Waste Isolation Pilot Plant

Compliance Certification Application

Reference 511

Popielak, R.S., R.L. Beauheim, S.R. Black, W.E. Coons, C.T. Ellingson, and R.L. Olsen, 1983.

Brine Reservoirs in the Castile Formation, Waste Isolation Pilot Plant (WIPP) Project, Southeastern New Mexico, TME 3153, Albuquerque, NM, U.S. DOE.

Submitted in accordance with 40 CFR §194.13, Submission of Reference Materials.

TME 3153

BRINE RESERVOIRS IN THE CASTILE FORMATION WASTE ISOLATION PILOT PLANT (WIPP) PROJECT SOUTHEASTERN NEW MEXICO

March 1983

U.S. DEPARTMENT OF ENERGY
WASTE ISOLATION PILOT PLANT
ALBUQUERQUE, NEW MEXICO

TME 3153

BRINE RESERVOIRS IN THE CASTILE FORMATION WASTE ISOLATION PILOT PLANT (WIPP) PROJECT SOUTHEASTERN NEW MEXICO

AUTHORS:

Roman S. Popielak — 3/16/83
Roman S. Popielak — Date
D'Appolonia Consulting Engineers, Inc.

Richard L. Beauheim — 3/16/83
Richard L. Beauheim — Date
D'Appolonia Consulting Engineers, Inc.

for S. R. Black RLS — 3/23/83
Sara R. Black — Date
D'Appolonia Consulting Engineers, Inc.

William E Coons — 3/23/83
William E. Coons — Date
D'Appolonia Consulting Engineers, Inc.

Charles T Ellingson — 3/14/83
Charles T. Ellingson — Date
D'Appolonia Consulting Engineers, Inc.

for R. L. Olsen RLS. — 3/23/83
Roger L. Olsen — Date
D'Appolonia Consulting Engineers, Inc.

APPROVED FOR SUBMITTAL TO WESTINGHOUSE BY:

D. K. Shukla — 3/23/83
D. K. Shukla — Date
D'Appolonia Consulting Engineers, Inc.

COGNIZANT MANAGER

C. C. Little — 3/25/83
C. C. Little — Date
Westinghouse Electric Corporation

ACKNOWLEDGEMENTS

The authors would like to thank the many individuals who contributed to the development and production of this report. Westinghouse-TSC and DOE provided constant support for this task. For their technical review and suggestions, the authors would like to thank Isaac R. Kaplan and Paul J. Mankiewicz of Global Geochemistry Corporation; Ekwere J. Peters and T. William Thompson of Department of Petroleum Engineering at the University of Texas-Austin; and Bernard J. Wood, Lubor Jarolimek, and John T. Gormley of D'Appolonia Consulting Engineers, Inc.

Additional technical coordination and support was provided from within D'Appolonia by Joseph K. Register, Jeffrey W. Nelson, John Kubiczki, and Dann Meyer.

TABLE OF CONTENTS

TABLE OF CONTENTS
(Continued)

PART III - HYDROLOGY

TABLE OF CONTENTS
(Continued)

TABLE OF CONTENTS
(Continued)

PART IV - CHEMISTRY

TABLE OF CONTENTS
(Continued)

TABLE OF CONTENTS
(Continued)

BACKGROUND

The Waste Isolation Pilot Plant (WIPP) project is a U. S. Department of Energy (DOE) research and development facility to demonstrate the safe disposal of radioactive wastes resulting from the defense activities and programs of the United States. This demonstration consists of two parts. First, about six million cubic feet of TRU waste will be emplaced in the thick bedded-salt deposits of the Salado Formation in southeastern New Mexico at a depth of about 2150 feet. Second, the WIPP will provide for research relative to the interactions of defense high-level waste with bedded salt, though all high-level waste will be removed prior to facility decommissioning.

A potential location was selected for the WIPP in the northern Delaware Basin of New Mexico, and three exploratory core holes were drilled (AEC-7, AEC-8, and ERDA-6; Figure 1). While drilling the third such hole (ERDA-6), substantial geologic structural deformation was noted, and brine and gas sufficiently pressurized to flow to the surface were encountered. The unpredictability of the geology led to relocation of the site to its present location in 1974 (Figure 1). Since relocation, an extensive site characterization program has been conducted, and the adequacy of the site has generally been demonstrated.

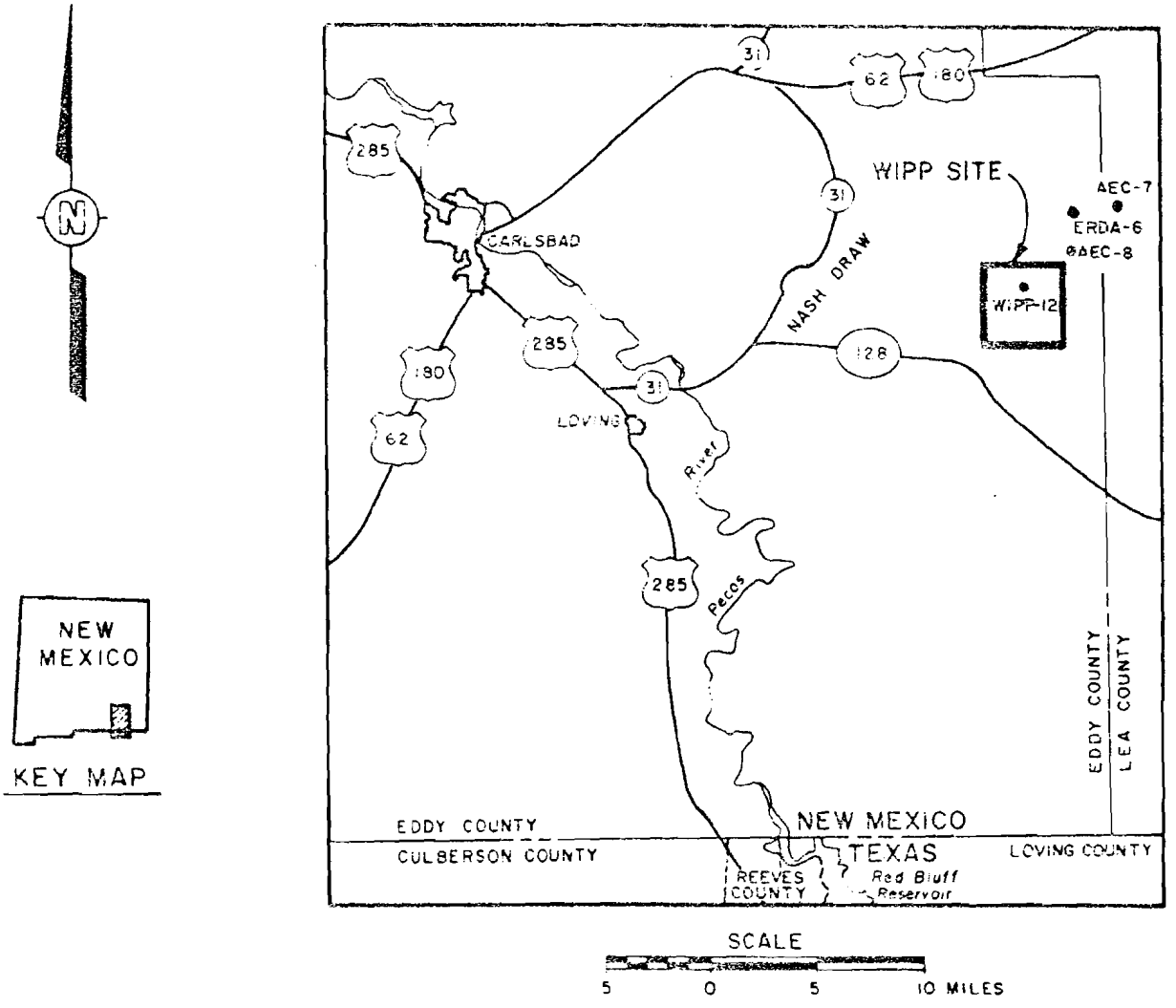

Figure 1 — Location of WIPP Site and Boreholes AEC-7, AEC-8, WIPP-12 and ERDA-6

In 1981, an agreement was signed between the State of New Mexico, the DOE, and others which included several studies intended to address the State's concerns relative to the suitability of the proposed WIPP site. Some of these studies addressed an area of geologic interest north of the proposed site, and pressurized brine reservoirs in the Delaware Basin. The work was begun in October 1981 and included the reopening and testing of ERDA-6, and the deepening and testing of WIPP-12, an exploration borehole which also encountered pressurized brine and gas. This report provides an account of these studies.

These studies and preparation of the brine reservoir report were performed by the WIPP Technical Support Contractor (TSC), primarily by D'Appolonia Consulting Engineers, Inc. (a member of the WIPP-TSC) under subcontract to the Westinghouse Electric Corporation (the TSC prime contractor). Sandia National Laboratories, Albuquerque, N.M. provided critical review of the studies and report; the U. S. Geological Survey also made comments.

The occurrence of pressurized brine reservoirs in the Castile Formation (underlying the Salado Formation) of the Delaware Basin has been documented over the past 40 years by reports of reservoir encounters by hydrocarbon exploration drilling. In general, these reservoirs were known to be contained in fractured anhydrite with associated hydrogen sulfide gas and were thought to be related to antiforms in the Castile.

Various theories were advanced to explain the origin of reservoirs, which included dissolution of evaporites by recent ground waters, dehydration of gypsum to form anhydrite, entrapment of ancient seawater during evaporite deposition, and ancient dissolution and reprecipitation of evaporite minerals. Should certain of these theories be correct, the suitability of the WIPP site could be in question. Thus, the purpose of this study was to determine the characteristics and origin of these reservoirs and evaluate their potential impact on the integrity and stability of the WIPP site.

Data used in the performance of this study were obtained from drilling and hydrological testing in boreholes ERDA-6 and WIPP-12 and from chemical analyses of samples of reservoir brine and gas collected at these two wells. Information was also obtained from a review of published and unpublished literature on the geology and hydrology of the basin. The principal data reviewed and analyzed in this report are contained in "Data File Report - ERDA-6 and WIPP-12 Testing" (D'Appolonia, 1982, 1983).

SUMMARY OF FINDINGS

The analyses and interpretations by three disciplines -- geology, hydrology, and chemistry — have been integrated to form a model of brine reservoir genesis, and to assess the current and future status of brine reservoirs as they relate to the WIPP site. The development of the brine reservoirs began in the Permian Period about 235 million years before present. The Castile evaporites, consisting primarily of anhydrite and halite as shown in Figure 2, were deposited at that time. During the initial chemical sedimentation (or precipitation) period, the solids were poorly consolidated and highly porous. Much or all of this pore space was filled with Permian seawater that had been enriched in dissolved solids, oxygen-18, and probably deuterium by evaporation. As sedimentation in the basin continued, the seawater became trapped as an interstitial fluid between individual grains of anhydrite and halite. As compaction increased, grain boundary accretion of halite probably surrounded some of the pore fluids and gave rise to fluid inclusions in halite crystals. Examination of ratios of major and minor element concentrations in the brines leads to the conclusion that the reservoir brines originated from ancient seawater with no evidence for fluid contribution from present meteoric waters.

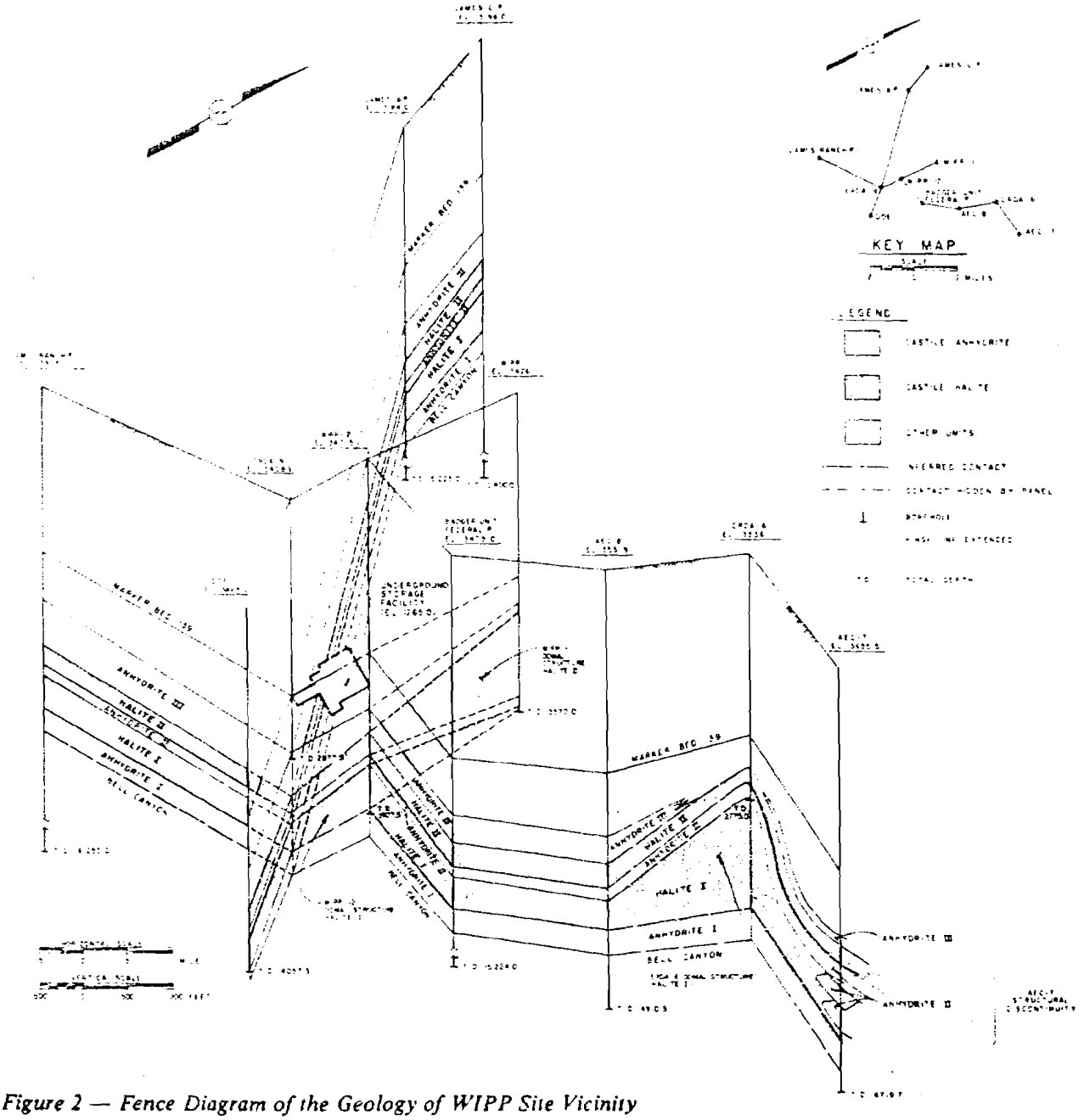

Figure 2 — Fence Diagram of the Geology of WIPP Site Vicinity

Subsequent to compaction and lithification of the sediments, the evaporite sequence was deformed. Deformation is represented, in part, by the localized elongate, salt-cored anticlines associated with the Castile brine reservoirs (e.g., Figure 2). These features were probably generated by flow of halite in response to differential stress. Several plausible mechanisms for salt flow have been proposed which would lead to the observed deformation. By whatever mechanism, the upward flow of salt locally deformed the overlying anhydrites and caused them to fracture as a result of extension (see Figure 3).

The waste disposal horizon, which is separated from the locally fractured anhydrite by about 600 feet of unfractured, low-permeability halite of the Salado Formation (Figure 2), was minimally deformed by the flow of Castile salt. The open fractures in the anhydrite acted as unfilled voids to attract the most mobile phases (i.e. brine and associated gases) present in the evaporite sequence. Flow into the fractures of the anticlines released some of the pressure on the brine and resulted in the current reservoir pressures which are somewhat less than present lithostatic pressure, but greater than present hydrostatic pressure.

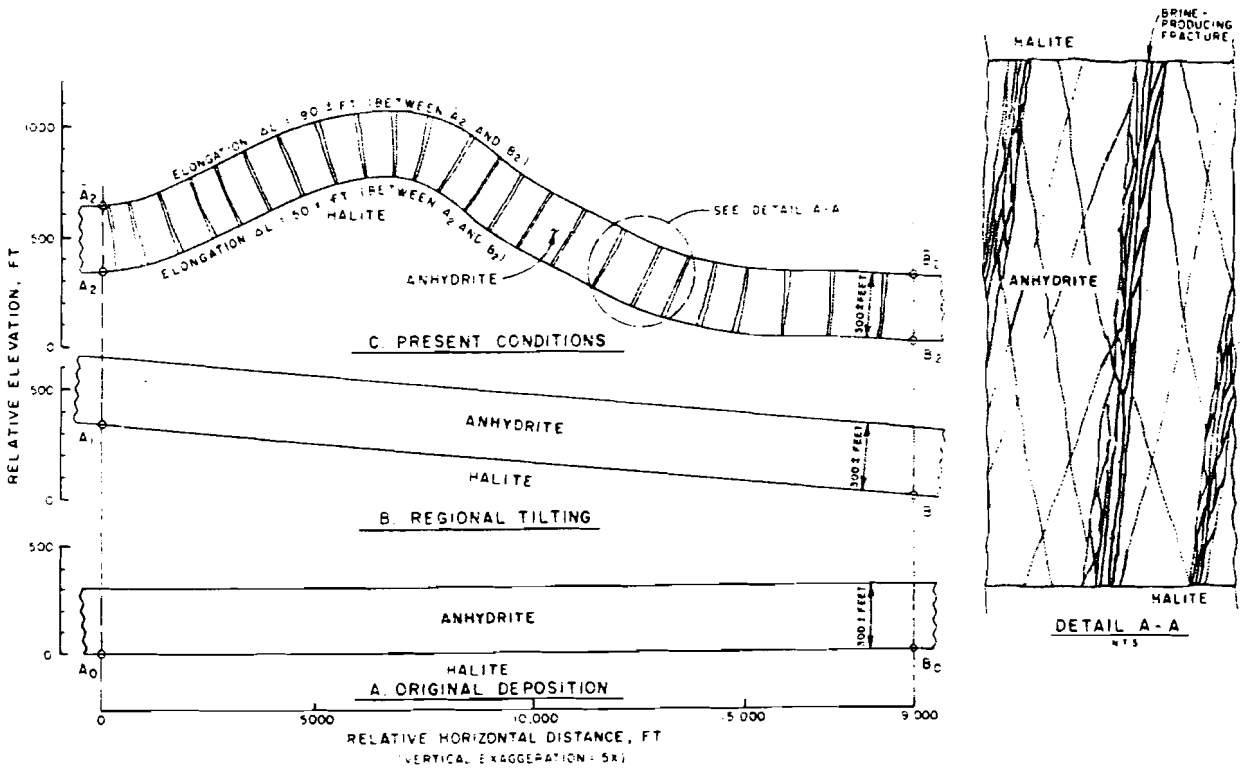

Figure 3 — Schematic of Brine Reservoir Formation

As the pore waters migrated toward fractures, they reacted with calcite to yield dolomite. This accounts for the presence of dolomite in the anhydrite and the relative depletion of magnesium in the brine. The reaction also further enriched the brines in oxygen-18 to give them the isotopic compositions observed. Additionally, during this local flow of brine, some halite, and in the case of WIPP-12, glauberite, were probably dissolved. Alternatively, minor dissolution (on the order of a fraction of an inch) of the confining halite beds (top and bottom) may have resulted in the halite saturation of the WIPP-12 reservoir.

Accompanying brine flow, or somewhat later, methane gas was both generated and trapped in place. In the case of ERDA-6, methane was generated biologically, whereas in WIPP-12 most or all of the methane was produced thermogenically (by the thermal degradation of organic matter). In both reservoirs, the hydrogen sulfide was produced largely by biological activity after the physical processes of reservoir formation were completed. However, a portion of the hydrogen sulfide may have had a thermogenic origin and been trapped similarly to the methane. At this stage, the evolution of the brine may have been complete.

The ERDA-6 and WIPP-12 brine reservoirs, which are located in fractured anhydrites above thickened halite (Figure 2), may be modeled as fractured heterogeneous systems. The volumes of the ERDA-6 and WIPP-12 brine reservoirs are estimated, within an order of magnitude, to be about 630,000 barrels and 17,000,000 barrels, respectively. The vast majority of brine is stored in low-permeability microfractures, and therefore is not readily released in the event the reservoirs are intercepted. In fact, less than three percent of the reservoir fluids would flow unassisted to the surface if encountered during exploration drilling. About five percent of the overall brine volume in each reservoir is stored in large, open fractures. The large fractures form an infiltration gallery or extended well, providing a collection mechanism and relatively high-permeability conduit for brine flow (Figure 3). The large fractures provide an initially vigorous flow or pressure-buildup response.

The microfractures provide a slow, sustained response. Given sufficient time, flow from the microfractures can largely replenish any depletion which has occurred in the large fractures.

At present, the Castile brine reservoirs appear to be isolated. There is no evidence to suggest hydraulic or chemical connection between reservoirs, or between reservoirs and other ground-water systems, either at the present or in the past. The persistence of high and different hydraulic heads in Castile brine reservoirs for at least one million years (the age of the most recent tectonic activity) is the principal hydrologic evidence for their isolation. The four Castile brine reservoirs for which accurate data are available show differences in hydraulic head ranging from 280 to 871 feet of water. Similarly, measured heads in the brine reservoirs are at least 1330 feet higher than heads in aquifers in the subjacent Delaware Mountain Group, and at least 1530 feet higher than heads in the overlying Rustler Formation (Figure 4). Hence, there is no physical mechanism for the brine reservoirs to receive recharge from these underlying and overlying units.

As regards chemical mechanisms, the gas and brine chemistries of the two reservoirs are distinctly different from each other and from local ground waters. For example, large differences in the reservoir gas compositions exist between WIPP-12 and ERDA-6. The gas in WIPP-12 is composed mostly of methane and has little or no carbon dioxide. The ERDA-6 reservoir contains substantial quantities of carbon dioxide, and more hydrogen sulfide than WIPP-12. Differences observed in the brine composition include boron, bromide, magnesium, potassium, and lithium concentrations. Connection between reservoirs would eliminate or mitigate these differences, especially with respect to the highly mobile gases. Accordingly, if connected in the past, the current brine (and associated gas) compositions of the two reservoirs would be more similar.

In addition to being isolated, the brines appear to be in chemical equilibrium with their surroundings, and they are stagnant. For example, the brines are chemically saturated with the primary phases of the reservoir host rock (anhydrite and calcite). WIPP-12 brine also appears to be saturated with halite, the principal phase of the confining strata. Furthermore, calculations indicate bulk system equilibrium among solid, liquid, and gas.

In summary, the brine reservoirs appear to be local, isolated features that have reached equilibrium with their environment. Evidence for long-term hydraulic and chemical isolation includes:

- Hydraulic heads that are substantially different from reservoir to reservoir and higher than the heads of local ground waters.
- The containment of gas by the reservoirs.
- Brine and associated gas chemistries that differ from reservoir to reservoir.
- Geographic separation and non-uniform distribution of reservoirs, i.e., extensive drilling has taken place in this area, but only a few wells have intercepted pressurized brines. There is no evidence for a continuous, extensive aquifer in the Castile.
- Bulk chemical equilibrium between the brine, gas, and reservoir rock in the ERDA-6 and WIPP-12 reservoirs.

Portions of the study presented in sections of this report centered around natural factors which could cause pressurized brine to contact the radioactive waste stored in the WIPP underground facility, and eventually transport radionuclides to the biosphere. Specifically, the potential for migration of brine as a result of hydraulic and/or chemical disequilibrium, with resultant dissolution of halite, was evaluated. At

present, the brine reservoirs studied are chemically and hydraulically stable. The brines are either at, or very near, saturation with respect to halite, and consequently have little or no halite-dissolution potential. Additionally, the brine reservoirs have maintained hydraulic heads greatly in excess of those in neighboring ground-water systems over at least a million years. These factors, combined with the extremely low permeability of intact halite and the absence of fractures which would increase that permeability in the halite separating the disposal horizon from the brine reservoirs, nullify the potential for upward vertical seepage of brine. For these reasons, pressurized brine reservoirs occurring in the Castile Formation do not affect the suitability of the present WIPP site.

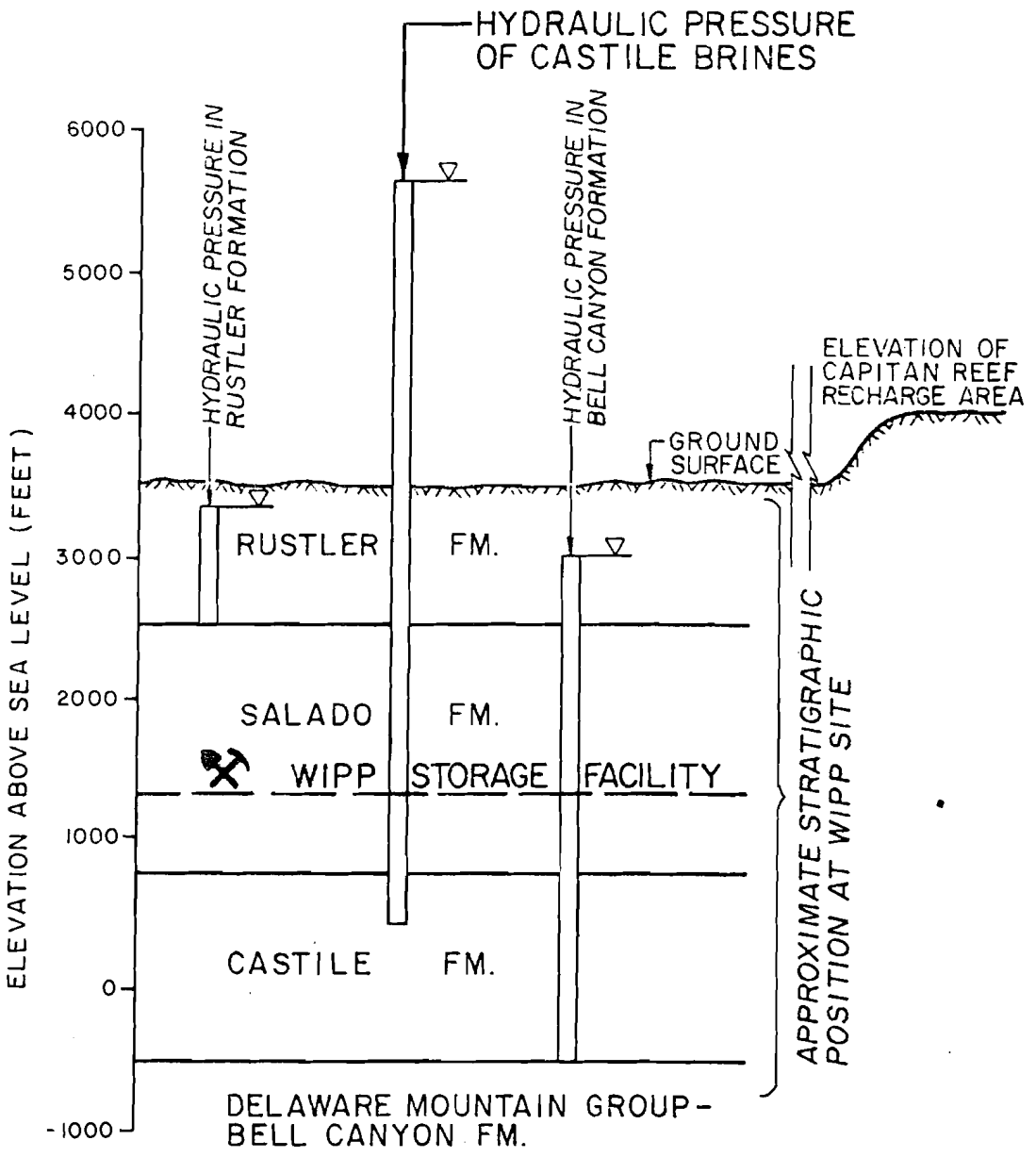

Figure 4 — Comparison of Standardized (Pure Water) Hydraulic Heads of Castile Formation Brines with Rustler Formation and Delaware Mountain Group

PART I - PREFACE AND INTRODUCTION

1.0 PREFACE

1.1 BACKGROUND

The Waste Isolation Pilot Plant (WIPP) project is a U.S. Department of Energy (DOE) research and development activity designed to demonstrate safe disposal of radioactive wastes resulting from the defense programs. The WIPP project mission consists of two parts. First, safe disposal of TRU waste in bedded salt will be demonstrated by placing approximately six million cubic feet of radioactive material in the facility. Second, a research facility for in-situ examination of the interactions between bedded salt and high-level radioactive waste will be provided by the WIPP. All high-level waste will be removed from the WIPP prior to decommissioning. A description of the planned WIPP is given in the WIPP Final Environmental Impact Statement (DOE, 1980a) and the WIPP Safety Analysis Report (SAR, DOE, 1980b).

The site for the WIPP is located in the Los Medanos area of the northern Delaware Basin, Eddy County, New Mexico (Figure 1). The selection of a bedded salt site was initiated in 1957 when the National Academy of Sciences (NAS) and the Atomic Energy Commission (AEC) stated that salt deposits provide the most promising medium for disposal of radioactive waste. Subsequently, several years of research associated with waste disposal in salt were undertaken, and led the NAS to reaffirm its 1957 position on radioactive waste disposal. Initially, a Lyons, Kansas salt mine was used for in-situ experimentation and was identified as a potential waste disposal site; however, the site was abandoned in 1972 due to the number of drillholes penetrating the beds and the likelihood that the salt beds were highly fractured. After a comprehensive search for a suitable disposal site, the Los Medanos area was chosen and field investigations were begun in 1974. Two core holes (AEC-7 and AEC-8) were drilled, both of which indicated acceptable subsurface geology (Figure 1). The third exploration hole, ERDA-6, revealed severe deformation of salt and anhydrite beds which dip up to 75 degrees. Additionally, fractured anhydrite produced a significant volume of brine and associated gas to

the surface from a depth of about 2700 feet. Due to the unpredictability of the subsurface geology and the difficulty that would result from underground construction in the steeply dipping strata at ERDA-6, the site was moved about six miles to the southwest, to its present location, in 1975.

An extensive site characterization program has been conducted for the past seven years. It has required drilling many (more than fifty) boreholes, conducting numerous geological, geophysical, geochemical, and hydrological studies, and performing a multitude of experiments on the suitability of bedded salt as a waste disposal medium. The results of these studies generally demonstrate the adequacy of the WIPP site for safe storage of radioactive waste; they are summarized in the WIPP Geological Characterization Report (GCR, Powers et al., 1978) and the WIPP SAR (DOE, 1980b).

In May, 1981, the State of New Mexico filed a lawsuit in Federal District Court against the DOE and the U.S. Department of the Interior (DOI) to enjoin WIPP activities. As a result of this filing, the DOE and DOI entered into a Stipulated Agreement with the State in July, 1981. Under this agreement, the DOE undertook studies addressing the State's concerns relative to the safety of the WIPP site. Three of these studies follow:

- Test Brine Reservoir in Deformation Zone: Reopen ERDA-6 and allow it to flow for at least ten days to measure the depletion of pressure at regular intervals in this well, and if access can be obtained, in Pogo #1 Federal well. Perform other necessary tests to determine the size, age, origin, and possible association with aquifers or other brine pockets.

- Report on Brine Reservoirs: Provide a comprehensive topical report on available information concerning brine reservoirs in evaporite beds in the Delaware Basin, including the results of tests at ERDA-6. This should include available information on the location, sizes, quantity, pressures, quality, ideas on origin, and methods of handling in mines.

- Horizontal Exploration of the Disturbed Zone: At the earliest possible stage of construction, and before

> emplacement of waste at the WIPP repository, provide for an additional 3000 feet of drift north of presently planned station #2, which is approximately 2500 feet north of ERDA #9, and drill 3000 feet horizontal cores to the north from this new location.

An alternative to the horizontal exploration of the "disturbed" zone was proposed by the DOE because the ability to drill 3000 feet, interpret the core, and seal the coreholes was questionable; the new plan included deepening ERDA-6 and WIPP-12 at least to the base of the Castile Formation. The State of New Mexico accepted the DOE proposal and work began in October, 1981.

In November, 1981, during the deepening of WIPP-12, pressurized brine was encountered at a depth of about 3000 feet in fractured anhydrite in the Castile; testing of this reservoir was added to the investigation.

This report is an account of the above-mentioned studies performed under the Stipulated Agreement between the DOE and the State.

1.2 PROJECT ORGANIZATION

The DOE assembled and manages a project team which consists primarily of the following organizations:

- Sandia National Laboratories (SNL) - the scientific advisor to the DOE on the WIPP project.
- Bechtel, Inc. - the architect/engineer for underground and above-ground facilities.
- WIPP Technical Support Contractor (TSC) - a group consisting of the prime contractor, Westinghouse Electric Corporation (Westinghouse), and subcontractors, D'Appolonia Consulting Engineers, Inc. (D'Appolonia), Dravo Engineers, and Gibbs and Hill, Inc. that provides technical support to the DOE on a variety of WIPP technical matters.
- U.S. Geological Survey (USGS) - responsible for site hydrology and an independent review of certain facets of site characterization.

- U.S. Army Corps of Engineers - responsible for site construction management.

The relationship among these groups is shown on Figure 2.

The studies reported herein were conducted for the DOE by the WIPP-TSC, primarily by D'Appolonia, under subcontract to Westinghouse Electric Corporation, Advanced Energy Systems Division. The objectives of these studies and the methods used were outlined by SNL and the WIPP-TSC with significant input from the USGS. Analysis and interpretation of the field data were performed by the WIPP-TSC, primarily by D'Appolonia, under Westinghouse direction, with suggestions and recommendations from SNL and USGS.

Most of the background information on the geology and hydrology of the northern Delaware Basin was derived from the exploration efforts of SNL and the USGS during the period from 1975 to the present. References for information extracted from documents prepared by these organizations are cited frequently in the text.

2.0 INTRODUCTION

2.1 BRINE OCCURRENCES IN THE CASTILE FORMATION

The WIPP site is located within the northeastern part of the Delaware Basin, a structurally downwarped crustal area of about 12,000 square miles. The Delaware Basin contains about 18,000 feet of sediments, dominated by strata of Permian age. It is a subbasin of the much larger Permian Basin, which includes the Midland Basin to the east, and the Palo Verde Basin to the northeast. The Capitan reef bounds the Delaware Basin on the north, west and southwest and is, in effect, the boundary of the basin. The Castile Formation halite and anhydrite beds were deposited in a deep inland sea within the Delaware Basin delimited by the reef, while the overlying Salado Formation bedded salt was deposited over the reef and ultimately covered a larger area. The Salado Formation is the unit currently under investigation as a containment for radioactive waste.

The occurrence of pressurized brine reservoirs in the Castile Formation has been documented over the past 40 years. Most of these reservoirs were encountered during exploratory drilling for hydrocarbons, and reliable information on reservoir flow rates, volumes, and pressures is not available. In general, the reservoirs encountered were contained within fractured anhydrite layers in the Castile Formation, and they were sufficiently pressurized for brine to flow to the surface. Further, all known reservoirs contain hydrogen sulfide gas and are associated with antiforms in the Castile. The occurrence of reservoirs is unpredictable however, in that reservoirs are not found in association with all antiforms. Available information on these reservoirs is included with this report.

2.2 PURPOSE OF STUDY

Various theories proposed for the origin of brine reservoirs in the Delaware Basin include:

- Dissolution of evaporites by fluids from underlying aquifers followed by fracturing of overlying anhydrite and migration of aquifer fluids into the fractures.
- Dehydration of gypsum to form anhydrite, accompanied by fracturing due to volume change and storage of fluids of dehydration in the fractures.
- Collection of entrapped ancient seawater in fractures formed during the structural evolution of the basin.
- Dissolution of evaporite minerals by meteoric water, closely followed by recrystallization, and fluid entrapment; subsequent fluid migration into fractures formed during salt flowage or tectonic activity.

At issue is the potential impact the brine reservoirs might have on the WIPP facility. Questions related to this impact include the following:

- Is there interconnection of local aquifers with brine reservoirs?

- Are brine reservoirs in the basin interconnected by a regional hydrologic system?
- Is brine reservoir formation an ongoing process, or has the system remained essentially static during the recent geologic past?
- Is the occurrence of brine reservoirs structurally controlled?

The purposes of this report are to address the above questions and in doing so, develop a supportable hypothesis on the origin of the reservoirs. Included is a prediction of the potential impacts of the reservoirs on the integrity of the WIPP site based on this information.

2.3 SCOPE OF STUDY

Information relative to pressurized brine reservoirs was obtained from two sources -- drilling reports, and extensive testing of the reservoirs intersected by ERDA-6 and WIPP-12. The investigations at the two boreholes required the integration of geology, hydrology, and chemistry. Geologic information on the reservoir rock and associated structures was obtained largely through examination of core from the boreholes and from geophysical logs. Hydrologic data were obtained by performing reservoir tests in the boreholes, and chemical data were gathered by analyzing brine and gas samples in the field and in various laboratories. Additional information on the topics of study was obtained from materials published on the Delaware Basin and WIPP site.

ERDA-6 and WIPP-12 field and laboratory data have been reviewed, reduced, and interpreted. A hypothesis explaining the characteristics and genesis of brine reservoirs in the Delaware Basin has been developed and substantiated. Though many data were considered, the focus of the studies is on recent data collected from ERDA-6 and WIPP-12.

During the testing activities conducted at ERDA-6 and WIPP-12, the New Mexico Environmental Evaluation Group observed portions of the tests and obtained a

small number of samples for limited chemical analysis in the New Mexico Bureau of Mines laboratory at Socorro. The results of the State's studies have not been included in this report because the Environmental Evaluation Group is in the process of publishing its own reports. The results of the State's studies are not expected to conflict in any way with the analyses and conclusions presented in this report, because their work is a subset of the studies performed by the TSC.

2.4 ORGANIZATION OF REPORT

The main body of the report is divided into four parts, each with a table of contents, tables, and figures. The final section of the report integrates and summarizes the findings.

Part II, Geology, presents the regional geologic setting and history of the Delaware Basin, and the WIPP site vicinity geology and history. In addition, features of note in the cored intervals are described and discussed in relation to the occurrence and genesis of brine reservoirs and deformation of the basin.

Part III, Hydrology, describes the data obtained from reservoir testing at ERDA-6 and WIPP-12, and from the literature. It also includes a discussion of the methods used to evaluate the data and presents a hydrologic model of the reservoirs which includes degree of connectivity and estimates of reservoir volume. A discussion of the hydrologic evidence on brine reservoir formation is included.

Part IV, Chemistry, is a summary of the data obtained on the chemical and isotopic composition of the reservoir brine, gas, and rock. A detailed discussion of the significance of the chemical data is included and an hypothesis is developed and supported to explain the origin and history of the reservoir fluids.

Part V, Summary and Conclusions, is a synthesis of the conclusions reached in Parts II, III, and IV, and presents a description of the evolution of brine reservoirs in the basin and the potential impact that these reservoirs could have on the WIPP facility.

LIST OF REFERENCES

Powers, D. W., S. J. Lambert, S. E. Shaffer, L. R. Hill, and W. D. Weart (editors), 1978, Geological Characterization Report, Waste Isolation Pilot Plant (WIPP) Site, Southeastern New Mexico: SAND 78-1596, Sandia National Laboratories, Albuquerque, New Mexico.

U.S. Department of Energy, 1980a, Final Environmental Impact Statement, Waste Isolation Pilot Plant: DOE/EIS-0026.

U.S. Department of Energy, 1980b, Waste Isolation Pilot Plant Safety Analysis Report (as amended in September, 1982).

DRAWN BY	CHECKED BY	S&B	5/18/82	DRAWING NUMBER NM78-648-A2
R. Bricker 21 Apr. 82	APPROVED BY	OPW/pkd	5/18/82	

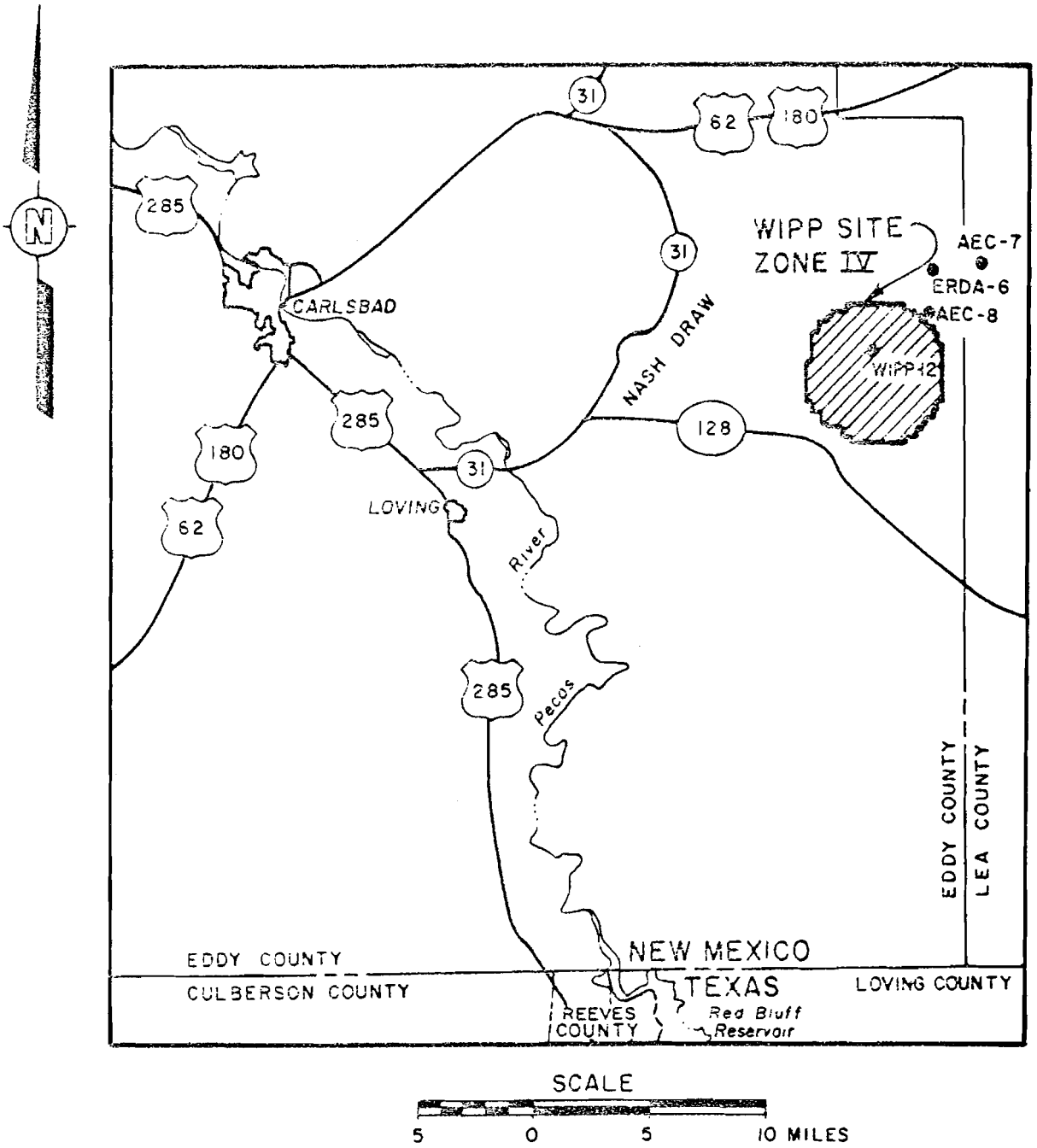

KEY MAP

FIGURE 1

LOCATION OF WIPP SITE AND
BOREHOLES WIPP-12 AND ERDA-6

PREPARED FOR

WESTINGHOUSE ELECTRIC CORPORATION
ALBUQUERQUE, NEW MEXICO

D'APPOLONIA

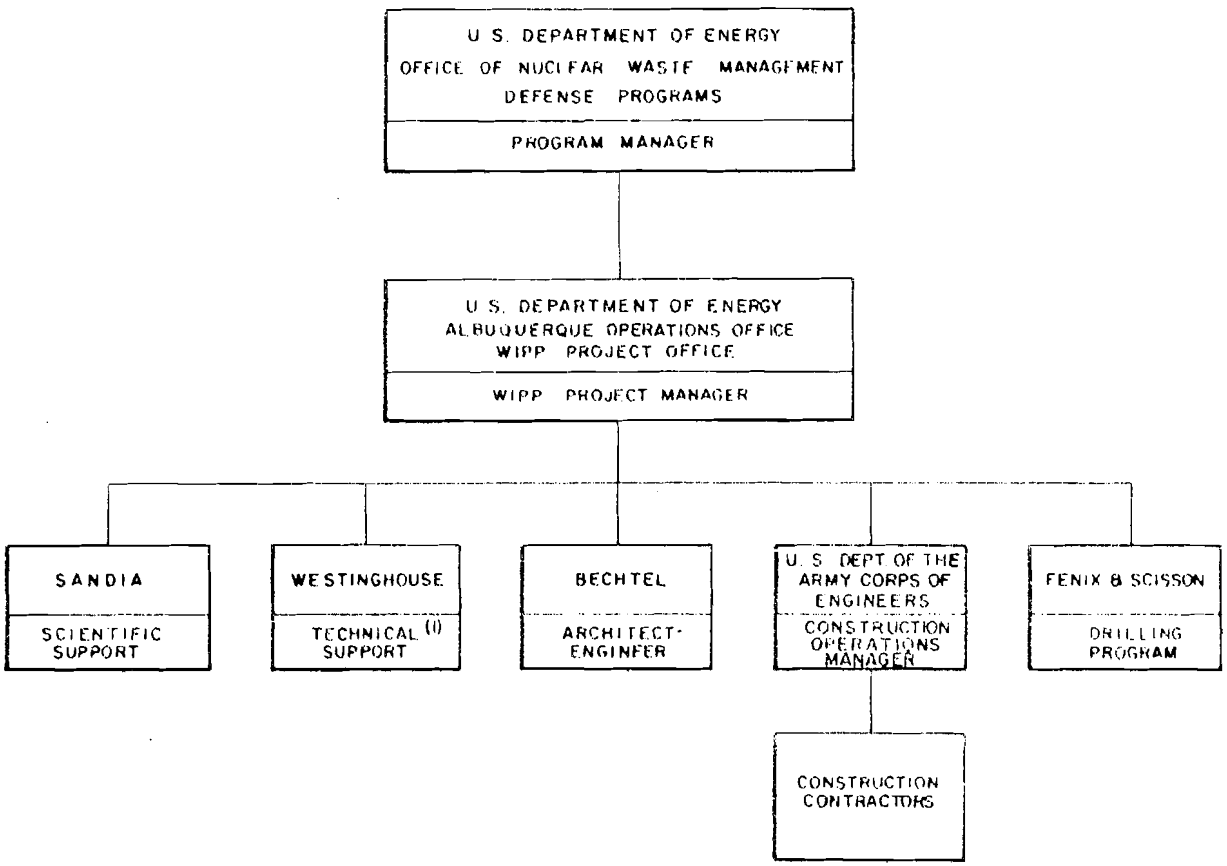

FIGURE 2

WIPP MANAGEMENT RELATIONSHIPS

PREPARED FOR

WESTINGHOUSE ELECTRIC CORPORATION
ALBUQUERQUE, NEW MEXICO

D'APPOLONIA

TWE 3153

(1) INCLUDING THE FOLLOWING SUBCONTRACTORS:
- D'APPOLONIA
- DRAVO
- GIBBS AND HILL

TABLE OF CONTENTS

TABLE OF CONTENTS
(Continued)

LIST OF TABLES

LIST OF FIGURES

PART II - GEOLOGY

1.0 INTRODUCTION AND SUMMARY

The geology section presents the interpretation and analysis of geologic data acquired during WIPP-12 and ERDA-6 testing, and related information from other pressurized brine occurrences in the Castile Formation, deep boreholes penetrating the Castile, and pertinent published information.

The geologic framework of southeastern New Mexico is formed by the Delaware Basin, the Central Basin Platform, Midland Basin, Capitan reef zone, Northwestern Shelf and Guadalupe Mountains. The WIPP site is located in the northeastern quadrant of the Delaware Basin, a structurally-downwarped basin of 12,000 square miles, approximately 90 miles from east to west and 150 miles north to south. The Delaware Basin is bounded on the north, west and southwest by the Capitan reef, an extensive basin-margin reef deposit. About 18,000 feet of sediments are present in the Delaware Basin, providing a nearly complete record of Paleozoic sedimentation. The Permian strata are the thickest of these sediments and include a thick section of evaporites that consist primarily of intercalated halite and anhydrite beds. The Castile and Salado formations comprise the major portion of this evaporite section.

At WIPP-12 the Castile Formation is comprised of five members (in ascending order): Anhydrite I, Halite I, Anhydrite II, Halite II, and Anhydrite III. Halite I is somewhat thicker than the typical section in the basin. The anhydrite rock is microcrystalline and dense, with thin bedding laminae made up of carbonates, organic material, and clays. Fractures are present in Anhydrite III, Anhydrite II, and an anhydrite stringer within Halite II, which dip between 70° and vertical. The fracture at 3016 feet depth produced brine. No fractures were detected in the halite members. At ERDA-6, the Anhydrite III member is apparently missing, based on previous geologic interpretation (Jones, 1981a). High-angle fractures are located in Anhydrite II which contain pressurized brine.

Information on other brine occurrences was analyzed and compared with WIPP-12 and ERDA-6 data to determine any basic patterns. Brine occurrences are associated with a belt of deformation in the Castile that parallels the Capitan reef subcrop and underlies the WIPP site. The brines appear to be located in the uppermost Castile anhydrite unit present at each location. At WIPP-12, Anhydrite III produced brine; at ERDA-6 the brine is thought to be located in Anhydrite II. Brine occurrences are associated in every known case with anticlinal structures of varying size within the belt of deformation.

The cause of fracturing of the anhydrites in the Castile Formation is thought to be the result of salt movement in the intercalated halite units. Examination of the anticlinal structures at WIPP-12, ERDA-6, and several other reservoir locations where data are available, shows that the halite units in the Castile vary in thickness. Thickening of the halite resulted from salt deformation. Initiation of deformation was caused by one of the following mechanisms: (1) gravity foundering of anhydrite; (2) tilting of the basin due to tectonic stresses which led to gravity sliding of the salt; (3) dissolution mechanisms; or (4) fluid generated by gypsum dehydration to anhydrite. The age of deformation is subject to discussion, but can be widely bracketed between late Miocene and Pleistocene time. The deformations appear to have created extensional fractures in the anhydrite overlying the halite at WIPP-12 and ERDA-6. Interstitial fluids were probably present in the Castile and migrated to the developing fractures due to differential pressure.

Geologic evidence alone cannot reveal the source of the fluids. However, there is no evidence of dissolution of evaporites by undersaturated fluids, which suggests that the brines are not of meteoric origin.

2.0 PURPOSE AND SCOPE OF STUDY

The purpose of the geologic portion of this study was to investigate the geology of the Castile Formation near the WIPP site in terms of its significance to pressurized brine occurrences. The following issues or areas of interest were addressed:

- Detailed geologic description of the Castile Formation, in the vicinity of WIPP.
- The relationship between structure/stratigraphy and reservoir occurrence.
- The mode of origin and timing of reservoir formation.
- The origin of brine present in the reservoir.

To address these items, WIPP-12 was re-entered and deepened into the basal member of the Castile by coring. The geologic investigation included:

- Logging of recovered core.
- Analysis of geophysical logs run in the borehole.
- Determination of the nature and intensity of deformation at WIPP-12, based on microstructures observed in core and other evidence of disturbance.
- Determination of orientation of deformation structures in oriented core intervals.

The related geologic investigations undertaken at ERDA-6 were limited because a complete data report on the ERDA-6 geology was issued in 1981 (Jones, 1981a). The investigations for the current program included:

- Logging of recovered core through the previously plugged interval.
- Logging of about 150 feet of drill cuttings samples.

In addition to ERDA-6 and WIPP-12 data, available data on deep boreholes penetrating the Castile which encountered pressurized brine were assembled and analyzed, as well as any data on deep boreholes not encountering brine. Numerous published reports and scientific literature concerning WIPP, the Castile Formation, and brine reservoir development were consulted.

3.0 GEOLOGY OF THE DELAWARE BASIN

Following is a precis of numerous previous investigations of the regional geology in the WIPP vicinity. The area has attracted much geologic study not only because of WIPP siting considerations, but also oil, gas, and potash resources, and a thick, well-preserved evaporite sequence. This geologic overview is provided here as a framework within which the site-specific geologic investigations are better understood.

3.1 REGIONAL GEOLOGIC AND PHYSIOGRAPHIC SETTING

The WIPP site is located in Eddy County, New Mexico, about 30 miles southeast of the city of Carlsbad. The site is within the Pecos Valley subdivision of the southern Great Plains physiographic province. The Pecos Valley is flanked to the west by the Guadalupe and Delaware Mountains which are within the Basin and Range physiographic province. To the east lies the relatively flat and undissected High Plains of the Great Plains physiographic province, known in southeastern New Mexico as the Llano Estacado. The significant topographic features are formed by the mountainous terrain to the west, the Pecos River Valley, and scattered swales and sinks, formed by dissolution of soluble strata underlying the area (Powers et al., 1978).

The geologic framework of the region is formed by the Delaware Basin, the Central Basin Platform, Midland Basin, Capitan reef zone, Northwest Shelf, and Guadalupe Mountains. The WIPP site is located in the northeastern quadrant of the Delaware Basin (Figure G-1), a structurally-downwarped basin of 12,000 square miles approximately 90 miles from east to west and 150 miles north to south. The Delaware Basin forms a part of the much larger Permian Basin. During its development, the Permian Basin was split into several subbasins, two of which are the Delaware Basin and the Midland Basin to the east, which is similar to the Delaware Basin but shallower. They are separated by the Central Basin Platform, an uplifted horst block bounded by faults.

The Delaware Basin is bounded on the north, west, and southwest by the Capitan reef, an extensive basin-margin reef deposit. The reef crops out and forms an

escarpment to the west of Carlsbad; this escarpment forms the eastern boundary of the Guadalupe Mountains. Behind the reef to the northwest of the Delaware Basin is the Northwest Shelf area, underlain by flat-lying rock strata deposited in shallow water (King, 1942). The Northwest Shelf is considered part of the Permian Basin, but was an area which did not undergo subsidence like the Delaware Basin.

Other structural features which played a role in the development of the Delaware Basin are the Huapache, Bone Spring, and Victorio flexures (Figure G-1). These features are related to the deformation which accompanied the rapid subsidence of the Delaware Basin (King, 1942). All of the elements which comprise the geologic framework will be discussed in greater detail in the following three sections.

3.2 REGIONAL STRATIGRAPHY

The Delaware Basin historically has been an important oil-producing area, as well as an important source of potash. The stratigraphy of the basin is therefore well documented in numerous published reports as well as unpublished oil exploration drilling data. Briefly summarized, about 18,000 feet of sediments are present in the Delaware Basin. A nearly complete record of Paleozoic sedimentation has been preserved (with the exception of Cambrian strata). In particular, the Permian evaporite sequence is one of the thickest and best preserved in the country. Figure G-2 is a regional east-west cross section across the Delaware and Midland basins, showing the thickness, extent, and continuity of the various rock strata. The Permian Age was obviously the dominant interval of deposition, indicated by comparison of thickness of Permian and Pre-Permian strata. The Mesozoic and Cenozoic eras are poorly represented, because erosion has removed most Mesozoic strata, and depositional activity was very limited during Tertiary and Quaternary periods.

Figure G-3 is a stratigraphic column of rock units underlying the WIPP site, describing in more detail the age, thickness, and characteristics of each stratigraphic unit shown in Figure G-2. The formations of primary interest to

the WIPP project are the Castile and Salado Formations of Ochoan Age (upper Permian). The Salado Formation, comprised primarily of bedded salt, is the stratum proposed for waste disposal. The Castile, underlying the Salado, is comprised of anhydrite with interbedded halite and is the reservoir rock containing pressurized brine encountered in several wells in the northern Delaware Basin. The Castile Formation is of primary interest and was investigated in detail in relation to brine occurrences. Figure G-4 is a simplified cross section of the Castile Formation in the Delaware Basin, showing the relationship of the halite and anhydrite units from north to south.

3.3 REGIONAL AND LOCAL STRUCTURES

Regional Structures

The large-scale tectonic features which form the structural framework of the region include the Delaware Basin, Central Basin Platform, Capitan reef, Northwest Shelf area, and several monoclinal flexures, all of which developed from Late Pennsylvanian to Early Permian time. The Guadalupe and Delaware Mountains and regional tilting of the region were developed during middle to late Tertiary time. The following are brief summary descriptions of the major structural elements.

Delaware Basin - As described earlier, the Delaware Basin is a structural downwarped basin encompassing southeastern New Mexico and western Texas. The basin is oval and slightly asymmetrical with a northerly trend and southward plunge (Powers et al., 1978). The Delaware Basin is the area of maximum subsidence of the larger Permian Basin, with more than 20,000 feet of structural relief (Powers et al., 1978) and contains the thickest sequence of Permian strata in the Permian Basin.

Faults and flexures developed in the Delaware Basin as a result of rapid basin subsidence in late Pennsylvanian - Early Permian time. These include the faults bounding the Central Basin Platform, and several monoclinal flexures including the Bone Spring and Huapache monoclines, which in part determined the configuration of the Delaware Basin.

Central Basin Platform - The Central Basin Platform is a subsurface structural feature that separates the Delaware and Midland Basins (Figure G-1). It may represent a structurally weak zone which underwent movement from Precambrian through early Permian time (Powers et al., 1978). According to Adams (1965), the uplift of the platform was necessary to compensate for compressional stresses generated by rapid, deep subsidence in the adjacent basins. The faults bounding the platform trend north to northwest, and predate the Permian evaporite deposits of the Delaware and Midland basins. Maximum structural relief between the Platform and the Delaware Basin is about 9000 feet and is fairly uniform from north to south (Powers et al., 1978). Because of movements of the Central Basin Platform from Precambrian through Pennsylvanian time, it exhibits a greater degree of structural disturbance, such as folding and faulting, than do adjacent basinal areas. The Platform has been relatively stable tectonically since early Permian time (Powers et al., 1978); minor low magnitude seismic activity has been recorded historically in the vicinity, but is generally attributed to hydrocarbon extraction activities in the area (Powers et al., 1978).

Capitan Reef Zone - Growth of the Capitan reef, and its predecessor, the Goat Seep reef, appears to have been controlled by flexures near the margins of the Delaware Basin (King, 1942). Reef growth during middle and upper Guadalupe time initiated on sloping sea floor overlying the flexures, at the transition between the shallow shelf area and the deeper, subsiding basin area. According to King (1942), the Goat Seep limestone reef is approximately 1200 feet thick, and the Capitan reef approximately 1800 to 2500 feet thick. Both of these reefs overlie an even older reef deposit (Abo reef) of Leonardian (early Permian) time, probably also controlled by the same flexures.

Erosion and Cenozoic uplift have acted to exhume the Capitan reef along the eastern edge of the Guadalupe Mountains where it forms an escarpment. The Castile Formation crops out adjacent to the escarpment. The Capitan reef outcrop disappears below Salado and younger sediments in the vicinity of

Carlsbad, continuing to subcrop in a horseshoe shape around the northern and eastern limits of the Castile Formation (Figure G-1).

Northwestern Shelf Area - This structural area extends northward and northwestward of the Delaware Basin. Some investigators consider the Capitan reef the element which divides the Northwestern Shelf from the Delaware Basin (Brokaw et al., 1972), while others argue that the Delaware Basin extends some distance into the back reef area (Powers et al., 1978). The shelf was in existence prior to Permian time, based on the rocks present. It probably formed the shelf margin of the early Tobosa sag, or Permian Basin (Powers et al., 1978). The shelf area exhibits many small flexures, folds, and domes, some of which may be related to the large basin-margin flexures such as the Bone Spring monocline discussed below.

Flexures - Near the western margin of the Delaware Basin, several structural flexures or monoclines are present which appear to have formed in response to rapid subsidence of the Delaware Basin (King, 1942). Two easily-identified features are the Bone Spring and Huapache monoclines. The Bone Spring directly underlies the Capitan reef escarpment, just south of the New Mexico - Texas border. The Huapache flexure is southwest of Carlsbad, along the eastern edge of the Guadalupe Mountains. Both features reflect similar flexures in the Precambrian basement, and may indicate historical zones of weakness dating from the Precambrian (King, 1942). Although the Huapache structure has the configuration of a monocline at the surface, evidence indicates that it overlies a thrust fault or series of faults in the Paleozoic section, thus representing draping of sediments over a fault zone (Powers et al., 1978). The fault zone was active up to Leonardian time in the Permian. Subsequent deposition over the fault zone produced the low eastward-dipping flexure configuration ranging from 0.5 to 2.5 miles in width. The Bone Spring and other similar flexures probably have a similar history (King, 1942).

Guadalupe-Delaware Mountains Uplift - The Guadalupe-Delaware Uplift is a fault block dipping gently northeastward, extending from Van Horn, Texas northwestward for about 110 miles. In New Mexico, the western boundary of the uplift is a great fault scarp produced by a system of nearly en echelon normal faults with displacements ranging from 2000 to 4000 feet (Powers et al., 1978). The eastern margin conforms to the Huapache Monocline, Bone Spring Monocline, and Capitan Reef Escarpment, discussed above. In cross section, the mountains exhibit an asymmetric profile with the fault scarp forming the steep western slope and the eastern slope dipping gently eastward at about 3 degrees. Structurally, the fault block is part of the Northwest Shelf, and it lies within the Basin and Range physiographic province. Faulting occurred during late Cenozoic time as a result of Basin and Range tectonic activity.

Regional Tilting - At least three episodes of gentle regional tilting have taken place in the Delaware Basin. The area was elevated and tilted slightly to the northeast during very early Tertiary time, during the Laramide Revolution which initiated mountain building in other parts of the Rocky Mountain Region. Minor igneous activity occurred in the Oligocene, producing the dike swarms observed in the northwestern Delaware Basin. Gentle tilting to the southeast occurred during late Tertiary (Pliocene) time, concurrent with basin and range activity to the west of the Delaware Basin. At this time, the Permian evaporites in the western part of the basin were elevated and exposed to erosion. During late Pliocene and early Pleistocene time, the main stage of uplift and faulting of the Guadalupe Mountains took place, which again may have contributed to minor gentle tilting of the basin to the southeast.

Local Structures

The preceding section focused on the major structural elements which form the tectonic framework of the Delaware Basin. On a smaller scale, structures in the vicinity of the WIPP site are associated with the origin and development of the Delaware Basin. The following discussion, taken primarily from Powers et al. (1978), briefly summarizes the types of local structures in the vicinity of WIPP.

Structure in Pre-Evaporite Rocks - Pre-Permian strata underlying the WIPP site have a regional dip of about 100 to 150 feet per mile (1 to 2 degrees) to the southeast reflecting the Delaware Basin downwarp. Minor faulting and warping is superimposed on this regional structural dip. The small faults tend to have a north-northeast trend, roughly parallel to regional strike, and are generally upthrown on the east. In Devonian strata, these small faults have displacements of up to 400 feet. Small arch-like swells are spaced several miles apart with amplitudes of several hundred feet and general east-west trends. These small-scale features are probably the result of basinal adjustment during late Pennsylvanian and early Permian time which accompanied the uplift of the Central Basin Platform. The subdued east-west-trending arches apparently serve as reservoirs for gas produced from the Morrow Formation of Pennsylvanian age. Small-scale structures in the Permian Delaware Mountain Group, about 9500 feet above the Morrow, do not show correlation with pre-Permian features. Warping is more subdued; small offsets of less than 50 feet are discontinuous and trend northwest. These small features, unrelated to underlying strata, probably formed in response to the very rapid accumulation of massive amounts of sediment during the Permian, which undoubtedly underwent differential subsidence, gravity creep, and other minor diagenetic adjustments.

Structure in Permian Ochoan Series - The Ochoan strata show a relatively uniform dip of one degree or less to the southeast, which is less than the dip of the underlying pre-Permian strata. Local variations in the regional dip of Ochoan strata have been observed in the underground excavations at the WIPP site (GFDR No. 7, 1983). Superimposed on the regional dip are areas of deformation attributable to mass migration or flow of salt. North and east of the WIPP site and immediately adjacent to the buried Capitan reef front, the Castile and the underlying Delaware Mountain Group are depressed into a structural trough paralleling the base of the reef and plunging southeastward. The most intense deformation in the Castile is related to this trough; intraformational "folding" or deformation appears to be best developed in a northwest-trending belt about 4 to 5 miles wide which coincides in trend and extent with the trough. All Castile members with the possible exception

of Anhydrite I have been involved in the deformation. Several large salt "anticlines" or antiformal structures have been recognized in the vicinity of the WIPP site on the basis of deep borehole data and surface seismic reflection data. The ERDA-6 borehole penetrates the crest of a large structure about ten miles long and three miles wide in which the Halite I member has apparently thickened from a normal 300 feet to over 1200 feet (Powers et al., 1978). Another similar structure is located about 9 miles southeast of ERDA-6, delineated by several deep oil exploration boreholes. A smaller similar structure was penetrated by borehole WIPP-12. Many investigators working in the area have noted these deformations in the Castile, and observed that the overlying Salado is also affected to a much lesser degree, as indicated by some warping. The deformation has been recognized through the use of deep borehole data, as well as seismic reflection data gathered during characterization of the WIPP site. These structures will be discussed in greater detail in later sections, in terms of the relationship of the structures to brine occurrences, the mode of formation, and time of formation.

3.4 SUMMARY OF GEOLOGIC HISTORY

The present configuration of the Delaware Basin was developed during Pennsylvanian time. The large Tobosa sag (also called the Permian Basin), in which sediments had accumulated from Ordovician through Mississippian time, was split by the rise of the Central Basin Platform; this median uplift created the Delaware Basin to the west and the Midland Basin to the east (Adams, 1965; King, 1942). During the early and middle Permian, the shelving margins of the rapidly subsiding basins were sites of extensive carbonate reef growth. The reefs eventually ringed much of the Delaware Basin, creating a nearly restricted, deep basin.

During early and middle Permian time, the basin became evaporitic and the Castile Formation (and overlying evaporites) was deposited. The depth of the basin during this period has been variously estimated to have been between 1000 and 2300 feet, with water depth ranging from several hundred to several thousand feet (Adams, 1944; Schmalz, 1969; King, 1947). Dean (1967, p. 130)

suggests that deposition in the Delaware Basin during Castile time proceeded slightly faster than subsidence, so that at the end of Castile time, the basin was filled. The uppermost portion of the Castile includes a thin tongue of magnesitic anhydrite, locally known as the Fletcher anhydrite, which was deposited over the Capitan reef and the Northwest Shelf area at the close of Castile time (Brokaw et al., 1972, p. 38; Adams, 1965, p. 2148). As a result of slight sagging and consequent rise in sea level following deposition of the Fletcher, deposition of evaporites continued and created the Salado Formation, which covers a much larger area than that occupied by the Castile Formation.

The mineralogic composition of the Castile is believed to have resulted from deposition in a basin nearly enclosed by the Capitan reef. King (1947) proposed the "reflux" theory to explain the fact that the Castile contains a greater volume of anhydrite than halite, when the volume ratio of halite to anhydrite components is 30 to 1 in sea water. In a typical evaporative sequence, calcium carbonate precipitates when sea water is evaporated to one-half the original volume; calcium sulfate is precipitated when the volume reaches about one-fifth of the original, followed by halite at about one-tenth of the original volume. To account for thick sequences of anhydrite, King (1947) proposed that the Delaware Basin was connected to the open sea by a shallow barred channel, sometimes referred to as the Hovey Channel (King, 1942, p. 665), in the southwest portion of the basin. New sea water was supplied by flow over the shallow bar through the channel to replenish water lost to evaporation. As evaporation proceeded and density of the water increased, the dense brine would sink below wave base. The heaviest brines enriched in sodium and chloride would, according to King (1947), reflux or percolate through the permeable bar back to the sea, maintaining the conditions necessary to precipitate calcium sulfate. Halite units within the Castile were precipitated subsequently in response to an increase in evaporation rates. Short-term fluctuations in salinity would result in fine laminations of different salts, such as those observed in the Castile (Dean, 1967). It has been suggested (Borchert and Muir, 1964; Udden, 1924; Anderson and Kirkland, 1966; Adams, 1944) that these laminations, or varves, of interlaminated anhydrite

and calcite with varying amounts of organic matter represent yearly depositional cycles during which the carbonates and organics accumulated during the winter months.

A point of considerable debate is whether the calcium sulfate of the Castile was deposited originally as anhydrite or gypsum. The predominance of gypsum in recent evaporite deposits tends to support the interpretation that most of the anhydrite in ancient deposits probably formed by recrystallization of primary gypsum (Dean, 1967). Experimental thermochemical and solubility data indicate that primary precipitation of anhydrite is entirely possible in the laboratory at normal basinal temperatures and pressures, depending on concentrations of other salts (Posnjak, 1940), or on the presence of organic compounds (Cody and Hull, 1980). Anhydrite has been observed as a recent primary precipitate in a few locations (Kinsman, 1966). Some investigators feel that the anhydrite of the Delaware Basin Castile Formation is primary (King, 1947; Dean 1967; Dean and Anderson, 1982), since evidence is limited for wide-scale conversion of gypsum to anhydrite.

Since the end of Permian time, the Delaware Basin has been relatively quiescent in terms of sediment accumulation and tectonic activity. During most of the Triassic the area was emergent; a thin blanket of sediments was deposited during late Triassic time (the Dockum Group) (Powers et al., 1978). During this period of emergence, some solution of soluble Permian rocks may have taken place. During Jurassic time, the area was uplifted slightly, with continuing erosion and solution of Permian formations (Powers et al., 1978; Bachman, 1980). Some sedimentation took place in the area during middle Cretaceous time.

During early Tertiary time, the Laramide orogeny created the Rocky Mountains, but this cycle of uplift seemingly had little impact on the Delaware Basin area. The region of southeastern New Mexico was elevated and tilted slightly to the northeast (Powers et al., 1978). Evidence of tectonism is indicated by minor flexing and folding in the Gaudalupe Mountains. The rocks deposited

during middle Cretaceous time were stripped off, and erosion of Triassic strata and solution of Permian evaporites continued. In late Tertiary, gentle uplift and tilting occurred again, creating an east-southeast regional dip throughout the basin. The Permian strata in the western part of the Delaware Basin were elevated as the western escarpment of the Guadalupe Mountains was uplifted due to basin and range activity, facilitating erosion, dissolution, and subsidence in the evaporites to the west of the Pecos River. The Ogallala Formation was deposited over most of the region during Miocene time, forming the High Plains surface (Powers et al., 1978). The main uplift and faulting of the Guadalupe Mountains occurred in late Pliocene to early Pleistocene time.

Since the beginning of middle Pleistocene time, erosion has been dominant in the Delaware Basin area. Most of the Ogallala sediments were removed, and solution subsidence features, such as Nash Draw and San Simon Swale, were established. The Gatuna Formation present in the vicinity of the WIPP site represents a valley-filling deposit consisting of coarse debris, possibly the remains of erosion of the Ogallala. The Mescalero caliche formed during this period. In conclusion, the Delaware Basin area has been remarkably stable in terms of tectonic disturbance since deposition of the Permian sediments.

4.0 GEOLOGIC ISSUES RELATED TO BRINE OCCURRENCES

As described in Section 2.0, the geologic issues important to an understanding of the brine occurrences are:

- Characterization of the Castile Formation
- The relationship between brine occurrences and geology
- The origin of the brine reservoirs.
- The origin of the fluids in the reservoirs.

The following major sections explore each of these issues in detail.

4.1 CHARACTERIZATION OF THE CASTILE FORMATION

4.1.1 Investigative Methods

Rationale

Characteristics of the Castile were determined in both ERDA-6 and WIPP-12 from examination of rock core obtained during drilling. ERDA-6 was drilled originally in the summer of 1975 to a depth of approximately 2775 feet and partially plugged after brine was encountered (Jones, 1981a). ERDA-6 was re-entered during this study and the cement plug and surrounding rock were cored to the previous total depth and the well was reopened to the brine reservoir.

WIPP-12 was drilled initially in 1978 to a depth of about 2775 feet, just below the top of the Castile Formation. During the present investigation, the well was re-entered and deepened to about 3925 feet into the top of the Anhydrite I member of the Castile.

The core obtained from both wells was logged by visual examination, and a lithologic description was prepared. This lithologic description and the details of coring are presented in the Data File Report issued by D'Appolonia in February 1982 (D'Appolonia, 1982).

Samples of the WIPP-12 and ERDA-6 core were selected for further testing, including microscopic analysis (petrography), X-ray diffraction, scanning electron microscopy, energy-dispersive X-ray spectroscopy, and isotopic analysis. This further testing was undertaken to determine:

- Elemental and mineralogic composition of selected zones of interest.
- Extent of brine-rock interactions in the fractured zones.
- Evidence of the presence of fluids in the rock during rock diagenesis and reservoir formation.

Limitations

Most of the information presented, including hydrologic and geochemical data, is based on two 8-inch drill holes located approximately 4 miles apart. While the assumption has been made that the characteristics of the host rock exhibited in WIPP-12 and ERDA-6 are representative of the Castile throughout the areal extent of the brine reservoirs, in reality the cores are specific only to the hole locations. Variations in stratigraphy and lithology are present elsewhere due to structure and slight variations in depositional environment. The results and interpretations presented in this report should be considered in this context.

4.1.2 Stratigraphy of the Castile Formation at the WIPP Site

When WIPP-12 was originally drilled in 1978, about 50 feet of the top member of the Castile Formation were penetrated. For this investigation, the well was deepened into the Castile, and bottomed about 25 feet below the top of the basal member of the formation. Referring to Figure G-5, the stratigraphic units intercepted in WIPP-12 are (in descending order) Anhydrite III (or Anhydrite III-IV), Halite II, Anhydrite II, Halite I, and Anhydrite I. The following short table presents depth below ground surface, elevation relative to sea level, and thickness of each stratigraphic member at WIPP-12, with the exception of Anhydrite I, which was not fully penetrated. The Halite I member is thickened, probably due to salt flow which is discussed in a later section; the typical thickness of Halite I in areas not affected by deformation is about 315 feet (personal communication, R. P. Snyder, 1982). The members overlying Halite I are consistent with typical regional thicknesses.

Member	Drilled Interval (Ft.)	Elevation (Ft.)	Thickness (Ft.)
Anhydrite III-IV	2725.3 - 3053.9	746.2 - 417.6	328.6
Halite II	3053.9 - 3281.8	417.6 - 189.7	227.9
Anhydrite II	3281.8 - 3391.0	189.7 - 80.5	109.2
Halite I	3391.0 - 3901.6	80.5 - -430.1	510.6
Anhydrite I	3901.6 - 3925 (T.D.)	-430.1 - ?	?

ERDA-6 was originally drilled in the summer of 1975, and about 42 feet of the assumed Halite I member of the Castile were penetrated. During the present investigation, ERDA-6 was reopened and drilling did not proceed deeper than the 1975 investigation. Because of deformation in the vicinity of ERDA-6, the Anhydrite III member is presumed to be missing from the section. Both Jones (1981a) and Anderson and Powers (1978) interpret the anhydrite intercepted in the borehole as Anhydrite II, based on correlation of lithology with that of nearby boreholes. The intense deformation observed in the core supports the conclusion that thickening and uplift of underlying halite has created extension and separation of Anhydrite III, so that it is not present at the ERDA-6 location. Possible mechanisms for this deformation are discussed in Section 4.3. However, the possibility exists that the anhydrite unit encountered during drilling is Anhydrite III. Drilling of WIPP-12 revealed that Anhydrite III exhibits bedding laminae previously thought to be present only in the lower anhydrites. Since the ERDA-6 anhydrite is also laminated, its stratigraphic identity cannot be readily determined. For this report, the interpretation of Jones (1981a) and Anderson and Powers (1978) is accepted pending definitive borehole data from the ERDA-6 vicinity.

The following table relates stratigraphic depth of the Castile members present in ERDA-6 (from Jones, 1981a), as seen in Figure G-5.

Member	Depth Interval (Ft.)	Elevation (Ft.)	Thickness (Ft.)
Anhydrite III	Missing	-----	-----
Halite II	2400.5 - 2555.1	1139.7 - 985.1	154.6
Anhydrite II	2555.1 - 2732.5	985.1 - 807.7	177.4
Halite I	2732.5 - 2775 (T.D.)	807.7 - ?	?

Figure G-6 is a fence diagram of the WIPP site and vicinity, showing the stratigraphic relationships among WIPP-12, ERDA-6, and other nearby boreholes, including the WIPP exploratory shaft, as interpreted for this report. This representation shows the relative continuity of the Castile members within an approximate 4-mile radius of the center of the WIPP site. Variations in

thickness of the Castile members within this radius are evident from the figure. Outside this radius, and approaching the Capitan reef, the Castile Formation begins to exhibit evidence of significant deformation, an example of which can be seen in the correlation between the ERDA-6 and AEC-7 boreholes. The structures shown in Figure G-6 are interpretations based on geophysical logs, surface seismic data, available structure contour maps, and literature review. The structures, along with their possible modes of origin, are discussed in Sections 4.2 and 4.3.

4.1.3 Lithology and Texture - WIPP-12

The following is a summary description of the lithology and texture of the Castile Formation core recovered from WIPP-12, augmented with interpretation.

Anhydrite - The anhydrite observed in the WIPP-12 core is dense and microcrystalline, ranging in color from light gray (N7)[1] through medium-light gray (N6) light bluish-gray (5B 7/1), medium gray (N5), to dark gray (N3) and olive-black (5Y 2/1) in the Anhydrite II member. The anhydrite is translucent with a vitreous luster. Petrographic examination of the anhydrite reveals several crystal forms, ranging from very fine-grained granular to large blocky lath-shaped crystals to long acicular crystals. These acicular crystals are sometimes found in radiating groups with sweeping extinction. The acicular anhydrite crystals may be pseudomorphs of anhydrite after gypsum, since they resemble the crystal form of gypsum. Also, other criteria for identifying gypsum pseudomorphs are the observation of remnant gypsum cleavage parallel to the long crystal axis, and radiating clusters of acicular crystals, a common growth habit of gypsum. Possible pseudomorphs were observed near the base of Anhydrite III, in anhydrite stringers within Halite II, at the base of Anhydrite II, and in Anhydrite I. An example of a possible pseudomorph group is shown in Figure C-18, in the Chemistry section. Although this suggests primary precipitation of gypsum, the criteria described above are sub-

[1] Color designations taken from Geological Society of America Rock-Color Chart, and used here for consistency of description.

jective. The acicular growth habit could also be the result of primary anhydrite precipitation, possibly due to rapid crystal growth.

Some anhydrite crystals show weak pleochroism which is not characteristic of the mineral. Because pleochroism is differential absorption of transmitted light in different crystallographic directions, pleochroic anhydrite probably possesses a slight structural defect which creates unequal absorption. This crystal lattice defect could be the result of included cations of transition metals which deform the lattice slightly (Stoiber and Morse, 1972, p. 202). Microprobe analysis would be necessary to detect foreign cations in the anhydrite crystals. Lattice defects as described above may have been compounded due to strain caused by post-depositional movements or tectonic stresses during crystallization or recrystallization, but this is purely speculative.

Accessory minerals are rare but include carbonates, quartz, and clays; carbonates found in the bedding laminae are discussed below. Quartz was identified in the vicinity of the contact between Halite II and Anhydrite II, consisting of euhedral grains with the C-axis parallel to the contact (Figure C-18). The quartz grains are believed to be authigenic; this is discussed further in Part IV, Chemistry, Section 3.3.3. Clays, though rare, are not rich in magnesium.

The core demonstrates some textures often noted in anhydrite such as mosaic or "chicken-wire" texture (Riley and Byrne, 1961). The mosaic effect is created by small masses of anhydrite separated by thin stringers of dark organic (?) material. This texture is most apparent between 2818 and 2830 feet (depth below ground surface). Another texture noted in WIPP-12 resembles flocculent texture (Riley and Byrne 1961), in which irregular feathery masses of yellowish-gray (5Y 7/2) to light olive-gray (5Y 5/2) anhydrite float in the matrix of gray anhydrite. This texture is common between 2830 and 2940 feet.

The most notable textural feature in the anhydrite, other than the fractures discussed in Section 4.1.4, is the layering formed by very thin bedding laminae, probably a result of minor, short-term salinity variations during deposition (Section 3.4). The laminae range from white (N9) to yellowish-gray (5Y 7/2) to dusky yellowish-brown (10 YR 2/2) to dark yellowish-brown (10YR 4/2) and range from less than 0.03 inch to 0.5 inch thick. The laminae are composed primarily of calcium and magnesium carbonate, with minor amounts of clays and organic material. The carbonate is usually extremely fine grained in the form of wispy lamellae dispersed around anhydrite crystals. Dolomite is found in laminae adjacent to anhydrite/halite contacts; its abundance decreases away from the contacts and calcite becomes the dominant carbonate (Part IV, Chemistry, Table C-11). For example, Sample 18A was taken about 12 inches above the Anhydrite II/Halite I contact; x-ray data show that all the carbonate is calcite. Sample 18B, taken about 1 inch above the contact, contains roughly equal amounts of calcite and dolomite. Samples from the mid-parts of anhydrite units have laminar material of predominantly calcite with trace amounts of dolomite. Adams (1944), as well as Kirkland and Anderson (1970), report that the carbonate material is calcite, based on examination of cores from other parts of the basin. However, petrographic examination of both ERDA-6 and WIPP-12 core, as well as X-ray diffraction data and scanning electron microscopy, indicate that some of the material within the dark laminae is clearly dolomite, particularly in the vicinity of halite contacts. The presence of dolomite as opposed to calcite may be related to the chemical composition of the brine and its interaction with the rock (see Part IV, Chemistry, Sections 3.3.2 and 5.1.2.).

Anhydrite Microstructure - There are noticeable variations in the appearance of the laminae with depth. Throughout the anhydrite section (as noted below), the laminae locally exhibit evidence of deformation referred to here as "microstructure". Microstructure is used here to describe small folds and crenulations with amplitudes generally ranging from less than one inch to about one foot. The term microstructure was chosen to distinguish small-scale deformation features from the macrostructures or salt-cored antiforms in the Castile as described in Section 3.3.

The bedding laminae are indistinct and generally ill-defined in the upper portion of Anhydrite III. Below 2940 feet, thin bedding laminae become apparent, and were noted in groups of several laminae, spaced about one inch apart. Below 2943 feet, bedding laminae appear to be a result of cycles of deposition and are spaced quite regularly 1/2 inch apart. The laminae are in some cases slightly undulatory and slightly inclined from the horizontal. Below 3000 feet, some small microfolds are observed in the bedding laminae; these small deformations become more apparent with depth, particularly below 3030 feet. Three feet above the contact with Halite II, the bedding laminae become more steeply inclined until, at the contact, they are dipping about 30° from the horizontal (parallel to the contact).

In contrast, the Anhydrite II member exhibits thin bedding laminae throughout, generally consistent in appearance. Anhydrite II shows the most abundant evidence of microfolding of bedding, the small folds generally having an amplitude of less than 0.25 inch. In some cases these microfolds are very regular and symmetrical in appearance, while in others, such as at a depth of 3302 feet, the laminae appear irregularly contorted, resembling flow structures. The microfolding is disharmonic, meaning that adjacent layers show varying fold amplitudes. Figure G-7 shows a typical example of microfolding style in Anhydrite II.

The Anhydrite I member is similar to Anhydrite III in that the bedding laminae are very irregular and poorly defined in the upper part of the unit. From the contact of Anhydrite I with Halite I at 3902 feet to 3918 feet, the laminae vary from 0.25 inch to less than 0.04 inch in thickness, and are spaced from 0.13 to 2 inches apart. The laminae are undulatory and do not show uniform thickness, and in some cases are microfolded. However, below 3918 feet, the laminae are parallel, spaced regularly at 0.06 inch apart with no indication of deformation or folding.

Several explanations have been offered by various investigators to explain the origin of the microstructures in the Castile Formation. The excellent preservation of the laminae and accompanying microfolds suggests stagnant deep water, and appears to preclude strong currents or wave action. For example, current or wave action should have produced recognizable ripples, cross-bedding, or scour marks. As shown in Section 3.4, many investigators agree that the Castile sea was deep (up to several thousand feet) to allow for operation of the reflux precipitation model, and to be consistent with the observed elevation difference between the top of the Delaware Mountain Group and the top of the Capitan reef.

The microfolds may be a result of small movements due to sliding or slumping during or immediately following deposition. These penecontemporaneous movements could explain the presence of deformed laminae surrounded by apparently undeformed anhydrite. Kirkland and Anderson (1970) argue that the apparent correlation of deformed laminae over a distance of roughly 70 miles indicates that sliding would have to be uniform over large distances within the basin. However, they do not rule out mass gravitational gliding in response to tectonism or an initial slope as a cause of folding. Earthquakes could be a trigger which would result in widespread and consistent small-scale adjustments. Riley and Byrne (1961) have suggested on the basis of laboratory experiments that microstructures similar to those observed in the Castile could form by flowage due to slight density differences between anhydrite laminae and more dense carbonate and bituminous material.

The microstructures probably did not form during conversion of primary gypsum to anhydrite. This is not to suggest that this conversion did not take place; petrographic evidence in the form of crystal pseudomorphs (Section 4.1.3) suggests that at least some primary gypsum may have been replaced by anhydrite. Geochemical data also do not rule out the conversion process as a minor source contributing to the reservoir fluid. However, in spite of the fact that gypsum-anhydrite transitions have been cited historically as the cause of microfolding, there is no evidence of this in the Castile. As

Anderson and Kirkland (1966) point out, the microfolds are observed in both anhydrite and gypsum; the appearance of the folded laminae is the same whether observed in core or at the gypsified Castile outcrop southeast of Carlsbad on Route 62 just north of the Texas-New Mexico border.

Another explanation proposed by Kirkland and Anderson (1970) is that the microstructures formed due to tectonic stresses. Microfolds formed, according to their analysis of folding style, in the hinge areas of larger scale folds formed probably during Tertiary time. This mechanism does not appear to fully explain the presence of microfolded laminae intercalated with undisturbed, unfolded laminae, as is often observed in WIPP-12 core. Anderson and Powers (1978) have shown that microfolds have been subjected to extension at ERDA-6, which indicates that the formation of microfolds probably predated the development of the structure at ERDA-6 and by inference the structure at WIPP-12. Thus, several explanations exist for the origin of microstructures of the type observed at WIPP-12.

Halite - The halite present in the Castile Formation is typically slightly translucent with a faint light gray (N7) to olive-gray (5Y 4/1) cast. Purer halite sections are colorless and transparent. Halite crystal size varies from 0.125 to 0.5 inch along the longest crystal dimension, although some very large crystals up to 3 inches long were observed in Halite I. The halite contains an appreciable amount of anhydrite. According to a report which investigated halite impurities (Gevantman et al., 1981) the percentage of impurities in a halite deposit can range from less than one percent to thirty percent; the Salado Formation generally contains about 10 percent impurities (Gevantman et al., 1981). A reasonable estimate of the percentage of anhydrite within the halite units of the Castile at WIPP-12 based on core examination would be about five percent. The anhydrite impurities typically appear as white (N9) to medium gray (N5) thin beds and laminae 0.125 to 0.25 inch thick, within a band or zone of dark olive-gray (5Y 4/1) halite. Invariably the thin anhydrite beds, although often indistinct, are folded and display evidence of slight to intense deformation.

Halite crystals are typically anhedral, with irregular crystal boundaries. Masses are very friable. Cubic crystals are rare; hopper cubes were not observed. At the contact between Anhydrite II and Halite I, petrographic examination revealed cubic halite molds filled with fine-grained granular anhydrite; these molds may represent relict hopper cubes which could have subsequently been dissolved by fluids saturated in anhydrite. In many places, the elongated halite crystal axes show a lineation or fabric. These types of halite crystal textures suggest that the halite has recrystallized under the influence of stress and subsequent flow, possibly aided by interstitial fluids (Ode, 1968).

Halite Microstructures - As with the anhydrite, variations occur in the appearance of the halite and its impurities with depth. These variations might lend evidence of the deformation history of the strata and the origin of the brine reservoir. The Halite II member exhibits the greater amount of included anhydrite when compared to Halite I. The upper interval in Halite II between the contact with Anhydrite III and 3118 feet contains numerous anhydrite impurities which appear to have undergone considerable deformation. The most common pattern of anhydrite stringers or thin beds observed through this interval is a semi-circular or arc pattern. The core appears to have intercepted portions of small recumbent folds in the halite (with amplitudes of several inches to three feet) with their axial planes perpendicular to the long axis of the core. The folds are made visible by the more easily discerned anhydrite stringers, even though the halite is similarly deformed. For example, at a depth of 3074, the elongated halite crystals are aligned parallel to the deformed anhydrite stringers.

Between 3118 feet and 3198 feet, Halite II contains considerable amounts of anhydrite, including several beds up to three feet thick. The anhydrite beds through this interval contain crystals and blebs of halite, and bedding laminae containing calcium carbonate are present. Because of the greater thickness of anhydrite impurities which increases the strength of the halite

(Ode, 1962, p. 576), deformation is less through this interval. However, bedding laminae within the anhydrite beds are often inclined, as at 3128 feet.

Below 3198 feet to the contact with Anhydrite II, Halite II exhibits structure and patterns indicating considerable deformation. A common feature is a circular or elliptical thin bed or stringer of anhydrite, surrounded by halite as shown in Figure G-8. This type of feature could be a section through a sheath fold or closed fold. An analogy of this type of structure would be to take a flat hankerchief, pull it upward through the closed ring of your fingers, cut off the tip, and observe the closure outlined by the cloth, which would represent one of the thin anhydrite stringers (Muehlberger, 1968). Small isoclinal folds are also common, as at a depth of 3218 and 3223 feet. A section of core through one of these folds with an undeformed axial plane could also produce a circular outline in the core. The thin anhydrite stringers also show evidence of rigid behavior such as boudinage, as observed at a depth of 3218.3 feet. An interesting feature is that deformed intervals are often separated by inches from horizontal, apparently undeformed anhydrite impurities.

The Halite I member contains fewer anhydrite impurities than Halite II, especially in the upper portion. Anhydrite impurities which are present are indistinct, and evidence of salt flow or deformation is rare. Cubic halite crystals were observed throughout the interval. An isoclinally-folded, thin anhydrite stringer is locally observed, with an amplitude of one inch or less. Below 3600 feet, Halite I begins to show more evidence of deformation. Anhydrite impurities appear as very light gray (N8) or moderate yellowish-brown (10YR 5/4) mottles, circular patterns, and tight isoclinal folds. A commonly observed feature is a mass of highly contorted, fragmented anhydrite stringers, usually about 0.125 inch thick, such as in Figure G-9. Zones or bands of sulfate-rich impurities are spaced from 0.5 to three feet apart in the halite. The halite crystals exhibit elongation and a distinct lineation. Below 3750 feet and down to the lower contact with Anhydrite I, large macrocrystals of halite are often observed, up to 3 inches in length.

The variations in texture and microstructure in the halite units indicate that different intervals within the halite deformed or were stressed with varying intensity. Differences in amounts of impurities within the halites also contributed to variations in deformation styles due to differing properties.

Significance of lithology and texture to brine occurrence -- No evidence of dissolution of halite or anhydrite was encountered during analysis of the WIPP-12 core. All core was fresh and unweathered (fractures did exhibit some microscopic evidence of fluid movements and are discussed below). In particular, the contacts between the anhydrite and halite units were exceedingly clean, tight, with no open space or weathering. However, microscopic evidence of fluid movement exists, such as the halite molds filled with anhydrite at the Halite I/Anhydrite II contact. Thus, the rock matrix at WIPP-12 shows no evidence of large-scale undersaturated meteoric fluid flow having occurred.

4.1.4 Fractures - WIPP-12

Several fractures were encountered in Anhydrite III and in an anhydrite stringer near the top of Halite II during drilling of WIPP-12; one fracture was observed near the base of Anhydrite II. All fractures were readily observed in the rock core; the majority of fractures were also detected using a U.S. Geological Survey televiewer log, an acoustic electrical log which detects rock discontinuities at the borehole surface. No fractures were detected in halite units.

Fracture Characteristics - Table G.1 contains a summary of fracture data and characteristics of all fractures detected in the core. The fractures are all high-angle breaks, ranging from about 70° to vertical. An average true fracture spacing (as opposed to apparent) through the lower part of Anhydrite III (fractures C-G) has been estimated, based on the fracture distribution, at about two to three feet. The persistence of individual fractures is unknown; based on the properties of halite, none would be expected to extend into overlying and underlying halite units, and in fact, none were observed in

halite. The fractures are generally planar and fairly smooth. Wall strength, although not measured, would appear to be unaltered. An exception is the major brine-producing fracture (fracture D) with severely broken and crushed rock in the middle six inches of the fracture interval. Rock strength may have been reduced in this interval due to the presence of brine, or drilling could have crushed the interval. Fracture F includes an interval also crushed into small fragments. Fractures H and J are closed with visible halite filling. Fracture B is partially filled with halite, fracture G has a gapped appearance, and fractures A, C, D, E, F, and K have no filling.

In general, the apertures of all fractures appear to be quite small, although they were detected on the televiewer log as attenuations of acoustic signals. However, core fragments across open fractures can be mated together with either undetectable or very small displacement. As shown in Table G.1, the estimated aperture of fractures A, C, E, and K is less than 0.06 inch (2 mm). The estimated aperture for the brine-producing fracture D is less than 0.2 inches (5 mm) The aperture for fracture F could not be estimated because of severe breakage.

Fracture B is filled with halite; filling thickness is not greater than 0.03 inch. Petrographic examination reveals that there is bridging of anhydrite grains across the fracture plane. Drilling fluid may have dissolved the halite filling in several areas, especially at the upper extremity of the fracture, creating the appearance of gapped filling, and creating an open aperture of about 0.03 inch.

Fracture G is closed in the sense that the core is intact and not separated. However, visible open space, up to about 0.03 inch (1 mm), exists along the fracture, creating a gapped appearance. No filling is visible within the gaps. Anhydrite grains appear to have bridged across the fracture plane.

Fracture filling is also evident in fractures H and J. These are located in an anhydrite layer just below the top of Halite II. The filling is halite,

about 0.1 inch thick, clear, transparent, and very smooth; no other minerals are present. The very smooth and optically continuous halite suggests possible deposition by fluids. The filling is continuous with the halite beds below in the lower fracture. Short horizontal breaks associated with the vertical break are also halite-filled.

Evidence of seepage, such as obvious dissolution, dissolution residue, clays, or iron staining, is not readily apparent along any of the fractures, even though fracture D contains brine. The crushed interval at 3017 feet contains anhydrite fragments with powdery, apparently weathered or dissolved anhydrite on the surface, which may indicate some dissolution along this fracture.

As apparent from drilling records, gas was encountered at 3006 feet, presumably contained in fracture C. Fluid was reported at 3017 feet, from fracture D. Both fractures were examined for evidence of brine/rock interaction. No evidence of fracture coatings was apparent from megascopic examination of the core. Petrographic examination revealed some growth of anhydrite crystals radiating outward from the fracture plane at 3017 feet. However, minor dissolution by the drilling fluid (as evidenced during electron microscope examination by pitting and the presence of barium) along the fracture may have destroyed other subtle evidence of brine/rock interaction. Fractures E, F, and G may have also contained brine because of their proximity to the main fracture D, but again no direct evidence of fluid was indicated.

Fracture Orientation - Four core runs were drilled using an oriented core barrel: 3000.7 to 3016.1 feet; 3016.1 to 3047.3 feet; 3047.3 to 3107.2 feet; and 3349.2 to 3410.2 feet. The orientation of the fractures, as well as bedding and textural features, were measured using the core orientation information. Fracture orientation was also obtained from interpretation of the televiewer log run by the U.S. Geological Survey. Figure G-10 shows the fracture data from both sources, projected onto a Schmidt net or hemispherical projection. When the fracture orientations derived from both methods are compared, they are not in complete agreement. The core orienting mechanism

may not have functioned properly, producing inaccurate data, or conversely, the televiewer magnetic north may have malfunctioned, causing drift and resultant inaccurate data. The source of the discrepancy between the two methods cannot be determined.

The orientation of the fractures based on the televiewer log ranges from about N 10° E at 85 degrees dip to the west, to N 50° W at 70 degrees dip to the west. The orientation of the fractures based on the oriented core ranges from about N 15° W at 80 degrees dip to the east, to S 60° E at 80 degrees dip to the southwest.

Other Rock Discontinuities - In addition to the conspicuous near-vertical fractures discussed above, discontinuities or joints are present in Anhydrite III along bedding laminae. Hairline joints are present in Anhydrite II, but are not as numerous as in Anhydrite III. They are rare in Anhydrite I. In Anhydrite III, these "hairline" discontinuities are typically closed and tight, with no detectable secondary filling. Apertures are hard to detect macroscopically because of their small size; when stressed, the core invariably breaks along these joints. They are present below 2994 feet, typically spaced about one inch or less, although the frequency of occurrence varies. For instance, joints are absent between 3012 and 3018 feet. They are not present below 3028 feet. No evidence of seepage or dissolution was observed along these joints during core logging. Other near-vertical hairline discontinuities or microfractures were observed in thin sections from Anhydrite III.

4.1.5 Porosity and Formation Compressibility - WIPP-12

Porosity - Estimates of porosity of the host rocks can be made from laboratory porosity tests, information obtained from geophysical well logging, and visual logging of the rock core. The discussion herein is centered on the porosity of the anhydrite which forms the brine reservoir in WIPP-12, because this information is important to the hydrologic evaluations in subsequent sections of this report. Estimates of porosity are used to approximate formation compressibility and reservoir volumes.

Porosity of the rock is made up of two components: (1) porosity of the intact, unfractured rock (primary porosity); and (2) porosity resulting from the presence of fractures (secondary porosity). Porosity can also be expressed as "total" porosity or "effective" porosity. Effective porosity includes only those voids which are interconnected and through which fluid is able to move, and is the porosity which is important from a hydrologic standpoint. Total porosity includes all voids, including voids which are not interconnected. The primary effective porosity of nearly all the host rock (halite and anhydrite) is expected to be relatively low. Halite and anhydrite typically have primary effective porosities on the order of one percent or less. Secondary effective porosity is practically nil if the rock is unfractured or only slightly fractured, or it can be much more than a few percent if the rock is highly fractured.

Laboratory measurements of effective porosity have been made on anhydrite core from WIPP-12 and ERDA-6, as presented in Table G.2. (The tests were performed according to API standards; they measured effective porosity by saturating dried core with toluene.) The two cores from Anhydrite III in WIPP-12 indicate effective porosities of 0.2 and 0.8 percent. These values of porosity are so low that the uncertainty associated with the measurement technique is nearly as large as the measurement itself. Table G-2 also presents measurements of permeability on the anhydrite core. The values given for the two WIPP-12 cores are both less than 2×10^{-4} md, below the sensitivity of the measurement equipment. These low values of porosity and permeability suggest that whatever effective porosity exists in the core is capable of transmitting fluid only at extremely low rates, and that the effective porosity from a practical hydrologic standpoint is extremely small.

Quantitative information about porosity is also available from several of the geophysical logs run in WIPP-12. Geophysical logs measure total, rather than effective, porosity; however, the difference between total and effective porosity is very small for anhydrite. The neutron porosity log, gamma density

log, and acoustic log can each be used to estimate porosity of the Anhydrite III member at WIPP-12 (Dresser Atlas, 1974, 1981a, 1981b). Collectively, the logs indicate that the porosity ranges from essentially zero to possibly as high as five percent in some fractured zones. The methods used to calculate porosity from these logs all suffer from the same limitation; i.e., when the porosity is very low, minor (and unknown) changes in lithology and density can significantly affect the calculated value of porosity. Thus, while the logs indicate that the porosity is generally low, exactly how low cannot be firmly determined from them.

An estimate of fracture porosity (secondary porosity) can be made from estimates of fracture apertures in the anhydrite core. Using the data from Table G.1, fracture porosity is calculated from the following:

$$\phi_f = \frac{\Sigma a}{\ell \cos \alpha} \quad \text{[Eq. 1]}$$

where ϕ_f = fracture porosity

Σa = summation of reservoir fracture apertures

ℓ = apparent length of reservoir observed in well.

α = average dip of fractures

This calculation yields maximum porosity values of 0.3 percent and 0.6 percent for fracture dip angles of 80 degrees and 85 degrees, respectively. They are considered maximum values since the values of aperture given in Table G.1 are upper bound estimates. This calculation has considerable uncertainty due to the difficulty associated with estimating aperture from core and the possibility that the observed fractures may not be representative of the local large-fracture group. However, it does indicate that fracture porosity is probably very low.

Consideration of theoretical relationships between fracture porosity and permeability indicates that high permeabilities are possible in rock masses with extremely low fracture porosities. Snow (1968) developed a relationship

between permeability, fracture porosity, and fracture spacing and applied it to numerous pressure test data in fractured rock. He found that for all cases analyzed, the theoretical fracture porosity was less than 0.1 percent.

Potential fracture porosity presented in Section 4.3.2 shows average values from 0.4 to 0.7 percent, with local potential maximum porosity up to 2.2 percent.

From the above discussion, it is apparent that the effective porosity of the anhydrite reservoir at WIPP-12 is very low, but that there is considerable uncertainty associated with all quantitative estimates of porosity. The primary effective porosity is believed to be practically zero. The secondary (fracture) effective porosity is estimated to be very low, probably in the range from 0.1 to 1.0 percent. This range of porosity will be used for the compressibility estimates which follow below, and the hydrologic analyses of Part III.

Formation Compressibility

Formation compressibility (pore volume compressibility, c_p) is a property of the host rock which is important for characterization of the host rock as a brine reservoir. It is defined by Earlougher (1977) as:

$$c_p = \frac{1}{V} \left.\frac{\partial V}{\partial p}\right|_T \text{, or}$$

$$c_p = \frac{1}{V} \frac{\Delta V}{\Delta p} \quad \text{[Eq. 2]}$$

where V is the reservoir interconnected pore volume, ΔV is the change in that volume, and Δp is the associated change in reservoir pressure (under isothermal conditions). Thus, it represents the pore volume change of a reservoir per unit change in reservoir fluid pressure per unit reservoir pore volume.

Pore volume compressibility can also be expressed in terms of the bulk modulus (K) of the rock mass which forms the reservoir and the effective porosity (ϕ) of the reservoir. The bulk compressibility (c_B) of the reservoir is defined by Jaeger and Cook (1976) as the inverse of the bulk modulus, or:

$$c_B = \frac{1}{K} \qquad \text{[Eq. 3]}$$

The pore volume compressibility is then the bulk compressibility divided by the porosity:

$$c_p = \frac{c_B}{\phi} \qquad \text{[Eq. 4]} \qquad \text{(Van Golf-Racht, 1982)}$$

which may be written as:

$$c_p = \frac{1}{\phi K}, \quad 0 < \phi < 1 \qquad \text{[Eq. 5]}$$

As discussed above, the effective porosity of the anhydrite reservoir in WIPP-12 is estimated to range from 0.1 to 1.0 percent. The bulk modulus of the rock can be estimated from the acoustic log run in WIPP-12 and from laboratory testing of anhydrite core from other locations on the WIPP site.

The acoustic log, which measures compressional wave travel time through the rock, uses a correlation between the wave velocity and elastic rock properties to estimate the bulk modulus of the rock (Dresser Atlas, 1981b). The computed values of bulk modulus range from 8 to 11 x 10^6 psi over the Anhydrite III member of WIPP-12, with an average of approximately 10 x 10^6 psi. Laboratory compression tests on anhydrite from other WIPP locations indicate similar results (Teufel, 1981; Pfiefle and Senseny, 1981). This value is representative of the bulk modulus of relatively intact, unfractured rock, because the laboratory tests are performed on unbroken rock and the acoustic logging tool measures velocities over a relatively short distance with few if any fractures included.

The bulk modulus of the rock mass will be significantly reduced by the presence of fractures, because fractures are considerably more compressible. Relationships between rock mass modulus and intact rock modulus, fracture stiffness, and fracture spacing developed by Kulhawy (1978) were used to estimate that the intact rock modulus is reduced by a factor ranging from 0.1 to 0.5 by the presence of large fractures. Using these reduction factors, the bulk modulus of the rock mass ranges from 1.0 to 5.0 x 10^6 psi.

The pore volume compressibility can be calculated from Equation 5 using the estimates of K and ϕ given above. Since ranges are given for both K and ϕ, there is also a considerable range of compressibility resulting from these values: a maximum of 1000 x 10^{-6} psi^{-1} and a minimum of 20 x 10^{-6} psi^{-1}. This range is used and discussed further in the hydrologic analyses of Part III, Hydrology.

4.1.6 Lithology and Texture - ERDA-6

The geologic portion of the investigation at ERDA-6 was limited, because a geologic report had already been prepared based on the original drilling (Jones, 1981a). The present program consisted of geologic logging of a single core run, and logging of rock chips from the base of the core run to total depth. The logs have been presented previously (D'Appolonia, 1982, Volume IIIA); the following is a summary of the lithology presented in that document.

Coring commenced in the cement borehole plug at 2562 feet, to recover and examine the cement plug to evaluate its sealing effectiveness. Thus the upper nine feet of the core run consists of grayish-black (N2) to brownish-black (5YR 2/1) cement. The cement is fairly brittle and tends to break easily. Whipstocking away from the plug began at 2571 feet, evidenced by the appearance of the contact zone between cement and wall rock. The contact zone ranges in color from white (N9) to very pale orange (10YR 8/2), and is microcrystalline, very soft, almost chalky in texture. The contact zone is apparently calcareous due to reaction with the cement, and exhibits vigorous reaction to hydrochloric acid.

The Anhydrite II adjacent to the contact zone is white (N9) ranging to medium gray (N5) in color. Its texture is very fine granular with vitreous luster. Bedding laminae are apparent as in WIPP-12, and exhibit similar variations in appearance, ranging from very distinct, parallel and undeformed, to micro-folded and undulating. The laminae are typically inclined 60 to 70 degrees from the horizontal, and are occasionally vertical. Contrasting random patches of anhydrite are white, almost translucent, without bedding laminae. Between 2595 and 2596 feet, halite-filled vugs were observed in the anhydrite. The core-break surfaces often exhibit recrystallized anhydrite crystals, halite crystals, and gypsum crystals.

Drilling continued in the whipstocked hole with a rotary bit. The cuttings description, though imprecise, indicates the general location of the contact with Halite I (2732 feet), confirmed by geophysical logging. The anhydrite recovered in the cuttings appears similar to that observed in the core.

4.1.7 Fractures - ERDA-6

Based on the previous investigation at ERDA-6 (Jones, 1981a), the brine issues from fractures, similar to the situation at WIPP-12. According to Jones, narrow, open fractures lined with anhydrite crystals are present at 2702 feet. The zone between 2709 and 2718 feet is considered to be the main fracture location, with vuggy, porous, recrystallized anhydrite breccia cut by fractures dipping between 45 and 60 degrees (no core was recovered between 2711 and 2718 feet).

For the present study, only a small portion of the original core through the reservoir zone was available for study to determine, if possible, any further information on fracture characteristics. Between 2710.8 and 2711.25 feet, white (N9) to very light gray (N8) anhydrite was observed, with 0.04-inch thick brown bedding laminae oriented almost vertically. An irregular fracture plane cuts the sample at an angle between 75 and 85 degrees. Adjacent to the fracture planes is porous, vuggy, recrystallized anhydrite containing halite

in many of the vugs. Some halite crystals aligned parallel to the fracture are cubic, clear, transparent, up to one inch in length. A small sample of this core segment was obtained for petrologic analysis.

The fracture described above is considerably different from the fractures described at WIPP-12. The ERDA-6 fractures appear to be related to sites of extensive recrystallization, even brecciation, of the host anhydrite. The WIPP-12 fracture known to have produced brine is a relatively clean, smooth fracture with no secondary filling. These differences are apparently related to the degree of structural deformation at each site, ERDA-6 being located on an apparently larger, more intensely deformed feature, four miles closer to the buried Capitan reef margin than WIPP-12.

4.1.8 Porosity and Formation Compressibility - ERDA-6

Porosity

Estimates of porosity of the anhydrite reservoir at ERDA-6 can be made based on information similar to that used at WIPP-12 (see Section 4.1.5). Laboratory measurement of the effective porosity of rock core from ERDA-6 (see Table G.2) indicates a porosity value of 1.6 percent. Values from WIPP-12 core are lower, less than one percent. Neutron porosity and gamma density geophysical logs from ERDA-6 indicate that the porosity ranges from essentially zero to possibly as high as thirty percent in the zone with the main fracture (2711 feet deep). (Note that the highest value of porosity from the geophysical logs is measured with respect to a relatively small volume which represents primarily the fracture zone.)

The fractures at ERDA-6 appear to be different than those at WIPP-12 in that there appears to be a concentration of fractures (or some type of voids) over a ten-foot interval (2709 to 2719 feet), whereas the fractures at WIPP-12 are more or less interspersed throughout the reservoir. Not all core was recovered from the fracture zone interval at ERDA-6, however, and therefore the nature of this zone is not well known. Potential fracture porosity presented in Section 4.3.2 shows average values from 0.7 to 1.1 percent with local potential maximum porosity of 1.6 percent.

As with WIPP-12, the effective porosity of the anhydrite reservoir at ERDA-6 is very difficult to estimate. The porosity at ERDA-6 appears to be somewhat higher than at WIPP-12, although it is still quite low. For the purposes of compressibility estimates which follow and the hydrologic analyses of Part III, the effective porosity at ERDA-6 is estimated to range from 0.2 to 2.0 percent, approximately twice the values for WIPP-12.

Formation Compressibility

Formation (pore volume) compressibility can be estimated for ERDA-6 in the same manner as for WIPP-12 (see Section 4.1.5). The bulk modulus of the anhydrite reservoir at ERDA-6 is estimated to be approximately the same as at WIPP-12, or 1 to 5 x 10^6 psi. With an effective porosity ranging from 0.2 to 2.0 percent, the range in pore volume compressibility is 10 x 10^{-6} psi^{-1} to 500 x 10^{-6} psi^{-1}. This range is used and discussed further in the hydrologic analyses of Part III.

4.2 GEOLOGIC LOCATIONS OF BRINE OCCURRENCES

To understand the brine occurrences at WIPP-12 and ERDA-6 more fully, information on other brine occurrences in the northeastern part of the basin was assembled and analyzed in conjunction with WIPP-12 and ERDA-6 information. Figure G-11 shows the majority of boreholes in the vicinity of the WIPP site which have penetrated the Castile Formation. As shown, thirteen boreholes have intercepted pressurized brine. Table H.1 in Part III, Hydrology, lists available pressure and flow data for these thirteen occurrences. Based on available data, the number of reservoirs intercepted in these thirteen boreholes is unknown. Although many of the available data are vague and incomplete, two conclusions can be drawn regarding brine occurrences in the area covered by Figure G-11:

- In nearly all cases, brine issues from the uppermost anhydrite unit of the Castile encountered in each borehole.

- Pressurized brine occurrences appear to be associated with deformation in the Castile.

The following is a summary of information on locations of pressurized brine occurrences based on a review of geophysical logs, surface seismic data, and unpublished data (Snyder, 1982, personal communication,).

4.2.1 Spatial Distribution of Brine Occurrences

Pressurized brines encountered in the Castile Formation in the northeastern Delaware Basin are located in a band or belt that is adjacent to and parallels the buried Capitan reef margin. This band or belt extends underneath the WIPP site. Castile brine occurrences have been documented in other parts of the Delaware Basin; these however exhibit negligible flows, sub-artesian heads, and were not considered as pressurized brine reservoirs in this study. No sub-artesian brines have been reported in the area covered by Figure G-11. The brine closest to the Capitan reef was intercepted in the Bilbrey 5 Federal well #1 (roughly 1.75 miles southwest of the buried reef front). The brine farthest from the reef was discovered in the Belco-Hudson Federal #1 well, southwest of the WIPP site, and about 12.5 miles southwest of the reef. All reported brine occurrences are shown in Figure G-11, superimposed on the structure contours of the Halite II member of the Castile Formation.

4.2.2 Stratigraphic and Structural Control

Stratigraphic Control

Interpretation of geophysical logs provided by the U.S. Geological Survey (Snyder, 1982, personal communication) indicates that the brines are located in the uppermost Castile anhydrite unit intercepted in each borehole. This is not necessarily the Anhydrite III unit, but simply the uppermost anhydrite as determined by the structure at each location. In some cases, as in the Bilbrey 5 Federal and Tidewater Richardson-Bass wells, data are lacking and no estimate can be made.

Brine in WIPP-12 and ERDA-6, as well as in most of the brine occurrences, is produced from fractures near the base of the uppermost anhydrite member

intercepted by the borehole. Exceptions are the Pogo Federal #1 well, which produced from the middle of the uppermost anhydrite (in an area where Anhydrites III and II coalesce), and the Union Federal #1 well, which intercepted brine in the upper part of Anhydrite III.

Structural Control

Figure G-11 is a structure contour map drawn on the top of Halite II of the Castile Formation, based on borehole data. The figure indicates where the Castile is deformed into a series of anticlinal and synclinal structures. The structures are superimposed on the regional one to two degree east to southeast dip of the Castile. The structures appear to be most intense in a four to six mile wide belt adjacent to the reef; deformation becomes less pronounced over a short distance toward the center of the basin. The largest structure in the vicinity of the WIPP site, penetrated by ERDA-6, has a closure of between 500 and 600 feet based on borehole data. The structure eight miles to the east of the WIPP site has a closure of about 300 feet also based on the borehole data of Figure G-11. Figure G-11 shows WIPP-12 and borehole WIPP-11 located on a single large antiform. Due to the sparsity of boreholes in the vicinity of WIPP-11 and WIPP-12 however, the structural interpretation presented on Figure G-11 cannot be considered definitive. Figure G-12 is a map showing seismic isochrons in the middle portion of the Castile Formation. Conversion of the seismic isochrons to structural contours would require control data (i.e., seismic velocities of rocks down to and including the middle Castile Formation) which are lacking. Nevertheless, the seismic isochrons appear to indicate that the structure at WIPP-12 is separate and distinct from the structure at WIPP-11.

4.3 PROCESS OF RESERVOIR FORMATION

The preceding section suggests that a relationship may exist between brine occurrences and the structures interpreted in Figures G-11 and G-12, although borehole control data which could aid in delineating the structures are lacking. An investigation into the mechanisms(s) which formed the structures could provide information on the formation of the brine reservoirs, as well as

on the origin of the brines. In this context, information pertaining to the origin of the structural deformation was assembled, primarily Borns et al. (1983), for the following discussion.

4.3.1 Mechanism for Development of Structures

Examination of the structures in Figure G-6 reveals that deformation is mainly confined to the Castile Formation, although the overlying Salado Formation reflects the warping slightly. The underlying Delaware Mountain Group does not appear to be widely involved in the structures under discussion (Powers et al., 1978; Anderson and Powers, 1978). Further, the fact that the structures are not uniformly distributed throughout the basin, and that the Delaware Basin has been essentially unaffected by regional tectonic activity (Section 3.4) suggests that the structures were not formed by a regional tectonic event.

Closer examination indicates that variations in halite thickness occur in association with the structures. Halite II is thickened at the WIPP-11 location. At WIPP-12, Halite I is about 500 feet thick, 200 feet thicker than would be expected in undeformed areas of the WIPP vicinity. At ERDA-6, although Halite I has not been fully penetrated, it is assumed to be considerably thickened (Figure G-6). The Union Well, located about 4000 feet to the northwest of ERDA-6, apparently encountered only eleven feet of Halite I. From correlation of stratigraphic evidence from deep wells (Figure G-6), it appears that the structures are located over thickened sequences of halite, both Halite I and Halite II.

Local thickening of halite and/or disruption of bedded salt sequences is a commonly observed phenomenon well-documented in published literature (Borchert and Muir, 1964; Baar, 1977; Muehlberger, 1968). That halite creeps or flows under the action of differential stresses is well established (Wawersik and Hannum, 1979). The rate of movement depends on deviatoric stress, temperature, moisture content, and depth of burial. In particular, halite tends to move upward due to density contrast with overlying strata, the mechanism which

is believed to be responsible for the formation of salt domes. Halite is much more ductile than anhydrite. When these two rock types are intercalated and subjected to the same deformation, anhydrite will tend to behave in a brittle manner whereas halite will behave in a ductile manner.

Thus, in the absence of any major regional tectonic event, and given the observed thickening of halite units, local salt tectonics seems a reasonable explanation for the structures. However, more difficult to determine is the factor(s) which initiated the salt tectonics, the distribution of the structures, the timing of formation, and, most importantly, how the brine reservoirs are related to the structures. Several hypotheses which address the factor(s) which are responsible for salt tectonics are listed below, taken from Borns et al. (1983):

- Gravity foundering, or instability due to density contrast.
- Dissolution mechanisms.
- Gravity sliding.
- Gypsum dehydration.

Another theory which is related to the proposed gravity foundering hypothesis is differential lithostatic load. A brief discussion of each of these hypotheses with supporting or contradicting evidence follows.

Gravity Foundering - Gravity foundering is envisioned by Borns et al. (1983) as a possible explanation for localized structural development. Gravity foundering results from the inherent instability of layered materials of different densities. The tendency is for lighter halite to rise above denser anhydrite. To explain the presence of deformation in some areas (the reef front in the vicinity of WIPP) and the general lack of structure in the central portion of the basin, abnormal concentrations of fluids may have facilitated salt flow. In other words, irregularly dispersed pockets of interstitial fluid may have controlled the halite deformation, the brine

occurrences providing the evidence of this mechanism. Development of a fault(s) due to external tectonic forces could have initiated gravity foundering.

Another factor which could have initiated salt movement is differential lithostatic pressure, which would result if surface erosion produced lows or valleys (Jarolimek, 1982, personal communication). Lithostatic pressure on buried halite would be less under the valley, resulting in a tendency for halite to thicken under the valley. This mechanism however cannot explain the localization of structures in the absence of a knowledge of paleogeography.

Dissolution Mechanisms - Dissolution has been suggested as a mechanism which: (1) dissolved evaporites near the top of the section, causing collapse and reduced local density, which permitted local deformation to start via gravity adjustment (diapirism); or (2) dissolution in the Castile itself removed halite and caused deformation in surrounding and overlying beds. There is no definite indication of near-surface dissolution of the required scale overlying the deformed area. In WIPP-12, there is no evidence in the Castile Formation core of any dissolution or dissolution residues. Also, geochemical evidence for the origin of Castile brines does not support the idea that the fluid is introduced meteoric water which has dissolved quantities of halite.

Gravity Sliding - This mechanism involves movement of the halite due to basinal tilting; the halite flowed down a slight gradient buttressed by the Capitan reef. However, whether the slope created by basinal tilting was sufficient to initiate salt movement is indeterminable because the exact movement mechanism is unknown.

Gypsum Dehydration - Heard and Rubey (1966) have suggested that the conversion of gypsum to anhydrite with associated release of water under applied heat and pressure leads to significant strength reduction and facilitates tectonic movement. The anhydrite-plus-water system is ten percent greater in volume

than the gypsum system (Braitsch, 1971); if the fluid cannot escape because of an impermeable rock sequence, high pore pressures result which reduce rock strength. Possible anhydrite pseudomorphs after gypsum were observed locally in thin sections of WIPP-12 core, and the geochemistry of the brines does not rule out dehydration of gypsum as a minor source of fluids. However, several inconsistencies must be explained, such as the localization and irregular distribution of deformation features, which could only be explained by irregular distribution of pockets of gypsum.

Thus, based on review of a report on deformation of evaporites near the WIPP site (Borns et al., 1983) and other published sources, possible hypotheses for salt tectonics are gravity foundering, differential lithostatic load, dissolution mechanisms, gravity sliding, and gypsum dehydration. Selection of a favored hypothesis is beyond the scope of this report, although gravity foundering and gravity sliding appear to be the most plausible theories.

4.3.2 Timing of Structural Development

The timing of halite deformation is subject to discussion and cannot be definitively determined. Several investigators have made estimates of the age of deformation based on various assumptions and available evidence. These estimates are discussed below.

Jones (1981a) believes that the structure penetrated by ERDA-6 offers evidence of the age of deformation. He has observed that pre-Triassic strata are uplifted and arched as a result of salt thickening, but that the overlying Ogallala Formation of Pliocene age is undeformed. This would appear to indicate that the movement is pre-Pliocene in age. However, non-involvement of overlying strata may not be a reliable indicator of movement in an evaporite sequence, since strain can be accommodated by the halite units and not transmitted to overlying beds.

From examination of ERDA-6 core, Anderson and Powers (1978) believe the structural deformation due to salt thickening probably post-dated the

formation of small microfolds in Castile anhydrite laminae. Since the orientation of anhydrite microfolding is believed to be consistent with structural trends developed during the Tertiary in the Delaware Basin (Kirkland and Anderson, 1970), Anderson (1978) has inferred that the salt thickening and subsequent deformation is mid-to-late Tertiary. Anderson (1978) assumes that the salt structures developed in response to the latest stage of basinal tilting in late Pliocene to early Pleistocene time.

Thus the age of the deformation cannot be determined within narrow limits. The discussion presented above can be summarized by concluding that the deformation is probably Cenozoic, and could have occurred between 12 to 1 million years ago, although definitive evidence does not exist. The relationship beween the ages of the structures at WIPP-12 and ERDA-6 is also not known.

4.3.3 Brine Reservoir Formation

The mechanisms which could have initiated or created salt deformational thickening have been discussed above. This section discusses the effects of the salt deformation on the interbedded and overlying anhydrite layers.

The model employed to explain the development and location of fractures presumes that the anhydrite layers acted as brittle beams or plates pushed upward by the upward movement of the underlying salt.

Elongation/extension of the anhydrite layers due to thickening of underlying halite is believed to be the predominant mechanism resulting in fracturing of the brittle anhydrite. A secondary mechanism is the bending of anhydrite associated with the deformation. As shown in Figure G-13, the regional tilting had apparently negligible effect on the integrity of the anhydrite layers in comparison with the later effects due to the deformations producing the present structures.

The strain due to extension of the anhydrite can be quantitatively evaluated, as illustrated in Figure G-13. Elongation of the anhydrite can be calculated from a cross section through the structure as the difference in length of the member before and after deformation, assuming that the ends (A and B in Figure G-13) of the member have remained horizontally fixed. The anhydrite layer can be broken into a series of circular arc and straight line segments. The elongations of the segments resulting from vertical displacements may then be calculated and summed, and the overall elongation, as a percentage of the original length, can be calculated. Typical average elongations for the structures around WIPP-12 and ERDA-6 are 0.4 to 0.7, and 0.7 to 1.1 percent, respectively. Locally, such as in the anticlinal crests, the elongation could reach 2.2 percent around WIPP-12, and 1.6 percent around ERDA-6 structures. Such extensions are likely to exceed the tensile strength of the anhydrite, and thus fracturing from elongation would occur.

Quantitative consideration can also be given to the stress and strains associated with the observed bending of the anhydrite. Stresses due to bending of a beam under elastic conditions can be directly related to the radius of curvature of the beam by the following expression:

$$\sigma_{max} = \frac{E\ (d/2)}{\pm R} \quad [\text{Eq. } 6]^{(1)} \quad \text{(Merritt, 1976)}$$

where σ_{max} is the maximum stress (tensile or compressive) in the beam, E is Young's modulus, d is the beam thickness, and R is the radius of curvature of the centerline of the beam. Thus, for a given beam, the stresses are inversely proportional to the radius of curvature. Equation 6 can be used to calculate tensile stresses due to bending for various radii of curvature as shown by the structures in Figure G-13. Young's modulus for anhydrite is

---

(1) In reality, the anhydrite would fracture due to its low tensile strength long before the full stresses predicted by Eq. 6 were reached, and Eq. 6 would not be fully applicable. It is used here for illustrative purposes only.

approximately 10^7 psi, and the compressive strength at a confining pressure of 2900 psi (20 MPa) is about 28,000 psi (Pfiefle and Senseny, 1981; Teufel, 1981). The tensile strength may be approximated as ten percent of the compressive strength (Jaeger and Cook, 1976), or about 2800 psi. Calculations at points of maximum curvature in cross sections through the WIPP-12 and ERDA-6 structures (as defined in Figure G-11) indicate that the maximum tensile stresses in the WIPP-12 and ERDA-6 anhydrites would have ranged from about 28,000 to 172,000 psi, and from 48,000 to 111,000 psi respectively, if no fracturing had occurred.

These calculations indicate that bending alone would cause high tensile stresses which would exceed the tensile strength of the anhydrite for most areas with significant structure. In other words, very little bending is required to produce bending stresses which exceed the strength of the rock, and therefore bending is a contributing factor in fracture development in the anhydrite due to salt movement. Equation 6 also indicates that the bending stresses are directly proportional to the anhydrite thickness. Since Anhydrite II is thinner than Anhydrite III, this is a possible explanation why the Anhydrite II member appears to be generally less fractured than the Anhydrite III member.

The fracture distribution, spacing, and apertures are governed by extremely complex processes; detailed modeling is beyond the scope of this study. However, a qualitative evaluation of the distribution of the elongation throughout the structure results in the following:

1. The largest elongations are most likely to occur within the crests of the anticlinal structures, where main fractures are open at the base of the anhydrite member and their apertures increase upward.

2. Within the synclinal structures, the fractures are most likely to be closed or with minimum apertures at the top of the anhydrite, and widen toward the base.

3. Within the straight limbs of the structures, the fracture faces should be parallel. The apertures

will depend on the local elongation, and on the strain transfer from the synclinal flexures where the salt deformation is producing mainly tangential forces.

If all of the extension were to be taken up in fractures, then these values of extension may also be representative of fracture porosity of the anhydrite, as follows:

STRUCTURE AROUND:	APPROXIMATE POTENTIAL FRACTURE POROSITIES(%) MIN. AVERAGE	MAX. AVERAGE	MAX. LOCAL(1)
ERDA-6	0.7	1.1	1.6
WIPP-12	0.4	0.7	2.2

These calculations agree in general with the porosity estimates presented in Sections 4.1.5 and 4.1.8.

The model appears to explain the limited amount of geologic data available for the WIPP-12 and ERDA-6 structures. The fact that brine was encountered near the base of anhydrite units in the majority of brine occurrences is not inconsistent with the fracture model. The majority of brine producers may have been drilled into limb areas where fracture aperture, and therefore the brine production, is greater near the base of the unit, because of the greater statistical chance of intersecting a limb of a structure rather than a crestal area.

Several questions remain unresolved however. ERDA-6 and WIPP-12 appear to be located on the crests of structures (see Figures G-11 and G-12, respectively) where fracture apertures should be greatest at the top of the anhydrite units, and yet brine was encountered only near the bottom of the units. (The concentration of brine at the base of the anhydrite at WIPP-12 does not

(1)Such as in anticlinal crests.

indicate fluid flow along the lower contact of Anhydrite III; no evidence of such flow was observed in the core.) The depths of the brine encounters may be due to the two boreholes simply missing existing large fractures except near the base of the units, which is always possible with vertical boreholes and near-vertical fractures. Although possible, the above explanation is hardly conclusive. Additionally, no rationale has been developed explaining the hit-or-miss nature of the brine encounters. If brine occurrences were simply related to structural deformation, a number of the dry holes presented on Figure G-11 would have been expected to have encountered brine. The fact that the holes are dry indicates the localization of brine within particular parts of structures by an unknown mechanism.

4.3.4 Pressurization of Brine Reservoirs

Creation of fractures or open voids by extension or dilatancy (McNaughton, 1953; McNaughton and Garb, 1975) would result in a large pressure differential between the voids and rock matrix pores. Any fluids available in the matrix pores adjacent to the voids would have the tendency to migrate toward and eventually fill the voids. The fluids in the voids would thus be pressurized at some value less than ancient pore pressure. Differences in pressurization between reservoirs may be explained by varying fracture intensity and aperture.

There are other possible explanations for abnormal pressures within isolated reservoirs (Bradley, 1975). The theories appearing plausible for brines within the Castile Formation are:

- Uplifting of the reservoir (relative to its one-time recharge area) or surface erosion, both of which could result in the water pressure in the reservoir being too high for its current depth of burial.
- Increasing temperature, perhaps as the depth of burial increased, caused the brine to expand, thus increasing pressure.

- Mass transfer of water from zones of low salinity to zones of high salinity by osmotic forces. Hydrologic confining beds can serve as semi-permeable membranes.

- Molecular restructuring of original organic material in sediments by chemical, physical, and/or biological actions.

No viable theory is recognized that can explain the present hydraulic heads in the Castile Formation by referencing them to the present ground-water flow system. Therefore, the pore fluid pressures of all Castile brines are probably products of ancient pore pressures modified by rock dilatancy and perhaps by internal processes.

4.4 GEOLOGIC EVIDENCE OF BRINE ORIGIN

The preceding section dealt with the formation of the structures in the WIPP vicinity, and how the deformation led to the development of brine reservoirs. This section will discuss available geologic evidence, primarily negative in nature, which supports the conclusions reached in Part IV, Chemistry, Section 5.1, regarding brine origin.

Known pressurized-brine reservoirs are associated with salt-cored deformation structures within the Castile Formation. In the case of WIPP-12 and ERDA-6, the fluids are contained in high-angle fractures probably formed by extension of anhydrite during salt flow. Fluids may have been present within the rock matrix, and due to differential pressure accumulated in the fractures as they developed. Two types of fluids could be present in the rock matrix: (1) original connate water trapped interstitially or within grains of the evaporites at the time of deposition; or (2) water formed by the dehydration of gypsum to anhydrite. Carpenter (1978) cites previous work that indicates that evaporite mineral accumulations usually have initial porosities in excess of fifty percent. Although nearly all of this water is evaporated and squeezed out during subsequent compaction and diagenesis, the potential exists for small quantities of this water to be trapped interstitially or within grains.

Dehydration of gypsum to anhydrite as a general phenomenon is a concept supported by numerous investigators. A small amount of primary gypsum converted to anhydrite during diagenesis would provide a large volume of fluid, because about fifty percent of the original system volume of gypsum converts to water (Heard and Rubey, 1966). Evidence of conversion of gypsum to anhydrite is not readily apparent from macroscopic inspection of WIPP-12 or ERDA-6 core. Microfolds in anhydrite laminae are more readily explained by compressive forces than by conversion of gypsum to anhydrite (Kirkland and Anderson, 1970). Petrographic examination of the anhydrite in WIPP-12 reveals the presence of possible pseudomorphs of anhydrite after gypsum as discussed in Section 4.1.3. This evidence for primary gypsum is not compelling, although dehydration waters cannot be ruled out as a minor source of brine reservoir fluid. Ground water or meteoric water does not appear to be a plausible fluid source at WIPP-12, based on the lack of evidence of dissolution features and the tight contacts observed.

LIST OF REFERENCES

Adams, J. E., 1944, Upper Permian Ochoa Series of Delaware Basin, West Texas and Southeastern New Mexico: Amer. Assoc. of Pet. Geol. Bull., v. 28, no. 11, pp. 1596 - 1625.

Adams, J. E., 1965, Stratigraphic-Tectonic Development of the Delaware Basin: Amer. Assoc. of Pet. Geol. Bull., v. 49, no. 11, pp. 2140-2148.

Anderson, R. Y., 1979, Notes on Dissolution and Brine Chambers Related to the WIPP: Memo submitted to the State of New Mexico, Environmental Evaluation Group, 15 pp.

Anderson, R. Y. and D. W. Kirkland, 1966, Intrabasin Varve Correlation: Geol. Soc. of America Bull., v. 77, pp. 241-255.

Anderson, R. Y. and D. W. Powers, 1978, Salt Anticlines in Castile-Salado Evaporite Sequence, Northern Delaware Basin, New Mexico: New Mexico Bureau of Mines and Mineral Resources, Circular 159, pp. 79-83.

Baar, C. A., 1977, Applied Salt-Rock Mechanics 1: Elsevier Scientific Publishing Co., Amsterdam, 294 pp.

Bachman, G. O., 1980, Regional Geology and Cenozoic History of Pecos Region, Southeastern New Mexico: U.S. Geol. Survey Open-File Report 80-1099, 116 pp.

Borchert, H. and R. O. Muir, 1964, Salt Deposits - The Origin, Metamorphism, and Deformation of Evaporites: D. Van Nostrand Co. Ltd., Princeton, N. J., 338 pp.

Borns, D. J., L. J. Barrows, D. W. Powers, and R. P. Snyder, 1983, Deformation of Evaporites Near the Waste Isolation Pilot Plant (WIPP) Site: SAND82-1069, Sandia National Laboratories, prepared for U.S. Dept. of Energy, Albuquerque, New Mexico.

Bradley, J. S., 1975, Abnormal Formation Pressure: Amer. Assoc. of Pet. Geol. Bull., v. 59, pp. 957-973.

Braitsch, O., 1971, Salt Deposits - Their Origin and Composition: Springer-Verlag, New York, 297 pp.

Brokaw, A. L., C. L. Jones, M. E. Cooley, and W. H. Hays, 1972, Geology and Hydrology of the Carlsbad Potash Area, Eddy and Lea Counties, New Mexico: U.S. Geol. Survey Open-File Report, USGS 4339-1, prepared for U.S. Atomic Energy Comm., 86 pp.

Carpenter, A. B., 1978, Origin and Chemical Evolution of Brines in Sedimentary Basins: Oklahoma Geol. Survey Circular 79, pp. 60-77.

Cody, R. and A. B. Hull, 1980, Experimental Growth of Primary Anhydrite at Low Temperatures and Water Salinities: Geology, v. 8, pp. 505-509.

LIST OF REFERENCES
(Continued)

D'Appolonia Consulting Engineers, Inc., 1982, Data File Report - ERDA-6 and WIPP-12 Testing: Report prepared for Westinghouse Electric Corp. and U.S. Dept. of Energy, Albuquerque, New Mexico, 7 vols.

Dean, W. E., Jr., 1967, Petrologic and Geochemical Variations in the Permian Castile Varved Anhydrite, Delaware Basin, Texas and New Mexico: University of New Mexico, Ph.D. Dissertation, 326 pp. (University Microfilms Number 68-3463).

Dean, W. E. and R. Y. Anderson, 1982, Continuous Subaqueous Deposition of the Permian Castile Evaporites, Delaware Basin, Texas and New Mexico: Depositional and Diagenetic Spectra of Evaporites - A Core Workshop, Handford: Loucks, and Davies, eds., SEPM Core Workshop No. 3, Calgary, Canada, June, 1982, 395 pp.

Dresser Atlas, 1974, Log Review 1: Dresser Industries, Inc.

Dresser Atlas, 1981a, Neutron Logs: Dresser Industries, Inc.

Dresser Atlas, 1981b, Acoustic Logs: Dresser Industries, Inc.

Earlougher, R. C., Jr., 1977, Advances in Well Test Analysis: Soc. Pet. Engr. of AIME Monograph, v. 5, 264 pp.

Gevantman, L. H. (ed.), 1981, Physical Properties Data for Rock Salt: National Bureau of Standards Monograph 167, U.S. Dept. of Commerce, 282 pp.

GFDR (Geotechnical Field Data Report) No. 7, 1983, Geologic Mapping of Exploratory Drift: compiled for U.S. Dept. of Energy by TSC-D'Appolonia, February 17, 1983.

Heard, H. C. and W. W. Rubey, 1966, Tectonic Implications of Gypsum Dehydration: Geol. Soc. of America Bull., v. 77, pp. 741-760.

Hills, J. M., 1968, Permian Basin Field Area, West Texas and Southeastern New Mexico: Geol. Soc. of America Special Paper 88, pp. 17-27.

Jaeger, J. C. and N. G. W. Cook, 1976, Fundamentals of Rock Mechanics: Halsted Press, New York, 585 pp.

Jarolimek, L., 1982, personal communication: Senior Project Consultant, D'Appolonia Consulting Engineers, Inc., Pittsburgh, Pennsylvania.

Jones, C. L., 1981a, Geologic Data for Borehole ERDA-6, Eddy County, New Mexico: U.S. Geol. Survey Open-File Report 81-468, 59 pp.

Jones, C. L., 1981b, Geologic Data for Borehole ERDA-9, Eddy County, New Mexico: U.S. Geol. Survey Open-File Report 81-469, 50 pp.

LIST OF REFERENCES
(Continued)

King, P. B., 1942, Permian of West Texas and Southeastern New Mexico: Amer. Assoc. of Pet. Geol. Bull., v. 26, no. 4, pp. 535-763.

King. R. H., 1947, Sedimentation in Permian Castile Sea: Amer. Assoc. of Pet. Geol. Bull., v. 31, no. 3, pp. 470-477.

Kinsman, D. J. J., 1966, Gypsum and Anhydrite of Recent Age, Trucial Coast, Persian Gulf: in Proceedings, Symposium on Salt, 2nd, Northern Ohio Geol. Society, v. 1, pp. 302-326.

Kirkland, D. W. and R. Y. Anderson, 1970, Microfolding in the Castile and Todilto Evaporites, Texas and New Mexico: Geol. Soc. of America Bull., v. 81, pp. 3259-3282.

Kulhawy, F. H., 1978, Geomechanical Model for Rock Foundation Settlement: Jour. of the Geotech. Engr. Div., Proc. of the Amer. Soc. of Civil Engr., v. 104, no. GT2, pp. 211-227.

McNaughton, D. A., 1953, Dilatancy in Migration and Accumulation of Oil in Metamorphic Rocks: Amer. Assoc. of Pet. Geol. Bull., v. 37, pp. 217-231.

McNaughton, D. A. and F. A. Garb, 1975, Finding and Evaluating Petroleum Accumulations in Fractured Reservoir Rock: Exploration and Economics of the Petroleum Industry, v. 13, Matthew Bender and Company, Inc., pp. 23-49.

Merritt, F. S. (editor), 1976, Standard Handbook for Civil Engineers: McGraw-Hill Book Co., New York.

Muehlberger, W. R., 1968, Internal Structures and Mode of Uplift of Texas and Louisiana Salt Domes: Geol. Soc. of America Special Paper 88, pp. 359-364.

Ode, H., 1968, Review of Mechanical Properties of Salt Relating to Salt Dome Genesis: Geol. Soc. of America Special Paper 88, pp. 543-595.

Pfiefle, T. W. and P. E. Senseny, 1981, Elastic-Plastic Deformation of Anhydrite and Polyhalite as Determined from Quasi-Static Triaxial Compression Tests: SAND 81-7063, by RE/SPEC, Inc. for Sandia National Laboratories, Albuquerque, New Mexico, 123 pp.

Posnjak, E., 1940, Deposition of Calcium Sulfate from Sea Water: Amer. Jour. of Science, v. 238, no. 8, pp. 559-568.

Powers, D. W., S. J. Lambert, S. E. Shaffer, L. R. Hill, and W. D. Weart (editors), 1978, Geological Characterization Report, Waste Isolation Pilot Plant (WIPP) Site, Southeastern New Mexico: SAND 78-1596, issued by Sandia National Laboratories, for U.S. Dept. of Energy, Albuquerque, New Mexico.

Riley, C. M. and J. V. Byrne, 1961, Genesis of Primary Structures in Anhydrite: Jour. of Sed. Petrology, v. 31, no. 4, pp. 553-559.

LIST OF REFERENCES
(Continued)

Sandia National Laboratories and U.S. Geological Survey, 1982, Basic Data Report for Drillhole WIPP-11 (WIPP): SAND 79-0272, Sandia National Laboratories, Albuquerque, New Mexico.

Schmalz, R. F., 1969, Deep-Water Evaporite Deposition: A Genetic Model: Amer. Assoc. of Pet. Geol. Bull., v. 53, no. 4, pp. 798-823.

Snow, D. T., 1968, Rock Fracture Spacings, Openings, and Porosities: Jour. of the Soil Mech. and Found. Div., Proc. of the Amer. Soc. of Civil Engr., v. 94, no. SM1, pp. 73-91.

Snyder, R. P., 1982, personal communication: Geologist, U.S. Geological Survey, Denver, Colorado.

Stoiber, R. E. and S. A. Morse, 1972, Microscopic Identification of Crystals: Ronald Press Company, New York, 278 pp.

Teufel, L. W., 1981, Mechanical Properties of Anhydrite and Polyhalite in Quasi-Static Triaxial Compression: SAND 81-0858, Sandia National Laboratories, Albuquerque, New Mexico, 35 pp.

Udden, J. A., 1924, Laminated Anhydrite in Texas: Geol. Soc. of America Bull., v. 35, pp. 247-354.

Van Golf-Racht, T. D., 1982, Fundamentals of Fractured Reservoir Engineering: Developments in Petroleum Science 12, Elsevier Scientific Pub. Co., New York, 710 pp.

Wawersik, W. R. and D. W. Hannum, 1979, Interim Summary of Sandia Creep Experiments on Rock Salt From the WIPP Study Area, Southeastern New Mexico: SAND 79-0115, Sandia National Laboratories, Albuquerque, New Mexico, 69 pp.

TABLE G.1

SUMMARY OF FRACTURE CHARACTERISTICS
WIPP-12

CASTILE FORMATION MEMBER	FRACTURE DESIGNATION	FRACTURE DEPTH (FT.)	DIP ANGLE AND DIRECTION (DEG)[1]	STRIKE[1] (AZIMUTH)	APERTURE (ESTIMATED FROM CORE)	FILLING	REMARKS
	A.	2789.3 - 2797.0	Vertical[2]	---	<0.06 in.	None	Not detected on televiewer log.
	B.	2812.2 - 2828.8	Vertical	N-S	0.03 in. (partially open)	Halite (partially filled)	Orientation difficult to obtain from televiewer log.
	C.	3006.4 - 3008.3	78° SW	130°[3]	<0.06 in.	None	Produced gas during drilling.
Anhydrite III	D.	3016.1 - 3017.4	85° NW	10°[3]	<0.2 in.	None	Produced brine during drilling.
	E.	3044.2 - 3045.2	Vertical[2]	- -	<0.06 in.	None	Not detected on televiewer log.
	F.	3046.2 - 3047.0	80°[2]	---	---	None	Not detected on televiewer log.
	G.	3048.6 - 3051.6	72° SW	130°[3]	0 to 0.03 in.	None	Gapped appearance.
Anhydrite Stringer	H.	3057.5 - 3058.8	75°SW	170°[3]	0.1 in. (filled)	Halite	
In Halite II	J.	3060.6 - 3061.5	75°SW[2]	170°[2]	0.1 in. (filled)	Halite	Very indistinct on televiewer log.
Anhydrite II	K.	3335.6 - 3337.0	Vertical[2]	---	<0.03 in.	None	Televiewer log not run through this interval.
Halite I				No fractures observed			
Anhydrite I				No fractures observed			

[1] From televiewer log.

[2] Estimated.

[3] Orientations depicted on Figure G-10.

TABLE G.2

EFFECTIVE POROSITY, GRAIN DENSITY, AND PERMEABILITY LABORATORY TEST RESULTS FROM ANHYDRITE CORE

WELL	SAMPLE DEPTH (ft)	EFFECTIVE POROSITY (%)	GRAIN DENSITY (g/cm^3)	PERMEABILITY (md)
WIPP-12	2815	0.8	2.939	<0.0002
WIPP-12	3007	0.2	2.954	<0.0002
ERDA-6	2600	1.6	2.923	0.003

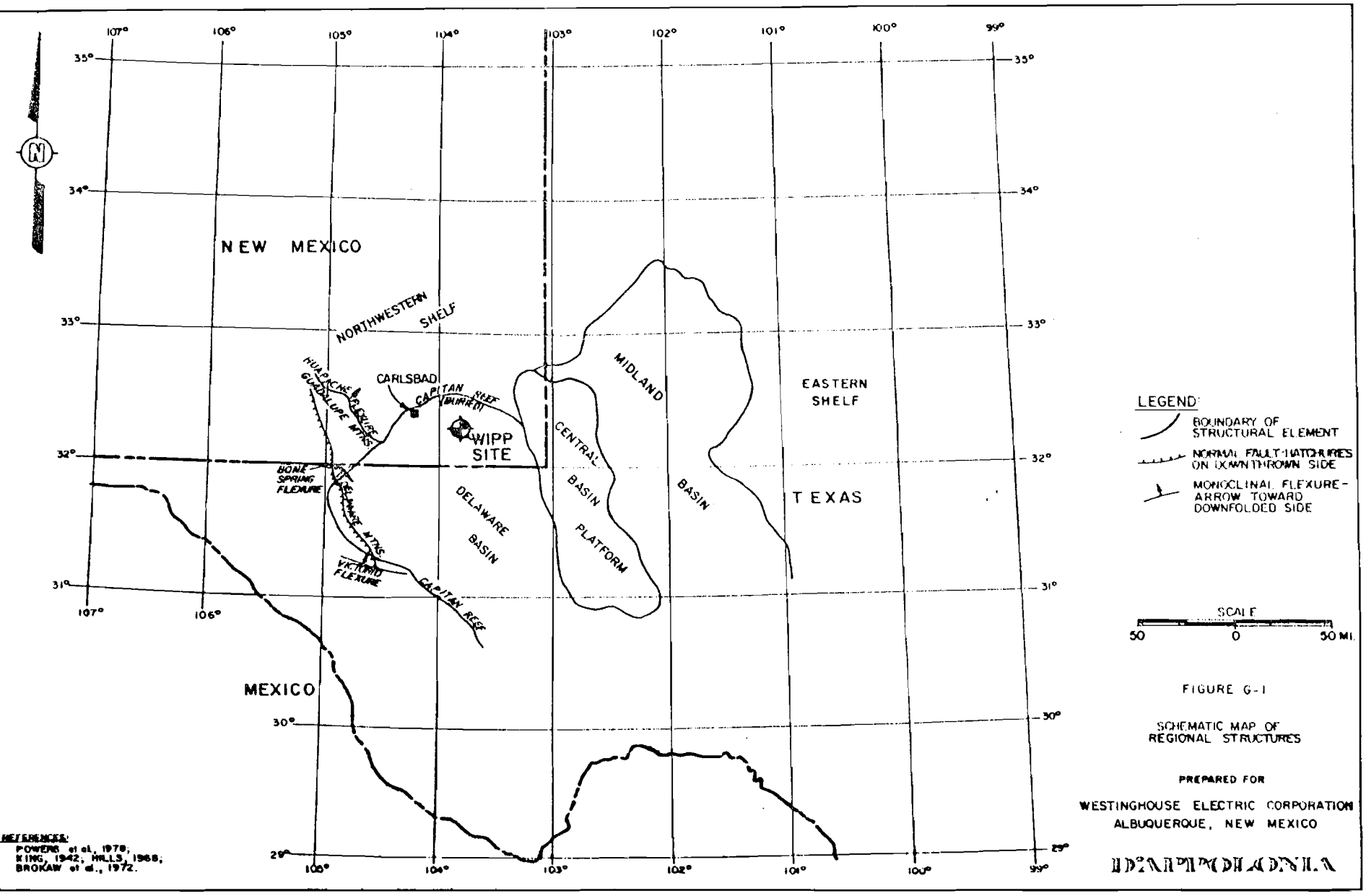

REFERENCES:
POWERS et al., 1978;
KING, 1942; HILLS, 1968;
BROKAW et al., 1972.

FIGURE G-1

SCHEMATIC MAP OF REGIONAL STRUCTURES

PREPARED FOR

WESTINGHOUSE ELECTRIC CORPORATION
ALBUQUERQUE, NEW MEXICO

IDAHO

TME 3153

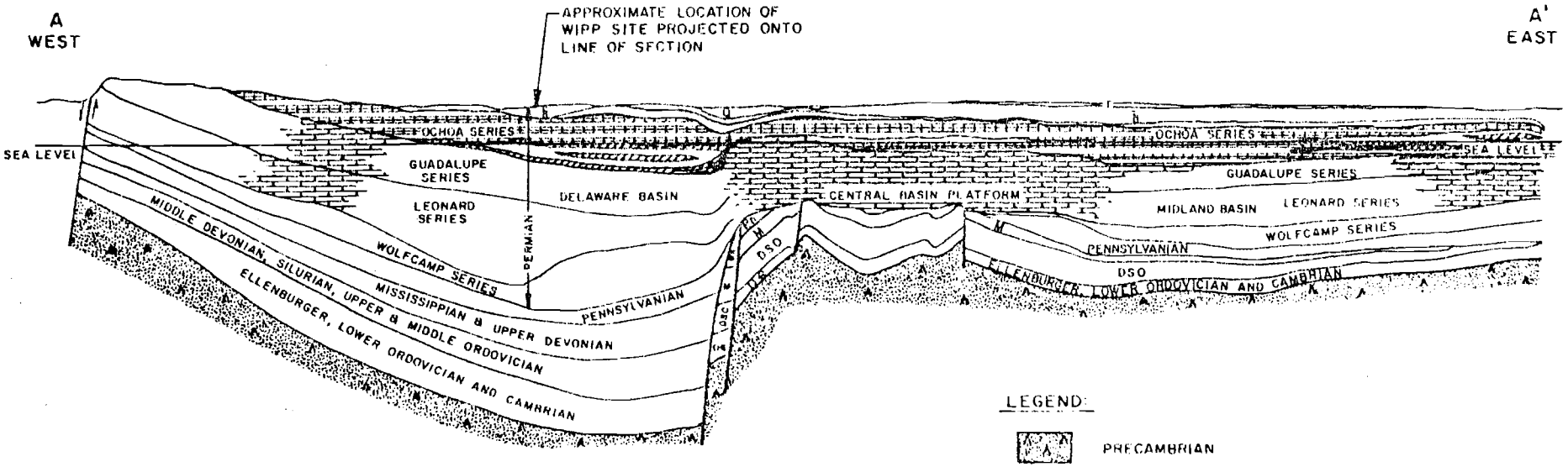

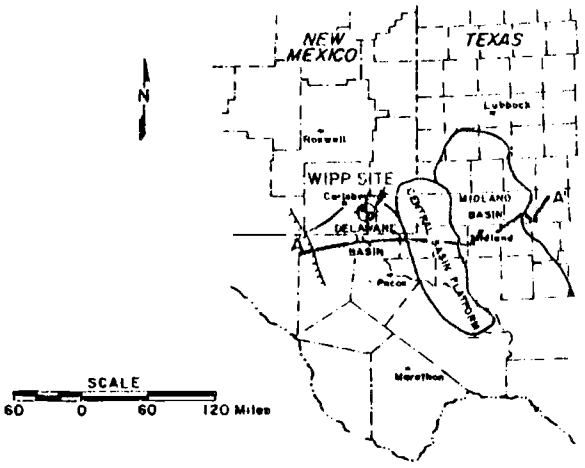

KEY MAP

REFERENCE:
HILLS, J.M., 1968

FIGURE G-2

REGIONAL CROSS SECTION SHOWING
STRATIGRAPHIC RELATIONSHIPS

PREPARED FOR

WESTINGHOUSE ELECTRIC CORPORATION
ALBUQUERQUE, NEW MEXICO

DAMES & MOORE

TME 3153

DRAWING NUMBER	NM78-648-B4
	5/18/82
APPROVED BY	DKS/CPW 5/18/83
DRAWN BY	SKB
	1-7-82

ERA	SYSTEM	SERIES	FORMATION	GRAPHIC LOG	APPROX. DEPTH TO CONTACT AT SITE	PRINCIPAL LITHOLOGY	APPROX. THICKNESS (feet)	APPROX. THICKNESS (meters)
CENOZOIC	RECENT		Surficial sand		(3)	BLANKET SAND AND DUNE SAND; SOME ALLUVIUM INCLUDED	0-100	0-30
CENOZOIC	QUATERNARY	PLEISTOCENE (Kansan?)	Mescalero caliche & Gatuna Fm.		10 40 (12)	PALE REDDISH BROWN, FINE-GRAINED FRIABLE SANDSTONE CAPPED BY 5-10 FT. HARD, WHITE CRYSTALLINE CALICHE (LIMESTONE) CRUST	0-35	0-10
MESOZOIC	TRIASSIC	UPPER TRIAS	Santa Rosa Sandstone		50 (15)	PALE RED TO GRAY, CROSS-BEDDED, NON-MARINE, MEDIUM TO COARSE-GRAINED FRIABLE SANDSTONE, PINCHES OUT ACROSS SITE	0-250	0-80
			Dewey Lake Redbeds		540 (165)	UNIFORM DARK RED BROWN MARINE MUDSTONE AND SILTSTONE WITH INTERBEDDED VERY FINE GRAINED SANDSTONE, THINS WESTWARD	100-550	30-170
			Rustler			GRAY GYPSIFEROUS ANHYDRITE WITH SILTSTONE INTERBEDS IN UPPER PART, REDDISH BROWN SILTSTONE OR VERY FINE SILTY SANDSTONE IN LOWER PART; HALITIC NEAR BASE; CONTAINS 2 DOLOMITE MARKER BEDS, MAGENTA (M) IN UPPER PART AND CULEBRA (C) IN LOWER PART; THICKENS EASTWARD DUE TO INCREASING CONTENT OF UNDISSOLVED ROCK SALT	275-425	80-130
			Salado — Upper member / McNutt member / Lower member		850 (259)	MAINLY HALITE (85-90%) WITH MINOR INTERBEDDED ANHYDRITE, POLYHALITE AND CLAYEY TO SILTY CLASTICS; TRACE OF POTASH MINERALS IN MC NUTT ZONE. THE MINOR INTERBEDS ARE THIN AND OCCUR IN COMPLEXLY ALTERNATING SEQUENCES. THICKEST NON-HALITE BED IS THE COWDEN ANHYDRITE (CA) 17 FT THICK. MULTIPLE ANHYDRITE INTERBEDS ARE MOST COMMON IMMEDIATELY BELOW THE COWDEN AND IMMEDIATELY ABOVE BASE OF SALADO	1750-2000	530-610
						APPROXIMATE LOCATION OF UNDERGROUND WIPP FACILITY		
			Castile — Anh. III / Halite III / Anh. II / Halite II / Anh. I		2825 (661)	(UNCONFORMITY) THICK MASSIVE UNITS OF FINELY INTERLAMINATED ("VARVED") ANHYDRITE-CALCITE ALTERNATING WITH THICK HALITE (ROCK SALT) UNITS CONTAINING THINLY INTERBEDDED ANHYDRITE TOP ANHYDRITE UNIT LACKS CALCITE INTERLAMINATIONS	1250±	380±
PALEOZOIC	PERMIAN	GUADALUPIAN	DELAWARE MOUNTAIN GROUP — Bell Canyon (Delaware sand)		4075± (1243)	MOSTLY LIGHT GRAY FINE-GRAINED SANDSTONE WITH VARYING AMOUNT OF SILTY AND SHALY INTERBEDS AND IMPURITIES. CONTAINS CONSIDERABLE LIMESTONE INTERBEDS AND LIME RICH INTERVALS. TOP UNIT IS LAMAR LIMESTONE MEMBER, A PERSISTENT SHALY LIMESTONE OR LIMY SHALE	1000±	300±
			Cherry Canyon		5100± (1560)	MOSTLY GRAY TO BROWN FINE TO VERY FINE GRAINED SANDSTONE SIMILAR TO BRUSHY CANYON, INTERBEDDED WITH SHALE, DOLOMITE AND SOME LIMESTONE	1100±	350±
			Brushy Canyon		6200± (1890)	PREDOMINANTLY FINE GRAINED, GRAY TO BROWN SANDSTONE INTERBEDDED WITH MINOR BROWN SHALE AND DOLOMITE	1800±	550±
		LEONARDIAN	Bone Springs — First sand / (2nd sand) / Third sand		8000± (2440)	THICK, PARTLY CHERTY BASIN LIMESTONE SEQUENCE IN UPPER PART UNDERLAIN BY ALTERNATING UNITS OF FINE TO VERY FINE GRAINED SANDSTONE AND LIMESTONE. SHALE IS NOT COMMON BUT THE LIMESTONES ARE COMMONLY ARGILLACEOUS	3400±	1050±
					11400± (3480)			

ERA	SYSTEM	SERIES	FORMATION	GRAPHIC LOG	APPROX. DEPTH TO CONTACT AT SITE	PRINCIPAL LITHOLOGY	APPROX. THICKNESS (feet)	APPROX. THICKNESS (meters)
PALEOZOIC	PENNSYLVANIAN	WOLFCAMPIAN	"Wolfcamp"			DARK COLORED BASIN LIMESTONE AND DOLOMITE WITH INTERBEDDED SHALE. SANDSTONE IS SCARCE. SHALE AND CARBONATE CONTENT ROUGHLY EQUAL. MAY CONTAIN A FEW HUNDRED FEET OF LITHOLOGICALLY SIMILAR UPPER PENNSYLVANIAN STRATA (CISCO AND CANYON EQUIVALENTS)	1400±	450±
		? DESMOINESIAN? DERRYAN?	Strawn		12800± (3900)	DOMINANTLY LIMESTONE WITH SOME CHERT AND INTERBEDDED SHALE IN UPPER PART. DOMINANTLY LIGHT GRAY, MEDIUM TO CONGLOMERATIC SAND IN LOWER PART	300±	90±
		MORROWAN?	Atoka		13100± (3990)	PRINCIPALLY LIMESTONE, CHERTY IN MIDDLE PART, ALTERNATING WITH DARK SHALE	650±	200±
			Morrow		13800± (4200)	MOSTLY FINE TO COARSE OR CONGLOMERATIC SANDSTONE WITH DARK GRAY SHALE. SOMEWHAT LIMY SEQUENCE NEAR TOP INTERBEDDED WITH SANDSTONE IS REFERRED TO AS "MORROW LIME"	1250±	400±
	MISSISSIPPIAN	UPPER MISS.	Barnett Shale		15000± (4570)	(UNCONFORMITY) LIGHT YELLOWISH-BROWN, LOCALLY CHERTY LIMESTONE OVERLAIN BY DARK BROWN SHALE (BARNETT)	650±	200±
		LOWER MISS.			(4760)			
	DEVONIAN	UPPER DEV.	Woodford Shale		15600± 15800± (4820)	BLACK, ORGANIC SHALE, PYRITIC (UNCONFORMITY)	175±	50±
	SILURIAN					LIGHT-COLORED, CHERTY DOLOMITE. CONTAINS TWO LIMESTONE INTERVALS IN UPPER HALF OF SECTION	1150±	350±
	ORDOVICIAN		MONTOYA GROUP		16900± (5150)	CHERTY LIMESTONE AND DOLOMITE	1300±	400±
			SIMPSON GROUP			ALTERNATING BEDS OF LIMESTONE AND GRAY OR GREEN SHALE, WITH MINOR SANDSTONE UNITS		
			ELLENBURGER GROUP			CHERTY DOLOMITE, INCLUDES BASAL SANDSTONE MEMBER		
PRECAMBRIAN					18200± (5550)	(UNCONFORMITY) IGNEOUS INTRUSIVE TERRANE (AGE 1.2-1.4 BILLION YEARS)		

EXPLANATION

LITHOLOGIC SYMBOLS

- Sandstone
- Mudstone; siltstone; silty and sandy shale
- Shale
- Limestone
- Dolomite
- Cherty limestone and dolomite
- Shaly limestone
- Anhydrite (or gypsum)
- Interlaminated anhydrite-calcite
- Halite (rock salt)
- Granitic rocks

NOTES:

1. FOR APPROXIMATE DEPTH TO CONTACT AT SITE, THE FOLLOWING NOTATION IS USED:
   (3) - METERS
   10 - FEET
2. THE LOCATION OF THE UNDERGROUND WIPP FACILITY IS BASED ON THE STRATIGRAPHY PRESENTED IN THIS FIGURE.

REFERENCE:

POWERS, et al., 1978

ELEVATION (FEET): 0, 300, 600, 1200, 1800, 2400
ELEVATION (METERS): 0, 200, 400, 600
VERTICAL SCALE

FIGURE G-3

SITE STRATIGRAPHIC COLUMN

PREPARED FOR

WESTINGHOUSE ELECTRIC CORPORATION
ALBUQUERQUE, NEW MEXICO

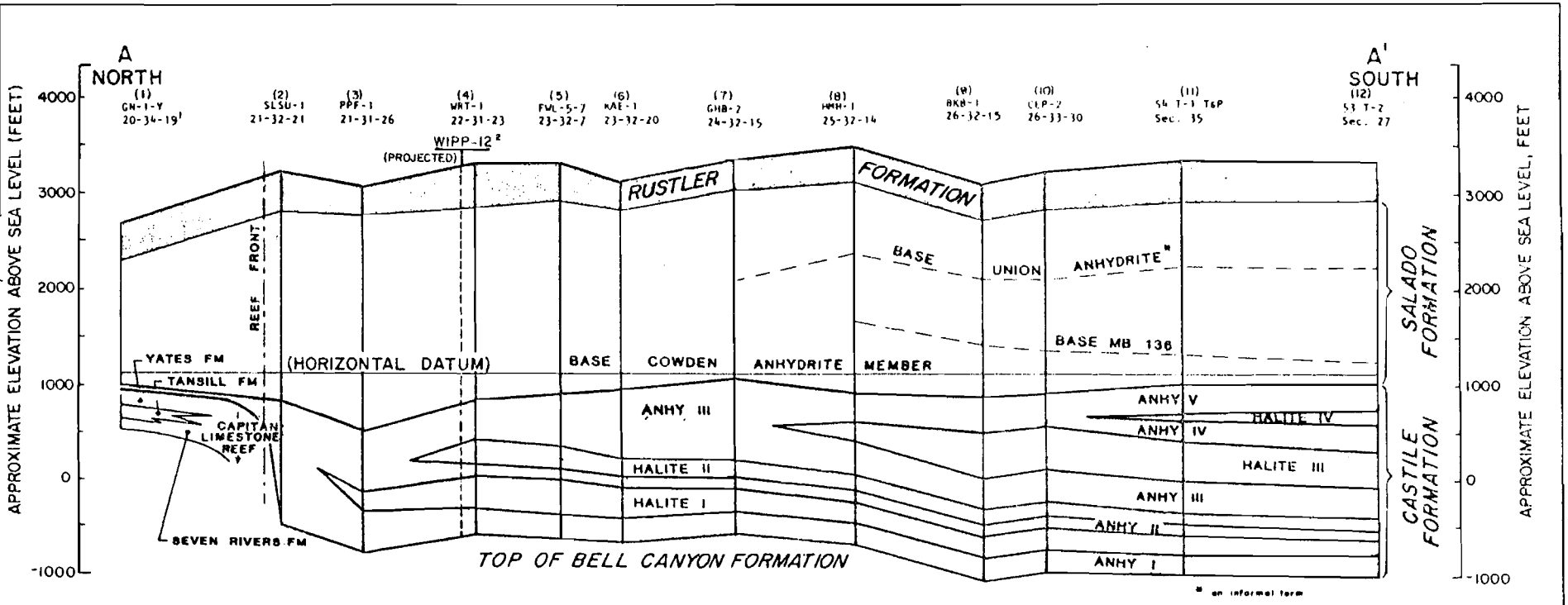

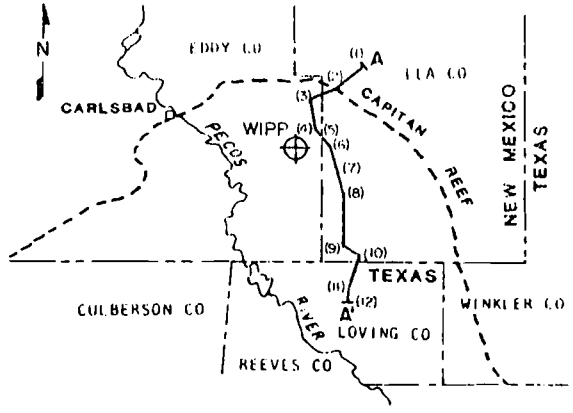

KEY MAP

NOTES:

1. CONTROL POINTS INDICATED BY OIL COMPANY ABBREVIATION, FOLLOWED BY TOWNSHIP, RANGE AND SECTION.
2. APPROXIMATE LOCATION OF WIPP-12 PROJECTED ONTO LINE OF SECTION.

HORIZONTAL SCALE
5 0 3 6 MILES
VERTICAL EXAGGERATION = 23 X

FIGURE G-4

SIMPLIFIED GEOLOGIC CROSS SECTION
OF OCHOA SERIES
NORTHEASTERN DELAWARE BASIN

PREPARED FOR

WESTINGHOUSE ELECTRIC CORPORATION
ALBUQUERQUE, NEW MEXICO

REFERENCE:

BACHMAN, 1980, USGS OPEN FILE REPORT 80-1099

DRAWN BY BKH 8-19-82 | CHECKED BY | APPROVED BY | DRAWING NUMBER NM78-648-B57

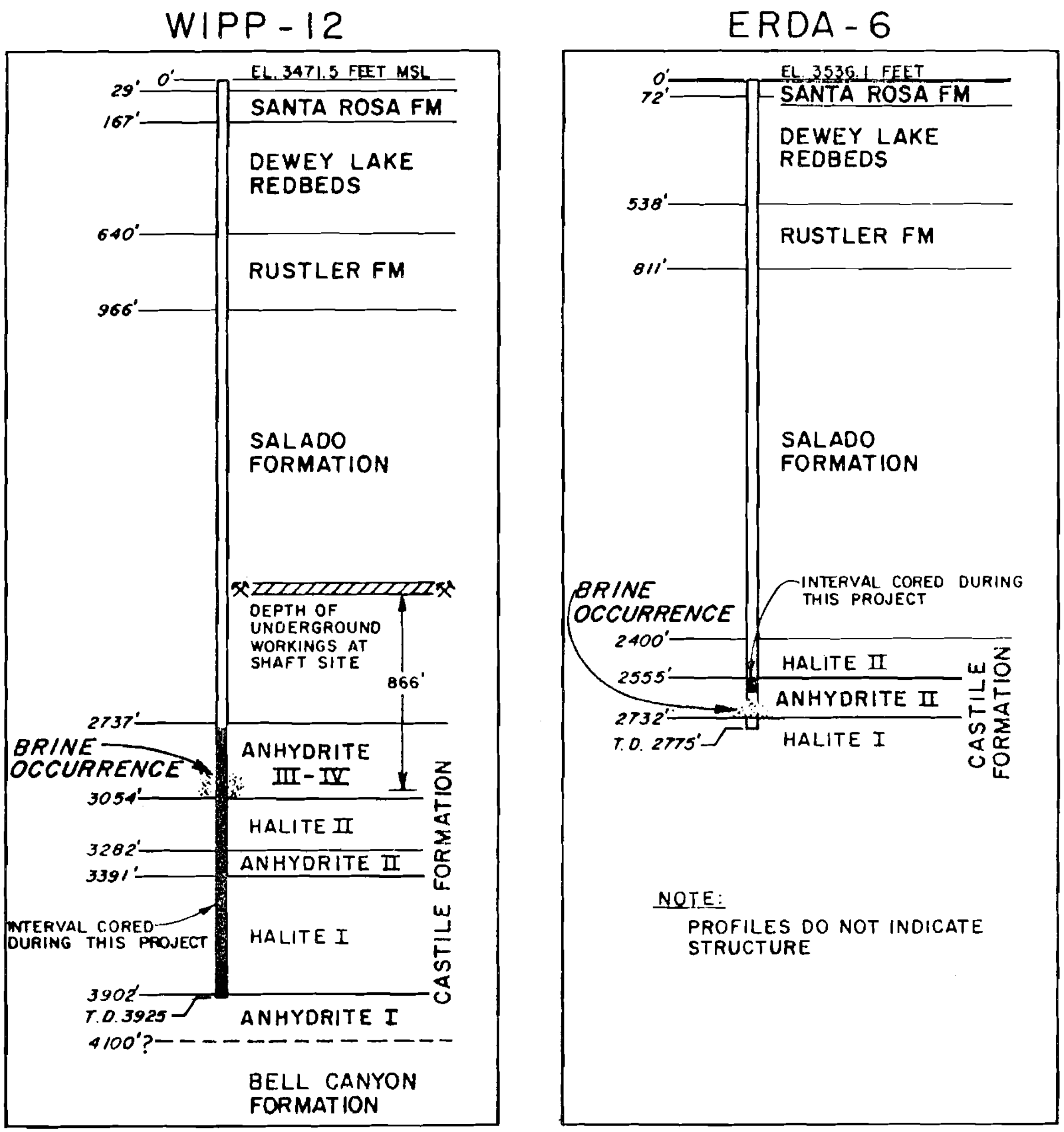

FIGURE G-5

SIMPLIFIED STRATIGRAPHIC PROFILE OF WIPP-12 AND ERDA-6 BOREHOLES

PREPARED FOR

WESTINGHOUSE ELECTRIC CORPORATION
ALBUQUERQUE, NEW MEXICO

TME 3153

TME 3153

DRAWN BY	CHECKED BY	DRAWING NUMBER
R.D.R. 3-8-83	APPROVED BY	NM78-648-MI

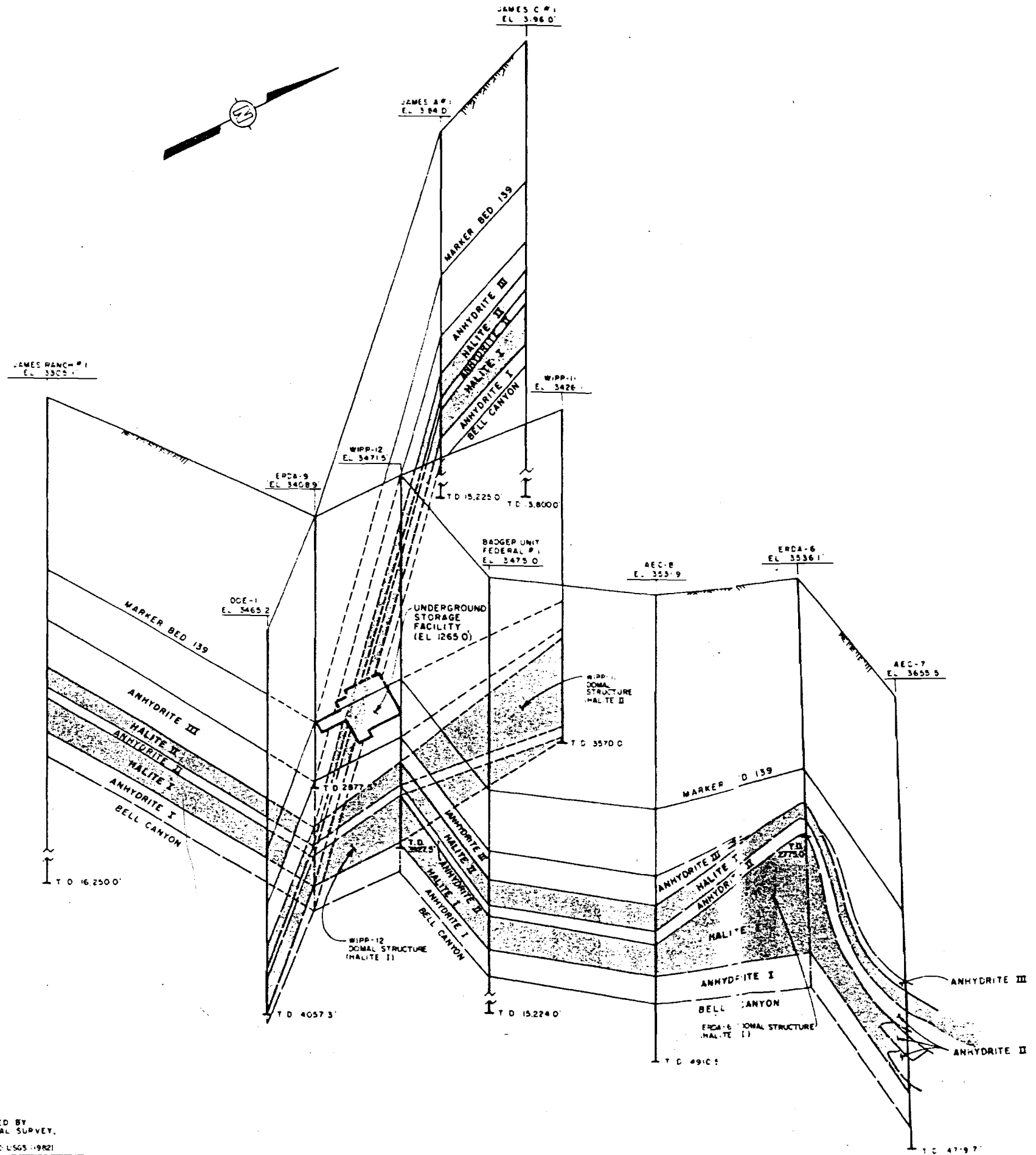

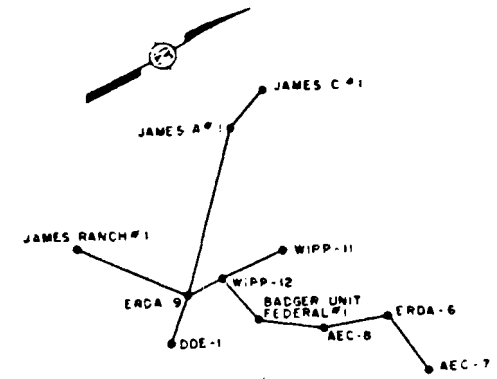

KEY MAP

SCALE
2 0 2 MILES

LEGEND

- CASTILE ANHYDRITE
- CASTILE HALITE
- OTHER UNITS
- INFERRED CONTACT
- CONTACT HIDDEN BY PANEL
- BOREHOLE
- HINGE LINE EXTENDED
- TD TOTAL DEPTH

HORIZONTAL SCALE
5 0 5 1 MILE

VERTICAL SCALE
500 0 500 1000 FEET

REFERENCES

GEOPHYSICAL LOGS PROVIDED BY R.P. SNYDER, U.S. GEOLOGICAL SURVEY, PERSONAL COMMUNICATION.
JONES (1981) & SANDIA AND USGS (1982)

FIGURE G-6

FENCE DIAGRAM OF THE GEOLOGY OF WIPP SITE VICINITY

PREPARED FOR

WESTINGHOUSE ELECTRIC CORPORATION
ALBUQUERQUE, NEW MEXICO

D'APPOLONIA

DRAWN BY R. Bricker 28 Sept.82
CHECKED BY SRB 11/4/82
APPROVED BY
DRAWING NUMBER NM78 648 ABI

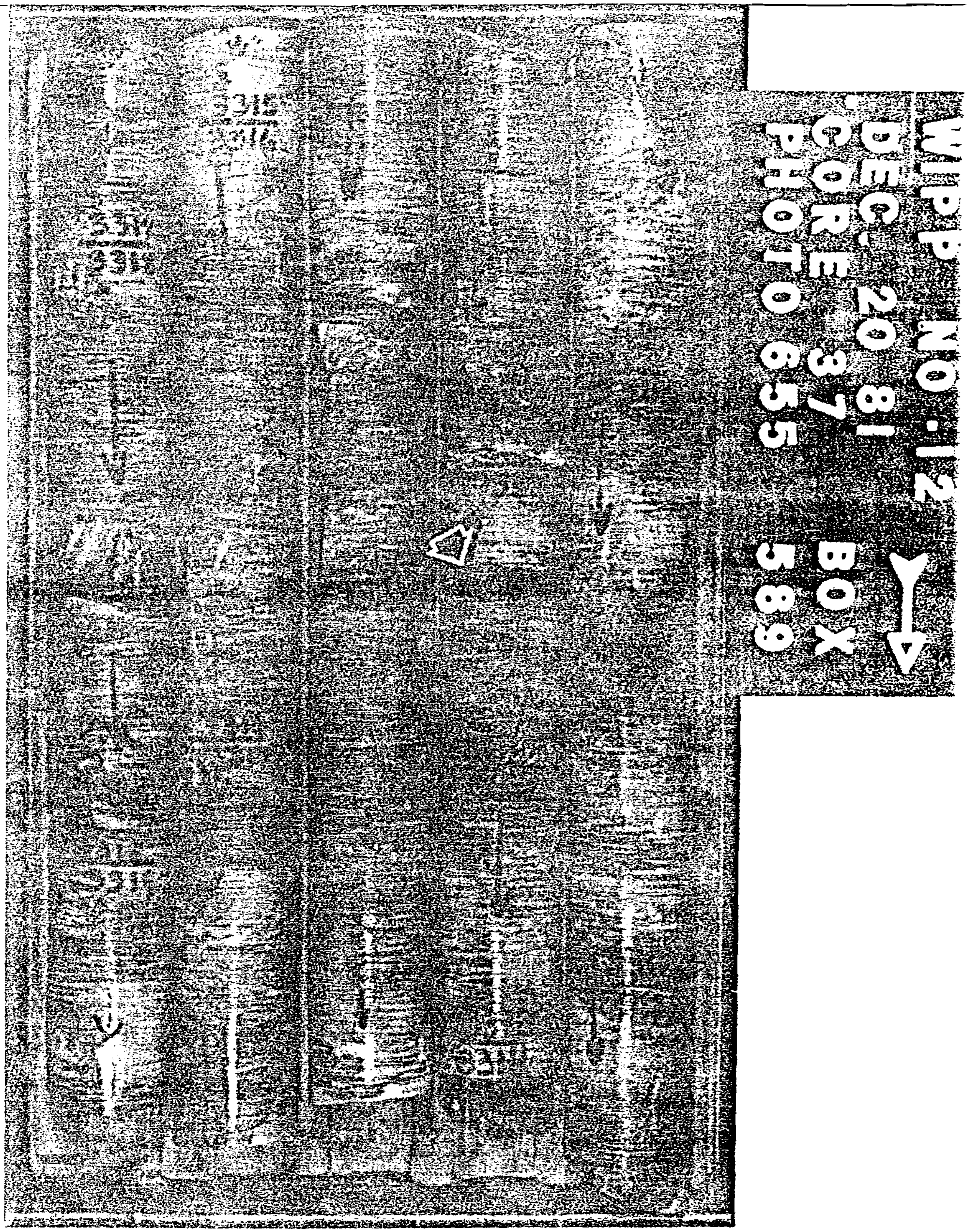

FIGURE G-7

EXAMPLE OF MICROFOLDING STYLE IN ANHYDRITE II

PREPARED FOR

WESTINGHOUSE ELECTRIC CORPORAT
ALBUQUERQUE, NEW MEXICO

D'APPOLONIA

PHOTO PROVIDED BY:
SANDIA NATIONAL LABORATORIES

DRAWN BY	CHECKED BY	APPROVED BY	DRAWING NUMBER
K Bricker 28 Sept 82	SRB		NM78 648 A82

FIGURE G-8
EXAMPLE OF MICROFOLDING
STYLE IN HALITE II
PREPARED FOR
WESTINGHOUSE ELECTRIC CORPORATIO
ALBUQUERQUE, NEW MEXICO

PHOTO PROVIDED BY:
SANDIA NATIONAL LABORATORIES
ALBUQUERQUE, NEW MEXICO

D'APPOLONIA

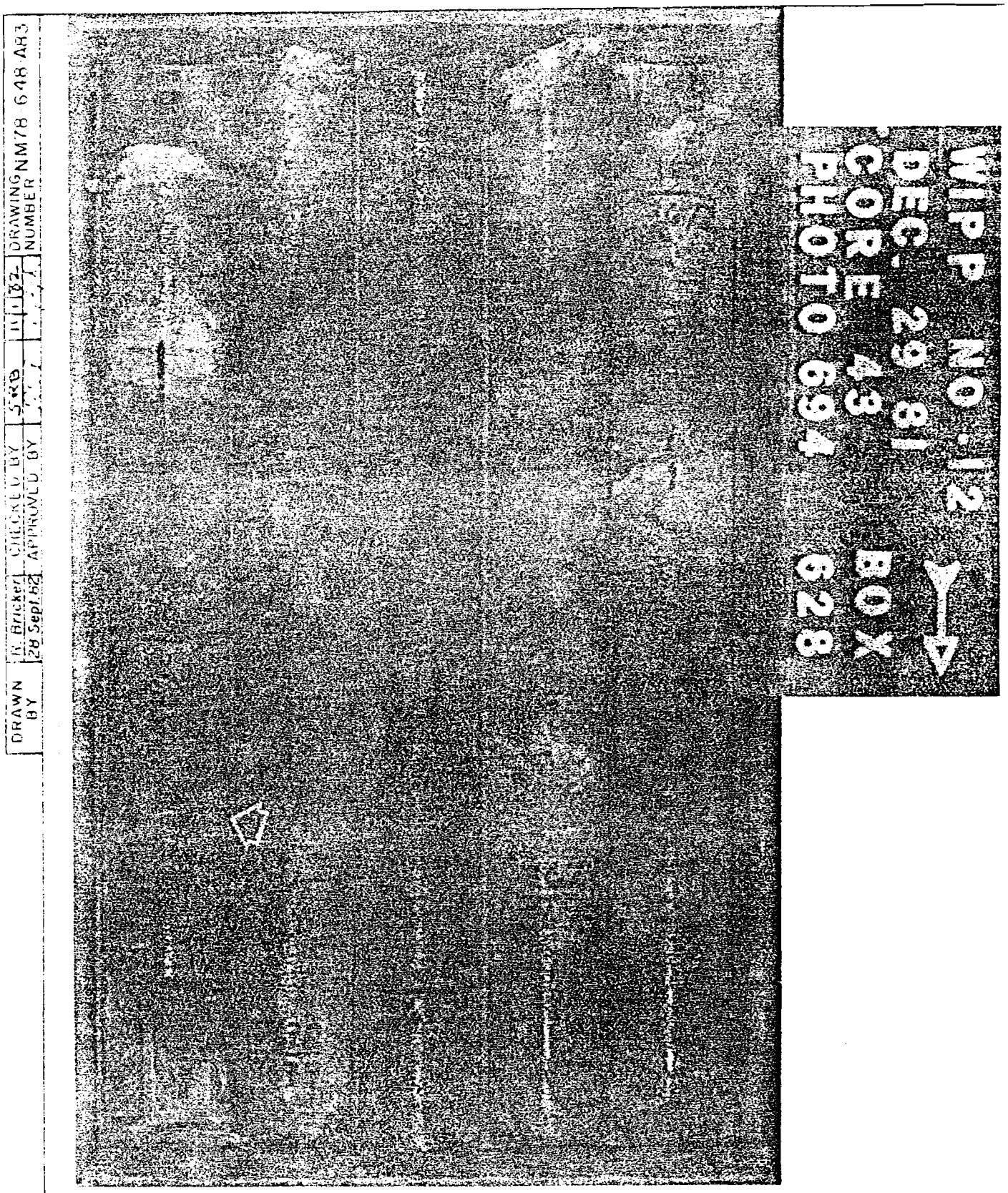

FIGURE G-9

EXAMPLE OF MICROFOLDING STYLE IN HALITE I

PREPARED FOR

WESTINGHOUSE ELECTRIC CORPORATIC
ALBUQUERQUE, NEW MEXICO

PHOTO PROVIDED BY:
SANDIA NATIONAL LABORATORIES
ALBUQUERQUE, NEW MEXICO

D'APPOLONIA

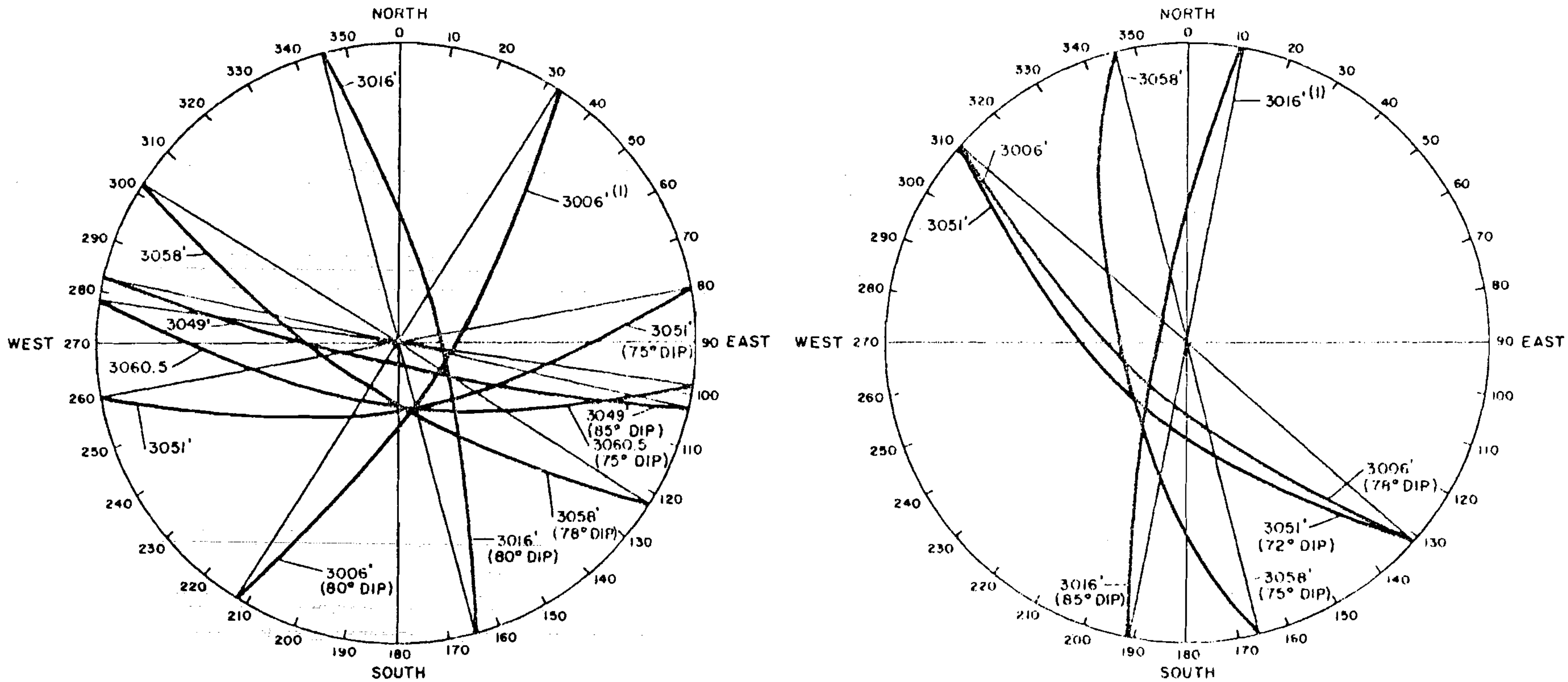

FRACTURE ORIENTATION FROM ORIENTED CORE

FRACTURE ORIENTATION FROM TELEVIEWER LOG

EQUATORIAL PROJECTION OF FRACTURE PLANES

(LOWER HEMISPHERE)

NOTE:
(1) DEPTH BELOW GROUND SURFACE

FIGURE G-10

ORIENTATION OF FRACTURES AT WIPP - 12

PREPARED FOR

WESTINGHOUSE ELECTRIC CORPORATION
ALBUQUERQUE, NEW MEXICO

DRAWN BY	CHECKED BY	DRAWING NUMBER
BKH 12-6-82	APPROVED BY	NM78-648-B31

TME 3153

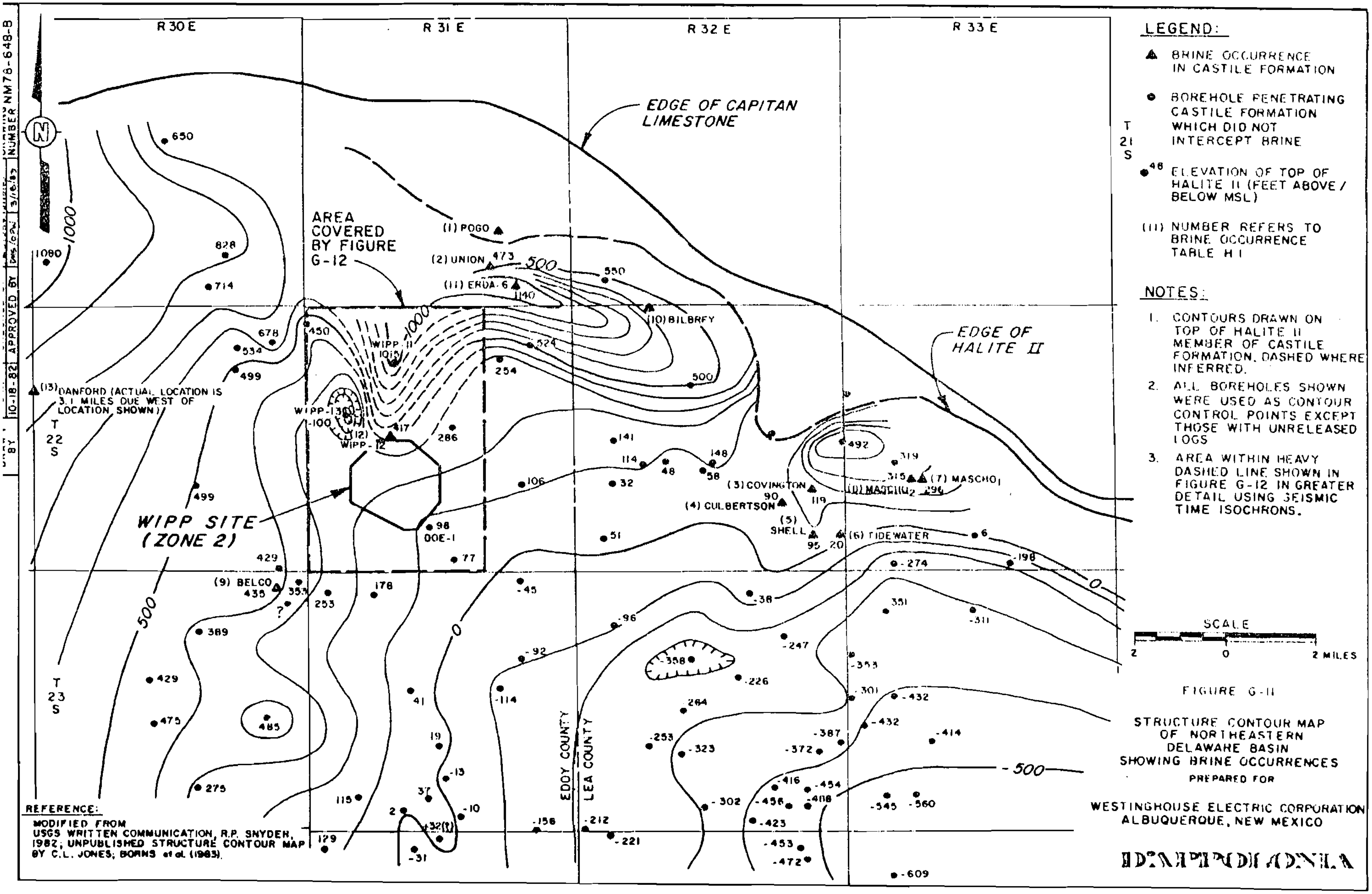

FIGURE G-11

STRUCTURE CONTOUR MAP OF NORTHEASTERN DELAWARE BASIN SHOWING BRINE OCCURRENCES

PREPARED FOR

WESTINGHOUSE ELECTRIC CORPORATION
ALBUQUERQUE, NEW MEXICO

TME 3153

DRAWN BY	CHECKED BY	APPROVED BY	DRAWING NUMBER
R. Bricker 6 Dec. 82			NM78-648-A88

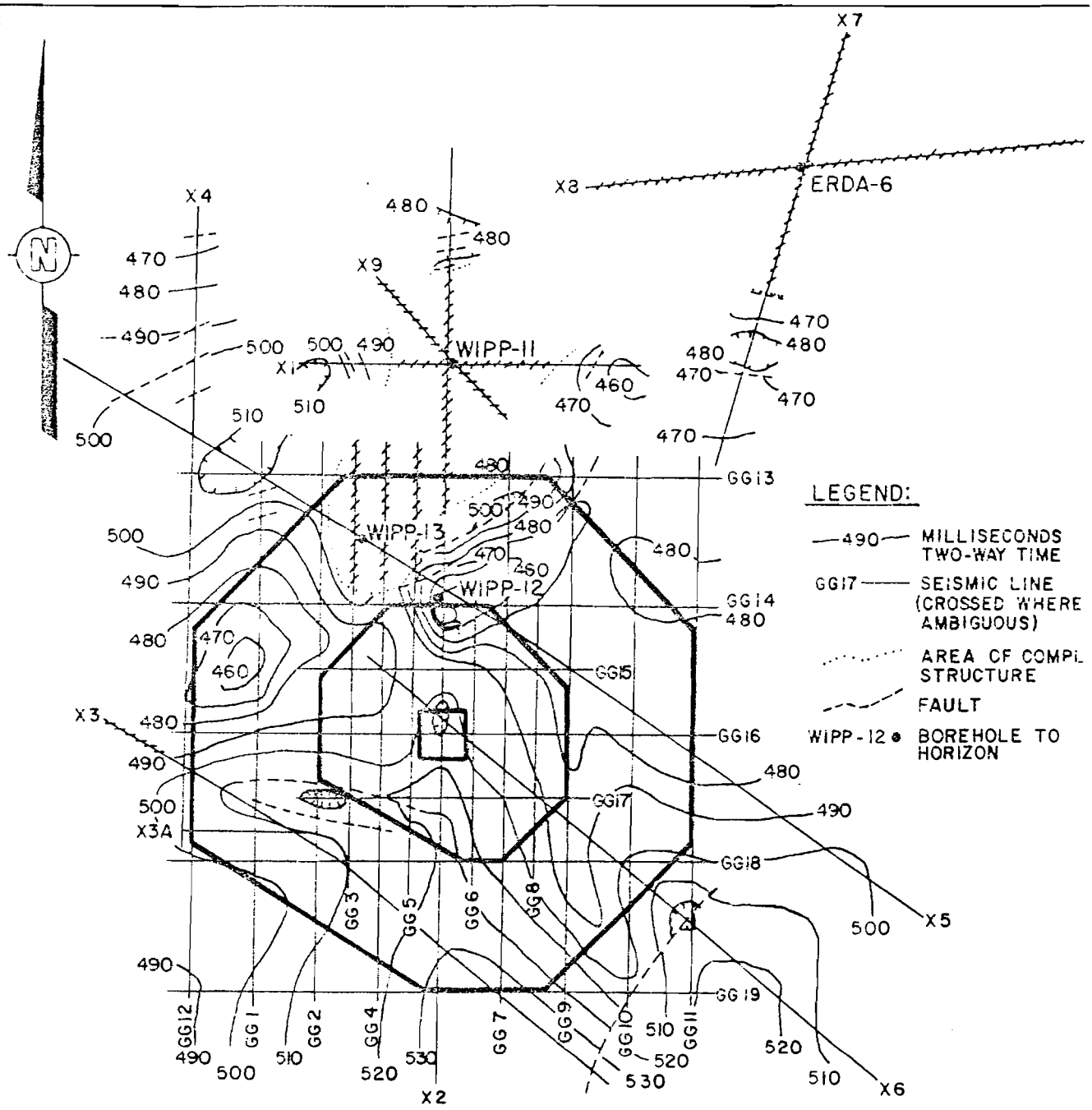

NOTES:

1. CONTOUR INTERVAL 10 MILLISECONDS; DATUM 3350 FEET ABOVE SEA LEVEL.
2. CONTOUR INTERVAL IN FEET WOULD BE APPROXIMATELY 75 FEET BASED ON AN AVERAGE SEISMIC VELOCITY OF 7620 FT./SEC. AVERAGED OVER THE ENTIRE STRATIGRAPHIC INTERVAL FROM GROUND SURFACE TO THE MIDDLE OF THE CASTILE FORMATION.

REFERENCE:

BORNS et al. (1983).

FIGURE G-12

SEISMIC TIME STRUCTURE
MIDDLE CASTILE FORMATION

PREPARED FOR

WESTINGHOUSE ELECTRIC CORPORAT
ALBUQUERQUE, NEW MEXICO

DAMPPODLONIA

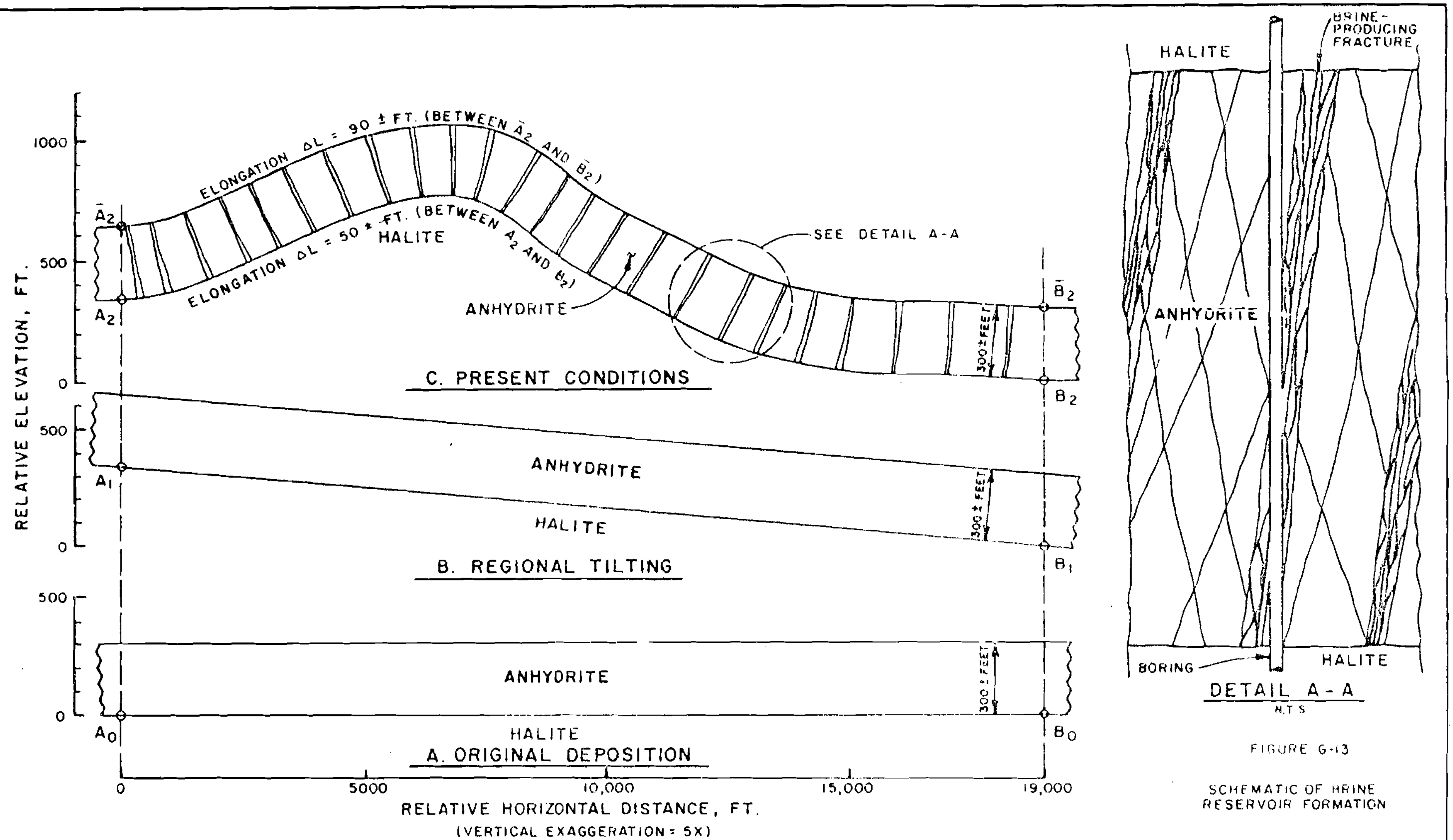

FIGURE G-13

SCHEMATIC OF BRINE RESERVOIR FORMATION

PREPARED FOR

WESTINGHOUSE ELECTRIC CORPORATION
ALBUQUERQUE, NEW MEXICO

D'APPOLONIA

TME 3153

DRAWN BY	R. Bricker	25 Oct. 82	DRAWING NUMBER	NM78-648-B55
CHECKED BY	KLB/GRA	12/16/83		
APPROVED BY	DKS/[illegible]	3/8/83		

TABLE OF CONTENTS

TABLE OF CONTENTS
(Continued)

LIST OF TABLES

LIST OF FIGURES

PART III - HYDROLOGY

1.0 INTRODUCTION AND SUMMARY

The hydrology section of this report presents the investigative methods, data, analytical methods, results, and conclusions of the hydrologic study conducted during this project. Data include those collected specifically for analysis of the Castile brine reservoirs (i.e., D'Appolonia, 1982, 1983) and those compiled from the drilling records of other wells in the Delaware Basin. Much of this drilling record data is used in analysis of the spatial distribution of the reservoirs and was developed in Part II, Geology. Included are indications of the quality of the field data and the applicability of the field data to several analytical methods.

The results of the hydrological investigations indicate that the ERDA-6 and WIPP-12 brine reservoirs, and probably the other Castile brine reservoirs, are isolated from each other and from ground-water systems in the overlying Rustler Formation and underlying Bell Canyon Formation. The persistence of high and different hydraulic heads in Castile brine reservoirs over at least the last million years is the principal hydrologic evidence for their isolation. Because all known Castile brine occurrences are associated with fractures, the reservoirs are thought to be comprised of localized systems of interconnected fractures. The ERDA-6 fracture system is estimated to contain about 630,000 barrels of brine and the WIPP-12 fracture system may contain about 17,000,000 barrels. The brines are thought to represent primary pore fluids within anhydrite which were isolated by overlying and underlying halites. The brine migrated to the fractures when the fractures opened.

In the absence of human intervention, no credible mechanism has been identified which could allow Castile brines to flow to the waste disposal horizon. An increased hydraulic gradient towards the waste disposal facility will exist during the hundreds of years the facility excavation is open, but flow from the Castile to the facility cannot occur in such a short geologic time. After salt creep seals the facility, hydraulic conditions will be similar to those

which have prevented flow from the Castile brine reservoirs for a million years.

2.0 PURPOSES AND SCOPE

2.1 SUMMARY OF PREVIOUS INVESTIGATIONS

The existence of brine reservoirs in the Castile Formation has been documented by forty years of observations made during oil and gas exploration drilling. During this period, little or no effort was made to organize the available data or characterize the reservoirs quantitatively. Indeed, the Castile Formation is considered an aquiclude by authors studying regional hydrogeology. Hiss (1975) published the first comprehensive ground-water report on the Delaware Basin and dealt with the topic on a regional scale, documenting flow patterns and regions of recharge and discharge for the aquifers of economic interest. Hiss (1975) relied on existing data and, as such, could say little about the hydrology of the Castile brine reservoirs. Mercer and Orr (1979) studied the hydrology of the region as it relates to the WIPP project. Their report concentrated on the Rustler and Bell Canyon formations, which constitute the closest overlying and underlying aquifers respectively, to the Castile and Salado formations. Powers et al. (1978) present these data in an extensive report on the geological characterization of the WIPP site. They established that the Salado and Castile formations separate the overlying and underlying flow systems by a combined thickness of hundreds of feet of very low-permeability material. The heads within the flow systems are below ground surface, and the aquifers are known to contain unsaturated (with NaCl) waters. Fluids encountered within the Salado Formation occur as small pockets with low pressure. Brine reservoirs in the Castile Formation are discussed, but little is quantified.

Register (1981) compiled existing data on the Castile brine reservoirs and produced the first report concentrating on this subject. His report was completed prior to the work of this present project, but remains a source of background information on, and documentation of, the reservoirs encountered during hydrocarbon exploration. Gonzalez (1983) studied fracture flow in the

Rustler Formation by pressure analysis and tracer techniques. He was able to determine effective porosity, dispersivity, and anisotropy values for several study locations surrounding the WIPP facility.

The first WIPP site-characterization exploration hole to indicate the presence of Castile brine reservoirs was ERDA-6. ERDA-6 was initially drilled to 2775 feet below ground surface in 1975 to evaluate the site for location of the WIPP facility (Jones, 1981a). Technical direction for the project was provided by Sandia National Laboratories. Examination of drill cuttings and core was the responsibility of the U.S. Geological Survey, and supervision of drilling operations was provided by Fenix and Scisson, Inc. After interception of the brine reservoir at 2711 feet in anhydrite, drilling continued into the underlying Halite I unit. A drill stem test (DST) was performed on the brine reservoir, after which a cement plug was emplaced from the total depth of 2775 feet to 2562 feet. The well was then abandoned until initiation of the present work.

2.2 PURPOSES OF STUDY

Prior to the investigation initiated in October, 1981, information on pressurized brine reservoirs within the Castile Formation was scarce and of a semiquantitative nature. Interest in a thorough understanding of brine occurrences within the Delaware Basin increased with intersection of the pressurized brine reservoir at ERDA-6 in 1975, initiation of Site and Preliminary Design Validation (SPDV) construction at the WIPP site, and intersection of a reservoir by WIPP-12, located about one mile from the site center, in 1981. The lack of quantitative information prompted investigations at ERDA-6 which were later supplemented by work at WIPP-12. Table H.1 lists the available data on each reported brine occurrence in the Castile Formation. ERDA-6 and WIPP-12, drilled specifically for investigation of the WIPP project area, are the only wells in which reservoir characteristics have been quantitatively assessed. Tables H.2 and H.3 and Figures H-1 and H-2 present a summary of the hydrological tests performed in ERDA-6 and WIPP-12 during investigation of the brine reservoirs.

The hydrologic testing program was oriented toward establishing the relationship between brine reservoirs in the Castile Formation and the suitability of the WIPP site. The hydrological issues which determine the impact of reservoir occurrence on site suitability are summarized below.

2.2.1 Connectivity of Brine Reservoirs With Other Water Sources

The brine reservoirs in the Castile Formation are stratigraphically and geographically the closest substantial volumes of liquids to the WIPP disposal horizon. The degree of isolation of these brine reservoirs from other water sources, especially those in close proximity to the site, enters into the assessment of the hydrological stability of the site. Intercommunication of widely spaced (stratigraphically or geographically) reservoirs could provide pathways for radionuclide migration away from the WIPP disposal area. Interconnection of brine reservoirs with local aquifers containing unsaturated (with respect to NaCl) fluids could lead to reservoir enlargement that could potentially affect the WIPP facility. Additionally, such interconnection would also provide potential pathways for radionuclide migration.

The results of hydrological investigations performed to determine whether interconnection exists are discussed in Section 3.4.1. The conclusions are supported by the results of the geochemical investigations discussed in Part IV, Chemistry, Sections 3.3 and 4.3.

2.2.2 Volume of Brine Held by Reservoirs

The drainable volume of brine (or the volume produceable at the facility horizon) stored within the anhydrite members of the Castile Formation was another factor thought to have a bearing on the suitability of the WIPP site. Knowledge of drainable volume is useful for assessment of the geographical extent of the reservoirs and to provide input data for consequence modeling. The only two brine reservoirs in the Castile Formation for which volumetric analyses were performed are those intercepted by ERDA-6 and WIPP-12. Results of reservoir volume analyses are presented in Sections 3.4.3 and 3.4.4.

2.2.3 Hydrologic Evidence of Brine and Reservoir Origin

Identification of the mechanism responsible for development of the brine reservoirs, the age-dating of reservoir development, and the length of time they have been isolated are relevant to the assessment of site stability. These data will help answer questions concerning whether reservoir development is an active process or ended in the geological past and is currently dormant. The contribution that hydrologic analyses can make toward identifying the brine origin and migration history is to explain:

- What could be (or could not be) the source of the brine?
- What was the mechanism of brine migration and accumulation in the fractured anhydrites?
- Are the processes of reservoir development or brine migration still active?

Hypotheses on brine origin, migration, and accumulation can be developed in light of the reservoirs' undisturbed (maximum) pressures and reservoir responses to brine removal. A discussion of the origin of the reservoirs and brines is in Section 4.4 of this report. The majority of the evidence pertaining to the origin of the brine, however, is derived from the geochemical investigations discussed in Part IV, Chemistry, Section 5.1.

2.2.4 Potential for Brine to Migrate From Reservoirs to Waste Facility

An assessment of the potential for brine migration into the underground waste facility is important due to the possible mobilization of the waste following brine intrusion. Mechanisms that could cause inflow of brine to the waste disposal horizon are:

- Upward seepage of brine through the halite of the Salado Formation under the induced hydraulic gradient.
- Dissolution of evaporites and associated movement of brine.

- Movement of brine through unplugged boreholes which connect the disposal horizon and brine reservoirs either directly or through interconnecting fractures.
- Flow of brine through fractures induced by mining activities.

A discussion of the potential for brine movement into WIPP underground openings via upward seepage through the Salado Formation is offered in Section 3.4.2 of this report. The potential for dissolution of evaporites is addressed in Part IV, Chemistry, Section 3.3.5. The last two possibilities are not within the scope of this report. The consequences of interconnecting the WIPP underground with a brine reservoir through drilling, however, have been shown to be insignificant (Woolfolk, 1982).

2.3 SCOPE OF STUDY

The initial phase of the current study involved a thorough review of data on brine occurrences in the Delaware Basin. The data were examined to determine if relationships could be defined between brine occurrences and local stratigraphy or geologic structures. Evidence of connections between reservoirs was also sought. Data on brine occurrences in other parts of the world, as well as data on fractured reservoirs in general, were also reviewed to provide a broader background for the study. Following the data review, a conceptual hydrogeological model was developed of the area around the WIPP site. A study plan was then developed to test, refine, and verify the model.

The field efforts undertaken to characterize the hydraulic properties of the brine reservoirs in ERDA-6 and WIPP-12 consisted of drill stem tests (DST's) and flow tests with subsequent pressure-recovery monitoring. Two drill stem tests and three flow tests were performed in each tested well. Whenever possible, tests were designed to complement or supplement previous tests. The hydrological testing program was developed to accomodate geochemical sampling, as well as geophysical logging.

3.0 HYDROLOGIC CHARACTERIZATION OF BRINE RESERVOIRS

Brine flow rates from the reservoirs, and reservoir pressures measured prior to, during, and after flow periods, were the key data used to characterize the hydrology of the reservoirs. In particular, these data were used in determination of:

- Reservoir undisturbed pressure.
- Reservoir transmissivity.
- Reservoir flow-system model.

3.1 TESTING

Detailed information on the hydrological testing procedures and volumes of brine produced from the reservoirs was presented by D'Appolonia (1982) in "Data File Report - ERDA-6 and WIPP-12 Testing" and "Addendum 1" to that report. The discussion below briefly summarizes the tests performed at ERDA-6 and WIPP-12. Figures H-1 and H-2 show the sequence of testing events, with pertinent depths.

3.1.1 Drill Stem Testing

A drill stem test (DST) is a short duration, single borehole flow and buildup test conducted through downhole packers and steel tubing. The technology was developed by and for the petroleum industry to test the hydraulic properties of deep-seated reservoirs and allow the collection of reservoir fluids for analysis. The drill stem tests performed in ERDA-6 and WIPP-12 produced an initial set of data on the brine reservoirs' hydraulic properties including: (1) reservoir pressure; (2) reservoir temperature; and (3) reservoir transmissivity. In addition, observations of reservoir behavior during drill stem tests were used to develop programs for subsequent flow tests in both wells.

Drill Stem Tests in ERDA-6 were performed at two intervals. The first tested interval was located between 2472 and 2562 feet (top of cement plug). The test, designated as "DST-2472", was performed prior to reopening the well to the brine-producing horizon, and its primary purpose was to test the in-situ integrity of the cement plug emplaced in ERDA-6 in 1975. The second interval

tested by the DST method was between the depths of 2676 and 2748 feet (bottom of the hole). This interval straddled the main brine-producing fracture located in Anhydrite II at 2711 feet. This test, designated "DST-2680", produced an initial set of data concerning the hydraulic properties of the ERDA-6 brine reservoir.

Drill Stem Tests in WIPP-12 were also performed at two intervals. The first tested interval was between 3020 and 3047 feet (bottom of the hole). The purpose of testing in this interval was to gather data from below the then-known fractured zone located in Anhydrite III approximately between 3010 and 3020 feet. During this test, designated "DST-3020", the packer could not be set below 3020 feet due to the configuration of the DST tool; thus, the fractured zone may not have been totally sealed off from the tested interval. The second tested interval extended from 2986 to 3047 feet. This DST, designated "DST-2986", produced an initial set of data on the hydraulic properties of the brine reservoir at WIPP-12.

3.1.2 Flow Testing

A flow test, as used in this report, refers to a relatively long-term flow and pressure buildup test. Flow tests were conducted to provide further information on reservoir hydraulics and to allow for substantial fluid removal for estimation of reservoir volumes and collection of representative samples for chemical analysis. The longer duration of the flow tests also provided reservoir-hydraulics data representative of regions remote from the well. The data on brine production during these tests and the associated reservoir pressure responses were used to calculate reservoir fluid volumes.

All flow tests in ERDA-6 and WIPP-12 were designed to be constant-pressure, variable-flow-rate tests. This method is applicable to situations in which a well intersects a reservoir with a pressure head above ground surface. Such a condition was encountered in ERDA-6 and WIPP-12. However, technical difficulties prevented the maintenance of constant pressure during some of the tests.

Flow and Buildup Tests in ERDA-6 provided further information on the hydraulic properties of the brine reservoir, as well as data for reservoir volume calculations. Flow Test 1 immediately followed DST-2680. It was performed through steel tubing with a DST tool isolating the tested interval between 2676 and 2748 feet (bottom of hole) from the remainder of the hole. Due to the risk of hydrogen sulfide embrittlement of the tubing, which could result in the loss of the DST tool, this test was terminated after 5.6 hours of flow and 3 hours of buildup. Total brine production during this test was 153 barrels.

Flow Test 2 and Flow Test 3 were designed to provide data on the response of the reservoir to long-term stress. Significantly larger volumes of brine were allowed to flow from the well: 1030 barrels during Flow Test 2 and 444 barrels during Flow Test 3. The pressure buildup following shut-in was monitored to provide a basis for the evaluation of long-term reservoir response. Both Flow Test 2 and Flow Test 3 were run with an open borehole with all instrumentation above ground surface. Currently, ERDA-6 is shut-in and will soon be cemented and plugged to the surface.

Flow and Buildup Tests in WIPP-12 provided further information on the hydraulic and geochemical properties of the brine reservoir, as well as data for reservoir volume calculations. Prior to the initiation of the formal hydrologic testing program at WIPP-12, over 27,000 barrels of brine were unavoidably produced from the well during drilling and geophysical logging.

Flow Test 1 was designed primarily to allow the collection of gas and brine samples at the wellhead and, using a downhole sampler, under in-situ reservoir conditions. The brine flow was restricted during this test to maintain the backpressure necessary to operate the gas/liquid separator and to optimize sample-collection conditions. The collection of hydrologic data was of lesser concern, and in fact, no interpretable data were obtained. Total brine production during this test was 489 barrels. Between Flow Tests 1 and 2, an additional 25,000 barrels of brine were unavoidably produced during additional drilling and logging activities.

Flow Test 2 was a short-term test designed to provide data on the fracture response to short-term stress. It was expected that the data would be useful in assessing fracture permeability and the ratio of fracture-to-total storage volume. Total brine production during this test was 2258 barrels.

Flow Test 3 was designed to provide data on the response of the reservoir to long-term stress. Total brine production during this test was 24,800 barrels. Currently, WIPP-12 is shut-in and will soon be plugged through the producing zone. Final plugging to the surface will be a part of the borehole plugging program.

3.2 MEASUREMENTS

Detailed information on flow-monitoring-system configurations, flow-meter specifications, and pressure-monitoring devices is presented by D'Appolonia (1982). The discussion below briefly summarizes the methods of flow and pressure data acquisition, type of instrumentation, factors affecting quality of flow and pressure data, and special concerns regarding data acquisition techniques.

3.2.1 Flow Measurements

The flow rates and volumes of brine produced from the reservoirs were measured with a variety of metering devices. During periods when drilling or activities other than hydrological testing (e.g., geophysical logging or packer installation) were in progress, flow rates were approximated by pump stroke counters and fill-up rates of the mud pits. This type of flow rate approximation was especially important during the deepening of WIPP-12. During efforts specifically designed for hydrologic testing, various flow meters were installed to monitor flow rates, and during DST's, downhole transducers measured inflow rates into the tubing. Tables H.2 and H.3 briefly summarize the flow monitoring in ERDA-6 and WIPP-12, respectively. Information on instrumentation and factors affecting the quality of measurements is also provided.

During testing at ERDA-6 and WIPP-12, the flow rate measurements were at times affected by:

- Gas liberated from the brine passing through the flow meters, causing them to register erroneously high flow rates.
- Salt precipitation within the flow lines or flow meters restricting flow and often incapacitating instruments.
- Deterioration of flow meters due to the corrosiveness of the brine and hydrogen sulfide.
- Choke effects during DST flow periods.

The problem of gas liberation in the flow system upstream of the flow meters was noticed only at ERDA-6 where the gas bubbles were large and often completely filled the discharge pipe. At WIPP-12, no large gas bubbles were noted at the position of the flow meters, but the possibility of small bubbles remains. The analyses presented in Part IV, Chemistry, Section 4.3.2, indicate that even under flowing conditions no more than about two percent of the fluid volume at the WIPP-12 reservoir level is occupied by gas, and no gas at all should exist in the ERDA-6 reservoir. Therefore, most of the gas probably was liberated during travel up the well. The much slower flow rate of ERDA-6 is likely responsible for the existence of more gas in the discharge line by allowing longer travel times under reduced pressure. Problems with gas/brine separation were rectified when gas/liquid separators were used. Brine flow rates were measured downstream from the separator after most of the gas had been removed from the flow line.

Salt buildup within the flow lines and meters occurred because the drop in pressure as the brine flowed to the surface was apparently sufficient to cause salt precipitation from the halite-saturated brine (see Part IV, Chemistry, Section 3.3.2). The problem was overcome by using several flow meters in a parallel arrangement and bypassing the brine flow from an obstructed flow

meter to a clear one. The obstructed meter would then be flushed with fresh water to prepare for its future use. The extremely high corrosiveness of the brine, coupled with the presence of hydrogen sulfide, also caused frequent flow meter failures. The parallel arrangement of flow meters allowed switching to an alternate whenever a meter needed to be repaired. As a last resort or as a check on flow meter accuracy, the brine could be channeled through a cutthroat flume.

Choke effects were noted during the flow periods of the DST's conducted at WIPP-12 (D'Appolonia, 1982, v. II). These effects are present when pressure at the instant of flow period initiation is not as low as would be expected based on the pre-test static pressure exerted by water in the tubing. Choke effects are caused by the reservoir yielding fluid at a greater rate than can easily pass through the DST tool, causing backpressure to build up on the reservoir side of the restriction or "choke." Because the DST transducer is also located on the reservoir side of the choke, this choke pressure is registered instead of the desired pressure of the water column in the tubing. For this reason, the DST's conducted in WIPP-12 were not used for quantitative analysis.

Problems encountered during the flow tests were identified in the field and corrective measures were implemented. Their bearing on the overall quality of the test data was considered during selection of data for quantitative analysis.

3.2.2 Pressure Measurements

Reservoir pressures were measured during all buildup tests, all phases of DST's, and during some flow tests. Depending on the type of test, its duration, and operational concerns, pressures were measured either downhole at the production horizon or at the wellhead. The methods of pressure measurement, instrumentation, and limitations are presented briefly in Tables H.2 and H.3. For detailed information, refer to D'Appolonia (1982, 1983).

Downhole Pressure Measurements

Electronic pressure transducers connected via wireline with surface-located computers were used to acquire and record reservoir pressure and temperature data. The downhole pressure-monitoring systems allowed measurement of these parameters at reservoir depth. For all tests except Flow Tests 2 and 3 in WIPP-12, a Lynes Triple Conducting Wireline (TCWL) transducer probe was coupled with an HP-9825 desktop computer for data acquisition and manipulation. During Flow Tests 2 and 3 in WIPP-12, a Johnston-Macco Downhole Pressure-Temperature Transducer -- Surface Pressure Readout (DPTT-SPRO) system was used (D'Appolonia, 1982). The seals between the wireline and the wellhead often proved troublesome, causing leaks and affecting pressure readings. For extended periods of pressure monitoring, the downhole monitoring systems proved impractical.

Surface Pressure Measurements

Electronic pressure transducers, the same as those used for downhole monitoring, and mechanical pressure gages were utilized for pressure measurements at the surface. By measuring the pressure at the surface, no wireline was needed, thus leakage of pressure between the cable and wellhead was eliminated. However, monitoring pressure at the surface has some drawbacks affecting data quality.

To correlate pressures read at the surface to those at the reservoir level, the pressure exerted (fluid pressure gradient x thickness) by the fluid column in the wellbore above the reservoir must be known. One fluid pressure gradient survey was performed in ERDA-6, which indicated a pressure gradient of 0.5326 psi/ft of brine. Four fluid pressure gradient surveys were run in WIPP-12. The surveys indicated fluid pressure gradients in the brine-filled portion of the wellbore ranging from 0.5345 to 0.5433 psi/ft of brine, with an average of 0.5378 psi/ft.

The pressure gradient survey run in WIPP-12 after four months of shut-in prior to Flow Test 2 also revealed the presence of a gas cap in the wellbore

extending to approximately seven feet below the ground surface. The presence of a gas cap at the wellhead creates a problem in converting wellhead (surface) pressure to reservoir (downhole) pressures because gas is much lighter than brine and the location of the gas-brine interface in the wellbore could not be monitored on a continual basis. With an expanding gas cap, wellhead pressures will rise at a faster rate than reservoir pressures because as a gas cap expands, the gas pressure must rise to compensate for the pressure exerted by the displaced brine. Even if the reservoir pressure is static, the gas pressure in an expanding gas cap will continue to rise. The effect of gas cap development on the shape of a pressure buildup curve plotted from wellhead data will be very small due to the slow formation of the gas cap. The gas cap factor must be eliminated, however, when estimating reservoir pressure depletion for reservoir volume calculations. Accordingly, on March 7 and 8, 1983, the gas caps on the WIPP-12 and ERDA-6 wellbores were released to obtain data needed to calculate the reservoir pressures accurately (see Sections 3.4.3 and 3.4.4).

Another drawback to surface pressure measurements was that ambient temperature variations caused the pressure readings to fluctuate. The temperature effect was largely eliminated by insulating the wellhead.

3.2.3 Special Concerns

All pressure recovery tests in ERDA-6 and WIPP-12, with the exception of the buildup period following Flow Test 1 in ERDA-6, were conducted in uncased, open boreholes. The entire 1600-foot thickness of the Salado Formation, containing numerous clay seams of total thickness under ten feet, was exposed to the pressurized brine. Cross-flow between the Castile reservoirs and sections of the Salado with locally elevated permeabilities was therefore possible. The impact that inter-reservoir cross-flow could have on buildup pressure has been examined for WIPP-12. The maximum inflow into the Salado Formation, based on shut-in conditions, was estimated to be 25 bbl/day and this in turn could lower the buildup pressure by approximately 6 to 7 psi over a long-duration buildup period. This inflow rate is likely lower than outflow rates from the Salado would be under evacuated-borehole conditions.

3.3 DATA REDUCTION AND ANALYSIS

Data reduction and analysis were guided by an evolving working hypothesis for a reservoir model. Qualitative examination of geologic and hydrologic data provided a preliminary indication of appropriate flow-system models to be used to analyze the hydrologic data quantitatively. As the analyses progressed, the models were tested and refined until the most appropriate model was developed.

3.3.1 Working Hypothesis for Reservoir Model

A general reservoir model of the ERDA-6 and WIPP-12 brine reservoirs was developed largely from information gained from drilling records, core, and other data from ERDA-6, WIPP-12, and other wells in the Delaware Basin. This model was used as a working hypothesis during analysis of the hydrologic data. Refinement of the working model continued during hydrological testing and data analysis. The following is a list of preliminary information from which the reservoir model was originally developed:

- Both the ERDA-6 and WIPP-12 brine reservoirs were encountered in the uppermost anhydrites in the Castile Formation. Flow was detected from the lower portion of each anhydrite only (Register, 1981; D'Appolonia, 1982). The anhydrite beds are bounded on the top and bottom by massive salt beds.

- Brine was produced from ERDA-6 and WIPP-12 when coring intercepted large, near-vertical fractures. No brine flow was noted from non-fractured intervals within the borehole.

- Near-vertical microfractures were noted in thin sections of core samples from the fractured zones in WIPP-12.

- Geophysical logs run in ERDA-6 and WIPP-12 indicate that intact anhydrite has a porosity of about 0.01 or less (D'Appolonia, 1982, v. III A, 6.5; IVA, 12.5; and Addendum 1, 12.19).

- The occurrence of brine is apparently associated with antiform features (Figure G-11) which may be controlling factors in the density, distribution, and orientation of fractures.

Analysis of core and geophysical logs indicates that the brine reservoirs probably consist of multiple interconnected fracture sets of various apertures and extents. The large fractures are probably most limited in extent, and are expected to have high permeabilities but relatively little brine storage capacity. Different large-fracture sets may be interconnected by smaller fractures (see Figure G-13). The smaller fractures probably have greater geographical extent, and account for the majority of brine storage while having relatively low permeabilities. The density of fractures is probably greatest along the flanks of the antiforms (Aguilera, 1980), which may explain the distribution of highly productive reservoirs (cf. reservoir locations on Figure G-11 with flow rates in Table H.1). At some point in every lateral direction, the fractures, both large and small, probably end in massive anhydrite of extremely low permeability. The reservoirs are also bounded above by low-permeability anhydrite and massive salt, and below by massive salt.

The conditions noted above suggest that the expected pressure and flow behavior in the Castile reservoirs would be different than that predicted by homogeneous, infinite reservoir models. For this reason, in selecting analytic methods, several reservoir models were considered in addition to the standard homogeneous, infinite model. These included: homogeneous, finite models; double-porosity models; and single vertical fracture (both infinite and finite fracture permeability) models.

3.3.2 Analytic Methods for Connectivity/Isolation Assessment

Three main categories of hydrologic information can be used to assess the degree of isolation of the Castile brines: (1) observations of hydraulic heads in the brine reservoirs and other ground-water systems; (2) observations of brine occurrences (or the lack of occurrences) throughout the basin; and (3)

pressure changes in observation wells during hydrological testing in ERDA-6 and WIPP-12 (interference testing). Section 3.4.1 presents the results of this assessment.

3.3.3 Analytic Methods for Brine Migration Potential

Four scenarios have been identified that might cause brine stored in the Castile Formation to contact the waste disposal facility. As outlined in Section 2.2.4, these are: (1) upward seepage of brine through halite of the Salado Formation; (2) dissolution of evaporites and associated movement of brine; (3) flow of brine through fractures induced by mining activities; and (4) movement of brine through unplugged boreholes. The first scenario, upward seepage of brine through halite of the Salado Formation, is the only scenario which does not rely on human influence that can be evaluated solely on the basis of hydrologic evidence. This will be the only scenario addressed in this section. The second scenario, dissolution of evaporites and associated movement of brine, will be treated in Part IV, Chemistry, Section 3.3.5.

The potential for upward seepage of brine through halite of the Salado Formation can be evaluated most simply by considering the present-day flow regime, and changes that could occur in that regime as a result of opening up the WIPP facility. Much of the same evidence used to assess the connectivity/isolation of brine reservoirs can be brought to bear on this problem. The results of this evaluation are presented in Section 3.4.2.

3.3.4 Analytic Methods for Flow System Characterization

Early examination of the buildup data from the tests in ERDA-6 and WIPP-12 indicated that the reservoirs were not responding as simple, textbook examples of idealized systems. Preliminary analyses were therefore conducted with the extensively used and versatile Horner (1951) method. Although originally developed to analyze infinite-acting radial flow in an isotropic, homogeneous medium, the Horner method allows the recognition and interpretation of non-ideal behavior caused by such factors as wellbore storage, skin (near-well radial heterogeneities), boundary effects, double porosity, fractures, and

other reservoir heterogeneities. Other, more specialized methods of analysis may then be selected accordingly and applied to the data to quantify or characterize the non-ideal conditions.

In the Horner method, buildup pressure (Δp) is plotted versus log [(t_p + Δt)/Δt] to produce a Horner plot (see Nomenclature at end of Hydrology text for definition of symbols). If the conditions of infinite-acting radial flow are met, a straight line will be present on the Horner plot. Deviations from the straight line during early and late buildup times are indicative of deviations from these conditions.

Figure H-3 presents a hypothetical Horner plot showing the signatures of many deviations and their causes; in general, wellbore conditions will affect the early data (far right) and boundary effects will influence the late data (far left). Figures H-4 and H-5 show Horner plots from reservoir tests in ERDA-6 and WIPP-12, respectively. Comparison of these Horner plots with Figure H-3 shows that: (1) both wells have large negative skins or intersect major fractures; (2) both reservoirs show infinite-acting radial flow during intermediate times; (3) both reservoirs show boundary effects; and (4) both reservoirs show recharge (repressurization) after interception of the boundary, although this is more pronounced in ERDA-6 (Figure H-4). Furthermore, the shapes of the Horner plots suggest that the effects of major vertical fractures may continue into the infinite-acting radial-flow period, and that the recharge effects noted at very late times may be due to non-uniform pressure distributions in the heterogeneous reservoirs prior to testing.

Initial qualitative interpretation of the Horner plots suggested that the following reservoir models might be used to guide interpretation of at least a portion of the data; under each model type are listed some of the analytical methods which can be used for that particular model. Included are both flow and buildup period analytical methods.

- Infinite-acting, homogeneous, radial-flow model
  - Theis method (Theis, 1935)

- Jacob-Lohman method (Jacob and Lohman, 1952)
- Horner method (Horner, 1951)

- Infinite-acting, heterogeneous, radial-flow model (double porosity)
  - Horner method (Warren and Root, 1963)
  - Bourdet and Gringarten method (Bourdet and Gringarten, 1980)
  - Mavor and Cinco-Ley method (Mavor and Cinco-Ley, 1979)
- Finite-acting, radial-flow model
  - Jacob method (Cooper and Jacob, 1946)
  - Horner method (Horner, 1951)
  - Da Prat et al. method (Da Prat et al., 1981)
  - Muskat method (Muskat, 1937)
- Model for well intersecting a major vertical fracture (linear flow)
  - Locke and Sawyer method (Locke and Sawyer, 1975)
  - Horner method (Russell and Truitt, 1964; Raghavan et al., 1972)
  - Gringarten et al. method (Gringarten et al., 1972)
  - Jenkins and Prentice method (Jenkins and Prentice, 1982)

A systematic series of analyses was conducted using many of the techniques mentioned above. The results of each analysis were used as an indication of whether or not the reservoir actually conformed to the assumptions inherent in the method. In this way, the results of all the analyses supplied either positive or negative information on the reservoir characteristics and helped to refine the working model of the Castile brine reservoirs. In the end, the Horner method proved to be best suited for analysis of the available data. All the other methods either produced ambiguous or qualitative results, or provided nothing that could not also be obtained from the Horner method.

Over the following pages each of the major analytical methods used are discussed. The information gained from each analysis is noted, as well as the

reasons why each was ultimately dismissed in favor of the Horner method. A listing of the quantitative results from many of the methods is presented in Table H.4.

Horner Semi-Log Method of Analyzing Buildup Period Data

The applicability of previously derived heat flow solutions to ground-water flow problems was first demonstrated by C.V. Theis (1935). The theory and technique of buildup period semi-log analysis was expanded by D.K. Horner (1951), who brought the procedure to widespread use in the petroleum industry.

The Horner method is based on the radial ground-water flow equation:

$$\frac{\partial^2 H}{\partial r^2} + \frac{1}{r}\frac{\partial H}{\partial r} = \frac{S}{T}\frac{\partial H}{\partial t} \qquad \text{[Eq. 1]}$$

subject to the following assumptions:

1. A well of negligible storage capacity fully penetrates a homogeneous, isotropic, horizontal, infinite, confined reservoir.
2. The hydraulic head everywhere within the reservoir is equal and constant prior to initiation of flow.
3. At initiation of the flow period, fluid withdrawal from the well begins and is maintained at a constant rate.
4. Flow towards the well is radial.
5. The fluid is homogeneous.
6. At the beginning of the buildup period, flow from the formation into the well instantaneously ceases.

Given these conditions, the following equation defines the pressure changes in the pumped well during the buildup period:

$$p_w = p_o - \frac{2.3\ Q\mu}{4\pi kh} \log \frac{t_p + \Delta t}{\Delta t} \qquad \text{[Eq. 2]}$$

Beginning at the start of the buildup period, pressure data are collected as a function of elapsed buildup time. A plot is then prepared of buildup pressure versus the log of $\frac{t_p + \Delta t}{\Delta t}$. During the buildup period when the assumptions of the method are met, the data will plot as a straight line. As can be seen from the previous equation, the slope of this line is equal to

$$m = \frac{2.3\ Q\mu}{4\pi kh} \qquad \text{[Eq. 3]}$$

and thus the kh product (transmissivity) can be calculated if Q and μ are known.

Horner (1951) suggested a modification of this method for flow periods in which the flow rate was not held constant. This procedure was later theoretically verified for the case of constant-pressure, non-constant-rate production (Ehlig-Economides, 1979). The procedure involves calculating a modified production time, t_p^*, with the equation:

$$t_p^* = \frac{\Delta V}{Q_f} \qquad \text{[Eq. 4]}$$

With this modification, the equation describing pressure buildup at the well becomes:

$$p_w = p_o - \frac{2.3\ Q_f\ \mu}{4\pi kh} \log \frac{t_p^* + \Delta t}{\Delta t} \qquad \text{[Eq. 2A]}$$

Recognition of skin effects, wellbore storage, double-porosity behavior, lateral or radial inhomogeneities, and boundary effects are possible on the Horner plot, as shown on Figure H-3. Calculation of permeability from the Horner plot requires the identification of data representing radial flow; as shown in Figure H-3 these data may not constitute the only straight line

present on the Horner plot. Recognition of the various flow regimes represented during a buildup period can be aided by log-log analysis, as discussed below.

The Horner plot was the first method by which modern double-porosity analysis was conducted (Warren and Root, 1963; Odeh, 1965; Kazemi, 1969). Although differing in certain analytical assumptions, these authors agree that, under certain ideal conditions, two straight, parallel lines may develop when data are plotted by the Horner method. The first straight line represents fracture-dominated pressure buildup and the second straight line represents fractures and matrix block response. The vertical separation between the two lines is proportional to the amount of fluid storage in the fractures. An example of this type of behavior is included on Figure H-3. The difficulty in using the Horner method for double-porosity analysis of actual test data is that wellbore storage and skin effects often obscure the initial line, while boundary effects may influence the development of the second line. Even under ideal wellbore and boundary conditions, the two lines will not develop for all combinations of reservoir characteristics (fracture-to-matrix permeability ratio, fracture-to-matrix storage ratio).

The Horner method may also be used for analysis of buildup data affected by the presence of a major vertical fracture in connection with the wellbore (Russell and Truitt, 1964; Raghavan et al., 1972). The effect of such a fracture is to reduce the slope of the apparent Horner straight line, causing an overestimation of kh, and to create a general upward concave shape to the Horner plot similar to the effect of a large negative skin. A method of correcting the results of analyses based on the maximum slope of this plot was developed by Russell and Truitt (1964). The correction factor (F) is multiplicative and ranges between about 0.3 and 1.0 for most practical purposes, depending on the extent of the fracture. The determination of the correction factor requires previous knowledge of the size of the well's drainage area.

The Horner buildup curves obtained from tests performed in both ERDA-6 and WIPP-12 show combinations of most of the features discussed above, i.e., negative skin at early times and negative and then positive (recharge) boundaries at late times, resulting in curves with some features that resemble those typical of double-porosity models. These features, in conjunction with the observation that the wells intercept near-vertical fractures, strongly influenced the way in which the reservoir model was developed and analyzed.

The reservoir tests conducted in ERDA-6 and WIPP-12 can be grouped into two major categories:

- Relatively short tests, the results from which represent the characteristics of the local large-fracture group intercepted by each well.
- Relatively long tests, the results from which represent the characteristics of each reservoir averaged over an extensive area.

The shapes of the Horner plots from these two categories are distinctly different in terms of early large-fracture response and boundary effects, and indeed, this was a major influence in grouping the tests this way. Figures H-4 through H-7 show Horner plots of tests classified as short term, and Figures H-8 and H-9 show Horner plots from the long-term tests. The length of the flow and buildup periods and the reservoir tested are indicated on the figures.

Interpretation of Responses to Short-Term Tests - All the responses shown in Figures H-4 through H-7 show similar characteristics. In consideration of the large, near-vertical fracture intercepting the WIPP-12 borehole, the early- and intermediate-time data probably represent transition from some degree of linear flow to radial flow. The data from the WIPP-12 test indicate a larger degree of fracture influence by their more pronounced curvature than do the data from ERDA-6. In this situation, the best approximation of the Horner straight line is the steepest portion of the curve (Russell and Truitt, 1964). The fracture-influenced Horner straight line ends with boundary

effects on all the short-term tests. These boundary effects are due to the limited nature of the high-permeability local large-fracture group. The classical boundary-affected regions of the plots end in data dominated by recharge (repressurization) of the local large-fracture group. This recharge emanates from lower permeability regions of the reservoirs. The fact that the wellhead pressures continue to recover to values higher than existed at the start of each flow test indicates that pressures were not uniform throughout the high-permeability and low-permeability regions of the reservoirs prior to each test. The very late-time buildup represents a superposition of buildup responses of the low-permeability material from all previous tests, and possibly the effects of rock creep in response to lowered pore pressures.

Interpretation of Responses to Long-Term Tests - Figures H-8 and H-9 show curvatures distinctly different from the short-term responses shown in Figures H-4 through H-7. These long-term responses are typical of fractured or stimulated wells in low-permeability reservoirs (Peters, 1982, personal communication). Over the long duration of these tests, the volume of influence migrated well beyond the local large-fracture group into the surrounding low-permeability material. In this way, the local large-fracture group acts as an extended well in a reservoir with permeability equal to that of the medium surrounding the major fractures connected to the well.

Jacob-Lohman Method of Analyzing Constant-Pressure Flow Data

C.E. Jacob and S.W. Lohman (1952) developed a method for analyzing variable-flow-rate data gathered during constant-pressure production similar to the methods developed by Theis (1935) and Cooper and Jacob (1946) for analyzing pressure-drawdown data gathered during constant-rate production. The conditions which must be met in order to maintain constant reservoir pressure are: (1) constant friction head loss in the well casing and discharge line; (2) constant fluid density; and (3) constant backpressure or unrestricted flow. Although all flow tests conducted in ERDA-6 and WIPP-12 were free-flow tests, only ERDA-6/Flow Test 3 and WIPP-12/Flow Test 2 meet the three requirements for true constant-pressure production (D'Appolonia, 1982, v. IIIB,

Addendum 1). These are the only tests that were analyzed by the Jacob-Lohman method. ERDA-6/Flow Tests 1 and 2 were eliminated due to non-constant fluid density (discharge of heavy drilling fluids) (D'Appolonia, 1982, v. IIIA). WIPP-12/Flow Test 3 was eliminated due to changing backpressure caused by salt crystallization in the flow lines (D'Appolonia, 1982, Addendum 1).

The Jacob-Lohman method was used to test for the degree of conformance to assumptions of homogeneity and infinite-acting behavior. It was not relied on for quantification of reservoir properties because the brine reservoirs were found to be finite, heterogeneous, and probably anisotropic, and thus in violation of assumptions on which the analytical technique is based. The field data, plotted as 1/Q versus log t, did not plot as the desired straight line until near the end of the flow tests. This indicated that the flow rate was dropping more quickly than the theory predicted, suggesting depletion of fractures (heterogeneity) and/or boundary effects. For this reason, the method was more useful in defining what the reservoirs are not, than what they are. The results of the Jacob-Lohman analyses were not used quantitatively, although they agreed reasonably well with the Horner analyses (see Table H.4).

Log-Log Type-Curve Analysis

Modern type-curve analysis is the most versatile method of reservoir evaluation available. This versatility is due to the fact that type curves can be developed for any reservoir model for which analytical equations exist (in more complex situations, numerical models can be used). The type curves under consideration were developed for analysis of pressure-drawdown data during a constant-rate flow period in a reservoir showing double-porosity response (Bourdet and Gringarten, 1980). They may also be used to analyze buildup data under certain conditions.

The tests analyzed with the Bourdet-Gringarten type curves are: ERDA-6/DST-2680-2/Second Buildup, ERDA-6/Flow Test 1/Buildup, ERDA-6/Flow Test 2/Buildup, WIPP-12/Flow Test 2/Buildup, and WIPP-12/Flow Test 3/Buildup. The data from the ERDA-6 tests were analyzed by D'Appolonia personnel, and the data from the WIPP-12 tests were analyzed by Johnston-Macco petroleum engineers.

The hypothetical Horner plot showing double-porosity response in Figure H-3 and the Bourdet-Gringarten type curves are based on the same theory with the exception of wellbore conditions being included in the type curves. Because the Horner plots of the actual field data do not show two parallel straight lines, the argument for analyzing the data with the double-porosity type curves is questionable. This is especially true considering the apparent influence of boundaries on the data; boundaries were not included in development of the type curves. The basic difference between the actual reservoir conditions and the assumptions used to develop the double-porosity model is that of the uniformity of heterogeneity distribution. The Castile brine reservoirs do not behave as infinite, uniformly-distributed heterogeneous reservoirs, as evidenced by the shape of the Horner plots. For this reason, and in spite of the fact that data can be matched to a double-porosity type curve, the parameters resulting from such an analysis cannot be trusted.

Although log-log type-curve analyses were not used quantitatively, log-log plots of test data were used to indicate the proper portions of the curves to be used for Horner analyses. For example, a unit slope in the data on a log-log plot indicates wellbore storage-affected data, and these data should not be used for reservoir characterization.

Extended Muskat Method of Analyzing Late Buildup Data

A method of estimating permeability, average reservoir pressure, and reservoir volume was developed by Muskat (1937). The method is based on radial flow in a bounded, cylindrical reservoir, and uses data that are clearly influenced by the boundaries. Because of the boundary effects visible on Horner plots, this method was thought to hold promise for analyzing the boundary-affected data from ERDA-6 and WIPP-12. Since Muskat's original work, other researchers have found that the method is very sensitive to reservoir shape (e.g., Earlougher, 1977). Furthermore, whether the flow and buildup periods were maintained long enough to elicit the behavior predicted by the Muskat method is difficult to determine. Probably because of a lack of data on the shape of the ERDA-6

reservoir, the analysis of the buildup data from Flow Test 1 by this method yielded permeabilities somewhat inconsistent with those calculated by the Horner method. Although the reservoir volumes were in general agreement with those calculated in Section 3.4.3, without definite information on the shape of the reservoir, little confidence can be placed in the results of the method. For this reason, the results of the Muskat volumetric analysis are not reported. Boundary effects were not sufficiently well delineated in data from WIPP-12 to warrant application of the Muskat method to those data.

Linear-Flow Analysis Method for Flow Period Data

The majority of analytic methods for reservoir testing are based on the assumption that fluid flows radially towards the producing well. However, if a well intersects a highly conductive fracture, the liquid-production surface may no longer be limited to the wellbore, but may include the fracture. In this situation, the flow pattern may become linear with equipotential surfaces parallel to the plane of the fracture. In light of the observations of brine flow from fractures in the ERDA-6 and WIPP-12 boreholes, linear-flow analysis techniques appeared appropriate.

Muskat (1937) first recognized and developed solutions for linear flow. Earlougher (1977) presented a review of analytical methods for many types of fracture-affected test data. The method used here is after Jenkins and Prentice (1982). This method is restricted to absolutely linear flow, whereas the modification of the Horner method for correction of the effects of a major vertical fracture is applicable to all degrees of radial and linear flow. The method was developed for analyzing drawdowns given a constant discharge rate. Because the ERDA-6 and WIPP-12 flow periods were conducted as variable-discharge-rate, constant-pressure tests, the field data required conversion to the corresponding constant-rate data. This conversion was conducted based on a process developed by Jacob and Lohman (1952) who noted that the difference between the ratio of discharge to drawdown for the two testing procedures quickly becomes small during a flow period.

This method was used to analyze the flow period data from ERDA-6/Flow Test 3 and WIPP-12/Flow Test 2. The remaining flow tests did not meet the requirements of constant-pressure production as detailed in the discussion on the Jacob-Lohman method. For this reason, the conversion of flow-rate-decline data to pressure-decline data could not be performed for utilization of this technique.

The only factor that introduced uncertainty into this analysis was the use of calculated drawdown data instead of true field measurements. The error in this conversion is a function of elapsed flow time, being greatest at the beginning of the test and quickly becoming small as flow time increases. Because the plots of $\sqrt{t}$ versus calculated drawdown for ERDA-6/Flow Test 3 and WIPP-12/Flow Test 2 show linearity only in mid- to late-time data, no analysis error due to the data manipulation is expected.

Under common fracture conditions, linear flow predominates in early time, followed by elliptical flow, and eventually radial flow at late times (Jenkins and Prentice, 1982). Linearity of the ERDA-6/Flow Test 3 plot begins at 1440 minutes of flow time, and that of the WIPP-12/Flow Test 2 plot begins at 100 minutes of flow time; in both cases the linearity extends to the end of the test, possibly indicating a very long period of linear flow. A major problem with this interpretation is that for infinite-acting linear flow to occur at late times, the fracture connecting with the wellbore must extend nearly the entire width of the reservoir, and the reservoir must be effectively infinite in the directions perpendicular to the plane of the fracture. A highly anisotropic medium, with the major principal direction of permeability perpendicular to the plane of the fracture, could also prolong linear-flow time.

Although this technique indicated the possibility of linear flow to major vertical fractures connected to both the ERDA-6 and WIPP-12 wells, this type of analysis cannot explain the data as fully as the modified radial-flow method. Due to the concerns stated above and the availability of an alternate

interpretation (radial flow), the absolutely linear flow model is not considered tenable. Furthermore, without data from an observation well, this method can only provide the value of a lumped parameter involving fracture length, transmissivity, and storativity. As such, its utility in quantifying reservoir properties is limited. This method was therefore not used quantitatively.

Conclusions

As explained over the preceeding pages, the Horner method was initially used in qualititative interpretation of the buildup data. These interpretations were used to select specific analytical methods which would test the validity of the qualitative interpretations. The results of these various analytical methods, and their implications relative to the proper reservoir model choice, are also discussed. The result of this elimination process was that the Horner method, modified for the effects of fracturing, was selected as the most appropriate analytical method. All permeabilities reported in Sections 3.4.3 and 3.4.4 are the results of Horner analyses.

3.3.5 Analytic Methods for Reservoir Volume Determination

The volume of brine reservoirs in the Castile Formation was thought to have a potential bearing on the suitability of the WIPP site. Knowledge of reservoir volumes is of interest because it contributes to the assessment of the geographical extent of the reservoirs, to a determination of the origin of these features, and to modeling the consequences of interconnecting brine reservoirs and the WIPP facility.

Before the volume of a reservoir can be determined, the reservoir must be defined. The simplest reservoirs consist of homogeneous media with single types of porosity and distinct impermeable boundaries. With such a reservoir, the pore volume may be determined by measuring the permanent pressure depletion caused by removing a measured volume of fluid. The brine reservoirs in the Delaware Basin, however, are more complex. They are typically associated with antiform features within the anhydrite members of the Castile Formation,

and consist of heterogeneous media with multiple fracture sets and poorly-defined boundaries. As described in Section 3.3.1, the working hypothesis is that the ERDA-6 and WIPP-12 brine reservoirs consist of multiple interconnected fracture sets of various sizes. The large fractures intersected by the wells, designated the "local large-fracture group", have high permeabilities but little brine storage capacity because of their low density. The microfractures have relatively low permeabilities, but account for the majority of the brine storage because of their greater density and/or because they may act as low-permeability conduits connecting other large-fracture groups to the wellbore.

In a sense, the large fractures have created the reservoirs (Aguilera, 1980). The large fractures provide a collection system similar to an infiltration gallery for the brine in the microfractures. They provide production surfaces which concentrate diffuse flow from large volumes into discrete channels. Jenkins and Prentice (1982) have termed such a production surface intercepted by a well an "extended well." Without the large fractures, the low-permeability microfractures would be unable to supply significant quantities of brine to any discrete location. The flow tests at ERDA-6 and WIPP-12 demonstrate that after initial high flow rates, pressures in the large fractures decrease and flow rates decrease. If the well is then shut in and brine in the microfractures is allowed to recharge the large fractures, the cycle may be repeated, albeit at slightly lower flow rates and pressures. If long-term constant-pressure production is sought however, flow rates will drop off as the low permeability of the microfractures comes to dominate the flow regime. Flow may continue indefinitely, but at miniscule rates. A lower limit for the volume of the reservoir may then be defined as the maximum volume which can be produced (by artesian flow and/or pumping) during the period when the high permeability of the large fractures dominates the flow system. This volume is the volume of the local large-fracture group plus whatever small contribution the microfractures can make during the short time required to drain the large fractures.

The ERDA-6 and WIPP-12 brine reservoirs are interpreted to be fractured heterogeneous reservoirs. In a fractured heterogeneous reservoir, the fluid pressure in the large fractures may react quickly when fluid is removed, while the fluid pressure in the microfractures may exhibit a delayed response due to low permeability. The effect of the microfracture response is to counteract the pressure depletion in the large fractures as the entire system strives to regain equilibrium. This creates difficulties in measuring the pressure depletion in the large fractures which has resulted from the removal of fluid, because that depletion is not permanent. To quantify large-fracture volume, the response of the fluid present in the large fractures must be separated from the response of the fluid in the microfractures.

A semi-log Horner plot of pressure-buildup data collected after a short-term flow test offers the opportunity to separate large-fracture response from microfracture response. If a flow period is very short, the fluid produced will come predominantly from the large fractures because the microfractures will not have time to respond significantly. The buildup from such a flow period should likewise show an initial response due predominantly to large fractures before the microfractures have a chance to respond. (In the buildup from a long flow test, the large-fracture response will comprise a smaller percentage of the total pressure recovery.) Figure H-4 provides an example of this. The segment of the buildup curve labeled "A" represents the large-fracture response alone. The segment labeled "B" represents the effects of the large-fracture boundaries. In segment "C", production comes predominantly from the microfractures. If the "C" segment is extrapolated to infinite time, the corresponding pressure approaches full recovery, representing the infinite-acting nature of the microfractures. Some portion of the buildup in segment "C" may be caused by rock creep physically decreasing the size of the reservoir, which would raise the pressure in the reservoir.

In the buildup from a very short flow test, the local large-fracture group may respond as a bounded system before the low-permeability microfractures have

the time to react significantly. The pressure depletion measured by extrapolating the "B" segment to infinite time may therefore be used to calculate the large-fracture volume, with a small allowance for flow from the microfractures.

Reservoir fluid volume can be calculated using the equation:

$$V = \frac{\Delta V}{\Delta p \; c_t} \qquad \text{[Eq. 5]}$$

where V is the reservoir fluid volume, ΔV is the volume produced from the reservoir, Δp is the change in pressure of the reservoir, and c_t is the total system compressibility.

Total system compressibility (c_t) is equal to pore compressibility (c_p) plus fluid compressibility (c_f). Pore compressibility was discussed in Part II, Geology, Sections 4.1.5 and 4.1.8. Fluid compressibility is a combination of brine and gas compressibility, and is defined as:

$$c_f = (1 - x)\, c_b + x\, c_g \qquad \text{[Eq. 6]}$$

where c_b is the brine compressibility, c_g is the gas compressibility, and x is the volumetric proportion of undissolved gas present in the reservoir. Estimates of the volumetric proportion (x) of undissolved gas under static reservoir conditions have been made for WIPP-12 and ERDA-6 (see Part IV, Chemistry, Section 4.3.2). At ERDA-6, all of the gas is estimated to be dissolved and x is zero. At WIPP-12, small amounts of methane and nitrogen are not dissolved, and x is estimated to be approximately 0.7 percent. The compressibility of the undissolved gas is approximately 600×10^{-6} psi^{-1}. Due to the small percentage of gas present, the effect on fluid compressibility is small. Using the above figures, fluid compressibilities of the ERDA-6 and WIPP-12 reservoirs are approximately 2×10^{-6} psi^{-1} and 6×10^{-6} psi^{-1}, respectively. Because these fluid compressibilities are considerably smaller than the uncertainties in the pore compressibility estimates, total system

compressibilities will be approximated simply by the estimates of pore compressibilities.

Equation 5 may be used to estimate a minimum value for the total reservoir volume, using the total volume produced from the reservoir and the difference between the initial shut-in pressure prior to all flow and the most recent pressure measurement. This volume will be much greater than the volume calculated for the local large-fracture group due to contributions from micro-fractures, but will only represent the portion of the reservoir affected up to the time of the measurement. If the pressure transient continues to expand in the reservoir, the shut-in pressure will continue to increase, increasing the reservoir volume estimate. Alternatively, if any portion of the late-time buildup is due to rock creep, the reservoir volume estimate will be too large.

See Sections 3.4.3 and 3.4.4 for the volume estimates of the ERDA-6 and WIPP-12 brine reservoirs, respectively.

Limitations of Analytic Methods for Reservoir Volume Determination

The largest degree of uncertainty in using the fracture volume equation presented above (Equation 5) is associated with the pore compressibility, c_p. The wide range of estimated pore compressibilities presented in Part II, Geology, Sections 4.1.5 and 4.1.8, reflects this degree of uncertainty. Estimates of reservoir volume which follow show a range of values corresponding to the range of compressibilities. Uncertainties regarding rock creep also serve to render total reservoir volume estimates tentative.

3.3.6 Analytic Methods for Prediction of Future Brine Production

In modeling the possible consequences of interconnecting a brine reservoir with the WIPP facilities, the volumes of brine which could conceivably flow from the Castile brine reservoirs might be of interest. However, the magnitudes of these volumes in no way affect the extreme unlikelihood of such an interconnection occurring in a time frame of interest without human intervention.

The volume of brine which can be produced from a reservoir is always less than the volume in storage. Artesian flow ceases as the pressure head is depleted, and pumping stops when the formation can no longer supply enough fluid to keep the pump operating, even though in both cases there remains substantial fluid in storage. For any single flow period, the maximum volume of brine which can flow at a given elevation is governed by the head in the reservoir which is in excess of that elevation. By rearrangement of Equation 5, this may be expressed as:

$$\Delta V = V \Delta p c_t \quad [Eq. 5A]$$

From the standpoint of radionuclide mobilization, which may involve time-dependent reactions, the rate of flow is, in some respects, more important than the total quantity of flow. An effort was made, therefore, to quantify the flow rates which might be expected were the reservoirs allowed to flow unhindered. In the petroleum industry, this procedure is known as decline curve analysis. In a very general sense, it involves the extrapolation of observed flow-rate declines during long flow periods to longer periods of time. Extrapolation techniques may be either theoretically or empirically based. Fetkovich (1980) presented empirically derived methods of predicting declines in flow rates with time for homogeneous systems. Jacob and Lohman (1952) presented a theoretically derived type curve for flow-rate declines in infinite, homogeneous systems (see Figure H-10). Da Prat et al. (1981) presented a type-curve method for predicting production declines in finite homogeneous and double-porosity systems (see Figure H-10). Because of the dual response common to both classical double-porosity and fractured heterogeneous sytems, double-porosity decline curves may be used qualitatively to predict general features of flow-rate declines in fractured heterogeneous systems. For double-porosity systems, Da Prat et al. found that after a sharp initial decline in flow rate, representing fracture depletion, there is a long period of relatively constant flow, representing combined matrix and fracture flow, before the final decline in flow rate representing total system

depletion. A similar response may be expected from a fractured heterogeneous system, as first the local large-fracture group is depleted, followed by the more prolonged depletion of the microfracture system.

3.4 RESULTS OF TESTING

Data from the hydrologic testing program were analyzed using the methods discussed above. All data acquired during the present testing program were thoroughly examined. In many cases, however, the data had to be rejected as unreliable because of technical limitations of the instrumentation used (e.g., the choke effect in DST tool entry ports) or operational/mechanical deficiencies (e.g., heavy mud in the hole affecting flow rates; leaky blowout preventer or lubricator). In some cases, the discrepancies between the assumptions of certain analytical methods and existing conditions were too large to consider analysis results reliable. Only the most reliable data and only the analytical methods best suited to the actual reservoir conditions were used to quantify reservoir properties in this report. Less reliable results were used as qualitative backup. All data not explicitly interpreted in this report are contained in D'Appolonia (1982).

3.4.1 Hydraulic Connectivity/Isolation Assessment

This section presents the results of analyses performed to assess the degree of hydraulic connection between the Castile reservoirs of ERDA-6 and WIPP-12, and between these reservoirs and other ground waters. Three types of approaches were outlined in Section 3.3.2 for use in this analysis: (1) implications of high (and different) hydraulic heads observed for various brine reservoirs and ground-water systems; (2) analysis of the distribution of brine occurrences in the Delaware Basin; and (3) interference testing (monitoring of pressure in observation wells during flow and buildup tests).

Implications of the High (and Different) Hydraulic Heads Observed in the Castile Formation

All known Castile brine reservoirs flow at ground surface and have hydraulic heads higher than any other water-bearing formation known in the Delaware Basin. Figures H-11 and H-12 present the hydraulic heads of the reservoirs

and formations of interest in this discussion. Figure H-11 presents these data as a plot of pressure versus depth, and Figure H-12 presents total hydraulic head values referenced to mean sea level and calculated for the specific gravity of pure water. Figure H-13 presents the spatial distribution of known reservoir heads.

Because the hydraulic heads of the Castile reservoirs are higher than those of the fluid-bearing formations both above and below the Castile Formation, the only potential flow direction between formations is from the Castile both upwards and downwards. Furthermore, because the Castile heads, which range from 4680 feet in WIPP-12 to 5551 feet in ERDA-6, are higher than heads at the highest known potential recharge zone for Delaware Basin ground waters (3900 feet at the outcrop of the Capitan reef) (Powers et al., 1978), the Castile reservoirs cannot receive recharge through infiltration from the surface.

Given that the most recent tectonic event which could have contributed to the formation of the Castile domal structures (and by inference, the reservoirs) occurred over one million years ago (Part II, Geology, Section 4.3.2), along with the fact that Castile brine reservoirs can receive no recharge from an outside source, the maintenance of these high hydraulic heads can only be due to the extremely low permeabilities of the Castile and Salado Formations and the resulting isolation of the Castile brines. A similar argument can be applied in concluding that the WIPP-12, ERDA-6, Belco, and Gulf Covington reservoirs shown in Figure H-13 are isolated from one another due to the presence of non-communicative matrix. The persistence of high, and different, hydraulic heads within the Castile Formation is evidence of the lack of connectivity between the Castile brine reservoirs and between the Castile Formation as a whole and other ground waters in the basin.

The above argument explains the maintenance of the high hydraulic heads in the Castile Formation but does not explain their origin. Part II, Geology, Section 4.3.3 provides a discussion of possible origins of high hydraulic heads.

Observation of Brine Occurrences

Table H.1 presents data on the documented brine occurrences in the Castile Formation in the vicinity of the WIPP site. As indicated in Table H.1, all these wells flowed at ground surface with initial flow rates ranging from about 700 to 20,000 barrels per day, indicating substantial elevated local permeability. Drilling data from the northern Delaware Basin in general suggest that substantial volumes of brine are encountered only in discrete locations in fractures which appear to be associated with antiformal structures; no evidence exists to suggest a regional, homogeneous aquifer in the Castile Formation.

In summary, observations of the occurrences of brine in the Castile Formation suggest the existence of separate reservoirs. This conclusion is supported by the following points: (1) measurable amounts of brine only occur in association with fractures; (2) fracturing of the anhydrite members of the Castile Formation appears to be associated with antiform structural features (Part II, Geology, Section 4.2); and (3) these antiform structural features are non-continuous. The number of reservoirs represented by the thirteen documented brine occurrences cannot be determined with the available data. Given the hydraulic head differences which exist between the WIPP-12, ERDA-6, Belco, and Gulf Covington wells, and chemical differences in the brines from the ERDA-6 and Union wells (see Part IV, Chemistry, Section 3.3), a minimum of five reservoirs is suggested.

Interference Testing

During testing of the ERDA-6 brine reservoir, pressures were monitored in observation well AEC-7 at the request of the New Mexico Environmental Evaluation Group. (AEC-7 encountered small quantities of fluid at sub-artesian pressure.) Upon interception of the brine reservoir and testing in WIPP-12, ERDA-6, at that time under shut-in conditions, was utilized as a primary observation well. Observations continued at AEC-7 until December 16, 1981. No pressure changes in any of these wells which could indicate any degree of hydraulic connection between flowing and observation wells were observed.

The pressure data obtained from ERDA-6 during flow testing (depressurization) of the WIPP-12 reservoir show continuously rising pressure (Figure H-14, tabulated data in D'Appolonia, 1982, Addendum 1, 12.19). This rising trend reflects pressure recovery in response to the last flow test performed in ERDA-6 in November, 1981. There is no indication that this pressure trend was affected by testing at WIPP-12. This was the expected result; the ERDA-6 and WIPP-12 reservoirs were intercepted in what are interpreted to be different anhydrite members of the Castile Formation which are thought to be continuously separated from each other by halite (Figure H-15). Furthermore, the reservoir tests at both sites indicate limited zones of large-fracture-enhanced permeability. Thus, the reservoirs are limited in areal extent even within their respective anhydrite members.

If the reservoirs were connected by a fracture system, the fracture distribution would be expected to coincide with the distribution of the antiforms. This distribution would not be uniform. Connection (if any) of highly fractured zones in the flanks or crests of different antiforms could be through interconnecting fold arms bounded by large zones of unfractured rock. The storage capacity of such a fractured reservoir system would be very small compared to a uniform fracture-distribution arrangement for the entire anhydrite layer. For this reason, interference test equations based on radial flow (uniform fracture distribution) could greatly underestimate the propagation of pressure drawdown in the reservoir. This fact made quantitative predictions of the pressure response which might have been expected during the interference tests impractical.

Pressure data recorded in AEC-7 during depressurization and testing of the ERDA-6 brine reservoir showed continuously falling pressure (Figure H-16, tabulated data in D'Appolonia, 1982, 12.19). This trend, however, began prior to depressurization of the ERDA-6 brine reservoir, and did not appear to be influenced by flow tests and pressure buildups either in ERDA-6 or WIPP-12.

This information however, should be treated with caution because the stratigraphic units from which brine was produced in ERDA-6 (Anhydrite II) and WIPP-12 (Anhydrite III) were not isolated (packed off) in AEC-7. The open borehole system is very insensitive to small pressure changes. A contributing factor to the pressure decline of 2.1 psi over two months in AEC-7 may have been the emplacement of the transducer in the wellbore, which would have displaced the water level by about one foot, followed by a slow decay to its original level.

In summary, the results of interference testing indicate that hydraulic connections between the ERDA-6 and WIPP-12 reservoirs, and the ERDA-6 or WIPP-12 reservoirs and AEC-7, do not exist, or the degrees of connection are too low to be measured by the methods employed in this investigation. Additionally, the fact that hydraulic head differences have persisted between the reservoirs and the AEC-7 fluid over at least a million years indicates that any degree of connection which might exist is of an order too low to be detected by any existing interference testing techniques, and therefore is of no significance to site suitability.

3.4.2 Potential for Brine Flow to WIPP Facilities

No attempt has been made to assess quantitatively the flow rate into the waste disposal horizon due to the presence of pressurized brine in the underlying Castile Formation. The following is a discussion of the general hydrologic features which would control such flow.

The fact that the Castile brine reservoirs have maintained high hydraulic heads over at least the last million years indicates that very little vertical migration of brine has occurred under the existing hydraulic gradient. In effect, the reservoirs appear to be totally isolated. The existing head at the waste disposal horizon prior to the construction of underground openings may be approximated by a column of brine extending from the surface to the disposal horizon. At a pressure gradient of 0.5378 psi/ft, such a column would exert a pressure of about 1154 psig at the disposal horizon. By comparison, the pressure in the WIPP-12 wellbore at the disposal horizon is

about 1395 psig. The pressure differential between the WIPP-12 reservoir and the disposal horizon under present conditions, which is directly proportional to the hydraulic gradient, is therefore 1395 - 1154 = 241 psi. When the waste disposal facility is opened, the pressure at the disposal horizon will drop to atmospheric (0 psig). The pressure differential will then be 1395 psi, approximately a six-fold increase. The disposal facility will only be open for a few tens of years, after which it will be sealed and the pressure will return to its present state as salt creep closes the facility openings over perhaps a thousand years (Case et al. (1982) suggest 35 percent closure after 250 years). If no flow has occurred under the existing hydraulic gradient over at least one million years, no flow will occur if the gradient is increased by a factor of six for a thousand years. Similar calculations can be made which show that no flow from any Castile brine reservoir will affect the waste disposal facility.

3.4.3 Quantification of ERDA-6 Reservoir Model Permeability Distribution

Hydrologic testing in ERDA-6 yielded information on the hydrologic properties of the Anhydrite II member of the Castile Formation. The results of these analyses were grouped into three categories: the first two listed below represent reservoir characteristics, the third is more characteristic of the intact anhydrite.

- Results from relatively short-term hydrologic tests representing the permeability of the local large-fracture group near the wellbore (DST-2680, Flow Test 1).
- Results of relatively long-term hydrologic tests representing the average permeability over an extensive region of the reservoir (Flow Test 2 and Flow Test 3). These values are substantially influenced by low-permeability reservoir components.

- Results of relatively short-term tests conducted at the contact of the Halite II and Anhydrite II members of the Castile Formation (DST-2472). There are no major fractures intercepting this portion of the well and it is not considered as part of the ERDA-6 reservoir.

The permeability of a rock mass does not usually change over the length of time necessary to run a hydrologic test. However, in a heterogeneous reservoir composed of fractures of different sizes with different hydrologic boundaries, the apparent permeability will change over the duration of a test as different elements of the reservoir affect the flow or pressure behavior. Modeling of the flow or pressure response based on boundary locations and shapes has not been attempted due to lack of data. Instead, the effects of these heterogeneities are lumped into the apparent-permeability term reported for the long-term tests. Another possible factor serving to reduce the long-term permeability is evolution of gas in the reservoir and the resulting reduction of permeability to brine. The results of chemical analyses indicate this may be a minor effect in WIPP-12, and will not be a factor in ERDA-6 (Part IV, Chemistry, Section 4.3.2), due to differences in gas contents and pressures in the two reservoirs.

Many terms in the permeability equations have values which are consistent throughout this report, and these are listed below:

$B = 1.0$ RB/STB

$\mu = 1.77$ cp

$r_w = 0.33$ ft

The parameter values unique to individual analyses are listed in the sections referencing those individual tests.

Short-Term Reservoir Tests - During short-term hydrologic tests with relatively high flow rates, pressure drawdown is initially restricted largely to the major fractures. Upon shutting the well in, pressure equalization occurs quickly throughout the well-fracture system, but complete recovery cannot occur without contribution from low-permeability reservoir components. Because of the high pressure gradient in the major fractures, the initial pressure change associated with pressure equalization is large. Analysis of pressure data from this type of test yields permeability values representative of the major fractures near the well.

Table H.2 presents a list of all hydrologic tests performed in ERDA-6; data from those tests marked with an asterisk (*) are analyzed in this report. The tests that fall into the short-term reservoir test category are DST-2680-1 and -2, and Flow Test 1. Flow Test 1 was run with the DST tool downhole and was determined to have the highest quality data. This test was therefore chosen to be representative for this group (tabulated data in D'Appolonia, 1982, v. IIIA, 6.7). Figure H-6 is the Horner plot of the buildup data from Flow Test 1, showing the straight line selected and its slope. The following are the input variables required for calculation of permeability (D'Appolonia, 1982, v. IIIA, 6.7):

ΔV = 152.6 bbl
Q_f = 528 bbl/day
t_p^* = 6.94 hrs
h = 56.5 ft
F > 0.8 (estimation based on curve shape)

As shown in Table H.4, the transmissivity of the local large-fracture group at ERDA-6 is equal to 600 md-ft as calculated by the Horner method. This value corresponds to a permeability of 11 md using a production zone thickness of 56.5 feet. This production zone thickness is equal to the distance from the bottom of the packer element to the bottom of the borehole (D'Appolonia, 1982, v. IIIA). The effect of the F factor is to reduce the estimated permeability

(presented above) by at most twenty percent to take into account the influence of fractures connected to the wellbore.

Long-Term Reservoir Tests - During long-term hydrologic tests when flow rates preceding shut-in are low, the pressure gradient throughout the major fracture system is small. Pressure depletion may occur throughout an extensive region of the reservoir. Upon shutting the well in, pressure equalization still occurs quickly throughout the major fracture system, but since the pressure gradient within the major fracture system is small, the pressure change measured at the well during this equalization will be small. In contrast to short-term testing, the majority of pressure recovery in this case is due to contributions from the low-permeability components of the reservoir. Analysis of pressure data from this type of test yields permeabilities averaged over a large volume of the reservoir.

Tests conducted at ERDA-6 that fall into the long-term reservoir test category are Flow Test 2 and Flow Test 3. The data from Flow Test 2 were determined to be of the highest quality and this test was chosen as representative of the group. Figure H-8 is the Horner plot used for analysis of the buildup data from Flow Test 2 (tabulated data in D'Appolonia, 1982, v. IIIA, 6.8). The Horner straight line and its measured slope are included on Figure H-8. The following are the input variables necessary for calculation of permeability from these data (D'Appolonia, 1982, v. IIIA, 6.8):

ΔV = 1030 bbl
Q_f = 120 bbl/day (liquid only, gas/liquid ratio = 0.43)
t_p^* = 206 hrs (total liquid produced ÷ final liquid flow rate)
h = 56.54 ft

As shown in Table H.4, these analyses indicate that the apparent transmissivity of the ERDA-6 reservoir is 120 md-ft as calculated by the Horner method for tests of this duration. This value corresponds to a permeability of 2.2 md. Tests of longer duration might indicate lower permeabilities than

reported here. This is not due to any time-dependent rock property, but rather the increasing influence of low-permeability heterogeneities on the pressure response. As tests become longer, the apparent reservoir permeability could decrease until it approached the limiting value of the permeability for intact anhydrite.

Short-Term Tests at the Contact of the Halite II and Anhydrite II Members

Tests conducted in ERDA-6 at the Halite II-Anhydrite II contact include DST-2472-1 and -2. The section of the well tested during DST-2472 is not a part of the brine reservoir; results of this test gave information on the average properties of the intact rocks near the contact. The data from DST-2472-1/SBU were determined to be of the highest quality and were therefore chosen to be representative for the group. Figure H-17 is the Horner plot used for analysis of these data (tabulated data in D'Appolonia, 1982, v. IIIA, 6.3). The following are the input variables necessary for calculation of the permeability (D'Appolonia, 1982, v. IIIA, 6.3).

$Q = 0.51$ bbl/day

$t_p = 0.53$ hrs

$h = 90$ ft

The production zone thickness for this test is equal to the distance from the bottom of the packer element to the top of the cement plug (D'Appolonia, 1982, v. IIIA, 6.3) and includes both halite (83 ft) and anhydrite (7 ft). As indicated in Table H.4, the transmissivity calculated from this Horner analysis is 0.23 md-ft and is representative of average rock properties at the contact. This corresponds to an average permeability of 2.5×10^{-3} md over the tested interval, but because anhydrite typically has a higher permeability than halite, this value is probably too low for the anhydrite tested and too high for the halite.

Under test conditions in low-permeability formations, it may take considerable time for the true Horner straight line to develop. As can be seen in Figure

H-17, an extensive straight line has not yet fully developed in the data. Because of this, the permeability value presented here should be considered as a maximum average value.

The permeability of the intact Anhydrite II member was also measured in a core sample using nitrogen as the permeating fluid. Table H.4 presents the results of this test, and as shown, the permeability is 3×10^{-3} md. The much smaller rock masses tested during core tests (core volumes vs. 90 feet of borehole wall) would be expected to have the effect of reducing the measured permeability due to the absence of elevated-permeability heterogeneities in small core samples.

Reservoir Pressure

The maximum pressure measured for the ERDA-6 brine reservoir at the wellhead is 604 psig. Extrapolated to a reservoir depth of 2711 feet below ground surface with a fluid pressure gradient of 0.5326 psi/ft of brine, this corresponds to a reservoir pressure of 2048 psig. As shown in Figure H-12, this pressure corresponds to a potentiometric surface at 5551 feet above mean sea level when calculated for the specific gravity of pure water. This is the highest hydraulic head of any ground-water body known in the Delaware Basin. Section 3.4.1 contains a detailed discussion of hydraulic heads throughout the Delaware Basin.

Following the end of testing in November 1981 and a BOP change in February 1982, the wellhead shut-in pressure at ERDA-6 rose steadily as a result of both reservoir recovery and gas cap formation in the wellbore. A series of apparent gauge-related malfunctions have left the pressure data collected before and after the gas cap release on March 8, 1983 of uncertain validity. The highest pressure measured before the gas cap release was 558 psig on March 5, 1983. Because of a possible fluid leak from a diaphragm assembly attached to the gauge, this value may be too low. The first fully reliable pressure measurement made after the gas cap release was 552 psig on March 19, 1983.

During the gas cap release on March 8, 1983, approximately 510 ft^3 of gas (at STP) were vented from the well (D'Appolonia, 1983). Under the pressure (558 psig?) and temperature (72°F) conditions then existing in the wellbore, this gas would have occupied a volume of about 14 ft^3, corresponding to a maximum gas cap thickness of about 40 feet. Some minor fraction of the gas released probably came from gas exsolution from the brine during the release, however, and is not representative of gas cap volume in the wellbore.

After more than one year of recovery, the ERDA-6 reservoir should be near equilibration. Future increases in wellhead pressure will be predominantly the result of renewed gas cap formation.

Volume and Distribution of Brine Storage

Brine reservoir volume is estimated for two portions of the reservoir: the total reservoir and the volume contained within the local large-fracture group. Volume is calculated using Equation 5 with values of ΔV and Δp considered appropriate for each portion of the reservoir. Total compressibilities of both portions of the reservoir are assumed to be the same. As discussed in Part II, Geology, Section 4.1.8, a range of pore compressibilities has been estimated for ERDA-6. This range of pore compressibilities is based on a porosity range of 0.2 to 2.0 percent, and a bulk modulus range of 1 x 10^6 to 5 x 10^6 psi. In the following volume calculations, single values of porosity and bulk modulus have been selected to provide a "representative" value of pore compressibility which lies approximately in the middle of the range. This representative compressibility value is 50 x 10^{-6} psi^{-1}, which represents a porosity of one percent and a bulk modulus of 2 x 10^6 psi.

Data from the buildup period following Flow Test 1 (D'Appolonia, 1982, v. IIIA, 6.7), were selected as the most suitable for use in calculating the volume of the local large-fracture group of the ERDA-6 reservoir. The reasons for this selection include:

- The flow period of Flow Test 1 was relatively short (5.6 hours), stressing the large fractures more than the microfractures.
- The buildup data exhibit fairly well-defined boundary effects.
- Flow Test 1 occurred early in the testing history of ERDA-6, and the data from that test are largely unaffected by pressure buildup stemming from previous tests.

Immediately prior to Flow Test 1, the downhole pressure in ERDA-6 was 2030 psia. The volume of brine produced during Flow Test 1 was about 153 bbl. Figure H-6 is the semi-log Horner plot for Flow Test 1. The boundary-affected data may be extrapolated to a pressure of 1930 psia at infinite time. The pressure depletion at this point is 2030 psia - 1930 psia = 100 psi. Using the values presented above, the volume of the local large-fracture group at ERDA-6 is:

$$V = \frac{153 \text{ bbl}}{(100 \text{ psi})(50 \times 10^{-6} \text{ psi}^{-1})} = \underline{30{,}600 \text{ bbl}}$$

This volume estimate is corroborated by analysis of buildup data following a minor flow period associated with a blow-out preventer (BOP) change. During the BOP change, 20 barrels of brine flowed from ERDA-6. The Horner plot of the buildup data (Figure H-7) shows very distinct boundary effects. The extrapolated depletion from the boundary-affected data on the Horner plot is about 16 psi. Therefore, the local large-fracture group volume is:

$$V = \frac{20 \text{ bbl}}{(16 \text{ psi})(50 \times 10^{-6} \text{ psi}^{-1})} = \underline{25{,}000 \text{ bbl}}$$

This value is only eighteen percent lower than the volume calculated from the Flow Test 1 data, a minor discrepancy in a mass balance analysis such as this.

The total ERDA-6 reservoir volume may also be estimated using Equation 5, with the total volume of flow since the reservoir was first penetrated and the total pressure depletion associated with that flow used as input parameters.

Approximately 1,650 barrels of brine have been produced from ERDA-6. The maximum surface shut-in pressure recorded at ERDA-6 was about 604 psig. As of March 19, 1983, the surface shut-in pressure was about 552 psig. The total reservoir volume is therefore at least:

$$V = \frac{1650 \text{ bbl}}{(52 \text{ psi})(50 \times 10^{-6} \text{ psi}^{-1})} = \underline{630{,}000 \text{ bbl}}$$

Total reservoir volumes have also been calculated for the ranges of pore compressibility discussed earlier. Figure H-18 presents a plot of total reservoir volume versus porosity and bulk modulus, indicating the probable range of volumes to be from approximately 63,000 barrels to 3,200,000 barrels. These volumes correspond to pore compressibilities of 500×10^{-6} psi^{-1} to 10×10^{-6} psi^{-1}, respectively. The volume estimate based on representative values of porosity and bulk modulus, 630,000 barrels, is also shown on the figure.

Fractures found in core from ERDA-6 indicate that the reservoir may be approximately 56.5 feet thick. Given that thickness and a total effective porosity of one percent, 630,000 barrels of brine could be stored within an area of 6.3×10^6 ft^2. The actual geometry of the reservoir is not known, but the area mentioned above could be represented either by a square 2100 feet on a side, or by a circle with a radius of 1200 feet. Alternatively, if the reservoir extends through the entire 177-foot thickness of Anhydrite II (with one percent porosity), 630,000 barrels of brine could be stored within an area of 2.0×10^6 ft^2.

Future Brine Production

For any single flow period, the volume of brine which could flow from ERDA-6 at the surface is governed by the surface pressure. The maximum surface shut-in pressure recorded at ERDA-6 was about 604 psig. The theoretical maximum volume which could be produced from the ERDA-6 reservoir by artesian flow is therefore:

$$\Delta V = (630{,}000 \text{ bbl})(604 \text{ psi})(50 \times 10^{-6} \text{ psi}^{-1}) = \underline{19{,}000 \text{ bbl}}$$

Likewise, the maximum volume of brine from ERDA-6 which could flow at the elevation of the waste disposal facility is only a fraction of the brine in storage. For the purpose of discussion, the assumptions can be made that the waste disposal facility directly overlies the ERDA-6 reservoir, and the two are connected by an open borehole. In the Exploratory Shaft station, the floor of the disposal facility is at an elevation of about 1265 feet (GFDR No. 5, 1983). The pressure head in ERDA-6 at that elevation is about 1814 psig, whereas the pressure in the disposal facility should be atmospheric (0 psig). The theoretical maximum volume which could flow at that elevation is:

$$\Delta V = (630{,}000 \text{ bbl})(1814 \text{ psi})(50 \times 10^{-6} \text{ psi}^{-1}) = \underline{57{,}000 \text{ bbl}}$$

The volumes of brine which would flow under the above scenarios are independent of the total system compressibility (because c_t cancels with its usage in the calculation of total reservoir volume), and are dependent only on the $\Delta V/\Delta p$ ratios from the flow tests (and the assumption of linearity). Thus, although the total system compressibility and therefore the total reservoir volumes are relatively uncertain, the above flow volumes are considerably less uncertain.

None of the flow tests at ERDA-6 were long enough to provide sufficient data to estimate the long-term flow rate from the microfractures. Based on observations made during Flow Test 2 however, some qualitative conclusions can be drawn regarding future flow rate declines. About 1030 bbl of brine were produced from ERDA-6 during Flow Test 2. During that test, the flow rate dropped from a maximum of about 473 bbl/day to about 120 bbl/day over a period of about 89 hours, with a flow rate half-life of about 50 hours. It is unlikely therefore, that more than a few thousand barrels would flow from ERDA-6 at the ground surface before the flow rate dropped to a few bbl/day. The flow rate would not drop to zero however, but would instead stabilize at

the rate at which the microfractures recharge the large fractures. Considering the slow long-term pressure buildup rate and the low permeability of microfractures, that rate would likely be less than one bbl/day.

3.4.4 Quantification of WIPP-12 Reservoir Model Permeability Distribution

Hydrologic testing in WIPP-12 yielded information on the hydrologic properties of the brine reservoir in the Anhydrite III member of the Castile Formation. The results of these analyses were grouped into similar categories as described for the ERDA-6 test results.

- Results from relatively short-term hydrologic tests representing the permeability of the local large-fracture group near the wellbore.
- Results of relatively long-term hydrologic tests representing the average permeability over an extensive region of the reservoir. These values are substantially influenced by low-permeability reservoir components.

The difference between the short- and long-term test responses is discussed in Sections 3.3.4 and 3.4.3.

As opposed to ERDA-6, no well-test information on intact anhydrite permeability was obtained at WIPP-12. However, permeabilities were measured in core samples from the Anydrite III member in WIPP-12. As shown in Table H.4, the measured permeabilities are less than 2×10^{-4} md. The very small sample volumes tested in core analyses will always have lower permeabilities than would be measured in well tests, due to the effects of rare, high-permeability heterogeneities which cannot be included in core analyses. For this reason, the large-scale, intact anhydrite permeability at WIPP-12 is likely larger than 2×10^{-4} md.

Some input variables, necessary for calculation of permeability, are common to all tests in the ERDA-6 and WIPP-12 reservoirs. The variables common to all

tests have been listed in Section 3.4.3, while the input variables unique to each test are listed in the following sections where reference is made to each test.

Short-Term Reservoir Tests - Table H.3 is a complete list of the hydrologic tests conducted in WIPP-12; data from those tests marked with an asterisk (*) are presented in this report. The tests that are included in the short-term reservoir test category are DST-3020-1 and -2, DST-2986-1 and -2, and Flow Test 2. Due to the very high production rates from the WIPP-12 reservoir and the DST-tool choke effect mentioned in Section 3.2.1, the standard DST's did not provide data of good quality. For this reason, Flow Test 2 was chosen as being representative for the group. Figure H-5 is the Horner plot used for analysis of Flow Test 2 buildup data (tabulated data in D'Appolonia, 1982, Addendum 1, 12.19). The input variables that are unique to Flow Test 2 and are necessary for calculation of permeability are as follows (D'Appolonia, 1982, Addendum 1, 12.19):

ΔV = 2258 bbl
Q_f = 8057 bbl/day
t_p^* = 6.73 hrs
h = 61 ft
F > 0.55 (estimation based on curve shape)

The Horner straight-line slope is shown on Figure H-5. As shown in Table H.4, the transmissivity of the major fractures near the WIPP-12 wellbore is about 1.2×10^5 md-ft as calculated from the Horner method. This value corresponds to a permeability of approximately 2000 md for a production zone thickness equal to the distance from the top of the fissured zone to the bottom of Anhydrite III in WIPP-12 (D'Appolonia, 1982, v. IVB, 12.16, Addendum 1, 12.20). The effect of the F factor is to reduce the estimated permeability (presented above) by at most forty-five percent to take into account the influence of fractures connected to the wellbore.

Long-Term Reservoir Tests - The only long-term hydrologic test conducted on the WIPP-12 reservoir that was controlled adequately for analytical purposes was Flow Test 3 (tabulated data in D'Appolonia, 1982, Addendum 1, 12.20). Figure H-9 is the Horner plot used for analysis of the buildup data from Flow Test 3. The input variables necessary for calculation of permeability from this analysis are as follows (D'Appolonia, 1982, Addendum 1, 12.20):

ΔV = 24,800 bbl
Q_f = 1097 bbl/day
t_p^* = 542.5 hrs
h = 61 ft

As shown in Table H.4, the apparent transmissivity of the WIPP-12 reservoir, for tests of this duration, is 1000 md-ft as determined from Horner analysis. This corresponds to a permeability value of 17 md. The relatively higher long-term permeability at WIPP-12 as compared to ERDA-6 is probably related to the greater large-fracture aperture at WIPP-12.

Reservoir Pressure

The maximum pressure measured for the WIPP-12 reservoir at the wellhead is 208 psig. Extrapolated to a reservoir depth of 3017 feet below ground surface with a fluid pressure gradient of 0.5378 psi/ft of brine, this corresponds to a reservoir pressure of 1831 psig. As shown in Figure H-12, this corresponds to a potentiometric surface at 4680 feet above mean sea level calculated for the specific gravity of pure water. Section 3.4.1 contains a detailed discussion of hydraulic heads throughout the Delaware Basin.

Following the end of testing in June 1982, the wellhead shut-in pressure at WIPP-12 rose steadily as a result of both reservoir recovery and gas cap formation in the wellbore. Just prior to releasing the gas cap on March 7, 1983, the wellhead pressure was about 175 psig. On March 7, 1983, approximately 173 ft^3 of gas (at STP) were released from the well (D'Appolonia, 1983). Under the pressure (175.2 psig) and temperature (58°F)

conditions then existing in the wellbore, this gas would have occupied a volume of about 14 ft^3, corresponding to maximum gas cap thickness of about 33 feet. Some minor fraction of the gas released probably came from gas exsolution from the brine during the release, however, and is not representative of gas cap volume in the wellbore. From March 8 through at least March 20, 1983, the wellhead pressure at WIPP-12 remained steady at about 162 psig. After more than nine months of recovery, the WIPP-12 reservoir should be near equilibration. Future increases in wellhead pressure will be predominantly the result of renewed gas cap formation.

Volume and Distribution of Brine Storage

As with ERDA-6, brine volumes are estimated for the local large-fracture group and the total WIPP-12 reservoir. Volume is calculated using Equation 5 with values of ΔV and Δp considered appropriate for each portion of the reservoir. Total compressibilities of both portions of the reservoir are assumed to be the same. As discussed in Part II, Geology, Section 4.1.5, a range of pore compressibilities has been estimated for WIPP-12. This range of pore compressibilities is based on a porosity range of 0.1 to 1.0 percent, and a bulk modulus range of 1×10^6 to 5×10^6 psi. In the following volume calculations, single values of porosity and bulk modulus have been selected to provide a "representative" value of pore compressibility which lies approximately in the middle of the range. This representative value is 100×10^{-6} psi^{-1}, which represents a porosity of 0.5 percent and a bulk modulus of 2×10^6 psi.

The data from the buildup period following Flow Test 2 were selected as the most suitable for use in calculating the local large-fracture group volume of the WIPP-12 reservoir. The reasons for this selection include:

- The flow period of Flow Test 2 was relatively short (5.54 hours), stressing the large fractures more than the microfractures.

- The buildup data exhibit fairly well-defined boundary effects.
- Flow Test 2 followed several months of undisturbed buildup, and the data from that test are largely unaffected by pressure buildup stemming from previous tests.

Immediately prior to Flow Test 2, the downhole pressure in WIPP-12 was 1808 psia. The volume of brine produced during Flow Test 2 was about 2258 bbl (D'Appolonia, 1982, Addendum 1, 12.19). Figure H-5 is the semi-log Horner plot for the buildup from Flow Test 2. The boundary-affected data may be extrapolated to a pressure of about 1787 psia at infinite time. The pressure depletion at this point is 1808 psia - 1787 psia = 21 psi. Using the values presented above, the volume of the local large-fracture group at WIPP-12 is:

$$V = \frac{2258 \text{ bbl}}{(21 \text{ psi})(100 \times 10^{-6} \text{psi}^{-1})} = \underline{1.1 \times 10^{6} \text{ bbl}}$$

The total WIPP-12 reservoir volume may also be estimated using Equation 5, with the total volume of flow since the reservoir was first penetrated and the total pressure depletion associated with that flow used as input parameters. Approximately 80,000 barrels of brine have been produced from WIPP-12. The maximum surface shut-in pressure recorded at WIPP-12 was about 208 psig. As of March 20, 1983, the surface shut-in pressure was about 162 psig. The total reservoir volume is therefore at least:

$$V = \frac{80{,}000 \text{ bbl}}{(46 \text{ psi})(100 \times 10^{-6} \text{ psi}^{-1})} = \underline{17{,}000{,}000 \text{ bbl}}$$

Total reservoir volumes have also been calculated for the range of pore compressibility discussed earlier. Figure H-19 presents a plot of total reservoir volume versus porosity and bulk modulus, indicating the probable range of volumes to be from approximately 1.7×10^{6} barrels to 8.7×10^{7} barrels. These volumes correspond to pore compressibilities of 1000×10^{-6} psi^{-1} to 20×10^{-6} psi^{-1}, respectively. The volume estimate based on representative values of porosity and bulk modulus, 1.7×10^{7} barrels, is also shown on the figure.

The thickness of the WIPP-12 reservoir is not determinable with the available data. Assuming that the reservoir thickness coincides with the 61-foot thickness tested during the DST's, and that the total effective porosity is 0.5 percent, 1.7×10^7 barrels of brine could be stored within an area of 3.1×10^8 ft^2.

As presented above, the reservoir volume estimates are based on assumptions of total effective porosity and bulk modulus with an associated uncertainty in excess of one order of magnitude. Additionally, the use of the observed pressure depletion in the estimates assumes that rock creep has not occurred.

Future Brine Production

For any single flow period, the volume of brine which could flow from WIPP-12 at the surface is governed by the surface pressure. The maximum surface shut-in pressure recorded at WIPP-12 was about 208 psig. The theoretical maximum volume which could be produced from the WIPP-12 reservoir by artesian flow is therefore:

$$\Delta V = (1.7 \times 10^7 \text{ bbl})(208 \text{ psi})(100 \times 10^{-6} \text{ psi}^{-1}) = \underline{350{,}000 \text{ bbl}}$$

Likewise the maximum volume of brine from WIPP-12 which could flow at the elevation of the waste disposal facility is only a fraction of the brine in storage. For purposes of discussion, the assumptions can be made that the waste disposal facility directly overlies the WIPP-12 brine reservoir, and the two are connected by an open borehole. In the Exploratory Shaft station, the floor of the disposal facility is at an elevation of about 1265 feet (GFDR No. 5, 1983). The pressure head in WIPP-12 at that elevation is about 1395 psig, whereas the pressure in the disposal facility should be atmospheric (0 psig). The theoretical maximum volume which could flow at that elevation is:

$$\Delta V = (1.7 \times 10^7 \text{ bbl})(1395 \text{ psi})(100 \times 10^{-6} \text{ psi}^{-1}) = \underline{2.4 \times 10^6 \text{ bbl}}$$

As noted in Section 3.4.3, these flow volume estimates are independent of total compressibility, and, therefore, are less uncertain than the total reservoir volume estimates.

The only long-term flow test at WIPP-12 was Flow Test 3. Unfortunately, salt precipitation in the flow lines during Flow Test 3 caused significant, unmeasurable variations in backpressure, thereby rendering the flow data unsuitable for analysis using flow-rate decline techniques. Based on observations made during Flow Test 3 however, some qualitative conclusions can be drawn concerning future flow rate declines. About 24,800 bbl of brine were produced from WIPP-12 during Flow Test 3. The flow rate dropped from about 14,700 bbl/day at the start of the test to about 1100 bbl/day at the end of the test, some 210 hours of flow time later, with an initial flow rate half-life of about 18 hours. It is unlikely therefore, that more than about 100,000 barrels would flow from WIPP-12 before the flow was reduced to a few bbl/day. The flow rate would not drop to zero however, but would instead stabilize at the rate at which the microfractures recharge the large fractures. Considering the slow, long-term pressure buildup rate and the low permeability of microfractures, that rate would likely be less than one bbl/day.

4.0 DISCUSSION OF DATA AS RELATED TO ISSUES

In this section, the results of the hydrological investigations are summarized from the viewpoint of their importance to the issues. The issue most relevant to the site's hydrological integrity, i.e., connectivity/isolation of Castile brines, is presented first, followed by the other issues of reservoir volumes, potential for flow to WIPP facility, and origin of brine.

4.1 RESERVOIR CONNECTIVITY

Examination of drilling records, study of reports from previous work, and, most importantly, the results of testing performed recently in the ERDA-6 and WIPP-12 wells, have produced the following observations:

- Hydraulic heads are different in all four Castile brine reservoirs for which pressure data are available.
- Hydraulic heads in the Castile Formation in general are higher than heads in all other ground-water bodies in the Delaware Basin, including potential recharge zones in the Capitan reef outcrop in the Guadalupe Mountains.
- All known brine reservoirs in the northeastern part of the Delaware Basin appear to be associated with antiforms which are geographically separated, although not all antiforms are known to be associated with brine reservoirs.
- No changes in existing pressure trends were detected in observation wells during flow tests performed in WIPP-12 and ERDA-6.

These observations have led to two conclusions concerning the connectivity of the Castile brine reservoirs:

1) The Castile brine reservoirs at ERDA-6 and WIPP-12 are not connected to each other, and other Castile brine reservoirs in the northeastern part of the Delaware Basin are probably also hydraulically isolated from one another.

2) The brine reservoirs of the Castile Formation, and probably all pore waters of the Castile Formation, are isolated from the hydraulic systems in the overlying and underlying Rustler and Bell Canyon formations.

Both of these conclusions were derived largely from consideration of the first two observations listed above.

Brine reservoirs in the Castile are known to have the highest hydraulic heads of any ground waters in the vicinity. In the vicinity of the WIPP site, Castile brine heads range from 1530 to 2570 feet (of pure water) above heads in the Rustler Formation. Similar differences exist between Castile brines and waters in the Bell Canyon Formation. The only other potential recharge

area is the outcrop of the Capitan reef. The highest known head in the Capitan reef aquifer in the vicinity of the WIPP site is 1680 to 2950 feet below the hydraulic heads of Castile brines. Thus, the Castile brines cannot be receiving recharge from these other sources.

The geologic environment with which the brine reservoirs are associated became tectonically stable over one million years ago. The maintenance of excessive and non-equilibrated pressures within the reservoirs over a million years is evidence of their degree of isolation. The only other mechanism for maintenance of these excessive pressures, in the absence of continued diagenesis, would be recharge, which in this case has been shown to be impossible. The isolation of the Castile reservoirs is due to the very low-permeability environment in which they exist. This environment includes 2000 feet of almost impermeable rocks of the Salado Formation ($k < 5 \times 10^{-5}$ md) (Powers et al., 1978) separating the Castile and Rustler formations, and approximately 1000 feet of Castile evaporites ($k \leq 2.5 \times 10^{-3}$ md) separating brines of the Castile from the Bell Canyon Formation.

The same argument, citing head differences, lack of recharge, and geographical separation by low-permeability anhydrite and halite, can be used to conclude that the reservoirs encountered in ERDA-6 and WIPP-12 are not connected. Although few data exist on other brine reservoirs, the conclusion that all other reservoirs are individually isolated is also suggested.

In summary, the findings of the recent study strongly suggest that no hydraulic communication exists between brine reservoirs within the Castile Formation, as well as between the Castile Formation as a whole and neighboring hydraulic systems. In other words, the reservoirs neither receive recharge from outside sources nor appear to contribute to other hydraulic systems.

4.2 RESERVOIR VOLUMES

Understanding the fractured heterogeneous reservoir model is essential to the calculation of brine volumes stored in the ERDA-6 and WIPP-12 reservoirs.

Evidence of the fractured nature of both the WIPP-12 and ERDA-6 reservoirs was gathered during examination of core, analysis of geophysical logs, and analysis of reservoir behavior during flow and pressure buildup tests. These data have led to the following interpretation:

- A limited system of large fractures, designated the local large-fracture group, was intercepted in each borehole. These large fractures serve as high-permeability brine collection systems, but comprise only a small portion of the reservoirs' brine storage capacity. The local large-fracture groups can be viewed as extensions of the wells, and are responsible for the initially vigorous production rates and pressure-buildup rates observed at the beginning of each test. Fracture permeability is a function of fracture aperture. The large-fracture permeability at ERDA-6 is about 10 md, and at WIPP-12 is about 2000 md.

- The large fractures are intersected by numerous microfractures. The microfractures have relatively low permeabilities, but provide access to the majority of the brine stored in the reservoirs. The majority of the brine in storage may be contained within the microfractures alone, or in other large-fracture groups which are only connected to the wellbores by microfractures. After the initially high rates of production and pressure buildup, the major fractures serve mainly as conduits for the brine produced from the microfractures. Production from the microfractures is observed as a prolonged slow production or slow buildup rate.

- The components described above comprise the brine reservoirs as defined for volume determination. These reservoirs are surrounded by intact anhydrite with extremely low permeability which contributes little, if any, brine to the reservoirs.

In summary, the reservoirs consist of large-fracture systems of limited volume subtending a system of matrix blocks cut by microfractures. These reservoirs are surrounded by very low-permeability anhydrite formations. Brine stored in the microfractures eventually recharges the large-fracture systems to near their original pressures. This phenomenon is illustrated by the late-time response on the Horner plot in Figure H-4.

The total brine storage in the WIPP-12 reservoir was estimated to be 1.7×10^7 barrels, with approximately one million barrels stored in large fractures. The ERDA-6 reservoir is significantly smaller. It is estimated to hold about 630,000 barrels, 30,000 of which are stored in large fractures. Part of the large difference in reservoir storage can be explained by the fact that the large fractures in WIPP-12 have permeabilities about 200 times higher than the large fractures in ERDA-6. Hence, their aperture and storage capacity must be correspondingly larger. Differences in storage capacity might also be related to the relative extents of the two fracture systems, but no data are available on that subject.

4.3 POTENTIAL FOR BRINE FLOW TO WIPP FACILITIES

There are several possible avenues for pressurized brines of the Castile Formation to enter the WIPP facility. These include:

- Upward seepage of brine through the halite of the Salado Formation under the induced hydraulic gradient.
- Dissolution of evaporites and associated movement of brine.
- Movement of brine through unplugged boreholes.
- Flow of brine through fractures induced by mining activities.

The only potential conduit which may be established without human intervention and which can be evaluated solely on the basis of hydrologic evidence is upward seepage through Salado halite from the upper Castile.

The Castile brine reservoirs have remained isolated for at least a million years under the existing hydraulic gradient. The six-fold increase in the hydraulic gradient between the WIPP-12 reservoir and the waste disposal facility which will accompany the opening of the facility will not be sufficient, in the thousand years the facility openings and the gradient

exist, to affect the isolation of the WIPP-12 reservoir. Other reservoirs will also be unaffected by the temporary opening of the WIPP facilities.

4.4 ORIGIN OF RESERVOIRS AND BRINE

The origin of fluids which have accumulated to create the Castile brine reservoirs is discussed in Part IV, Chemistry, Section 5.1. Explanation of the mechanism for brine accumulation into reservoirs is more an issue subject to hydrologic analysis. To this end, a general review of theories on the development of fractured reservoirs was conducted. The findings of this review were that many reservoir-creation mechanisms fit with the brine origin theory and could explain the observed pressures. The following is the simplest theory, which in our opinion, best accords with the data.

- The Castile evaporites, along with connate water, were deposited in a plastic, low-permeability stratigraphic sequence during Permian time. Increasing thickness of the overburden in combination with hydraulic isolation and high plasticity caused the connate water to become over-pressurized relative to present conditions.

- Density contrast between halite and anhydrite in the Castile Formation resulted in the formation of domal structures in the halite, possibly triggered by basinal tilting (Part II, Geology, Section 4.3). Anhydrite beds, being more rigid than the ductile halite, developed a system of tensional cracks over the domes as they underwent folding and lengthening.

- Upon fracturing of the brittle anhydrite by extensional forces, the brine migrated from the rock matrix toward the zone of dilatancy due to the relative vacuum produced by the fractures. Vertical confinement was provided by overlying and underlying halite beds. Development of fractures, in other words, provided additional room for brine storage and resulted in reduction of reservoir pressure to below ancient pore pressure. Different hydraulic heads noted in various Castile brine reservoirs may be explained by different degrees of fracturing in anhydrite beds.

No viable theory is recognized that can explain the present hydrostatic heads of the Castile Formation by referencing them to present ground-water flow systems.

NOMENCLATURE

SYMBOLS

B	Formation volume factor, RB/STB
C	Wellbore storage constant (coefficient, factor) RB/psi
c_b	Brine compressibility, psi^{-1}
c_f	Fluid compressibility, psi^{-1}
c_g	Gas compressibility, psi^{-1}
c_p	Pore compressibility, psi^{-1}
c_t	Total system compressibility, psi^{-1}
F	Fracture correction factor for Horner plots
H	Hydraulic head, ft
h	Formation thickness, ft
K*	Hydraulic conductivity, ft/day, cm/sec
K	Bulk modulus, psi
k	Permeability, md
k_f	Fracture permeability, md
k_m	Matrix permeability, md
L	Fracture length, ft
log	Logarithm, base 10
m	Slope of semi-log straight line, psi/log cycle
p	Pressure, psi
Δp	Pressure change, psi
p_{ext}	Extrapolated pressure, psi
p_i	Well pressure prior to test, psi
p_o	Initial pressure, psi
p_w	Bottom-hole pressure, psi
Q	Flow rate, bbl/day
Q_f	Final flow rate, bbl/day
r	Radius, ft
r_w	Wellbore radius, ft
RB	Reservoir barrels (volume at reservoir temperature and pressure)

SYMBOLS

S	Storativity
s	Van Everdingen-Hurst skin factor
STB	Stock tank barrels (volume at 60°F and 14.65 psi)
STP	Standard temperature (0°C) and pressure (1 atm)
T	Transmissivity, ft^2/day or cm^2/sec
t	Time, hours
t_D	Dimensionless time
Δt	Elapsed shut-in time
Δt_f	Final elapsed shut-in time
t_p	Equivalent time well was on production or injection before shut-in, hours
t_p^*	Modified production time for pressure buildup analysis with variable rate before shut-in, hours
V	Volume, bbl
ΔV	Volume produced, bbl
x	Volumetric proportion of undissolved gas in brine
α	Block shape parameter, ft^{-2}
γ	Specific gravity; referenced to water for liquids, to air for gases
Δ	Difference or change
λ	Interporosity flow parameter
μ	Viscosity, cp
ϕ	Porosity, fraction
ω	Storativity ratio
∂	Partial derivative

LIST OF REFERENCES

Aguilera, R., 1980, Naturally Fractured Reservoirs: Penn Well Publishing Co., Tulsa, Oklahoma, 703 pp.

Bourdet, D. and A. C. Gringarten, 1980, Determination of Fissure Volume and Block Size in Fractured Reservoirs by Type-Curve Analysis: paper SPE 9293 presented at the 55th Annual Fall Technical Conference and Exhibition of the SPE of AIME, Dallas, Texas.

Case, J. B., S. M. Dass, J. G. Franzone, and A. K. Kuhn, 1982, Analysis of Potential Impacts of Brine Flow Through Boreholes Penetrating the WIPP Storage Facility: TME 3155, U.S. Dept. of Energy, Albuquerque, New Mexico.

Cooper, H. H. and C. E. Jacob, 1946, A Generalized Graphical Method for Evaluating Formation Constants and Summarizing Well Field History: Trans. Amer. Geophys. Union, v. 27, pp. 526-534.

D'Appolonia Consulting Engrs. Inc., 1983 (in preparation), Data File Report: ERDA-6 and WIPP-12 Testing, Addendum 2: prepared for Westinghouse Electric Co. and U.S. Dept. of Energy, Albuquerque, New Mexico.

D'Appolonia Consulting Engrs. Inc., 1982, Data File Report: ERDA-6 and WIPP-12 Testing: prepared for Westinghouse Electric Co. and U.S. Dept. of Energy, Albuquerque, New Mexico, 7 volumes.

Da Prat, G. H., H. Cinco-Ley, and H. J. Ramey, Jr., 1981, Decline Curve Analysis Using Type Curves for Two-Porosity Systems: Soc. Pet. Engr. Jour., June, pp. 354-362.

Earlougher, R. C., Jr., 1977, Advances in Well Test Analysis: Soc. Pet. Engr. of AIME Monograph, v. 5, 264 pp.

Ehlig-Economides, C. A., 1979, Well Test Analysis for Wells Produced at a Constant Pressure: Ph.D. Dissertation, Dept. of Pet. Engr., Stanford Univ. 117 pp.

Fetkovich, M. J., 1980, Decline Curve Analysis Using Type Curves: Jour. of Pet. Tech., June, pp. 1065-1077.

GFDR (Geotechnical Field Data Report) No. 5, 1983, Geologic Mapping of Access Drifts, "Double Box" Area: compiled for U.S. Dept. of Energy by TSC-D'Appolonia, January 8, 1983.

Gonzalez, D. D., 1983, Groundwater Flow in the Rustler Formation: Waste Isolation Pilot Plant (WIPP) Southeast New Mexico (SENM): SAND82-1012, Sandia National Laboratories, Albuquerque, New Mexico.

LIST OF REFERENCES
(Continued)

Gringarten, A. C., H. J. Ramey, Jr., and R. Raghavan, 1972, Pressure Analysis for Fractured Wells: paper SPE 4051 presented at the 47th Annual Fall Meeting of SPE of AIME, San Antonio, Texas.

Hiss, W. L., 1975, Stratigraphy and Ground Water Hydrology of the Capitan Aquifer, Southeastern New Mexico and Western Texas: Ph.D. Thesis, University of Colorado, Boulder, Colorado.

Horner, D. R., 1951, Pressure Buildup in Wells: Proc., Third World Pet. Cong., The Hague, Sec. II, pp. 503-523. Also Reprint Series, No. 9 - Pressure Analysis Methods, Soc. Pet. Engr. AIME, Dallas, 1967, pp. 45-50.

Jacob, C. E. and S. W. Lohman, 1952, Nonsteady Flow to a Well of Constant Drawdown in an Extensive Aquifer: Trans. Amer. Geophys. Union, v. 33, no. 4, pp. 559-569.

Jenkins, D. N. and J. K. Prentice, 1982, Theory for Aquifer Test Analysis in Fractured Rocks Under Linear (Nonradial) Flow Conditions: Ground Water, v. 20, no. 1, pp. 12-21.

Jones, C. L., 1981a, Geologic Data For Borehole ERDA-6, Eddy County, New Mexico: U.S. Geol. Survey Open-File Report 81-468, 59 pp.

Jones, C. L., 1981b, Geologic Data for Borehole ERDA-9, Eddy County, New Mexico: U.S. Geol. Survey Open-File Report 81-469, 50 pp.

Kazemi, H., 1969, Pressure Transient Analysis of Naturally Fractured Reservoirs with Uniform Fracture Distribution: Soc. Pet. Engr. Jour., December, pp. 451-462.

Locke, C. D. and W. K. Sawyer, 1975, Constant Pressure Injection Test in a Fractured Reservoir - History Match Using Numerical Simulation and Type-Curve Analysis: paper SPE 5594 presented at the 50th Annual Fall Technical Conference and Exhibition of the SPE of AIME, Dallas, Texas.

Mavor, J. T. and H. Cinco-Ley, 1979, Transient Pressure Behavior of Naturally Fractured Reservoirs: paper SPE 7977 presented at the 1979 California Regional Meeting of SPE of AIME, Ventura, California.

Mercer, J. W. and B. R. Orr, 1979, Interim Data Report on the Geohydrology of the Proposed Waste Isolation Pilot Plant Site, Southeast New Mexico: U.S. Geol. Survey Water-Resources Investigations 79-98, 178 pp.

Muskat, M., 1937, The Flow of Homogeneous Fluids Through Porous Media: McGraw-Hill Book Co., 763 pp.

Odeh, A. S., 1965, Unsteady State Behavior of Naturally Fractured Reservoirs: Soc. Pet. Engr. Jour., March, pp. 60-66.

LIST OF REFERENCES
(Continued)

Peters, E., 1982, personal communication: Prof. of Pet. Engr., University of Texas, Austin.

Powers, D. W., S. J. Lambert, S. E. Schaffer, L. R. Hill, and W. D. Weart (editors), 1978, Geological Characterization Report, Waste Isolation Pilot Plant (WIPP) Site, Southeastern New Mexico: SAND78-1596, Issued by Sandia Laboratories for U.S. Dept. of Energy, Albuquerque, New Mexico.

Raghavan, R., G. V. Cady, and H. J. Ramey, Jr., 1972, Well-Test Analysis for Vertically Fractured Wells: Jour. of Pet. Tech., Aug., pp. 1014-1020.

Register, J. K., 1981, Brine Pocket Occurrences in the Castile Formation, Southeastern New Mexico: TME 3080, U.S. Dept. of Energy, Albuquerque, New Mexico.

Russell, D. G. and N. E. Truitt, 1964, Transient Pressure Behavior in Vertically Fractured Reservoirs: Jour. of Pet. Tech., Oct., pp. 1159-1170.

Sandia National Laboratories and U.S. Geological Survey, 1982, Basic Data Report for Drillhole WIPP-11 (WIPP): SAND 79-0272, Sandia National Laboratories, Albuquerque, New Mexico.

Snyder, R. P., 1982, personal communication: Geologist, U.S. Geological Survey, Denver, Colorado.

Theis, C. V., 1935, The Relation Between the Lowering of the Piezometric Surface and the Rate and Duration of Discharge of a Well Using Groundwater Storage: Trans. Amer. Geophys. Union, v. 16, pp. 519-524.

Warren, J. E. and P. J. Root, 1963, The Behavior of Naturally Fractured Reservoirs: Soc. Pet. Engr. Jour., Sept., pp. 245-255.

Woolfolk, S. W., 1982, Radiological Consequences of Brine Release by Human Intrusion into WIPP: TME 3151, U.S. Dept. of Energy, Albuquerque, New Mexico.

TABLE H.1

SUMMARY OF CASTILE BRINE OCCURRENCES IN THE WIPP VICINITY

NUMBER[1]	WELL NAME	PRODUCING FORMATION/MEMBER[2]	DEPTH TO BRINE RESERVOIR (FT)	FORMATION PRESSURE (psig) MEASURED	FORMATION PRESSURE (psig) ESTIMATED MINIMUM[3]	INITIAL FLOW RATE[4]	REMARKS
1	Pogo	Castile/Anhydrite II-III[5]	3322		2519	1200-1440 bbl/day	Minimum pressure needed to discharge weighted mud (14.6 ppg or γ = 1.75); no shut-in pressure available.
2	Union	Castile/Anhydrite III	2810		1460	720 bbl/day	Minimum pressure needed to discharge weighted mud (10 ppg or γ = 1.20); no shut-in pressure available.
3	Gulf Covington	Castile/Anhydrite III	3600	1972		Conflicting Data	Shut-in pressure of 100 psi reported on drill record (γ = 1.2).
4	Culbertson	Castile/Anhydrite III	3515		1858	2000 bbl/day	Brine γ = 1.22. 8 mcf/day gas emitted (estimated); no other data available.
5	Shell	Castile/Anhydrite III	3671		1941	20,000 bbl/day	Minimum pressure needed to discharge brine of γ = 1.22; no other data available.
6	Tidewater	Castile/Unknown	3730		2325	No data	Minimum pressure needed to discharge weighted mud (12 ppg or γ = 1.44).
7	Mascho 1	Castile/Anhydrite III	3322		1800	8000 bbl/day	Minimum pressure needed to discharge brine of γ = 1.217[6]; no other data available.
8	Mascho 2	Castile/Anhydrite III	3298		1740	3000 bbl/day	Minimum pressure needed to discharge brine of γ = 1.217[6]. Also encountered water at 3235, with head of 300 feet.
9	Belco	Castile/Anhydrite III	2802	2075		12,000 bbl/day	Shut-in pressure at wellhead 125 psi when well filled with weighted mud (13.4 ppg or γ =1.61).
10	Bilbrey	Castile/Anhydrite III	3090		1630	6000 bbl/day	Minimum pressure needed to discharge brine of γ = 1.217[6]; no other data available.
11	ERDA-6	Castile/Anhydrite II	2711	2048		685 bbl/day	Shut-in pressure prior to substantial brine flow.
12	WIPP-12	Castile/Anhydrite III	3017	1831		12,000 bbl/day	Shut-in pressure prior to substantial brine flow.
13	H & W Danford 1	Castile/Anhydrite III	1930		1018	No data	Brine flowed to surface for 48 hours and then stopped. Minimum pressure needed to discharge brine of γ = 1.217[6].

(1) For well locations refer to Figure G-11. For pressure/depth relationship refer to Figure H-11.

(2) Based on data provided by U.S. Geological Survey.

(3) Data should not be used as static formation pressure.

(4) Typically estimated by driller.

(5) Anhydrites II and III coalesce at this location. Brine was encountered in middle of anhydrite.

(6) Specific gravity of brines in WIPP-12 and ERDA-6.

TABLE H.2
SUMMARY OF HYDROLOGIC TESTING IN ERDA-6

TEST	D'APPOLONIA (1982, 1983) ACTIVITY DESIGNATION	PERIODS OF TEST	DURATION	INSTRUMENTATION[1]	REMARKS
Drill Stem Test 2472	ERDA-6.3	DST 2472-1[2] FFL FBU* SFL SBU* DST 2472-2[2] FFL FBU	Oct 23, 1981 (20:30) to Oct 25, 1981 (15:31)	Lynes TCWL-DST Tool[3] - single packer assembly. TCWL triple pressure transducer. HP-9825 computer, printer, and plotter.	Test performed prior to drilling cement plug in ERDA-6. This test was performed above brine reservoir. Test produced data on permeability of Halite II and Anhydrite II contact.
Drill Stem Test 2680	ERDA-6.6	DST 2680-1[2] FFL FBU* SFL SBU* DST 2680-2[2] FFL FBU* SFL SBU*	Oct 28, 1981 (16:45) to Oct 30, 1981 (12:20)	Lynes TCWL-DST Tool - single packer assembly. TCWL triple pressure transducer. HP-9825 computer, printer, and plotter.	Results of this test were used for preliminary hydrologic characterization of reservoir.
Flow Test 1	ERDA-6.7	Flow Period* Buildup Period*	Oct 30, 1981 (12:20) to Oct 30, 1981 (17:54) Oct 30, 1981 (17:54) to Oct 30, 1981 (20:52)	Rockwell 2" cumulative flow meter. Lynes TCWL-DST Tool - single packer assembly. TCWL triple pressure transducer. HP-9825 computer, printer, and plotter.	Flow Test 1 was conducted through DST tool and 2-7/8" tubing. Setup as for DST 2680. Test terminated because of potential for H_2S embrittlement. Flow rates affected by heavy mud discharge and gas within flowline. Data from this test were used for quantification of reservoir properties.
Flow Test 2	ERDA-6.8	Flow Period* Buildup Period*	Oct 31, 1981 (11:18) to Nov 04, 1981 (18:35) Nov 04, 1981 (18:35) to Nov 17, 1981 (20:41)	Rockwell 2" cumulative flow meter. TCWL triple pressure transducer in hydraulic connection with the wellhead. HP-9825 computer, printer, and plotter.	Initial flow rates affected for 9 hours by heavy mud discharge and gas within flow line. Pressure buildup data affected by temperature fluctuation. Data from this test used for quantification of reservoir properties.
Flow Test 3	ERDA-6.9	Flow Period* Buildup Period*	Nov 17, 1981 (20:41) to Nov 20, 1981 (20:53) Nov 20, 1981 (20:53) to Feb 19, 1982 (12:33)	Rockwell 2" cumulative flow meter. Nov 20 81 to Nov 22 81 - TCWL triple pressure transducer located at 2702 feet below surface. Nov 22 81 to Feb 19 82 - TCWL triple pressure transducer located at surface.	Pressure data collected downhole affected by a leak in lubricator. Pressure data collected at the wellhead affected by temperature fluctuation, and by gas cap formation.

TABLE H.2
(Continued)

TEST	D'APPOLONIA (1982, 1983) ACTIVITY DESIGNATION	PERIODS OF TEST	DURATION	INSTRUMENTATION[1]	REMARKS
BOP Change	ERDA-6.11	Flow Period*	Feb 19, 1982 (12:33) to Feb 19, 1982 (13:26)	Envirotech flow meter. Baski cutthroat flume.	Replaced blow-out preventer on wellhead. Pressure buildup data collected at the wellhead affected by gas cap formation.
		Buildup Period*	Feb 19, 1982 (13:26) to Mar 08, 83 (11:17)	Feb 19 82 to Feb 20 82 - TCWL triple pressure transducer in hydraulic connection with the wellhead Feb 19 82 to Feb 20 82 - HP-9825 computer, printer, and plotter. Feb 20 82 to Mar 08 83 - Weksler 0-600 psig mechanical pressure gage installed at the wellhead.	
Gas Cap Release	ERDA-6.12	Flow Period*	Mar 08, 1983 (11:17) to Mar 08, 1983 (13:25)	Barton 202A differential pressure recorder with 1/4" orifice plate. Fisher-Porter flow rate meter. Weksler 0-800 and 0-600 psig mechanical pressure gages installed at the wellhead.	Gas cap released from wellbore. No brine flow. Pressure data from 0-800 psig gage may be affected by fluid leak from diaphragm assembly. Static pressure following gas release used in total reservoir volume calculations.
		Buildup Period*	Mar 08, 1983 (13:25) Continuing as of Mar 21, 1983		

[1]For detailed information on instrumentation refer to D'Appolonia (1982, 1983).

[2]Drill stem test terminology:
FFL - first flow period; FBU - first buildup period;
SFL - second flow period; SBU - second buildup period.

[3]TCWL = Triple Conducting Wireline
DST = Drill Stem Test

* Data used in this report.

TABLE H.3
SUMMARY OF HYDROLOGIC TESTING IN WIPP-12

TEST	D'APPOLONIA (1982, 1983) ACTIVITY DESIGNATION	PERIODS OF TEST	DURATION	INSTRUMENTATION[1]	REMARKS
Pressure Buildup	WIPP-12.3	Pressure Buildup	Nov 23, 1981 (20:25) to Nov 25, 1981 (06:45)	Mechanical pressure gage, 0-300 psig, at the wellhead.	Maximum wellhead pressure recorded for WIPP-12. Data used in static reservoir pressure calculation.
Pressure Buildup	WIPP-12.6	Pressure Buildup	Nov 29, 1981 (14:00) to Dec 03, 1981 (18:06)	Mechanical pressure gage, 0-300 psig, at the wellhead.	Pressure buildup followed substantial flow of 27000 bbl of brine during drilling the well to 3047 feet. No data from this test used for quantification of reservoir properties.
Flow Test 1	WIPP-12.7	Flow Period*	Dec 03, 1981 (18:06) to Dec 04, 1981 (15:00)	Rockwell 2" cumulative flow meter, installed upstream of gas/liquid separator. Floco flow meter installed downstream of gas/liquid separator. No pressure measurements were taken.	Results of this test were not used for reservoir hydrologic characterization. Its primary purpose was to collect downhole and surface brine and gas samples.
Drill Stem Test 3020	WIPP-12.8	DST-3020-1[2] FFL FBU DST-3020-2 FFL FBU DST-3020-3 FFL (Slug test)	Dec 04, 1981 (15:00) to Dec 06, 1981 (09:50)	Lynes TCWL-DST Tool downhole[3], connected via wireline to Hewlett-Packard data acquisition computer at surface.	Choke effects were serious during flow periods. Results of this test were used for preliminary reservoir hydrologic characterization but not used for quantification of reservoir properties.
Drill Stem Test 2986	WIPP-12.9	DST-2986-1[2] FFL FBU* SFL DST-2986-2 FFL FBU* SFL DST-2986-3 FFL (Slug test)	Dec 06, 1981 (09:50) to Dec 07, 1981 (02:52)	Lynes TCWL-DST Tool downhole, connected via wireline to Hewlett-Packard data acquisition computer at surface.	Choke effects were serious during flow periods. Results of this test were used for preliminary reservoir hydrologic characterization and development of further testing procedure. Produced information on thickness of fractured zone.
Pressure Buildup	WIPP-12.10	Pressure Buildup	Dec 07, 1981 (02:52) to Dec 12, 1981 (00:30)	Lynes TCWL-DST Tool downhole, connected via wireline to Hewlett-Packard data acquisition computer at surface.	Results of this test were not used for reservoir hydrologic characterization.
Pressure Buildup	WIPP-12.12	Pressure Buildup	Dec 15, 1981 (20:04) to Dec 17, 1981 (06:45)	Mechanical pressure gage, 0-300 psig, installed at the wellhead. Switched to 0-50 psig gage for greater precision.	Results of this test were not used for reservoir hydrologic characterization.
Pressure Buildup	WIPP-12.14	Pressure Buildup	Dec 21, 1981 (07:40)	Mechanical 0-250 psig pressure [illegible]	[illegible]

TME 3153

TABLE H.3
(Continued)

TEST	D'APPOLONIA (1982, 1983) ACTIVITY DESIGNATION	PERIODS OF TEST	DURATION	INSTRUMENTATION[1]	REMARKS
Pressure Buildup	WIPP-12.18	Pressure Buildup	Jan 04, 1982 (14:00) to May 20, 1982 (15:02)	Lynes TCWL Probe connected to wellhead at surface, connected to Hewlett-Packard data acquisition computer with conducting wireline cable. Also used Metserco 0-100 psig pressure recorder and 0-200 psig mechanical pressure gage.	Pressure buildup period started after installation of three production-injection packers. Produced information on reservoir response to brine flow. Due to uncertainties regarding intermittent flow, data not used for quantification of reservoir properties.
Flow Test 2	WIPP-12.19	Flow Period*	May 20, 1982 (15:02) to May 20, 1982 (20:31)	Halliburton 2" flow meter Johnston-Macco DPTT[3], Weksler 0-200 psig pressure gage.	Constant-pressure, variable-rate flow test. Data used to characterize hydraulics of reservoir.
		Pressure Buildup*	May 20, 1982 (20:31) to May 21, 1982 (16:16)		
Flow Test 3	WIPP-12.20	Flow Period*	May 23, 1982 (13:00) to Jun 02, 1982 (11:39)	Halliburton 2", 3", and 4" flow meters, Rockwell 2" flow meter, 4" cutthroat flume installed in flow measurement manifold system.	Salt crystallization in flow lines created non-constant-pressure, variable-rate flow test. Modeling indicated low sensitivity to variable flow and pressure. Data used for characterization of reservoir properties. Pressure buildup data collected at the wellhead affected by gas cap formation.
		Pressure Buildup*	Jun 02, 1982 (11:39) to Mar 07, 1983 (20:29)	Johnston-Macco DPTT[3], Weksler 0-200 psig pressure gage, Metserco 0-250 psig pressure recorder.	
Gas Cap Release	WIPP-12.21	Flow Period*	Mar 07, 1983 (20:29) to Mar 07, 1983 (21:32)	Barton 202A differential pressure recorder with 1/4" orifice plate. Fisher-Porter flow rate meter. Weksler 0-200 psig mechanical pressure gage installed at the wellhead.	Gas cap released from wellbore. No brine flow. Static pressure following gas release used in total reservoir volume calculations.
		Pressure Buildup*	Mar 07, 1983 (21:32) Continuing as of Mar 21, 1983.		

[1]For detailed information on instrumentation refer to D'Appolonia (1982, 1983).

[2]Drill stem test terminology:
FFL - first flow period; FBU - first buildup period;
SFL - second flow period, SBU - second buildup period.

[3]TCWL - Triple Conducting Wireline
DST - Drill Stem Test
DPTT - Downhole Pressure and Temperature Transducer

* Data used in this report.

TABLE H.4

SUMMARY OF RESERVOIR TESTING RESULTS

TEST	ANALYTIC METHOD	k (md)	kh (md-ft)	C (bbl/psi)	s	ω	λ	$\alpha \frac{k_m}{k_f}$	$L(\pi khS)^{1/2}$	REMARKS
ERDA-6/DST-2472-1/FBU	Horner	1.5×10^{-2}	1.3×10^{0}	NC	NC	NA	NA	NA	NA	h = 6.9' Anhydrite II + 83.1' Halite II.
ERDA-6/DST-2472-1/SBU	Horner	2.5×10^{-3}*	2.3×10^{-1}*	NC	NC	NA	NA	NA	NA	h = 6.9' Anhydrite II + 83.1' Halite II. Permeability representative of lumped rock properties.
ERDA-6/DST-2680-1/FBU	Horner	9.2×10^{0}	5.2×10^{2}	NC	NC	NA	NA	NA	NA	
ERDA-6/DST-2680-1/SBU	Horner	8.9×10^{0}	5.0×10^{2}	NC	NC	NA	NA	NA	NA	
ERDA-6/DST-2680-2/FBU	Horner	7.6×10^{0}	4.3×10^{2}	NC	NC	NA	NA	NA	NA	
ERDA-6/DST-2680-2/SBU	Horner	7.7×10^{0}	4.3×10^{2}	NC	NC	NC	NC	NC	NA	
	Mod. Horner	7.1×10^{0}	4.0×10^{2}	NC	NC	NC	NC	NC	NA	Modified production time.
	Bourdet and Gringarten	1.5×10^{1}	8.4×10^{2}	6.6×10^{-4}	-2.6	2×10^{-2}	5.2×10^{-5}	4.8×10^{-4}	NA	Fit to second curve uncertain.
ERDA-6/Flow Test 1/BU	Horner*	1.1×10^{1}*	6.0×10^{2}*	NC	NC	NC	NC	NC	NA	Permeability representative of major fractures near ERDA-6 well.
	Bourdet and Gringarten	1.2×10^{1}	7.0×10^{2}	3.0×10^{-4}*	-2.6*	≤ 0.1	4.1×10^{-5}	3.8×10^{-4}	NA	Fit to second curve uncertain.
	Muskat	3.3×10^{1}	1.8×10^{3}	NA	NA	NA	NA	NA	NA	Non-unique solution.
ERDA-6/Flow Test 2/BU	Horner*	2.2×10^{0}*	1.2×10^{2}*	NC	NC	NC	NC	NC	NA	Permeability representative of averaged reservoir properties including substantial contribution from microfractures.
	Bourdet and Gringarten	3.4×10^{0}	1.9×10^{2}	1.2×10^{-2}	-5.2	1×10^{-5}	1.1×10^{-5}	1.0×10^{-4}	NA	Fit to second curve uncertain.
ERDA-6/Flow Test 3/Flow	Jenkins and Prentice	NC	NC	NA	NA	NA	NA	NA	3.3×10^{-2}	L unknown.
	Jacob and Lohman	9.1×10^{-1}	5.1×10^{1}	NA	NA	NA	NA	NA	NA	
ERDA-6/Flow Test 3/BU	Horner	8.1×10^{-1}	4.6×10^{1}	NC	NC	NC	NC	NC	NA	Erratic pressure buildup.
ERDA-6/Core Test	Nitrogen Permeameter*	3×10^{-3}*	NA	NA	NA	NA	NA	NA	NA	Permeability representative of intact anhydrite. One sample tested.
WIPP-12/DST-2986-1/FBU	Horner	5.9×10^{3}	3.6×10^{5}	NC	NC	NA	NA	NA	NA	Data influenced by choke effects.
WIPP-12/DST-2986-2/FBU	Horner	5.2×10^{3}	3.1×10^{5}	NC	NC	NA	NA	NA	NA	Data influenced by choke effects.
WIPP-12/Flow Test 2/Flow	Jenkins and Prentice	NC	NC	NA	NA	NA	NA	NA	3.6×10^{0}	L unknown.
	Jacob and Lohman	1.6×10^{3}	9.9×10^{4}	NA	NA	NA	NA	NA	NA	
WIPP-12/Flow Test 2/BU	Horner*	2.0×10^{3}*	1.2×10^{5}*	NC	NC	NC	NC	NC	NA	Permeability representative of major fractures near WIPP-12 well.
	Bourdet and Gringarten	2.1×10^{3}	1.3×10^{5}	7.0×10^{-1}*	-5.9*	0.1	6.9×10^{-8}	6.3×10^{-7}	NA	Fit to second curve uncertain.
WIPP-12/Flow Test 3/BU	Horner*	1.7×10^{1}*	1.0×10^{3}*	NC	NC	NC	NC	NC	NA	Permeability representative of averaged reservoir properties including substantial contribution from microfractures.
	Bourdet and Gringarten	6.1×10^{0}	3.7×10^{2}	2.8×10^{-1}	-9.1	NC	NC	NC	NA	Fit to single type curve.
WIPP-12/Core Test	Nitrogen Permeameter*	$<2 \times 10^{-4}$*	NA	NA	NA	NA	NA	NA	NA	Permeability representative of intact anhydrite. Two samples tested.

NOTES:

NC = Not Calculated
NA = Not Applicable
* = "Best" or "most reliable" method or result.
See Table H.5 for Hydrology Conversion Factors applicable to WIPP site brines with γ = 1.217 and μ = 1.77 cp.

TABLE H.5

BRINE HYDROLOGY CONVERSION FACTORS

A. CONVERSION TABLE FOR CONVERTING FROM INTRINSIC PROPERTIES TO PROPERTIES APPLICABLE TO BRINE FLOW

MULTIPLY PROPERTY DETERMINED FOR BRINE FLOW[1]	BY	TO GET INTRINSIC PROPERTY OF THE MEDIUM
K^*[2] (cm/sec)	1.503×10^6	k (md)
K^*[2] (ft/min)	7.634×10^5	k (md)
T (ft^2/min)	7.634×10^5	kh (md-ft)

MULTIPLY GIVEN INTRINSIC PROPERTY	BY	TO GET PROPERTY APPLICABLE TO BRINE FLOW[1]
k (md)	6.655×10^{-7}	K^*[2] (cm/sec)
k (md)	1.310×10^{-6}	K^*[2] (ft/min)
kh (md-ft)	1.310×10^{-6}	T (ft^2/min)

B. CONVERSION TABLE FOR HYDRAULIC CONDUCTIVITY UNITS

K^*[2] (Hydraulic Conductivity)	cm/sec	ft/min	ft/day	gpd/ft^2
1 cm/sec	1.000	1.969	2.835×10^3	2.121×10^4
1 ft/min	5.080×10^{-1}	1.000	1.440×10^3	1.077×10^4
1 ft/day	3.528×10^{-4}	6.944×10^{-4}	1.000	7.480
1 gpd/ft^2	4.716×10^{-5}	9.284×10^{-5}	1.337×10^{-1}	1.000

C. CONVERSION TABLE FOR TRANSMISSIVITY UNITS

T (Transmissivity)	ft^2/min	gpd/ft
1 ft^2/min	1.000	1.077×10^4
1 gpd/ft	9.284×10^{-5}	1.000

[1]For WIPP brine properties of μ = 1.77 cp, and γ = 1.217.
[2]K^* is the symbol for hydraulic conductivity in this table.

DRAWN BY	DJ Rodriguez	CHECKED BY	RLB	3/18/82	DRAWING NUMBER NM78-648-E6
	1-12-81	APPROVED BY	DKS/JPW	5/10/82	

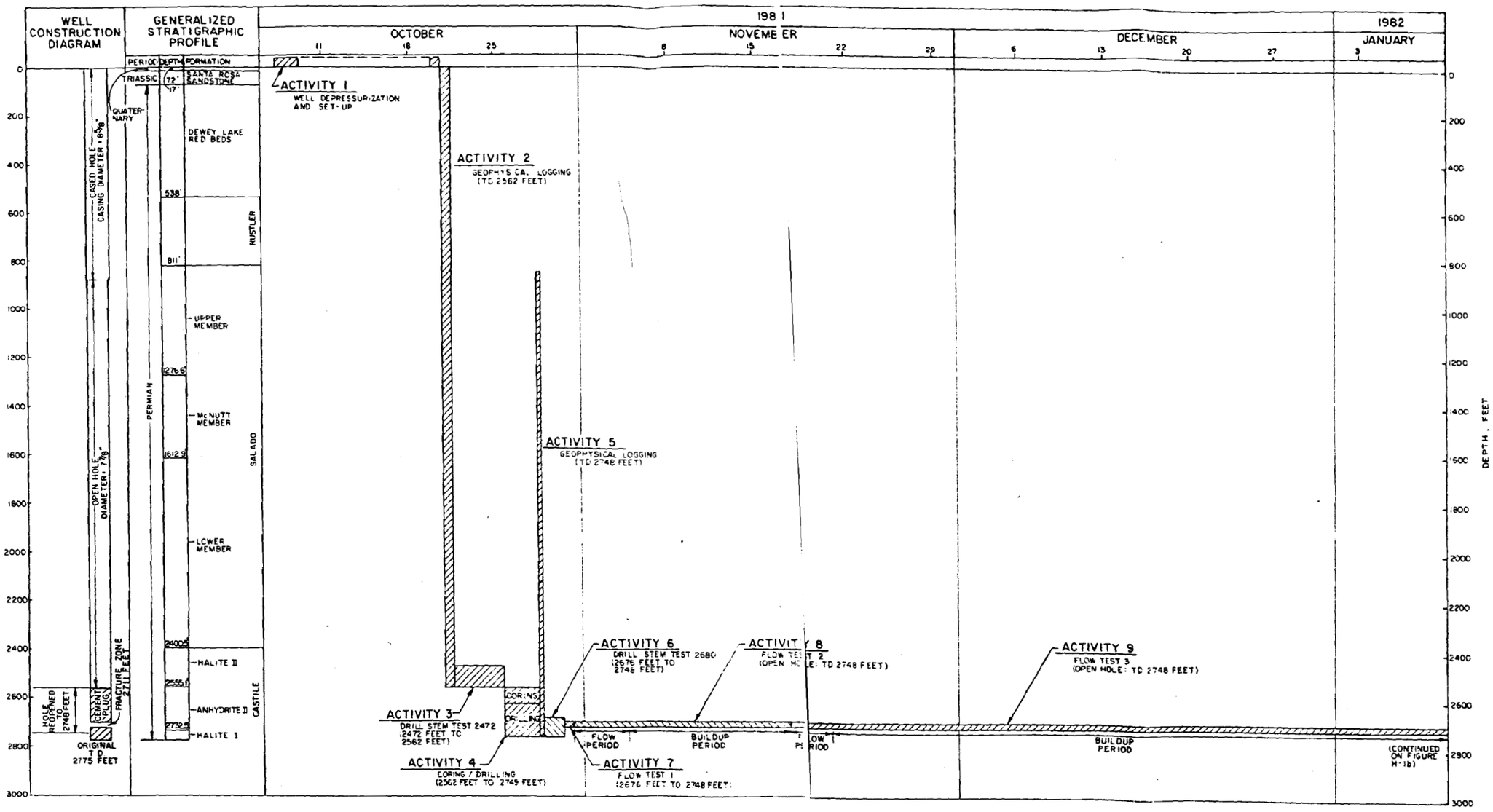

NOTES:
1. ALL DEPTHS ARE REFERENCED TO GROUND SURFACE ELEVATION 3536.1 FEET ABOVE SEA LEVEL.
2. ACTIVITY ERDA-6.10 TOOK PLACE AT AEC-7 WELL LOCATION AND IS NOT SHOWN ON THIS FIGURE.
3. STRATIGRAPHIC PROFILE FROM U.S. GEOLOGICAL SURVEY OPEN-FILE REPORT 81-468.

FIGURE H-1a

ERDA-6
TIME-VERSUS-DEPTH
ACTIVITY SUMMARY

PREPARED FOR

WESTINGHOUSE ELECTRIC CORPORATION
ALBUQUERQUE, NEW MEXICO

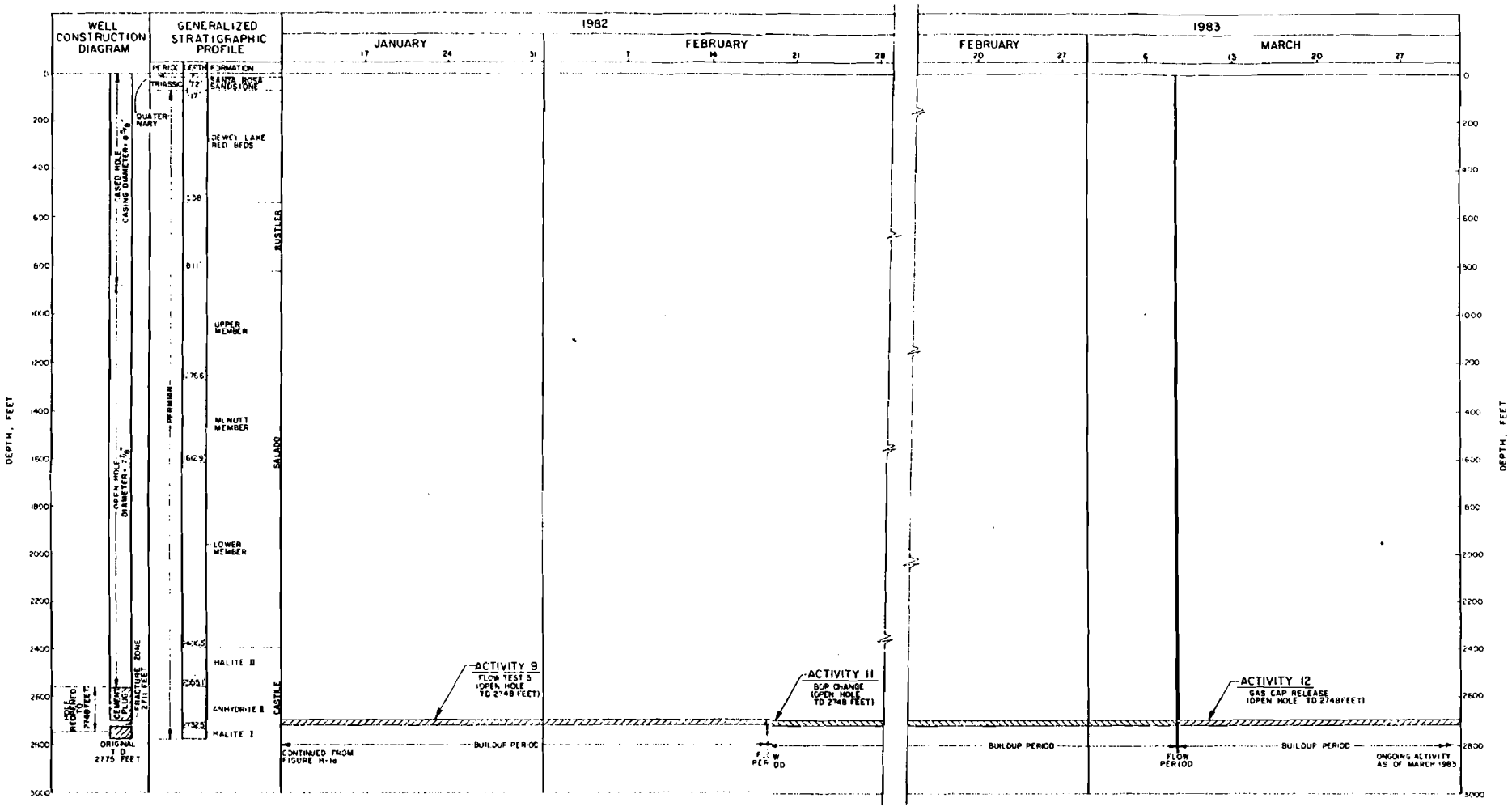

NOTES:
1. ALL DEPTHS ARE REFERENCED TO GROUND SURFACE ELEVATION 3536.1 FEET ABOVE SEA LEVEL
2. ACTIVITY ERDA-6 10 TOOK PLACE AT AEC-7 WELL LOCATION AND IS NOT SHOWN ON THIS FIGURE.
3. STRATIGRAPHIC PROFILE FROM US GEOLOGICAL SURVEY OPEN-FILE REPORT 81-468.

FIGURE H-1b

ERDA-6
CONTINUATION OF
TIME-VERSUS-DEPTH
ACTIVITY SUMMARY

PREPARED FOR

WESTINGHOUSE ELECTRIC CORPORATION
ALBUQUERQUE, NEW MEXICO

DRAWING NUMBER	NM78-648-E7
DRAWN BY	DJ Hodges
CHECKED BY	
APPROVED BY	
	1-18-82

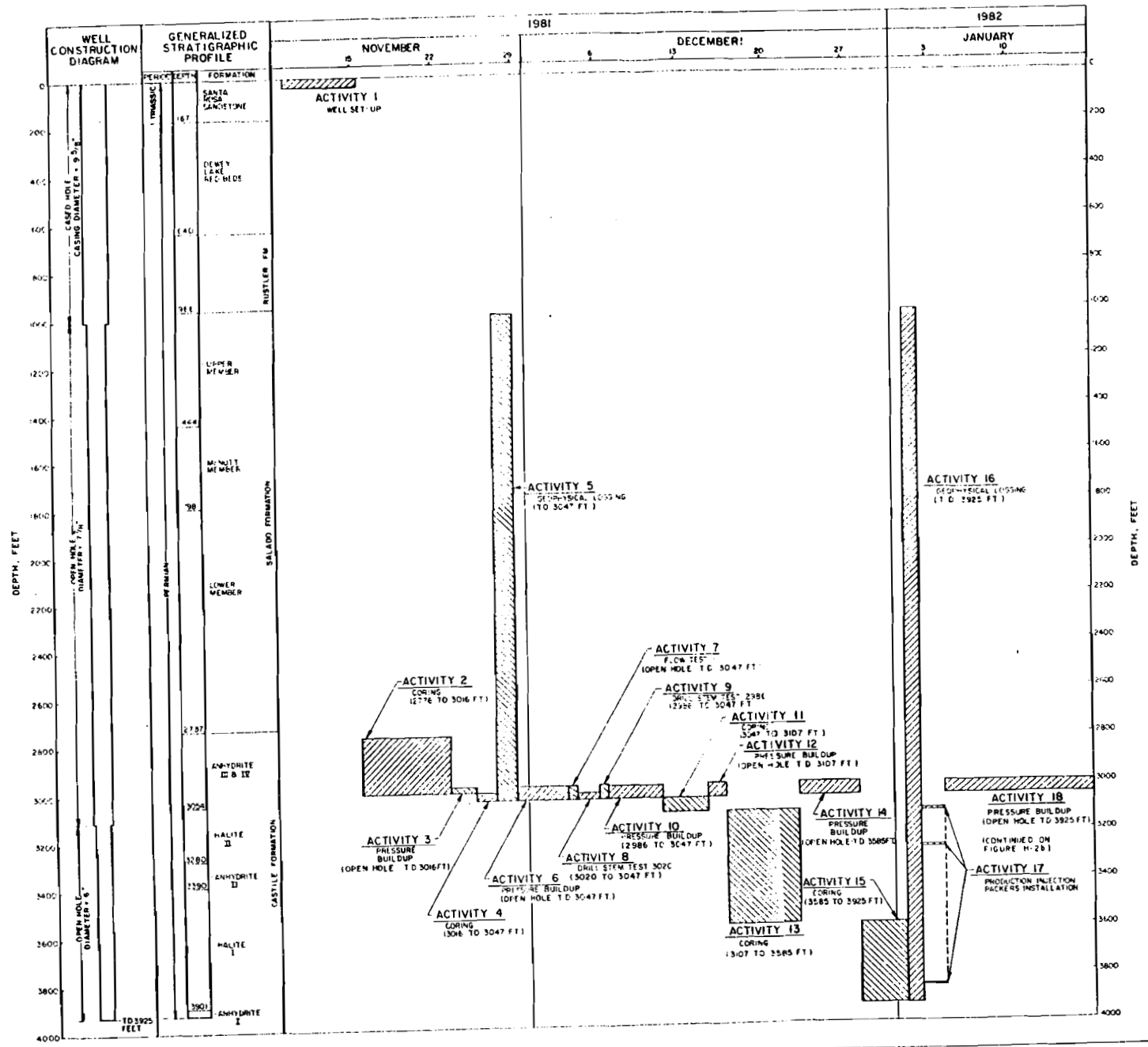

NOTES

1. ALL DEPTHS ARE REFERENCED TO GROUND SURFACE ELEVATION 3471.55 FEET ABOVE SEA LEVEL
2. STRATIGRAPHIC PROFILE FROM FREELAND AND DADOURIAN, GEOLOGIC DATA FOR BOREHOLE WIPP-12, D'APPOLONIA CONSULTING ENGINEERS, 1982, UNPUBLISHED REPORT.

FIGURE H-2a

WIPP-12
TIME-VERSUS-DEPTH
ACTIVITY SUMMARY

PREPARED FOR

WESTINGHOUSE ELECTRIC CORPORATION
ALBUQUERQUE, NEW MEXICO

D'APPOLONIA

DRAWN BY | 21 July 82 | A Brickert | CHECKED BY | APPROVED BY | UKD/CRM | DRAWING NUMBER NM78-648-E8

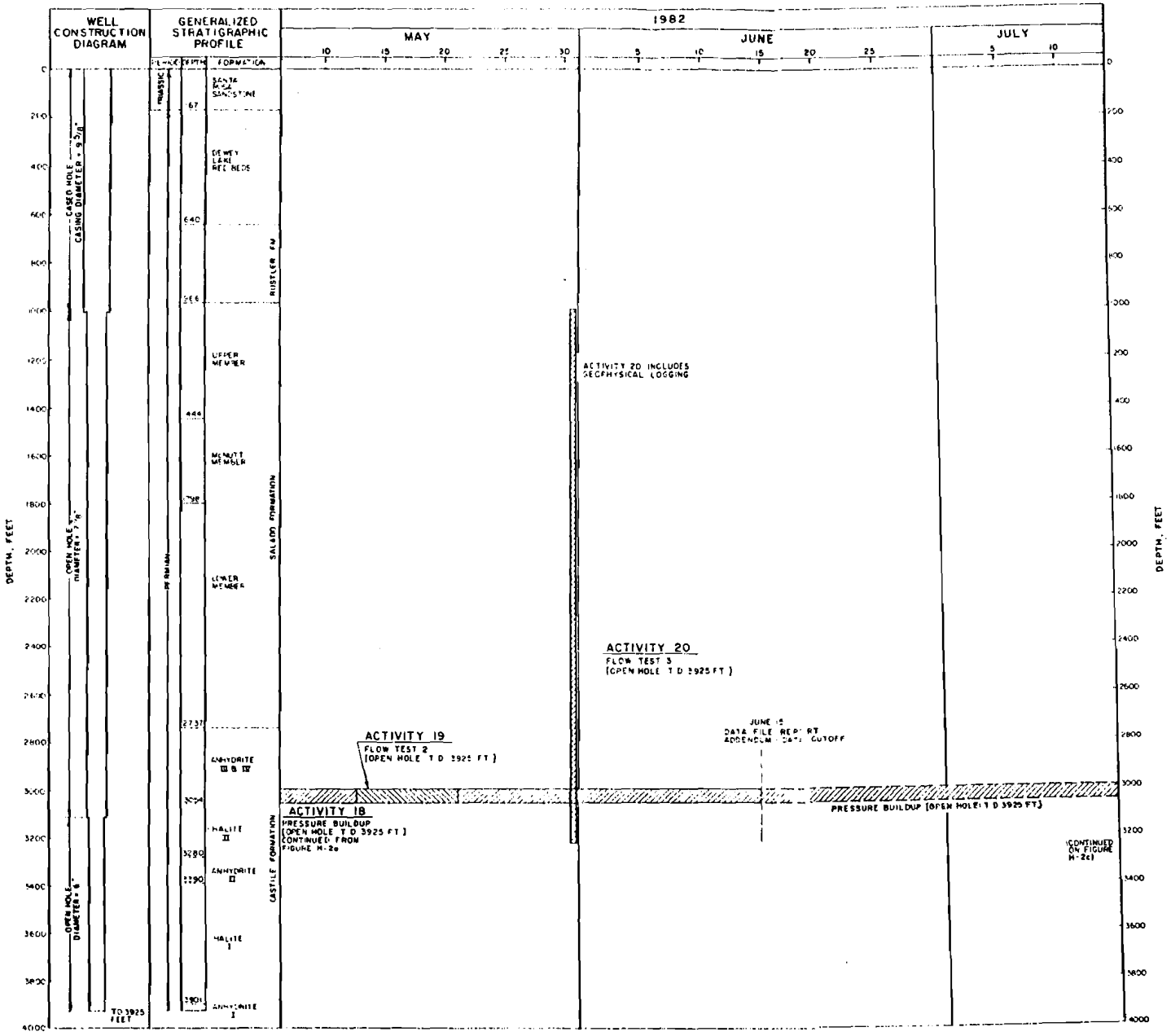

NOTES:

1. ALL DEPTHS ARE REFERENCED TO GROUND SURFACE ELEVATION 3471.8 FEET ABOVE SEA LEVEL.
2. STRATIGRAPHIC PROFILE FROM FREELAND AND DADOURIAN, GEOLOGIC DATA FOR BOREHOLE WIPP-12, D'APPOLONIA CONSULTING ENGINEERS, 1982, UNPUBLISHED REPORT.

FIGURE H-2b

WIPP-12
CONTINUATION OF TIME-VERSUS-DEPTH ACTIVITY SUMMARY

PREPARED FOR

WESTINGHOUSE ELECTRIC CORPORATION
ALBUQUERQUE, NEW MEXICO

D'APPOLONIA

DRAWN BY	CHECKED BY	APPROVED BY	DRAWING NUMBER
R. Bricker 23 Oct. 82	RLB 5/18/83	PKS 5/18/83	NM78-648-A89

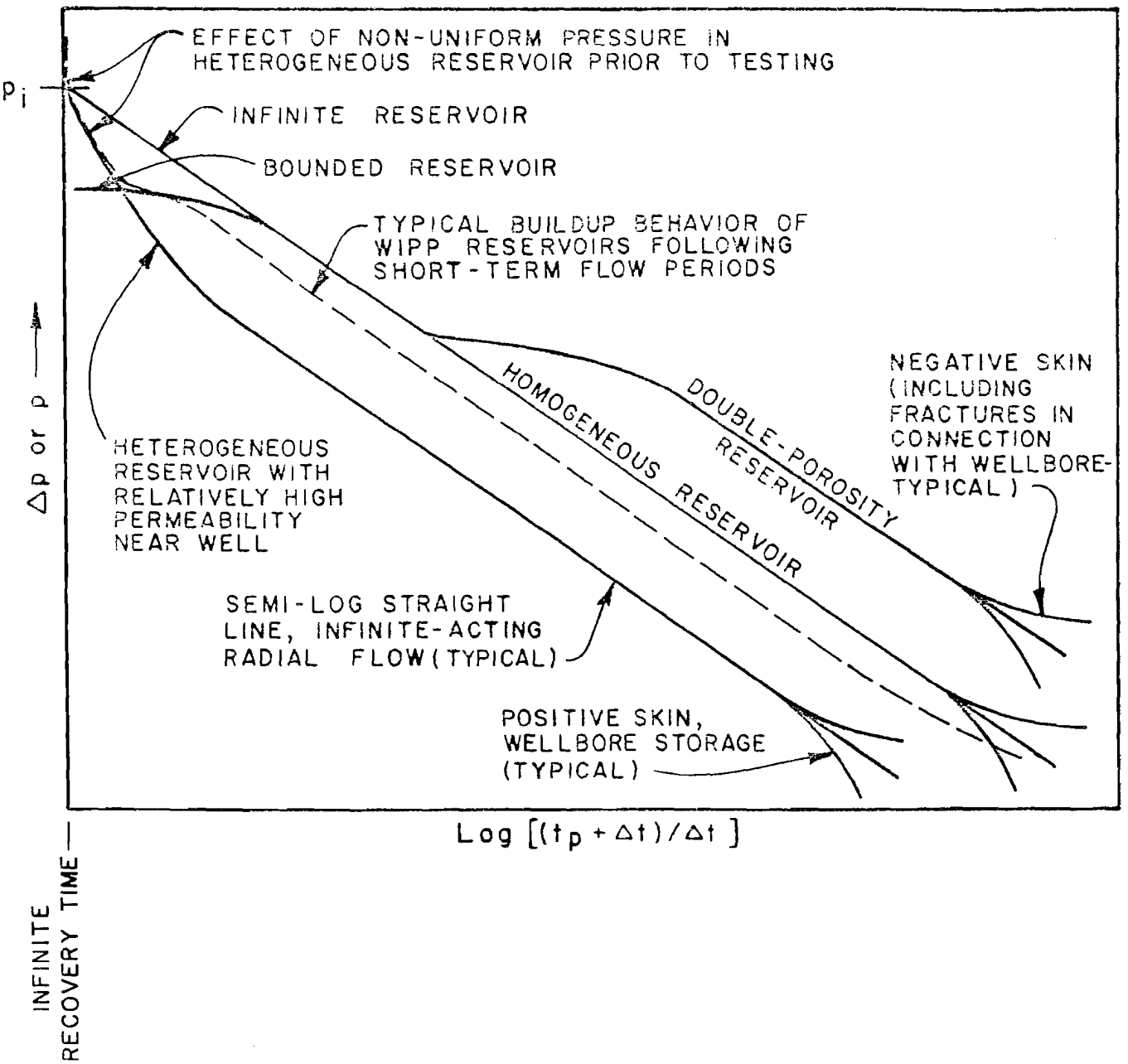

FIGURE H-3

FEATURES OF
TYPICAL HORNER PLOTS

PREPARED FOR

WESTINGHOUSE ELECTRIC CORPORATION
ALBUQUERQUE, NEW MEXICO

D'APPOLONIA

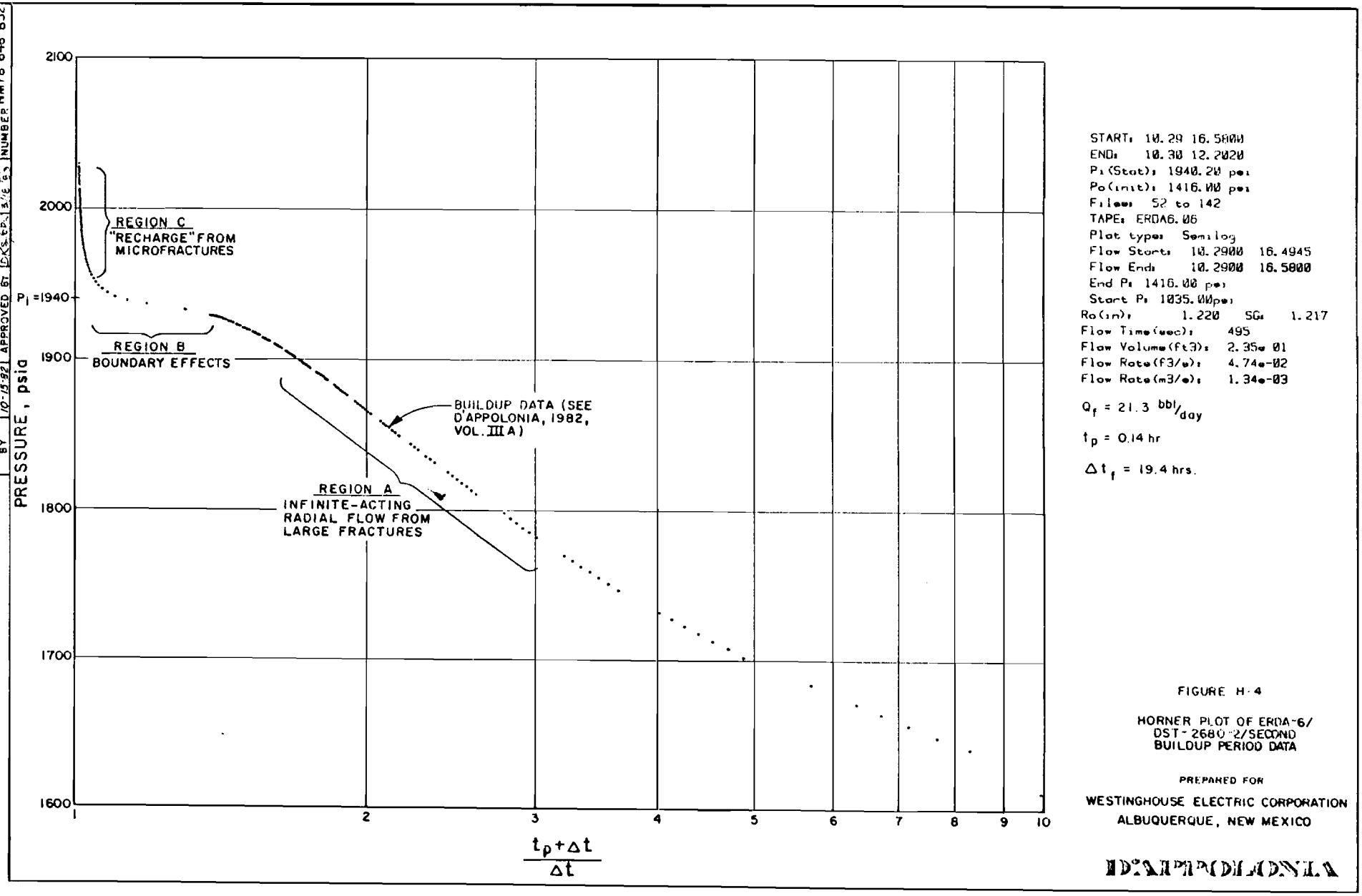

START: 10.29 16.5800
END: 10.30 12.2020
P_i(Stat): 1940.20 psi
Po(init): 1416.00 psi
Files: 52 to 142
TAPE: ERDA6.06
Plot type: Semilog
Flow Start: 10.2900 16.4945
Flow End: 10.2900 16.5800
End P: 1416.00 psi
Start P: 1035.00psi
Ro(in): 1.220 SG: 1.217
Flow Time(sec): 495
Flow Volume(ft3): 2.35e 01
Flow Rate(f3/s): 4.74e-02
Flow Rate(m3/s): 1.34e-03

Q_f = 21.3 $^{bbl}/_{day}$

t_p = 0.14 hr

Δt_f = 19.4 hrs.

FIGURE H-4

HORNER PLOT OF ERDA-6/
DST-2680-2/SECOND
BUILDUP PERIOD DATA

PREPARED FOR

WESTINGHOUSE ELECTRIC CORPORATION
ALBUQUERQUE, NEW MEXICO

D'APPOLONIA

DRAWN BY
CHECKED BY
APPROVED BY
DRAWING NUMBER NM78-646-B52

TME 3153

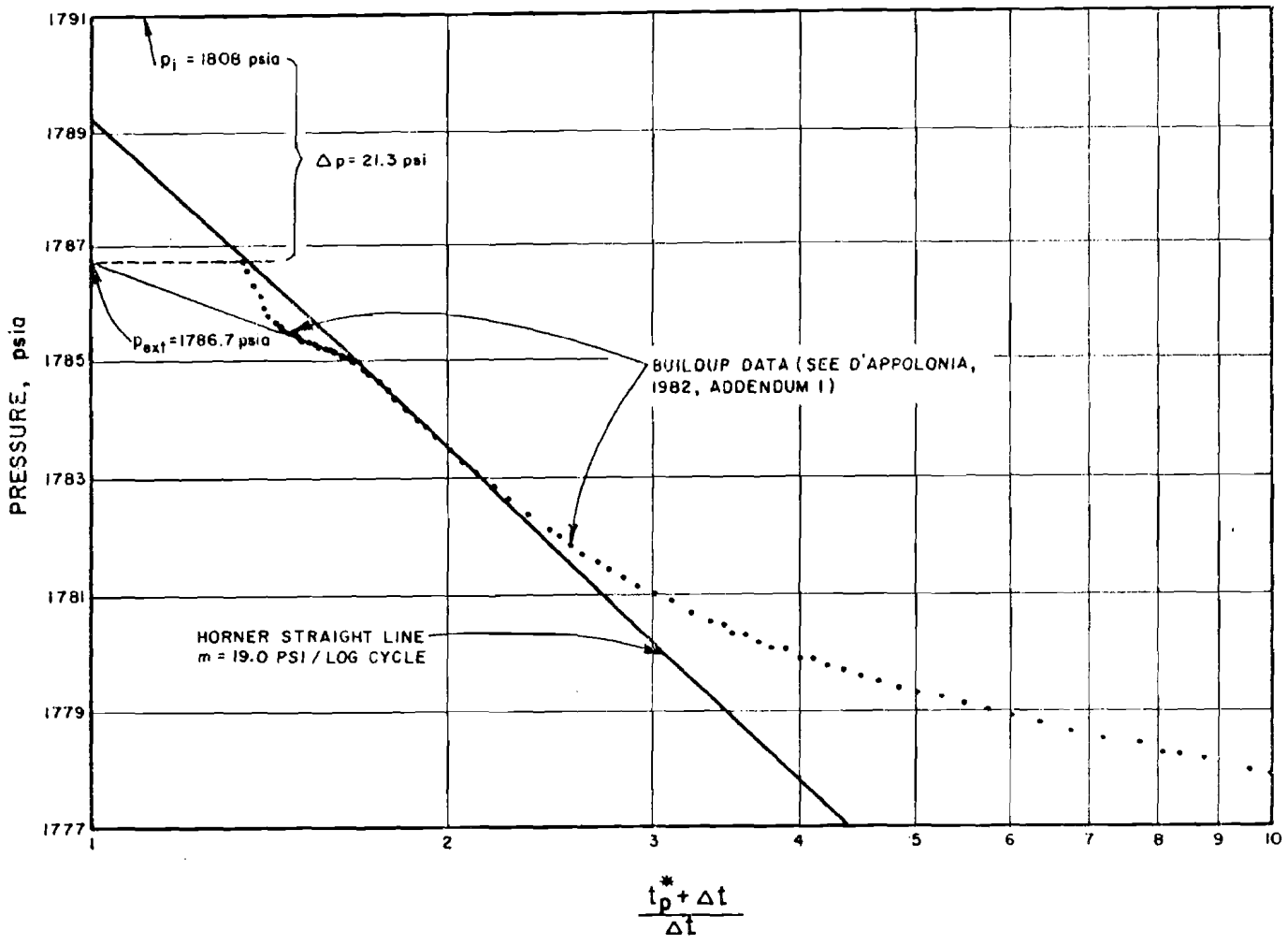

Q_F = 8057 $^{bbl}/_{day}$

t_p^* = 6.73 hrs.

Δt_f = 19.7 hrs.

FIGURE H-5

HORNER PLOT OF WIPP-12 / FLOW TEST 2 / BUILDUP PERIOD DATA

PREPARED FOR

WESTINGHOUSE ELECTRIC CORPORATION
ALBUQUERQUE, NEW MEXICO

D'APPOLONIA

DRAWN BY	B.K.H. 10-13-82	CHECKED BY	D.L.B. 12/8/82
		APPROVED BY	[illegible]

DRAWING NUMBER NW78-648-851

TME 3153

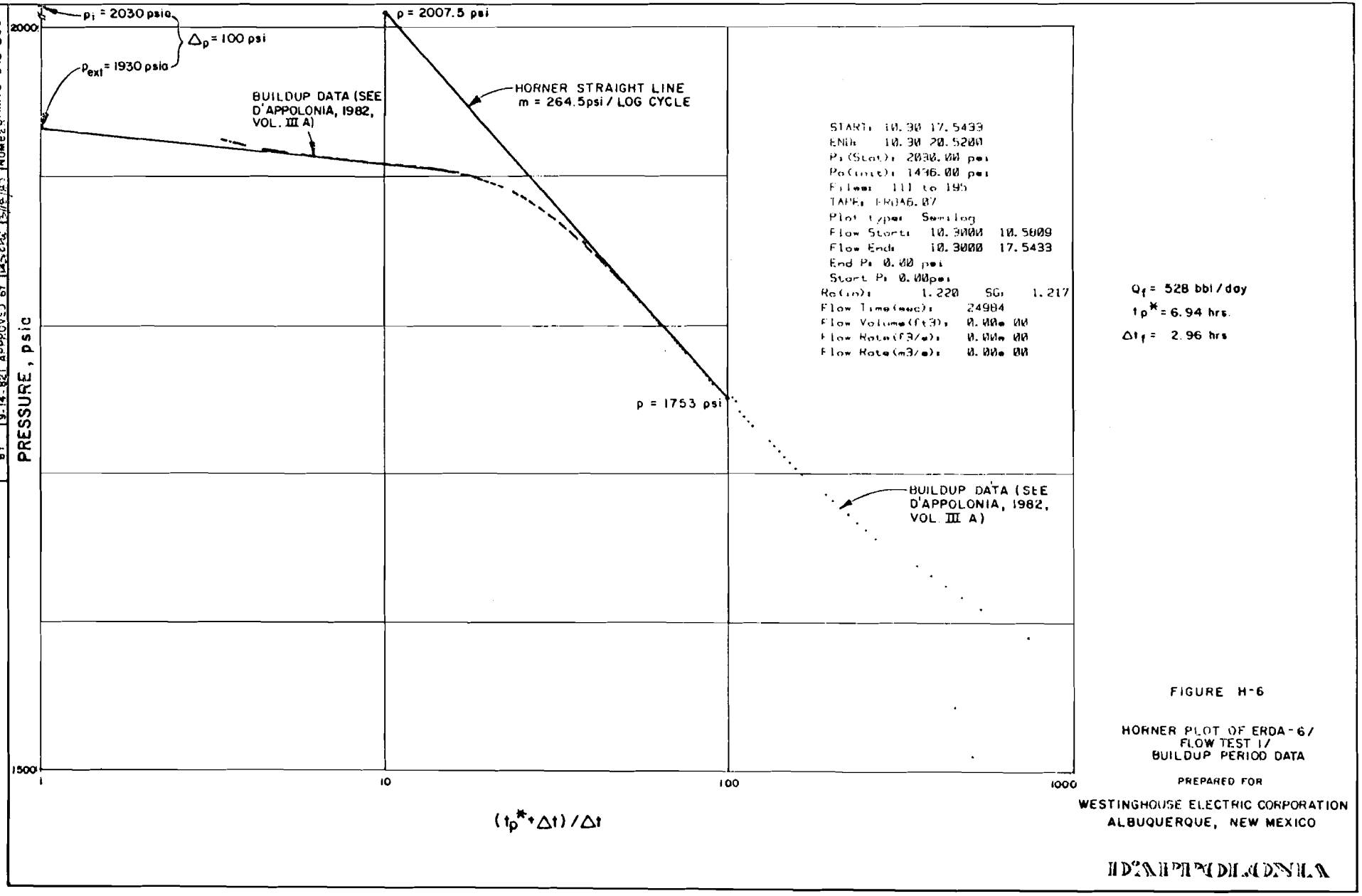

FIGURE H-6

HORNER PLOT OF ERDA-6/
FLOW TEST 1/
BUILDUP PERIOD DATA

PREPARED FOR

WESTINGHOUSE ELECTRIC CORPORATION
ALBUQUERQUE, NEW MEXICO

D'APPOLONIA

DRAWN BY | BAH | 9-14-82
CHECKED BY | RLS | 9/15/82
APPROVED BY | DA/CPA | 9/15/82
DRAWING NUMBER NM78-648-850

TME 3153

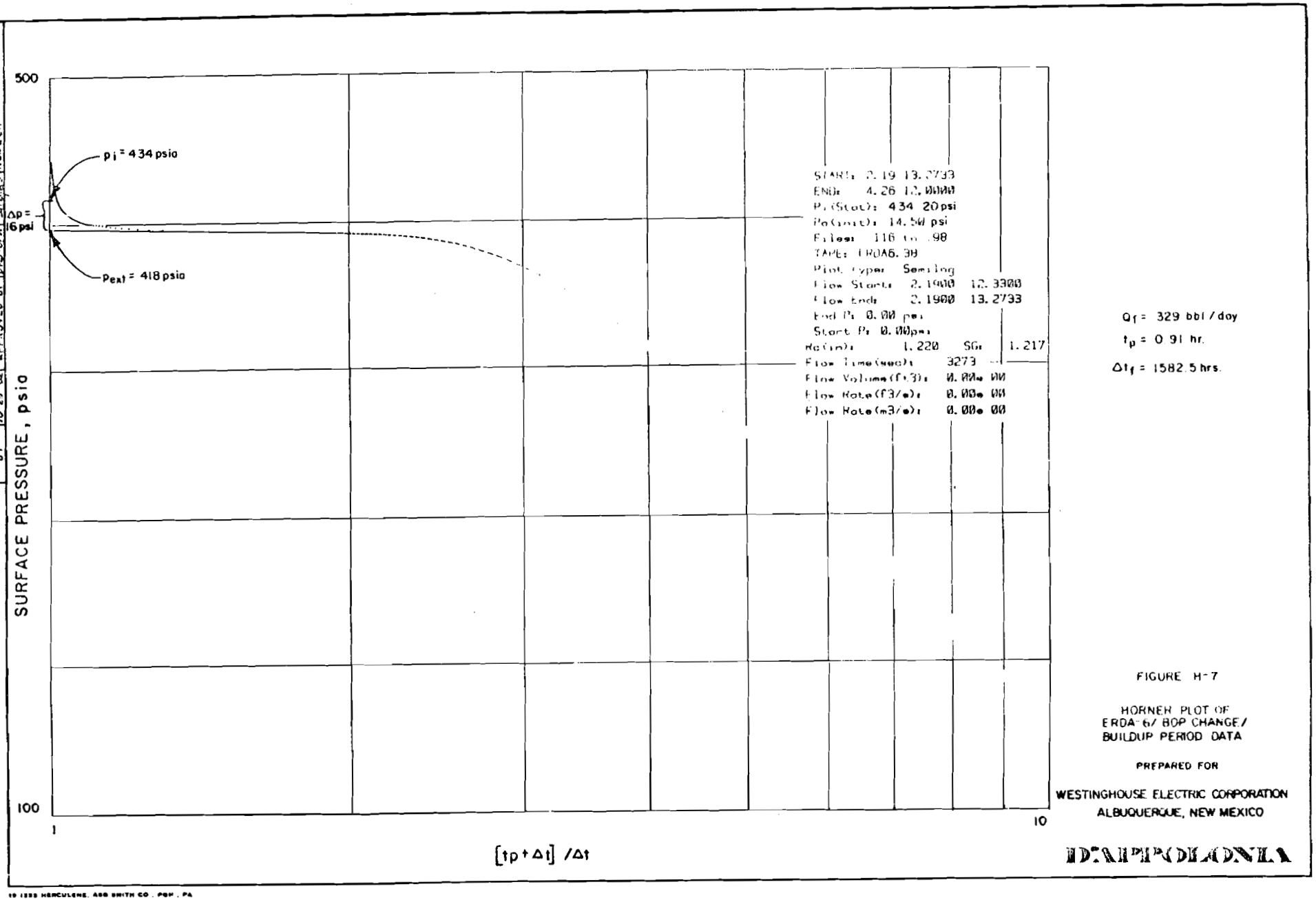

FIGURE H-7

HORNER PLOT OF
ERDA-6/ BOP CHANGE/
BUILDUP PERIOD DATA

PREPARED FOR

WESTINGHOUSE ELECTRIC CORPORATION
ALBUQUERQUE, NEW MEXICO

DRAWN BY | 10-26-82 | APPROVED BY | DRAWING NUMBER NM76-648-843

TME 3153

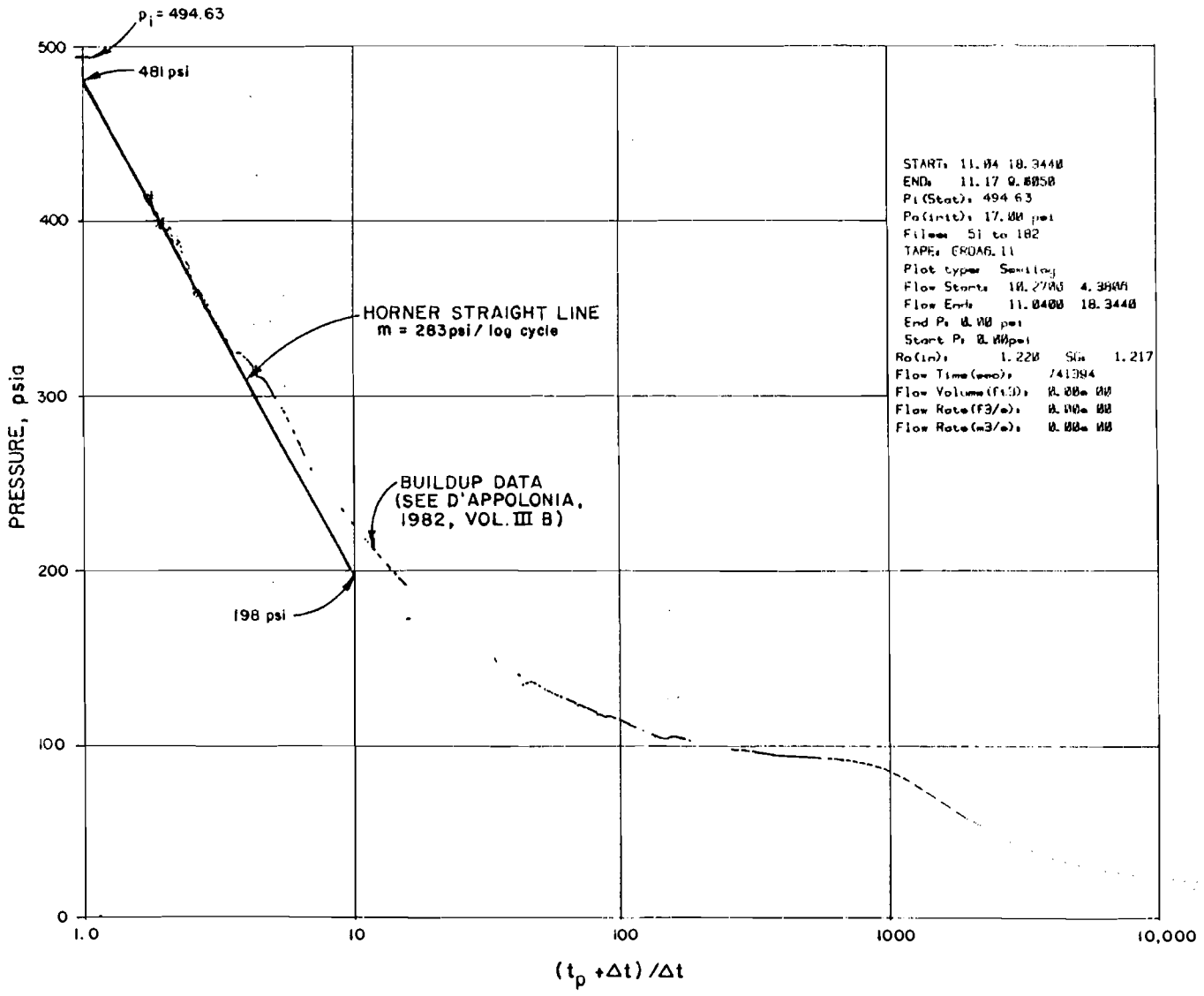

Q_f = 120 bbl/day

$t_p{}^*$ = 206 hrs.

Δt_f = 302.4 hrs.

FIGURE H-8

HORNER PLOT OF ERDA-6/
FLOW TEST 2/
BUILDUP PERIOD DATA

PREPARED FOR

WESTINGHOUSE ELECTRIC CORPORATION
ALBUQUERQUE, NEW MEXICO

D'APPOLONIA

DRAWN BY 9-15-82 | CHECKED BY | APPROVED BY | DRAWING NUMBER NM78-648-B62

TME 315

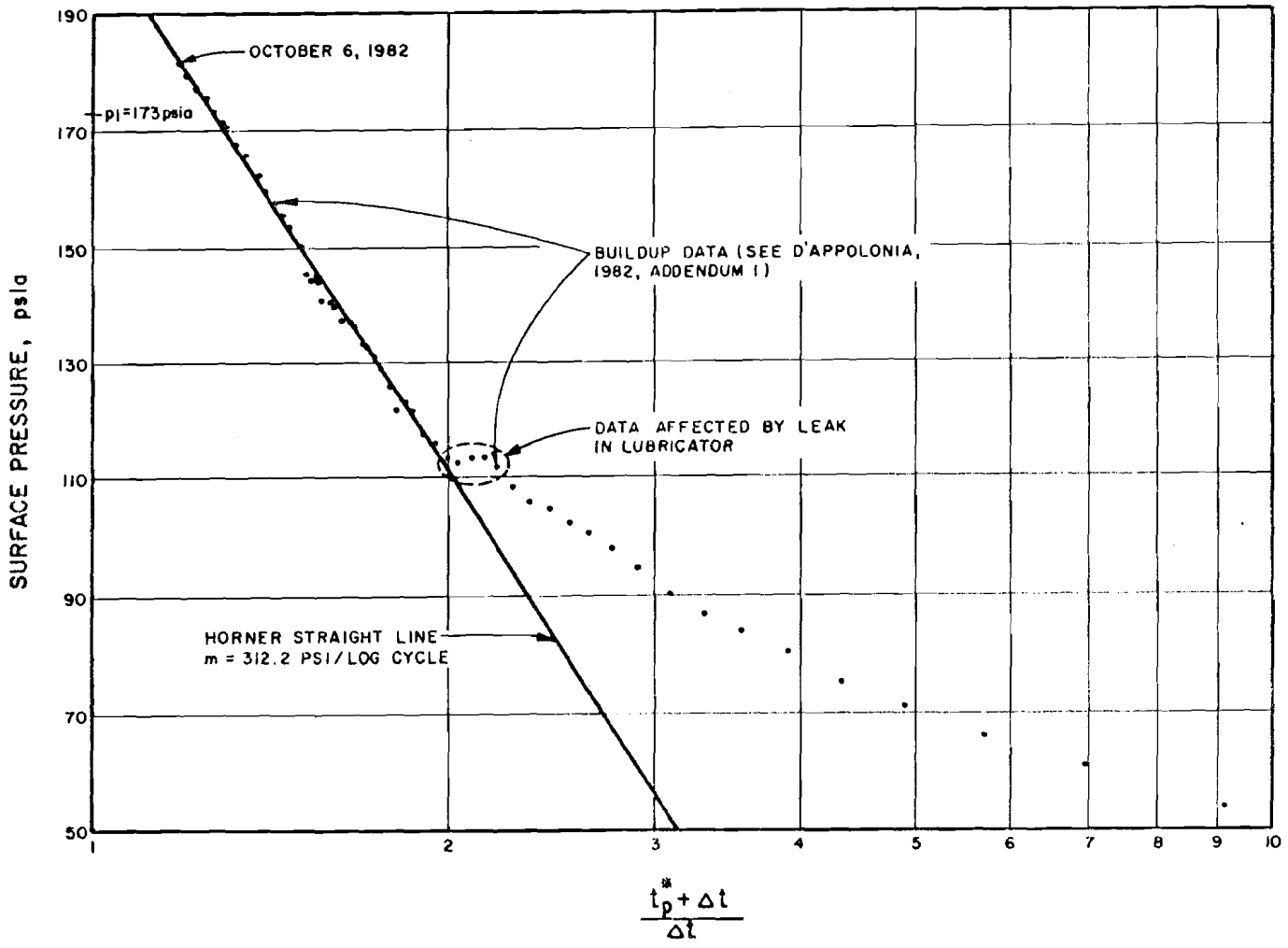

Q_f = 1097 bbl / day

t_p^* = 542.5 hrs.

Δt_f = 3020.5 hrs.

FIGURE H-9

HORNER PLOT OF WIPP-12 / FLOW TEST 3 / BUILDUP PERIOD DATA

PREPARED FOR

WESTINGHOUSE ELECTRIC CORPORATION
ALBUQUERQUE, NEW MEXICO

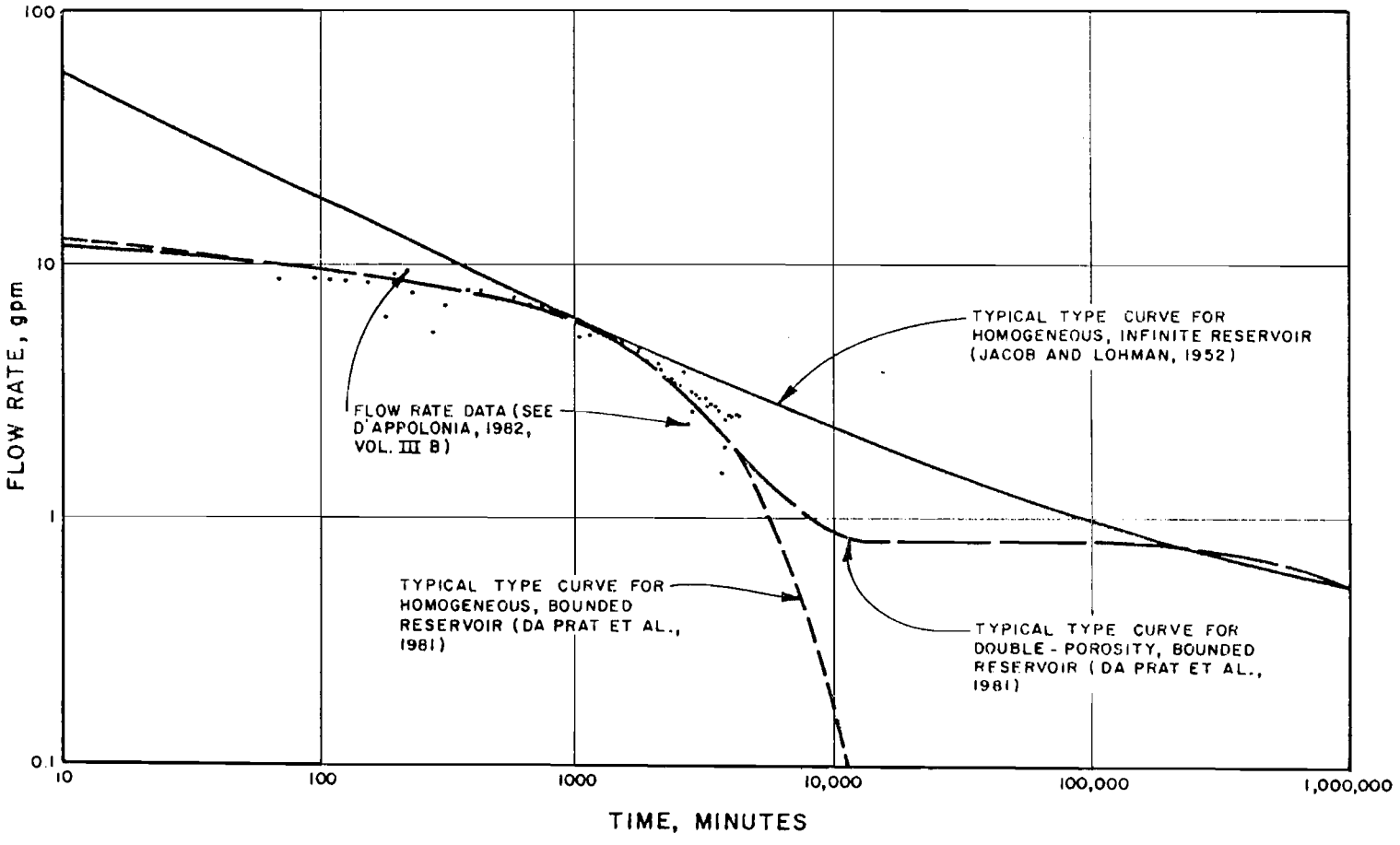

FIGURE H-10

COMPARISON OF OBSERVED AND THEORETICAL FLOW RATE DECLINE DURING ERDA-6/FLOW TEST 3

PREPARED FOR

DRAWN BY | B.K.H. | 10-13-82
CHECKED BY | K.L.B. | 3/18/83
APPROVED BY | [illegible] | 3/18/83
DRAWING NUMBER NM78-648-847

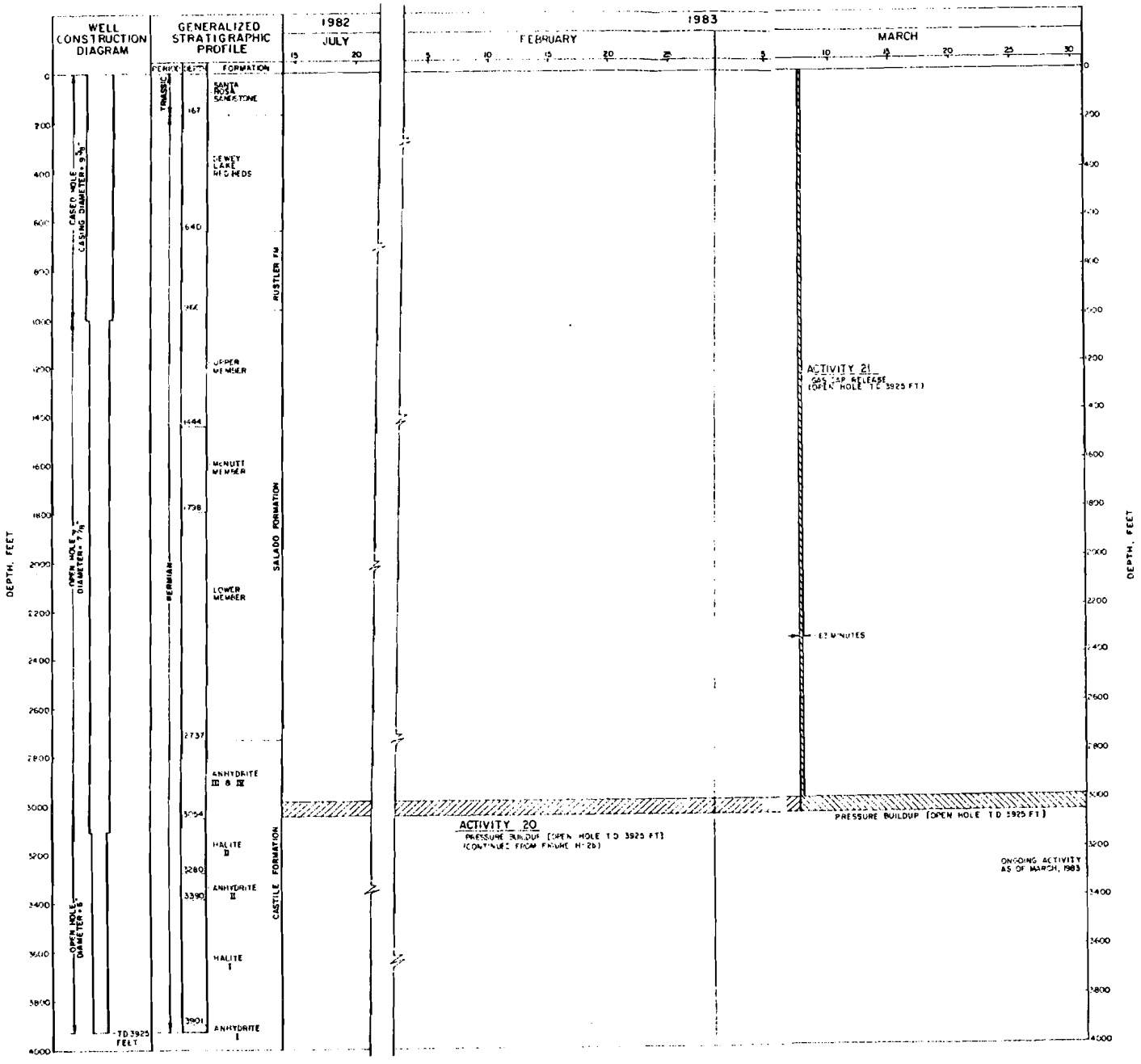

NOTES:

1. ALL DEPTHS ARE REFERENCED TO GROUND SURFACE ELEVATION 3471.2 FEET ABOVE SEA LEVEL
2. STRATIGRAPHIC PROFILE FROM FREELAND AND DAGOURIAN, GEOLOGIC DATA FOR BOREHOLE WIPP-12, D'APPOLONIA CONSULTING ENGINEERS, 1982, UNPUBLISHED REPORT

FIGURE H-2c

WIPP-12
CONTINUATION OF TIME-VERSUS-DEPTH ACTIVITY SUMMARY

PREPARED FOR

WESTINGHOUSE ELECTRIC CORPORATION
ALBUQUERQUE, NEW MEXICO

D'APPOLONIA

DRAWN BY | CHECKED BY RLB 3/18/83 | APPROVED BY | DRAWING NUMBER NM78-648-B63

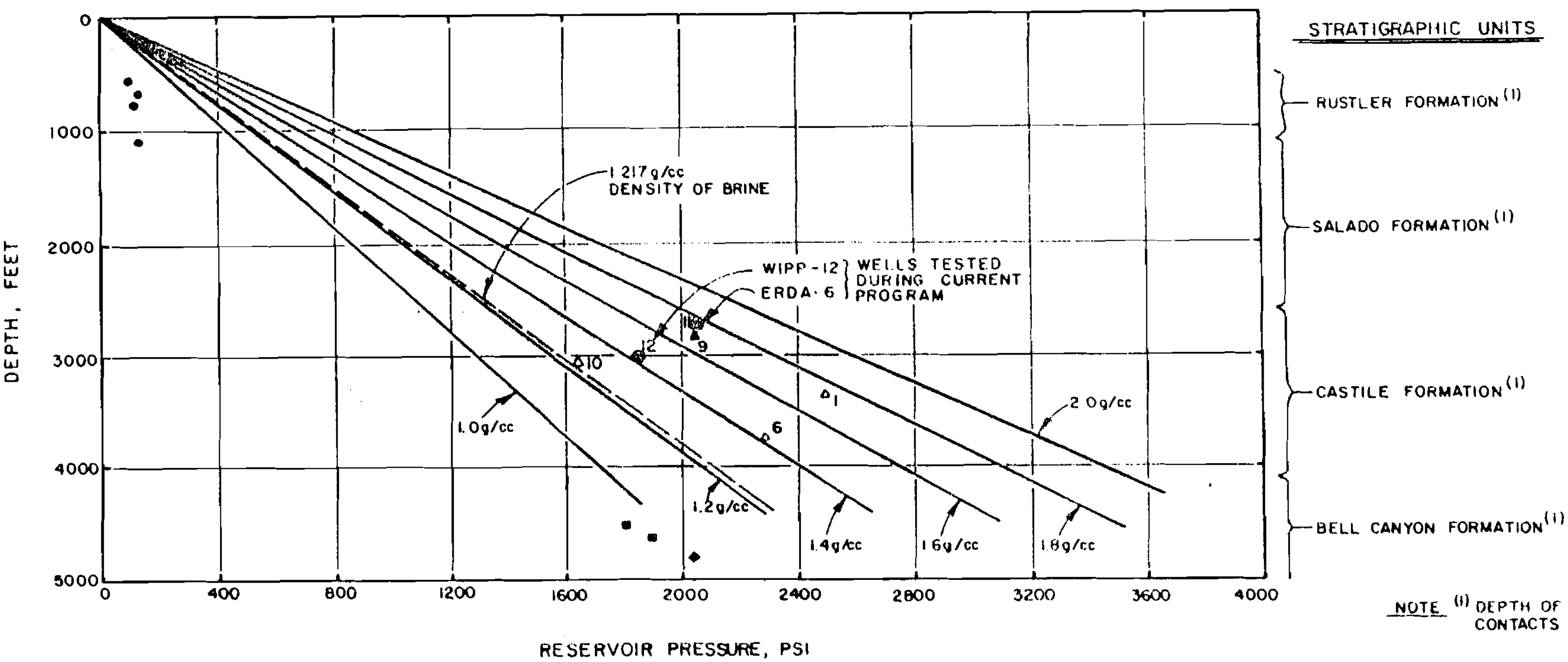

NOTE (1) DEPTH OF STRATIGRAPHIC CONTACTS AVERAGED.

LEGEND:

- ● PRESSURES MEASURED IN RUSTLER FORMATION
- ▲ PRESSURES MEASURED IN CASTILE FORMATION
- △ MINIMUM PRESSURE ESTIMATED IN CASTILE FORMATION
- ■ PRESSURES MEASURED IN BELL CANYON FORMATION, UPPER SAND
- ◆ PRESSURES MEASURED IN BELL CANYON FORMATION, LOWER SAND
- 1.0 g/cc ╲ PRESSURE GRADIENTS FOR MATERIALS OF SPECIFIED DENSITY (g/cc)

NOTE:
FOR WELL DESIGNATIONS REFER TO FIGURE G-11 AND TABLE H.1.

FIGURE H-11

PRESSURE VERSUS DEPTH FOR SELECTED BRINE RESERVOIRS IN WIPP VICINITY

PREPARED FOR

WESTINGHOUSE ELECTRIC CORPORATION
ALBUQUERQUE, NEW MEXICO

TME 3153

(815)

01	DRAWN BY	9-15-82	DRAWING NUMBER NM78-648-A2
	CHECKED BY	KLB	
	APPROVED BY		

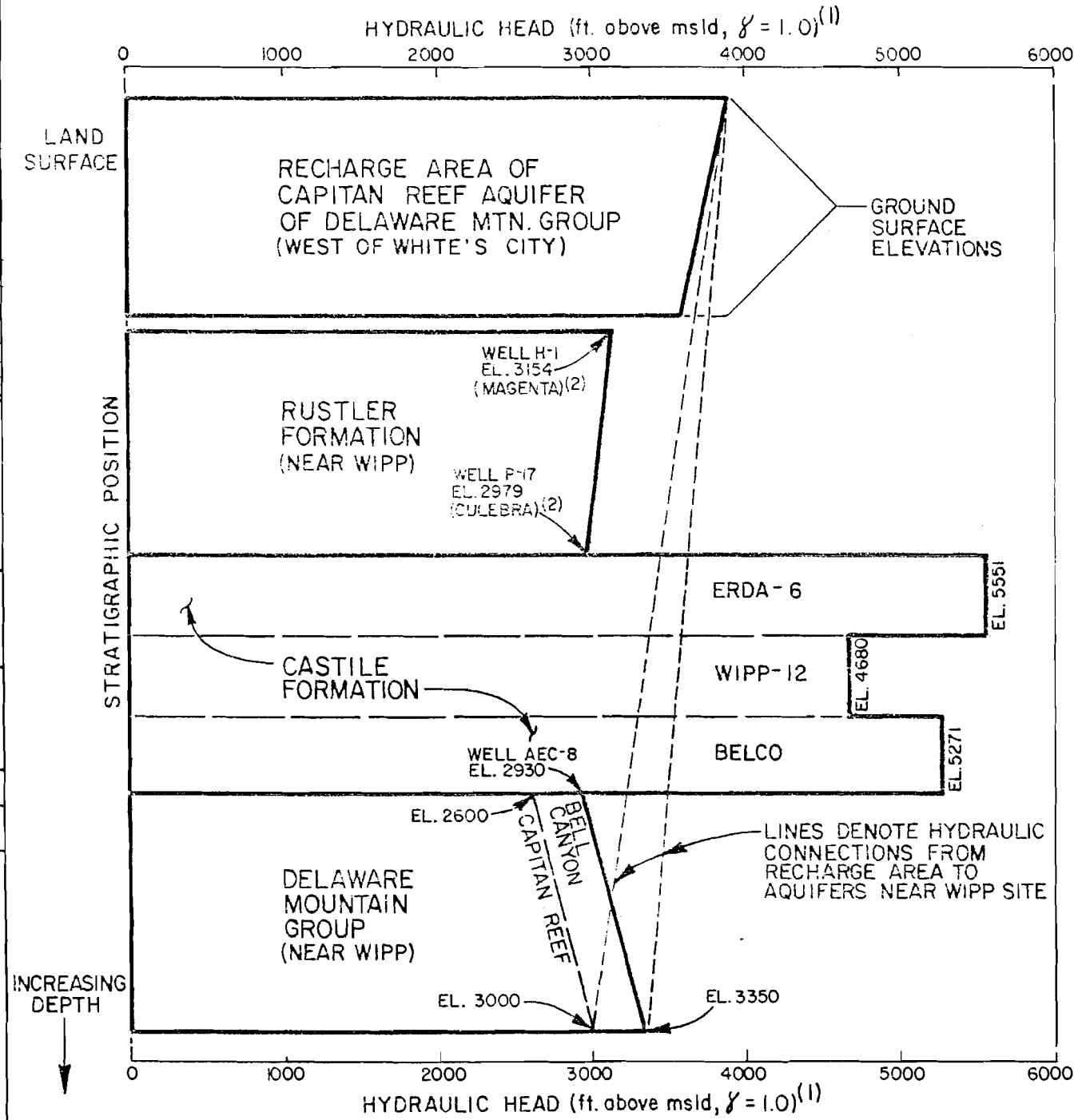

NOTE:

(1) HYDRAULIC HEAD VALUES ARE REFERENCED TO MEAN SEA LEVEL DATUM (msld) AND STANDARDIZED SPECIFIC GRAVITY OF WATER ($\gamma = 1.0$).

(2) MERCER AND ORR, 1979.

FIGURE H-12

COMPARISON OF STANDARDIZED HYDRAULIC HEADS OF RUSTLER AND CASTILE FORMATIONS AND DELAWARE MOUNTAIN GROUP

PREPARED FOR

WESTINGHOUSE ELECTRIC CORPORATIC

ALBUQUERQUE, NEW MEXICO

D'APPOLONIA

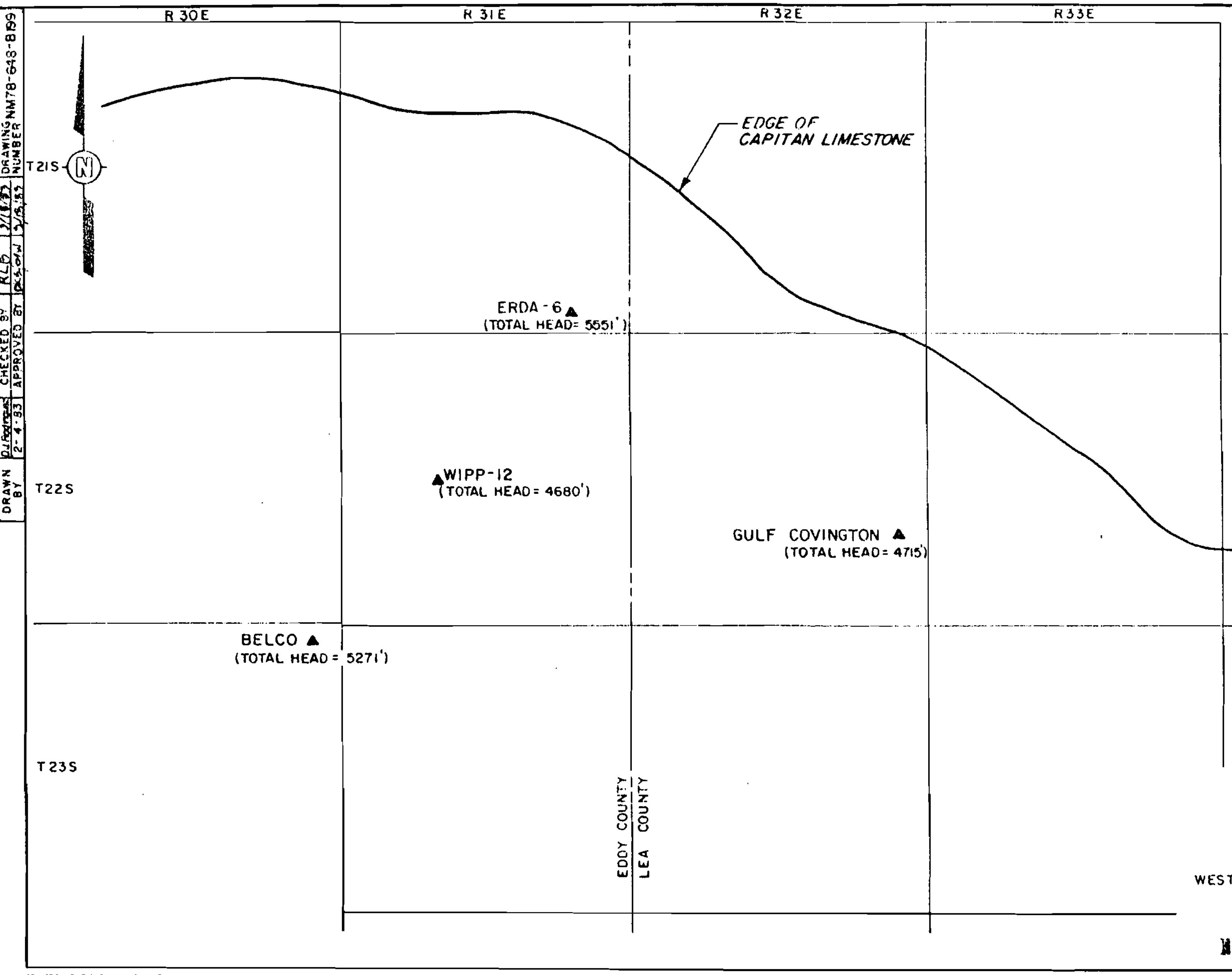

NOTE:
HEADS ARE CALCULATED FOR PURE WATER (γ = 1.0).

FIGURE H-13

HEAD DISTRIBUTION IN
CASTILE BRINE RESERVOIRS

PREPARED FOR

WESTINGHOUSE ELECTRIC CORPORATION
ALBUQUERQUE, NEW MEXICO

TME 3153

DRAWN BY	TEJ	CHECKED BY	KLJ	3/14/83
	6-23-82	APPROVED BY	D'APPOLONIA	3/15/83

DRAWING NUMBER NM78-648-B65

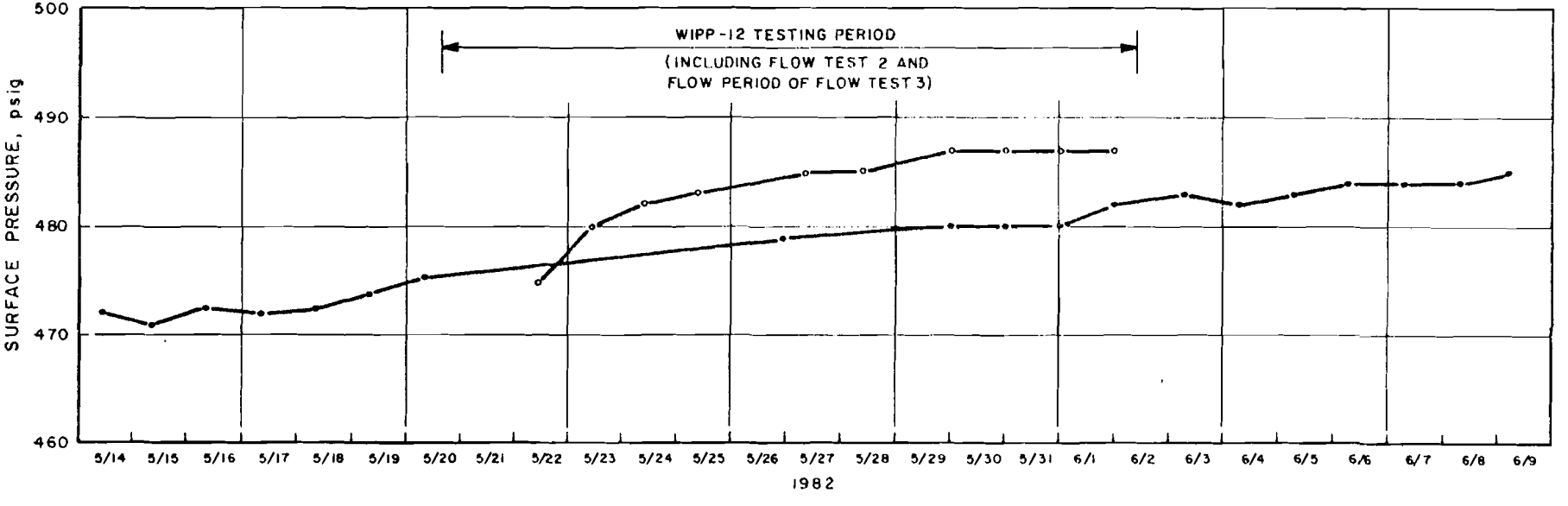

LEGEND

PRESSURE GAGE READINGS

PRESSURE RECORDER READINGS

NOTES:

1. DISCREPANCY DUE TO CALIBRATION OFFSET. PRESSURE RECORDER NEAR LIMIT OF OPERATING RANGE.
2. DATA TABULATED IN D'APPOLONIA (1982), ADDENDUM I.

START: 5.14 09:54
END: 6.9 07:10
PLOT TYPE: LIN-LIN

FIGURE H-14

PRESSURE IN OBSERVATION WELL ERDA-6 DURING TESTING OF WIPP-12 BRINE RESERVOIR

PREPARED FOR

WESTINGHOUSE ELECTRIC CORPORATION
ALBUQUERQUE, NEW MEXICO

D'APPOLONIA

TME 3153

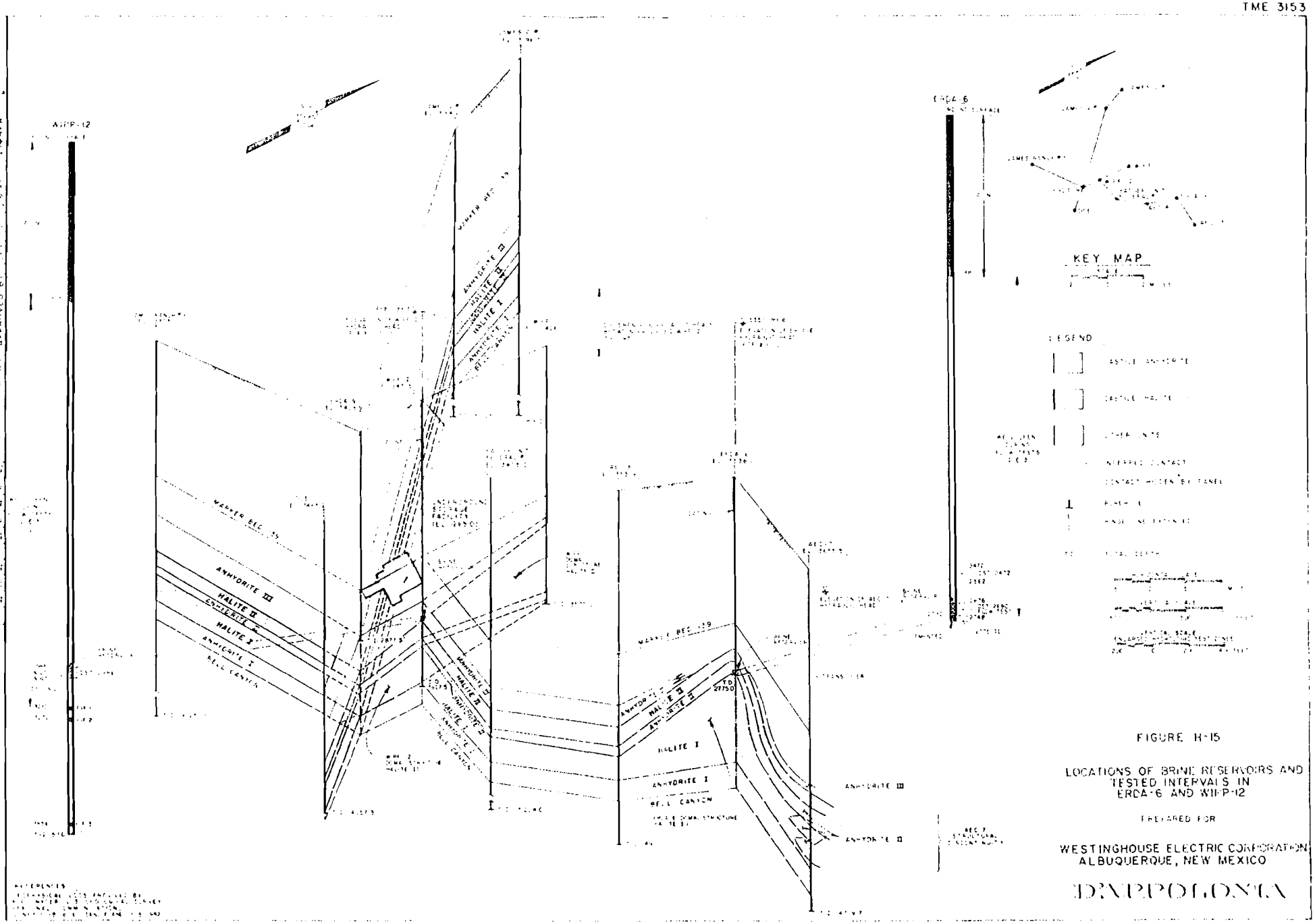

FIGURE H-15

LOCATIONS OF BRINE RESERVOIRS AND TESTED INTERVALS IN ERDA-6 AND WIPP-12

PREPARED FOR

WESTINGHOUSE ELECTRIC CORPORATION
ALBUQUERQUE, NEW MEXICO

DAPPOLONIA

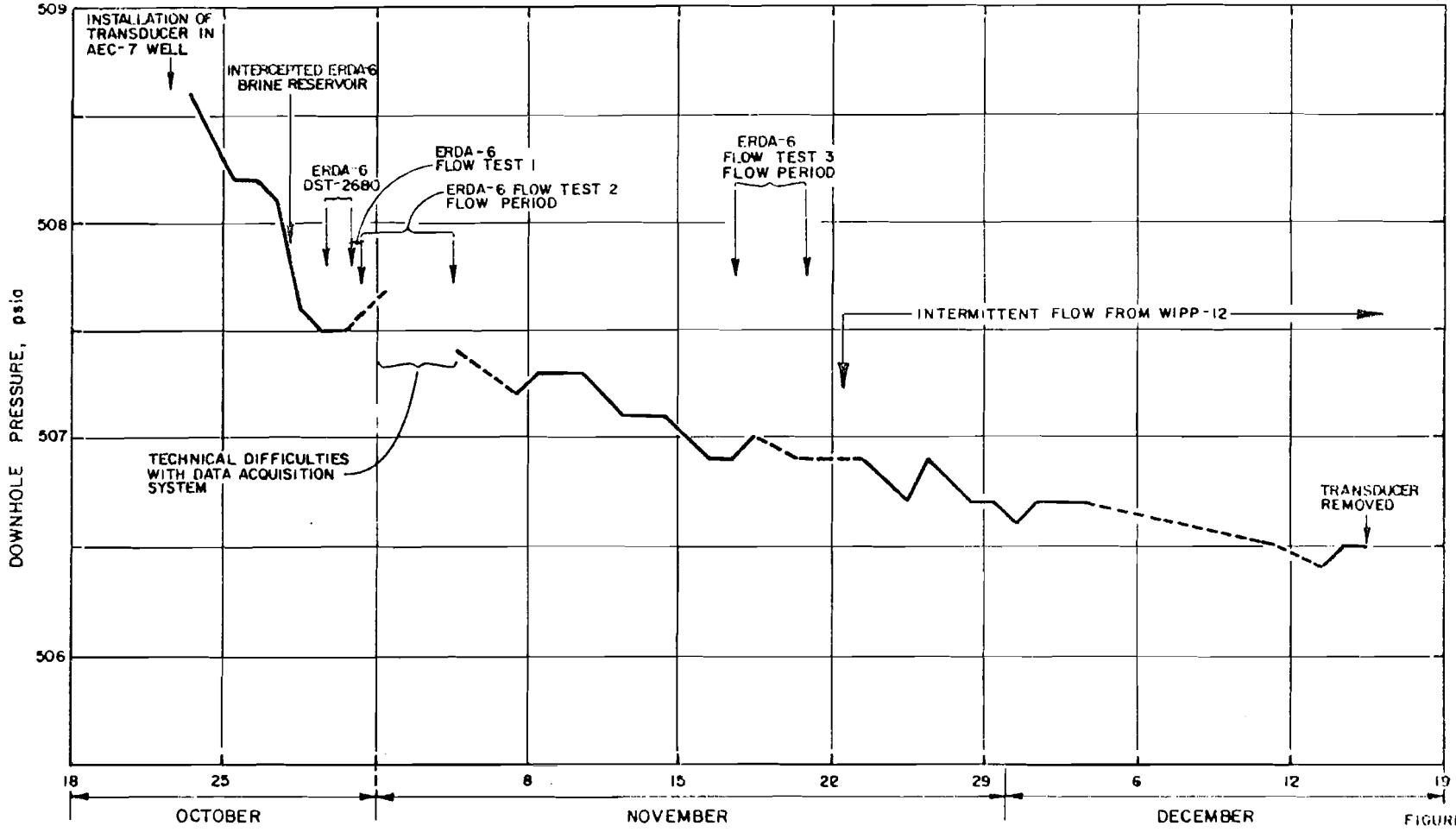

NOTE:
TRANSDUCER WAS SET 1300 FEET BELOW GROUND SURFACE.

FIGURE H-16
PRESSURE IN OBSERVATION WELL AEC-7 DURING TESTING OF ERDA-6 AND WIPP-12 BRINE RESERVOIRS

PREPARED FOR

WESTINGHOUSE ELECTRIC CORPORATION
ALBUQUERQUE, NEW MEXICO

DRAWING NUMBER NM78-648 B66

DRAWN BY | CHECKED BY | APPROVED BY | DATE 9/15/82

TME 3153

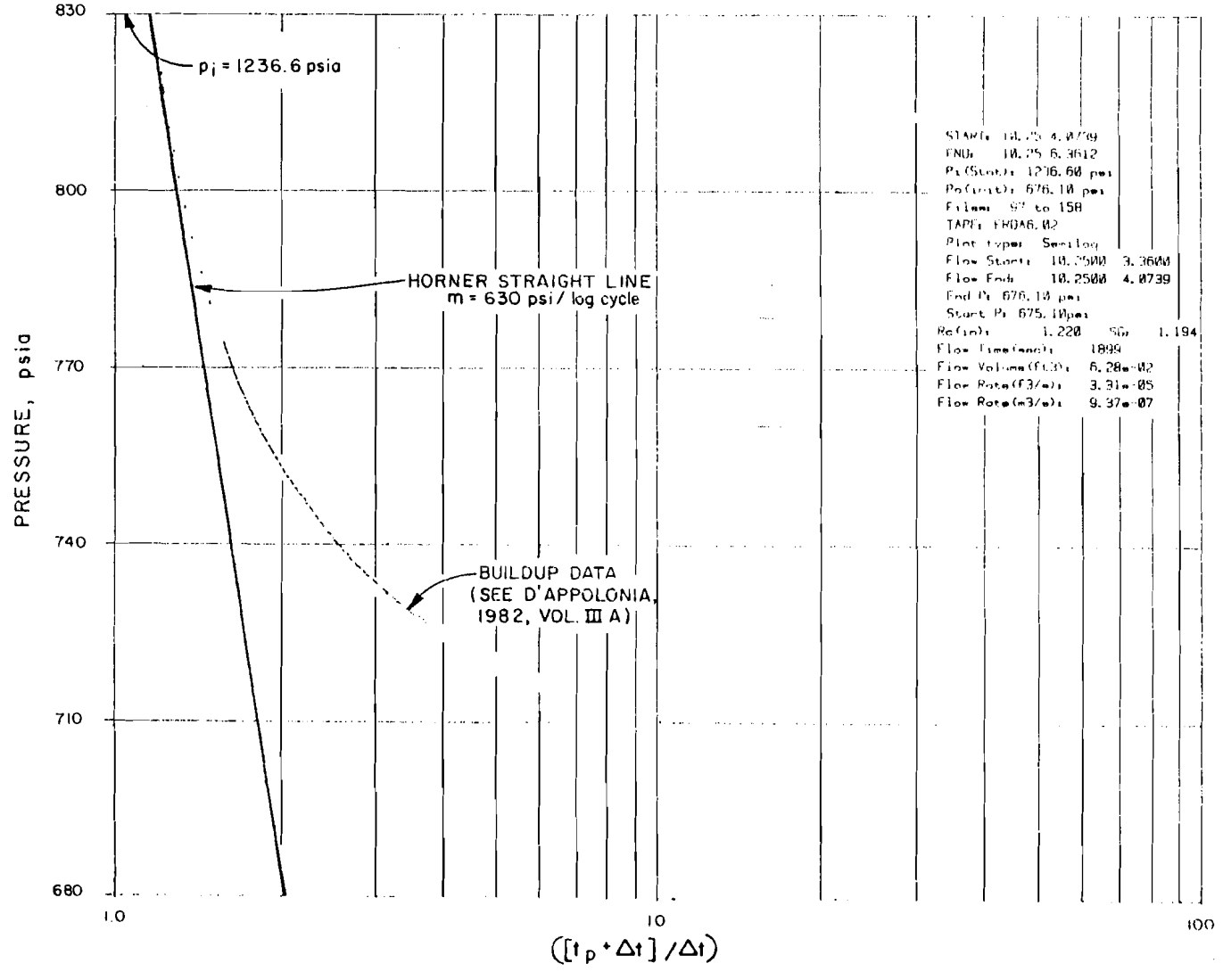

Q = 0.51 bbl / day

t_p = 0.53 hr.

Δt_f = 2.48 hrs.

FIGURE H-17

HORNER PLOT OF ERDA-6/
DST-2472-1/
SECOND BUILDUP PERIOD DATA

PREPARED FOR

WESTINGHOUSE ELECTRIC CORPORATION
ALBUQUERQUE, NEW MEXICO

DAPPOLONIA

TME 3515

03	DRAWN BY	R. Bricker 23 Oct. 82	CHECKED BY		DRAWING NUMBER NM78-648-A90
			APPROVED BY		

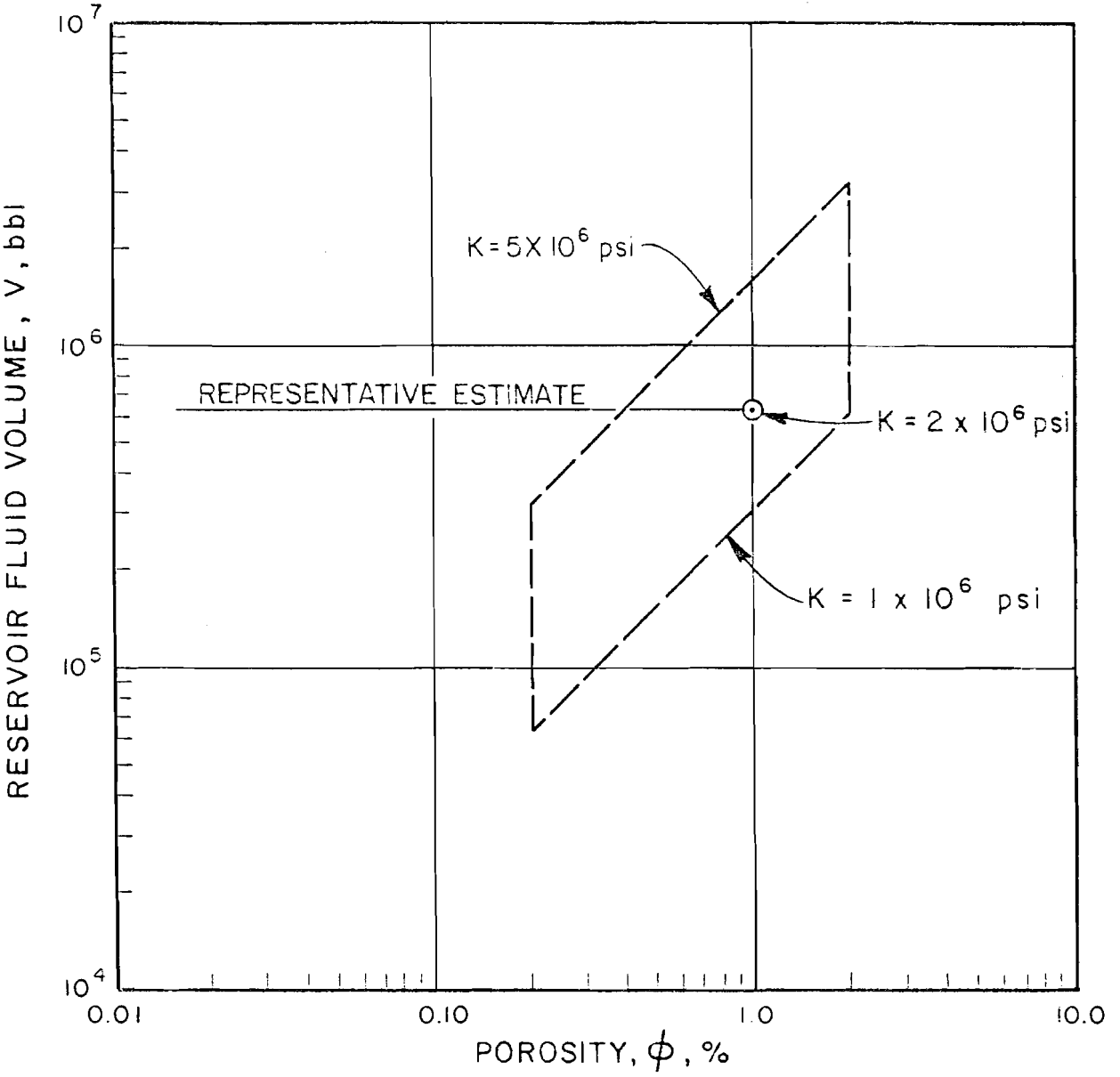

$$V = \frac{\Delta V}{\Delta p\,(1/\phi K)}$$

ΔV = 1650 bbl

$\Delta p \leq$ 52 psi

NOTE:

SEE SECTION 3.3.5 FOR DEFINITION OF VARIABLES.

FIGURE H-18

TOTAL RESERVOIR FLUID VOLUME
ERDA-6

PREPARED FOR

WESTINGHOUSE ELECTRIC CORPORAT
ALBUQUERQUE, NEW MEXICO

D'APPOLONIA

04	DRAWN BY	R. Bricker 23 Oct. 82	CHECKED BY		DRAWING NUMBER NM78-648-A91
			APPROVED BY		

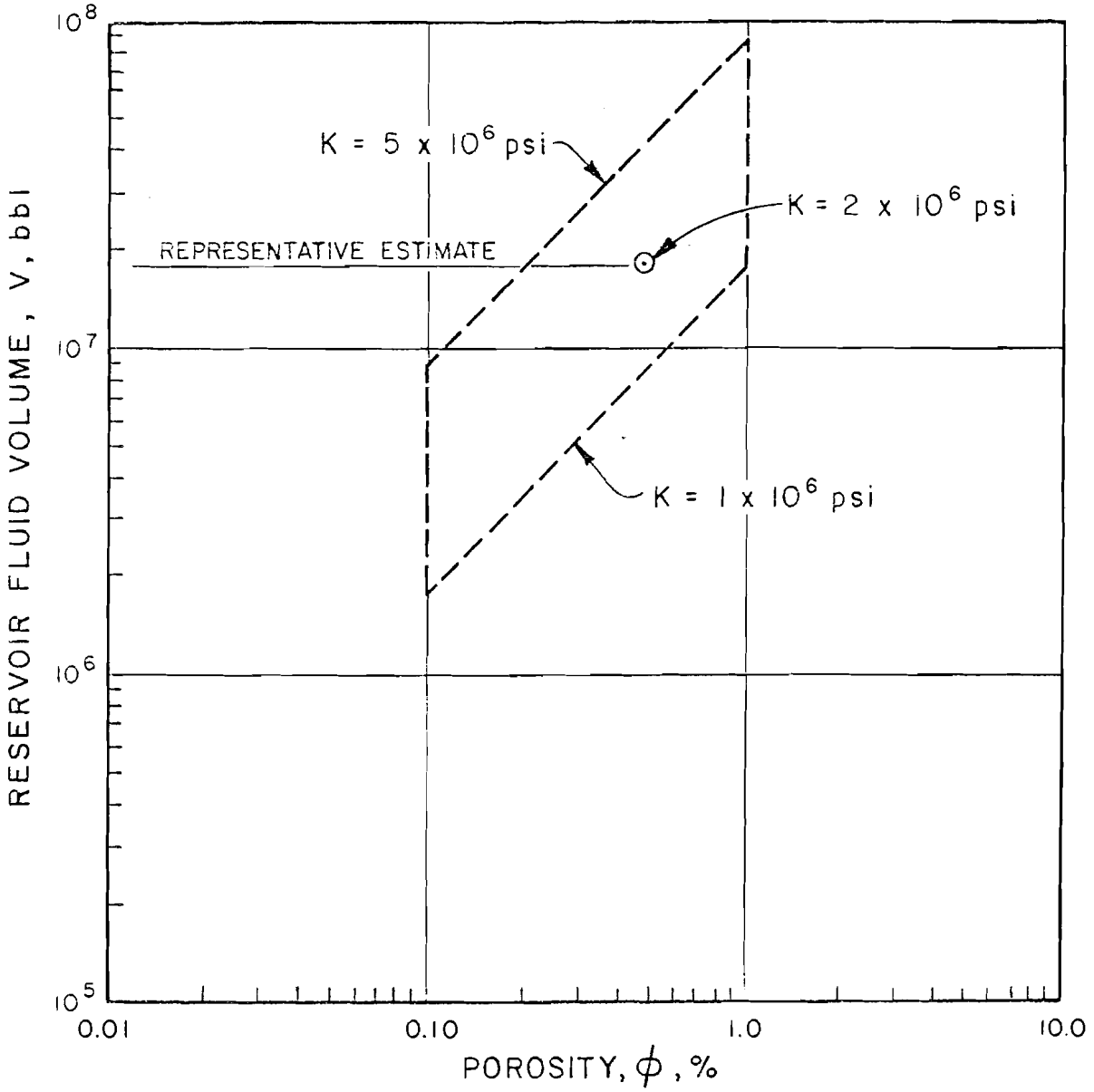

$$V = \frac{\Delta V}{\Delta p \ (1/\phi K)}$$

ΔV = 80,000 bbl

$\Delta p \leq$ 46 psi

NOTE:

SEE SECTION 3.3.5 FOR DEFINITION OF VARIABLES.

FIGURE H-19

TOTAL RESERVOIR FLUID VOLUME
WIPP-12

PREPARED FOR

WESTINGHOUSE ELECTRIC CORPORATION
ALBUQUERQUE, NEW MEXICO

D'APPOLONIA

TABLE OF CONTENTS

TABLE OF CONTENTS
(Continued)

LIST OF TABLES

LIST OF FIGURES
(Continued)

LIST OF FIGURES

PART IV - CHEMISTRY

1.0 INTRODUCTION AND SUMMARY

The chemistry of the Castile reservoir brines and coexisting gases have been evaluated to resolve issues related to the stability of the proposed WIPP site. The issues of concern are:

- The degree of isolation of the reservoirs.
- The potential for the fluids to degrade the host rock by chemical means (e.g., dissolution, reaction).
- The potential for the reservoirs to increase either in number, or in volume of fluid, within a short time frame.

Confident resolution of these issues depends on identifying the most likely origin of the reservoir fluids, and on evaluating the degree to which the fluids have equilibrated chemically with the host rock. These goals have been accomplished by assessing the major and minor element chemistries of the fluids, and by considering their isotopic compositions.

Prior to analysis of the data, several origins for the brine water were considered plausible. Possible water sources considered were:

- Meteoric water.
- Waters of dehydration (from gypsum).
- Ancient seawater.

Major and minor element chemistry and the isotopic character of the brines were used to evaluate these three models. Only one model appears to be internally consistent with all aspects of the chemistry. Specifically, the brine chemistry strongly indicates that the reservoir waters were derived from Permian seas. The ancient seawater was concentrated by evaporation in the open basin, and then trapped as pore water during sedimentation. The pore water was mobilized by structural deformations of the Delaware Basin, and

traveled along contacts and fractures to its point of collection. During this inferred ancient transport, the brine reacted with sedimentary carbonate minerals to form the dolomite observed in alteration zones. This reaction depleted the brines in magnesium, and increased the isotopic abundance of heavy oxygen (^{18}O). Either during transport, or subsequent to the entrapment of brine in the reservoir fractures, the waters of ERDA-6 and WIPP-12 also dissolved minor amounts of halite.

Although both ERDA-6 and WIPP-12 brines experienced similar histories, their individual chemistries are separate and distinct. This difference is probably a result of slightly different host environments, and different mineralogical interactions during transport to collection in the reservoirs. WIPP-12 brine is saturated with anhydrite, halite, calcite, and dolomite. These are the primary minerals occurring in the reservoir host rock. Accordingly, WIPP-12 brine is in chemical equilibrium with its environment, and has no potential for dissolving or reacting with host rock under present conditions. ERDA-6 brine is similarly saturated with anhydrite, calcite, and dolomite, but it appears to be slightly undersaturated with respect to halite. The potential for halite dissolution is small, however. Dissolution of less than one centimeter of the overlying salt will bring the brine to sodium chloride equilibrium, and cause dissolution to stop.

The most distinct compositional difference between ERDA-6 and WIPP-12 fluids is in their gas compositions. Gases in WIPP-12 are predominantly methane and hydrogen sulfide, while gases in ERDA-6 are predominantly carbon dioxide and hydrogen sulfide. Both reservoirs contain minor amounts(~ 10%) of nitrogen that is not due to air contamination. Both reservoirs have highly reducing (i.e., oxygen absent) environments.

The significance of the brine origin and the chemistry of the reservoir fluids is:

- The reservoirs are isolated. They are not connected to each other, or to any ground-water source. Moreover, the isolated condition of the reservoirs has probably existed since their formation at least a million years ago.

- The reservoirs are chemically stable. At the present temperature, the brines do not have the potential to impair the stability of the reservoir rock.

- The reservoir waters were formed from ancient seawater. Most of the brine, at one time, was pore water in the anhydrite. Accordingly, the potential for forming new reservoirs (or increasing the volume of existing reservoirs) is limited to the volume of pore water available through fractures. Whether or not such increases will occur is a function of geomechanical processes.

1.1 SUMMARY OF PREVIOUS INVESTIGATIONS

Rock and ground-water chemistries have been studied for several years, beginning in the early 1970's, in support of the WIPP project. The Geological Characterization Report, Waste Isolation Pilot Plant (WIPP) Site (Powers et al., 1978) summarized the data regarding the mineralogy of both evaporite and non-evaporite formations, as well as whole rock chemistry, and mineral paragenesis. In addition to ground-water compositions, the volatile phases in the evaporite sequence were investigated. Stable isotopes in area ground waters, and Rb/Sr and U systematics were also summarized. In addition to the comprehensive report by Powers et al. (1978), the geochemistry of the WIPP site and its environs are the subject of several shorter papers. Adams (1969) related the nature of trace elements in the Salado Formation, and Barr et al. (1979) have utilized uranium disequilibrium relations to infer ground-water residence times. Ground-water chemistry is discussed in Jones (1973), Mercer and Orr (1979), and Lambert (1978), and brines in the Castile Formation are examined in Anderson (1982), Anderson and Kirkland (1980), and Lambert (in preparation).

Previous geochemical studies of the WIPP site have concluded:

- It is unclear whether the brine occurrences at or near the WIPP site affect the stability of the geologic formation intended for nuclear waste disposal. Specific issues which are unresolved include the possibility of brine movement, the extent of brine accumulation, and the potential for dissolution at the site (cf. Anderson, 1982; Anderson and Kirkland, 1980; Lambert, 1978, and in preparation).

- The major mineral phases in the evaporite sequences are anhydrite, several clays, halite, loeweite, magnesite, polyhalite, quartz, and sylvite (Powers et al., 1978).

- Phases which occur in lesser amounts in the evaporites include kainite, iron oxide, feldspar, langbeinite, carnallite, and kieserite (Powers et al., 1978).

- Ground waters are chemically related to their host rock. Reactions between water and rock have influenced ground-water chemistry. Processes which have probably occurred include dissolution of evaporites, and isotopic and cation exchange between water and rock (Powers et al., 1978; Lambert, 1978).

- The origin of brines in the upper Castile Formation is uncertain. The meteoric-ground water, residual seawater, and the dehydration of hydrous phases origins have been proposed and defended (Lambert, 1978; Anderson, 1982; Anderson and Kirkland, 1980).

1.2 PURPOSE OF STUDY

The purposes of this study are to obtain chemical data about the brine reservoirs in the Permian Castile Formation and to interpret those data as they relate to the stability of the WIPP site. A major part of that assessment depends on an understanding of the processes that gave rise to the brine waters. Therefore, an integral part of the study is to establish the most likely genetic origin for the brines and associated gases. Of equal importance is to characterize the chemistries of the brines in sufficient detail that the brines may be evaluated for:

- Chemical communication between brine reservoirs or with local ground waters.
- Equilibrium with their geologic environments.
- Potential for degrading the proposed WIPP facility formation.
- Potential for increasing in volume (or in number of reservoirs) within a short (e.g., 10,000 year) time frame.

1.3 SCOPE OF STUDY

The scope of the present geochemical study includes consideration of all areas which pertain to the issues described briefly above and in more detail in Section 2.0. The main elements of this study, however, are the chemistries of the Castile brines, gases, and reservoir host rocks. Regional host rock and ground water data for the site and its environs will be drawn from D'Appolonia (1982) and other published reports. The objective of this study is to obtain as much chemical data on the brine, gas, and reservoir rocks as practically possible using a wide array of techniques. Thus, the scope of this study includes data obtained from:

- Chemical analyses of rock, gas, and brine for major, minor, and trace elements.
- Petrographic observations of the rocks.
- Scanning electron microscopy, with energy dispersive analysis of the rocks.
- Isotopic analyses of rocks, gases, and brines.
- Theoretical analyses of data.

Data generated during this study are sufficient to resolve the pertinent issues with a high degree of confidence; investigations to determine the uranium disequilibrium age of the brine and the origin of the evaporite deformation are continuing.

2.0 CHEMISTRY ISSUES RELATED TO BRINE RESERVOIRS

2.1 EXTENT OF CHEMICAL ISOLATION OR COMMUNICATION WITH OTHER WATER SOURCES

The issue of reservoir isolation is particularly critical to site suitability because if the brines communicate with other water sources, they represent a potential medium for transporting nuclides away from the proposed waste facility. Conversely, if the brines do not communicate with each other or with external water sources, they will have little capacity for dispersing nuclides. Analysis of the chemistries of the brines and coexisting gases is one means for determining the degree of present or past communication between reservoirs or among the brines and local ground waters. Because of the diffusive mobility of ions (near 10^{-4} to 10^{-5} cm^2/sec in standing water; Weast, 1971; Skelland, 1974) and of gases (near 10^{-1} cm^2/ sec; Skelland, 1974), chemical composition is a sensitive test for determining the extent of reservoir isolation. As an illustration, the linear diffusive distances for an average gas molecule have been calculated from: $x = (2Dt)^{1/2}$, where x = distance, D = diffusion coefficient, t = time. The calculation assumes that straight-line fractures exist between ERDA-6 and WIPP-12, and that the pore space of the rock is saturated with water. The assumptions are believed relevant because two isotopically distinct methanes and chemically distinct gases exist in the two wells.

The results compiled in Table C.1 for selected time periods show the distances over which near total equilibration (i.e., no concentration gradient) will exist. From the table, it can be seen that if the WIPP-12 and ERDA-6 reservoirs were well connected, significant mixing would occur between them in less than 80,000 years, and that no difference between reservoirs would be observed after 4.9 million years. Since the reservoirs were formed at least one million years ago (Jones, 1973, and see Part II, Geology, Section 4.3), the reservoir chemistry (particularly the gases) can be used to infer the extent of reservoir isolation. This determination can be made by detailed comparisons of major and minor element proportions and by comparing appropriate isotopic abundances.

2.2 GENERATION OF BRINE AND GAS COMPOSITIONS AND RELATION TO BRINE ORIGIN

The determination of the origin and composition of the ERDA-6 and WIPP-12 brines pertains to the potential for further brine generation, and the potential for (and effects of) brine migration. With respect to the WIPP site, the generation of more brine, or its migration over the long term have ramifications with respect to site stability and waste isolation. Several geochemical approaches can help determine brine origins, including major and minor element chemistry, and isotopic compositions of brines, gases, and host rocks.

2.3 EXTENT OF BRINE/HOST ROCK EQUILIBRIUM

Evaluating equilibrium between the brines and reservoir host rocks is a means for inferring the current and future chemical stability of reservoir formations; i.e., whether the brines are at rest or are being replenished with (or depleted of) water or other constituents, and whether or not the brines have a capacity for chemically degrading the host rock. In addition, evaluation of equilibrium may be an important input to safety analyses of the WIPP site because it may be useful to know if brine compositions are likely to change should the brine mobilize and gain access to buried waste. Equilibrium may be inferred by means of major and minor constituent chemistry of the brines, thermodynamic calculations, petrography of the host rocks, and by the isotopic compositions of the brines, gases, and host rocks.

2.4 CHEMICAL CONSTRAINTS ON RATE OF BRINE TRANSPORTATION

Any chemical data that relate to either the rate of brine transportation from its place of origin to its present reservoir, or to its movement (if any) subsequent to the siting of a nuclear waste disposal area will be critical to establishing site safety and stability criteria. As above, chemical information gained by major and minor element chemistry of the brines, reservoir rock petrography and mineral chemistry, and the isotope systematics of the rock-brine-gas assemblage may pertain to the resolution of this issue.

2.5 RESIDENCE TIME OF BRINES IN RESERVOIRS

Determining the residence time of the brine in the anhydrite reservoirs could provide information on the time of reservoir formation (time of deformation) and on the origin of the fluids. Simply stated, very long residence times could be evidence the brines and the reservoir systems have remained static for a significant period of time with no interconnection to active groundwater systems. Residence times can sometimes be inferred from brine origin or other geological or hydrological information, or they can be determined using geochronological methods. Few techniques exist to determine absolute residence times of fluids in reservoirs, and those that do exist require that significant assumptions be made to perform the "age" calculations. The uranium-isotope disequilibrium method can be used to determine the time of confinement or residence of the brines in the anhydrite reservoir rock. As with all geochronological techniques, however, determined "ages" must be interpreted in the context of the geologic setting and history of an area.

3.0 CHEMICAL CHARACTERIZATION OF GROUND WATER AND BRINE

In this section, the chemistry of the brine reservoirs will be presented, and where appropriate, compared to local or other related ground waters. The presentation of results will be preceded by a brief discussion of the sampling, storage, and analytical procedures employed. This discussion is provided to place the results in proper perspective and to apprise the reader of limitations in the data. Further information concerning the methodology is available in the companion data file report (D'Appolonia, 1982, Appendix A).

3.1 SAMPLES

Downhole and wellhead brine samples were collected at both ERDA-6 and WIPP-12. Downhole brine samples were collected at 2703 feet at ERDA-6 and at 3003 feet at WIPP-12. Most wellhead brine samples were collected at regular intervals during flow testing. During flow tests at ERDA-6, samples were collected for field analysis every one to two hours until chemical stabilization was evident. Thereafter, sampling occurred at six-hour intervals. At WIPP-12, sampling of brines at the surface occurred at two- to four-hour intervals.

Samples for laboratory analyses were collected simultaneously with those for field analysis, with all laboratory samples taken after the chemistry of the fluids from the wells had stabilized (i.e., contaminants were believed to have been flushed from the wells). The sampling program is summarized below and described fully in D'Appolonia (1982, Appendix A). Samples from the Union well were collected at the wellhead under flowing conditions.

3.1.1 Location and Rationale

The downhole brine (and gas) samples were collected in ERDA-6 near a presumed brine-producing fracture in Anhydrite II at a depth of 2711 feet. The contact with Halite I is located at about 2735 feet. In WIPP-12, the downhole samples were collected just above the probable fluid-producing fractures lying between 3016 and 3045 feet deep in Anhydrite III. The brine samples collected at the surface were collected as close to the wellhead as possible to minimize contamination. The surface brine sampling does not discriminate between brines from individual zones in the well. This results in an averaging of brine compositions near each well, and perhaps a more realistic view of the overall reservoir environment.

3.1.2 Techniques

Samples of brine for field analysis were collected at the surface in plastic bottles and analyzed immediately after collection. Brine samples for laboratory analyses by D'Appolonia, Export, Pennsylvania; Global Geochemistry Corporation, Canoga Park, California; New Mexico Bureau of Mines, Socorro, New Mexico; and Sandia National Laboratories, Albuquerque, New Mexico were collected in the quantities and containers specified by these laboratories. Bottled samples which required no filtration were sealed immediately after collection at the wellhead. Samples requiring filtering were collected in one-gallon plastic containers, and then filtered through a 0.45 micrometer filter, using nitrogen gas to pressurize the filtration apparatus. Samples that were to be preserved were treated with sulfuric or nitric acid, as instructed by the laboratories. Samples were transported to all laboratories

in sealed ice chests maintained at about 4°C. The details of sample collection are described more fully in D'Appolonia (1982, Appendix A). Preservation and shipment procedures are in accordance with recommendations of the U.S. EPA (1979) or APHA (1980). Downhole samples were collected in a K-500 MONEL sample chamber lowered to the sampling depth. The brine and included gas were transported in the chamber to Core Laboratories, Midland, Texas, for analysis. A portion of the brine was shipped to D'Appolonia laboratory and a portion of the gas was shipped to Global Geochemistry Corporation for additional analyses (see Section 4.1.2).

3.1.3 Storage

Samples were stored in their shipping containers until analyses were performed. Where prudent, samples were refrigerated or stored on ice.

3.1.4 Limitations

Prior to data reduction and analysis, concern was expressed that the utility of the data might have been decreased by the decision to sample at the wellhead. Specifically, collecting brine samples at the surface might limit the ability to estimate downhole conditions because of:

- Oxidation of the sample.
- Precipitation, resulting from changing pH, Eh, temperature, or pressure.
- Contamination due to wellhead and casing corrosion.
- Contamination with fluids from zones which are not connected to the brine reservoir in any way except through the borehole.
- Exsolution of gases from the liquids under atmospheric pressure.

Under isothermal conditions, the magnitude of the potential effects of these processes is dependent primarily upon kinetic factors and additions or subtractions of reservoir fluids by so-called "thief zones". In all cases, it is

reasonable to assume that slow flow rates should emphasize the effects (if any) of the spurious phenomena.

As a result, the chemical data were plotted as a function of both flow rate from the well and time after initiation of flow (Figure C-1). The samples investigated were all taken after field analyses indicated that the chemical system had stabilized (i.e., reached a pseudo-steady state). Because of the poorer analytical conditions that existed in the field, only samples that were analyzed in research laboratories have been used for the evaluation. These laboratory-analyzed samples were taken simultaneously with samples analyzed in the field, and they span the entire duration of the sampling period. All samples taken for laboratory testing were obtained at preset intervals (e.g. every 12-24 hours, depending on flow rate). All analyses are reported and these data form the basis for this report.

Three types of statistical analyses were performed on the chemical data from the analyses of brines. The Student's "t" test (parametric) and the Mann-Whitney test (nonparametric) were used to analyze the means and populations for data from two separate flow tests at ERDA-6 (Flow Tests 2 and 3). The chemical parameters used for the comparison of the brines were calcium, magnesium, potassium, sodium, bicarbonate, bromide, sulfate, δD, and $\delta^{18}O$. The hypothesis was that the chemical composition of the brine was constant throughout both flow test periods. This hypothesis was supported by the statistical tests, where no significant difference between the two flow periods was observed for any parameter in either test.

The possibility that the chemical compositions of the brines could have changed with the decreasing flow rates observed at each of the wells through time was tested by means of analysis of variance (ANOVA). The same chemical parameters were evaluated. The chemical analyses within each well were divided into three or four groups which represented decreasing flow rates through time. The within-group variance was tested against the among-group variance to indicate whether or not there was a significant change due to time

effects. For both wells no significant differences were observed at the 95% C.L., with the exceptions of δD showing a significant difference (C.L. = 98.9) in ERDA-6 and $\delta^{18}O$ showing a significant difference (C.L. = 98.5) in WIPP-12 due to time effects. These analyses substantiate the hypothesis that the observed changes in flow rates through time have no statistically verified effect on the chemical composition of the brines.

The consistency of the data shown in Figure C-1, the results of the statistical analyses, and the good agreement with established trends (see later discussion and Figures C-4 through C-14) indicate that concerns about wellhead sampling were not warranted for the major and minor element chemistry. In contrast, however, the reliability of trace metal data is still considered suspect in light of the potential for metal corrosion downhole and in the wellhead. Accordingly, no attempt to interpret the trace metal data has been made.

3.2 ANALYTICAL METHODS

3.2.1 Techniques

Analytical methods used by the D'Appolonia laboratory, and by Core Laboratories, Inc. are given in detail in D'Appolonia (1982, Appendix B). The δD and $\delta^{18}O$ methods used by Global Geochemistry are also given in D'Appolonia (1982, Appendix B). Global Geochemistry's $\delta^{13}C$ and $\delta^{34}S$ methods have not yet been reported, but they will be included in updates of the ERDA-6 and WIPP-12 Data File Report (D'Appolonia, 1982, Appendix A).

3.2.2 Limitations

All analytical methods used in this study are ASTM, API, APHA, U.S. EPA or U.S. Bureau of Mines published methods. Limitations of these methods are summarized in the references found in D'Appolonia (1982, Appendix B). Global Geochemistry has used its stable isotope methods successfully for a number of years. Precision is greater on solid and liquid samples than on gas samples. However, complex natural samples can produce unexpected interferences

and errors. In most cases, however, samples were analyzed for isotopic compositions in duplicate, and 10-13 samples of brine from each well were analyzed.

3.3 SUMMARY OF RESULTS

3.3.1 General Properties

Brines sampled from ERDA-6 and WIPP-12 have similar major element chemistries. Approximately ninety percent of the ions in the brines are either sodium or chloride. The other ten percent consist predominantly of calcium, lithium, magnesium, potassium, bicarbonate, sulfate, ammonium, nitrate, and boron. The average total dissolved solids (TDS) value for ERDA-6 samples is 330,000 mg/l, and for WIPP-12 samples, is 328,000 mg/l.

Although similar, the ERDA-6 and WIPP-12 brines are not identical. Student's "t" and Mann-Whitney tests were used to analyze the means and populations for chemical data from ERDA-6 and WIPP-12. The chemical parameters used for the comparison of the brines were calcium, magnesium, potassium, sodium, bicarbonate, bromide, sulfate, δD, and $\delta^{18}O$. Significant differences of the means/populations between ERDA-6 and WIPP-12 were observed at a greater than 99.8% confidence level (C.L.) for all parameters for both tests, except for bicarbonate, which showed a significant difference at a 98.6% C.L. for the "t" test and no significant difference at the 95% C.L. for the Mann-Whitney test. These results indicate that brines from the two wells have significantly different chemical compositions.

Average compositions for ERDA-6 and WIPP-12 are provided in Table C.2 along with data from the Union well. These compositions are shown diagramatically in Figure C-2. In the figure, the area of each circle is proportional to TDS. The proportion of each component in terms of equivalents is shown as a wedge, with exact values reported numerically (in percent equivalents). Charge balance may be assessed by comparing the size of the upper "hemisphere" (cations) with the lower shaded "hemisphere" (anions). Measured water temperature, TDS, Eh (oxidation-reduction potential), and pH are shown beneath each circle.

3.3.2 Major and Minor Elements

A later section (5.0) will include discussions of the origin of the brines and relate the data to issues of concern. To facilitate these discussions, the chemical data have been reduced and arranged in a convenient form. They are presented below, along with brief discussions of points of interest, in the following order:

- Evaluations of mineral saturation.
- Major and minor element concentration ratios.

Evaluations of Mineral Saturation

Evaluations of mineral saturations are helpful when attempting to infer the genetic histories of the brines, and are especially important when determining if the brines are in equilibrium with their surroundings. In making these evaluations, the equilibrium thermodynamic model developed by Harvie and Weare (1980) for brines was used. This model calculates the chemical activities of component ions, and permits calculation of ion activity products (IAP). The IAP of a mineral can then be compared with the solubility product (Ksp) of that mineral to evaluate whether or not the solution is saturated (i.e., in equilibrium) with the mineral. (If the IAP is equal to or greater than the Ksp, then the solution is saturated with the phase. If the IAP is less than the Ksp, then the solution is not saturated.) Since most of the Ksp values and all of the IAP values were generated using the model developed by Harvie and Weare (1980), the evaluation of phase equilibrium is internally consistent.

The IAP values are not exact and are subject to errors both in measurement and in computation. As a result, the calculated IAP values are reported as a range of possible values. Tables C.3 and C.4 contain evaluations of whether or not the ERDA-6 and WIPP-12 brines are saturated with common evaporite minerals. These evaluations are based on the reported Ksp and calculated IAP values included in the tables. In some cases, the range of calculated IAP's

spans the reported Ksp value; therefore, judgment was exercised, and the phase was described as "probably" saturated, or "probably not" saturated. In these instances, petrographic analyses or X-ray diffraction are probably the best means for establishing mineral stability. As with any theoretical evaluation, the model should be checked to ascertain its reliability. Checks on the evaluations contained in the tables are summarized in the column labeled "Physical Evidence" and discussed in the following paragraph.

In the original description of the model (Harvie and Weare, 1980), the computed results were compared with empirical laboratory results and agreement was found to be within five percent (relative). In its current application, the computed result can be compared with petrographic observations. The results are again in good agreement (see Part II, Geology, Section 4.1.3). A final, though less rigorous check on the model is to compare the computed results with established precipitation sequences (e.g., Grabau, 1920; Krauskopf, 1967). If inconsistencies arise, then the results of the model are doubtful.

Figure C-3 is a Janecke diagram of the type commonly used to report brine compositions. The diagram shows stability fields for common evaporite minerals that can coexist with halite. Brines of any given composition can be plotted in terms of their three Janecke components. The field bounding that composition determines the evaporite mineral that precipitates after halite for that particular brine, and descent lines govern subsequent precipitation. In this way, brine mineral precipitation sequences can be predicted for any brine composition. For example, the heavy line (with arrows) shows the common precipitation sequence for seawater. The WIPP-12 and ERDA-6 brines do not fall in the seawater field (bloedite), but instead plot in the thenardite (Na_2SO_4) region. Therefore, the Castile brines should precipitate thenardite (or a related phase) as the next mineral following halite. While ERDA-6 brine cannot be evaluated rigorously because it is not saturated with halite (therefore it does not plot on the plane of the diagram), the mineral saturation results calculated for WIPP-12 appear to be

consistent. That is, WIPP-12 brine (which is halite saturated) is also found to be saturated with glauberite, $CaNa_2(SO_4)_2$ (see Table C.4). Although glauberite is not shown on the Janecke diagram (Ca is not considered in the pseudo-ternary system employed for the diagram), glauberite would project into the thenardite (Na_2SO_4) field. Consequently, the calculated saturation for WIPP-12 brine with both halite and glauberite appears consistent with the bulk composition.

In general, ERDA-6 appears to be saturated in dolomite and calcite, and probably saturated in anhydrite. WIPP-12 is saturated with calcite and dolomite and probably saturated with anhydrite, glauberite, and halite. In most cases, these equilibria have been imposed on the brine by phases in the rock (i.e., the rock is controlling the solution chemistry). For dolomite, however, the rock appears to have equilibrated with the brine chemistry.

Major and Minor Element Concentration Ratios

The variations of major and minor element concentrations can be used to infer the genetic histories of aqueous solutions (e.g., Carpenter, 1978; Valyashko, 1956; Rittenhouse, 1967). The concept behind this practice is that brines formed by dissolution of halite (and other evaporites) become progressively enriched in ions such as sodium, choride, calcium, and sulfate because those ions are abundantly present in readibly soluble hosts. In contrast, brines which form by concentration of seawater become comparatively enriched in the normally less abundant incompatible elements (e.g., bromide, lithium, and boron) as the normal evaporation and precipitation sequence proceeds. Consequently, by comparing concentration ratios with normal seawater trends, brines which formed by dissolution (i.e., originated from meteoric waters or waters of dehydration) can be distinguished from those which are formed by concentrating seawater.

Figures C-4 through C-14 compare the ion ratios obtained from samples of ERDA-6 and WIPP-12 brines (D'Appolonia, 1982) with seawater evaporation trends

(Collins, 1975). Also shown for reference are brines that have been interpreted as seeps of meteoric waters into salt domes (Martinez, 1979) and some of the briney ground waters associated with the Los Medanos region (Hiss, 1975; Lambert, 1978). While limited data (Lambert, 1978) prevent comparing all of the regional ground waters with the brine occurrences, in most cases at least one ground water can be plotted. In these cases, the ground water is usually from the Bell Canyon Formation. Data from the Salado and Morrow ground waters are also frequently available, but sometimes they cannot be plotted on the scale of the figures. To avoid decreasing the clarity of presentation, on occasion the Salado and/or Morrow data were omitted.

As stated above, when seawater evaporates, all dissolved components become more concentrated but remain in the same relative proportions that existed in the original solution. These ratios remain constant until or unless a phase is precipitated or dissolved (e.g. Holser, 1966; Rittenhouse, 1967; Carpenter, 1978). For example, when precipitation of phase AB occurs from a solution containing A, B, C, and D, then the solution becomes depleted in A and B but not in the other components. As a result, the ratio C/D remains constant, but the ratios A/C, B/C, A/D, and B/D decrease.

In seawater, bromide (Br^-) is a relatively minor component (see Weast, 1971); however, since bromide does not partition appreciably into precipitating salts except in the very last stages of evaporation, it can be used to trace the addition or subtraction of other seawater components (e.g., Holser, 1966; Rittenhouse, 1967; Carpenter, 1978).

Although the chemistries of the brines are distinctly different, the WIPP-12 and ERDA-6 brines plot consistently near each other (see Figures C-4 through C-9). This general similarity probably indicates a similar source water for the Castile brines. The compositional differences among the Castile brines probably indicates separate histories following diagenesis and lithification of the basin. The fact that chemical differences persist indicates poor communication between reservoirs. While the Castile brines infrequently plot

near the regional ground waters and saline mine seeps, no trend among the brines and the latter waters is either consistent, or compelling. By comparison, the agreement with seawater evaporation is much better. Specifically, eight major brine components have been plotted as a function of coexisting bromide and/or chloride concentrations. These eight components comprise more than 99 percent of the dissolved material in the brine. Notably, six of the eight components either bracket, or fall very near to seawater evaporation trends (i.e., fall within 5 to 10 percent relative deviation). Of the remaining two components, only one (magnesium) shows a major departure from the seawater trend, and is significant to the origin of the brine. The other (boron) is significant only in that it occurs in excess. Implications of this excess are discussed later (Section 5.1.2).

The magnesium/bromide concentration plot (Figure C-9) of the brines shows that the reservoirs are depleted in magnesium relative to seawater. If the magnesium content of the brines were controlled by seawater evaporation, then magnesium and bromide would have become equally enriched until precipitation of magnesium-bearing phases such as epsomite ($MgSO_4.7H_2O$) or bloedite ($Na_2Mg(SO_4)_2.4H_2O$) occurred. That precipitation does not occur until the bromide content of the brine has reached 4,300 mg/l (Collins, 1975) which is far above the 510 mg/l and 880 mg/l bromide contents of the Castile brines. As a result, if the general agreement of the Castile brines and seawater evaporation trends are to be believed, magnesium depletion must have occurred because of water/mineral reaction. That reaction must have occurred after the brines were separated from waters in the basin, and must have generated a magnesium-bearing phase (e.g., dolomite, chlorite, or saponite).

In addition to the magnesium/bromide ratios, the slightly elevated sodium/bromide and chloride/bromide ratios are also significant. Elevation of these ratios above the seawater reference indicates that in addition to seawater concentration, minor dissolution of sodium- and chloride-bearing phases has occurred.

For ERDA-6, halite (NaCl) dissolution appears an adequate explanation for these elevated values. This statement can be made with some assurance because when sodium and chloride are subtracted from the brine compositions in equal molar amounts (i.e., halite stoichiometry), they reach the seawater solute/bromide reference curve simultaneously. This is not the case for WIPP-12. When the WIPP-12 brines have sodium and chloride subtracted, sodium still remains elevated above the seawater reference when chloride is coincident with the reference curve. This implies that the WIPP-12 brines may have dissolved another sodium-bearing phase--perhaps a sulfate (Lambert, 1978, and in preparation). The fact that WIPP-12 seems to be saturated with both halite and glauberite ($CaNa_2[SO_4]_2$) appears to support this contention (see Table C.4). Further support for this hypothesis is given by the WIPP-12 sulfate/bromide plot (Figure C-6) which shows a slight elevation of sulfate. Thus, the WIPP-12 brines have not only an excess of sodium and chloride but also of sulfate. However, due to the presence of other sulfates (e.g., anhydrite) and the complications of incongruent dissolution, quantitative confirmation of halite plus glauberite dissolution has not been attempted.

In addition to the solute versus bromide plots, chloride versus solute graphs have also been constructed. These figures (Figures C-10 through C-14) consistently show that the WIPP-12 and ERDA-6 brines do not relate well to local ground waters or to other brines of established meteoric origin (see Figures C-10 through C-14 and summary Figures C-15 and C-16). Instead, the chloride/solute plots support the bromide graphs by comparing well with seawater evaporation curves. Of note is that the WIPP-12 and ERDA-6 brines are slightly, but consistently enriched in chloride, which supports the interpretation of some halite dissolution.

3.3.3 Trace Elements

The reliability of transition metal trace element abundances is questionable because of the susceptibility of the metal well-casing to corrosion (e.g., reactions with hydrogen sulfide). Therefore, those data have not been evaluated in detail. The presence of silica (SiO_2) has been evaluated and is

interesting because of its high concentration. It is treated here as a trace element because of its commonly low concentration in most brines.

Figure C-17 plots silica concentration against bromide for the WIPP-12 and ERDA-6 brines. Also shown for reference are the expected seawater concentration curve (computed from Weast, 1971), and measured solubilities for amorphous silica (Chen and Marshall, 1982) and for quartz in brine.

As shown on the figure, the concentration of seawater will cause supersaturation of silica with respect to high quartz and amorphous silica. At low temperature, the common result of this phenomenon is the precipitation of amorphous silica (Iler, 1979). Rarely, however, quartz or another ordered silica phase may precipitate (e.g., Mackenzie and Gees, 1971).

The WIPP-12 brines are clearly supersaturated with respect to quartz and either saturated or supersaturated with amorphous silica. Since authigenic quartz is observed in the reservoir host rock as shown in Figure C-18 (see Part II, Geology, Section 4.1.3), the observed silica concentration is probably the result of a modified quartz solubility, i.e., solubility is controlled by the overgrowth of an amorphous surface coating on the quartz (Baumann, 1971).

The significance of the elevated silica concentration and the presence of authigenic quartz is at least three-fold. First, the silica contents of the brines are too high to have been generated by ground waters leaching quartz or clays (see Figure C-17). For example, the nearest ground-water source is the Bell Canyon aquifer. The water-bearing zones of this aquifer are dominantly quartz with clay accessory minerals (Powers et al., 1978). If quartz or clays exerted silica control on the leachate composition, then the Bell Canyon ground waters could not have attained the silica content of the brine. Moreover, the silica content of any saturated fresh-water source would be expected to decrease as the salinity of the water increased. Such a decrease would be

a general phenomenon attending brine formation, because an increase in dissolved solids decreases the chemical activity of water in solution (e.g., Weres et al., 1980). Thus, if a fresh-water source gave rise to the brines, then its silica content at low ionic strength would probably exceed that measured in the brine. Ground waters of such high silica content are not known near the WIPP-12 reservoir (Hiss, 1975). Second, the fact that quartz has precipitated implies that the silica concentration was probably somewhat higher than its present concentration (by perhaps a factor of 2) in order that homogeneous nucleation could occur (Harvey et al., 1976; Midkiff and Foyt, 1976, 1977). Such high concentrations would be consistent with those that might be produced by condensing seawater (see Figure C-17), but would not be consistent with dissolution of amorphous silica (or generation of amorphous silica by leaching). Third, the brines currently are saturated or slightly supersaturated with respect to amorphous silica. This equivalence, together with the observed quartz and its inferred surface coating, implies that the brines have reached a modified equilibrium with respect to SiO_2.

3.3.4 Isotopes

Major isotopes of the elements hydrogen, oxygen, carbon, and sulfur have been analyzed for both ERDA-6 and WIPP-12 brines. Results are summarized in Table C.5. These analyses were performed to support interpretations of the genetic origin of the brines, and to help evaluate the proximity to equilibrium and the extent of isolation of the brine reservoirs. The most heavily studied of these isotopes have been the deuterium and oxygen-18 ratios, where the ratios are defined (after Craig, 1961) as:

$$\delta D(^{o}/_{oo}) = \frac{\frac{D}{H}\ \text{sample} - \frac{D}{H}\ \text{SMOW}}{\frac{D}{H}\ \text{SMOW}} \times 1000,$$

and

$$\delta^{18}O(^{o}/_{oo}) = \frac{\frac{^{18}O}{^{16}O}\ \text{sample} - \frac{^{18}O}{^{16}O}\ \text{SMOW}}{\frac{^{18}O}{^{16}O}\ \text{SMOW}} \times 1000$$

The values for the WIPP-12 and ERDA-6 brines are shown in Figure C-19A, along with reference fields for Standard Mean Ocean Water (SMOW) and meteoric waters. As observed, the ERDA-6 and WIPP-12 values cluster together. Figure C-19B places the brine reservoir data in a regional context by including data for local ground waters. While the brine data plot at the extreme end of the trend, an apparent continuity between the ground waters and the brines is visible (Lambert, 1978).

Another valuable way in which to view the isotopic data is to plot them as a function of total dissolved solids (TDS) (Clayton et al., 1966). Such plots can sometimes be very informative about brine origins by revealing hidden trends, or by exposing incorrect assumptions (Clayton et al., 1966; Kharaka et al., 1973; Hitchon and Friedman, 1969). Graphical plots of δD versus TDS and $\delta^{18}O$ versus TDS can be found in Figures C-20 and C-21 for ERDA-6 and WIPP-12 brines. Also indicated in the diagrams are linear regression fits to the data, extrapolated back to the y-intercept (corresponding to zero TDS). These lines are an aid to identifying potential sources for the brine because parental waters <u>often</u> plot along those lines in both diagrams. For example, assume that the parent water which gave rise to the brine had a salinity lower than that now in the reservoir. To generate the current brine's composition, the parent water would have to react with rock to increase salinity. In so doing, the isotopic character of the water might change, but it must change along the regression line, provided that the isotopic fractionation mechanism has remained constant and that TDS evolved simultaneously with isotopic fractionation. In no case, however, can the regression line be extended beyond the y-intercept because no water has less than zero TDS. In interpreting these diagrams, however, caution must be exercised. Changes in reaction mechanism are not uncommon. Furthermore, the mechanisms which control isotopic composition are not necessarily the ones which control TDS (Clayton et al., 1966). Finally, regression lines through clusters of data around two points should not be considered definitive. Data from a third well could substantially alter the regression fits presented in Figures C-20 and C-21. With those

qualifications, it is worth noting that no regional ground waters currently in the basin plot near either regression line, nor do the regression lines converge on the current SMOW reference.

In addition to the deuterium and oxygen isotopes, the $\delta^{34}S$ values obtained from the sulfate in the brines and coexisting anhydrite are also informative. For these analyses, $\delta^{34}S$ was defined as:

$$\delta^{34}S(^{o}/oo) = \frac{\frac{^{34}S}{^{32}S}\ \text{sample} - \frac{^{34}S}{^{32}S}\ \text{Canyon Diablo Troilite}}{\frac{^{34}S}{^{32}S}\ \text{Canyon Diablo Troilite}} \times 1000$$

The measured $\delta^{34}S$ values range between 7.43 $^{o}/oo$ and 9.79 $^{o}/oo$ for the brines (Table C.5) and averages 11.6 $^{o}/oo$ for the anhydrites (Table C.6). These values are characteristic for Permian-aged materials of the Delaware Basin (Holser and Kaplan, 1966), and are outside the range for $\delta^{34}S$ values characteristic of any other time period (Nielsen, 1979; see Figure C-22).

Furthermore, the sulfur in the sulfate of the brines is consistently lighter than that of the coexisting anhydrite by about 3 $^{o}/oo$. Part of this difference is explained by the 1.65 $^{o}/oo$ (Holser and Kaplan, 1966) difference which would attend equilibrium fractionation between anhydrite and water. Since the reaction of water and sulfate minerals is hindered kinetically (i.e., coexisting anhydrite and brines have remained isotopically distinct for tens of millions of years; Holser et al., 1979), the brines are very old, and may well be Permian in age.

3.3.5 Statement of Findings

The major, minor, and isotope chemistries of ERDA-6 and WIPP-12 brines have been analyzed and the data reduced. Interpretation of the chemical trends has resulted in the findings below:

- The chemistries and histories of WIPP-12 and ERDA-6 brines are similar. Since the brine sampled at the Union well is chemically similar to WIPP-12 brine, it may also have had a similar history.

- The Castile brines bear little chemical resemblance to other regional ground waters or brines of established meteoric origin.

- While chemically similar, the Castile brines are distinctly different from each other. WIPP-12 brine is saturated with anhydrite, calcite, dolomite, halite, and glauberite; while ERDA-6 brine is saturated only with calcite, dolomite, and anhydrite.

- Both brines have apparently dissolved halite, and WIPP-12 brine may also have dissolved glauberite.

- WIPP-12 brine is saturated with halite and anhydrite; therefore, its potential for degrading overlying evaporites is negligible. ERDA-6 brine is saturated with anhydrite but somewhat undersaturated with halite. Consequently, ERDA-6 brine has a small potential for dissolving overlying evaporites. For example, if the ERDA-6 reservoir were to maintain its current areal dimensions (estimated at near 6.3×10^6 ft^2; see Part III, Hydrology, Section 3.4.3) and dissolve its way vertically through halite, it could proceed less than one centimeter before the entire volume of brine would be saturated.

- The sulfates in the brines have $\delta^{34}S$ values slightly lower than those of the coexisting anhydrites and reflect values characteristic only of the Permian.

- A continuous trend in $\delta D/\delta^{18}O$ values from regional ground waters to the brine reservoirs is apparent but may be misleading. Present day seawater and regional ground waters do not plot near regression lines established for the brine data.

- The brines have equilibrated chemically with calcite, dolomite, and quartz, and isotopically with anhydrite. These reactions are well-known for their sluggishness at low (25°C) temperatures. Accordingly, the brines are very old (and may be Permian age).

4.0 CHEMICAL CHARACTERIZATION OF GASES

In this section, the chemistry of the gases associated with the ERDA-6 and WIPP-12 brines will be presented. The presentation of results will be preceded by a brief discussion of the sampling, storage, and analytical procedures employed. Further information concerning methodology is available in the companion data file report (D'Appolonia, 1982, Appendix A). The analytical laboratories that produced the data, and the samples that were distributed to each of them are also identified in that report.

4.1 SAMPLES

The total number of samples collected and analyzed by the various laboratories is shown in Tables C.7 (ERDA-6) and C.8 (WIPP-12). These tables are divided into data from surface flow samples (C.7a and C.8a) and data from downhole samples (C.7b and C.8b).

4.1.1 Location/Rationale

Although small volumes of gas were sampled downhole (along with the brine), the majority of the data concerning gas composition were generated from samples discharged from a gas/liquid separator located near the wellhead. The separator has different efficiencies in separating the various gas components. For example, much of the hydrogen sulfide and carbon dioxide remains dissolved in solution, while most of the methane and nitrogen are exsolved. Therefore, the actual composition of the gases under downhole pressures and temperatures must be estimated using thermodynamic techniques in conjunction with the measured values.

The following types of containers were used for collection of the samples:

LABORATORY	CONTAINER
• Thurmond-McGlothlin	Metal (Iron) cylinders
• Global Geochemistry	100 ml glass cylinders

- Core Laboratories — Metal cylinders (MONEL and stainless steel lined with teflon)
- Sandia — 100 and 500 ml glass cylinders

Duplicate and triplicate samples using various container types were used for quality control.

4.1.2 Techniques

The following methods were used to collect gas samples:

- Surface samples:
  - gas from the gas outlet of a gas/liquid separator.
  - gas collected with brine under pressure in "in-line" sample containers.
  - gas from a vacuum extractor.
- Downhole samples:
  - gas collected under pressure with brine.

Continuous monitoring of the gas composition was performed in the field during ERDA-6 Flow Tests 1 and 2 by Profile Reservoir Analysis, Carlsbad, New Mexico, and during WIPP-12 Flow Tests 2 and 3 by Morco Geological Services, Carlsbad, New Mexico. The concentration of hydrogen sulfide in the gas was measured in the field every three to six hours by Thurmond-McGlothlin and D'Appolonia. Gas sampling techniques are described in detail in D'Appolonia (1982, Appendix A). Samples were analyzed by Core Laboratories and Thurmond-McGlothlin within 24 hours of collection. Samples collected in glass containers for Global Geochemistry and Sandia were placed in a freezer and shipped on dry ice.

4.1.3 Limitations

Limitations on the surface sampling of gas are similar to the limitations on brine sampling at the surface. Some degree of reactivity or reequilibration may take place during the flow of brine. The degree that this sampling limitation affects results can best be appraised in the consistency of results, and the usefulness of data to interpret downhole conditions.

Some degree of air contamination occurred in several samples. Contamination is easily recognized by increased abundances of nitrogen and carbon dioxide, and the presence of oxygen and argon. The data from suspect samples have not been considered in this report.

The reactions of the gases (especially hydrogen sulfide) with metal surfaces in the flow lines, separator, and sample cylinders will cause some decrease in the concentrations measured. However, the metal surface usually stops reacting after an initial "wearing-in" period. As a result, gas samples taken later in the sampling program are considered more reliable. Replicate analyses of gases taken in different containers showed little appreciable difference, indicating that sampling and storage precautions were successful in alleviating reactions with container walls.

4.2 ANALYSES

4.2.1 Techniques/Instrumentation

Analytical techniques used by the respective laboratories are described in detail in D'Appolonia (1982, Appendix B). Hydrocarbons, nitrogen, and carbon dioxide were analyzed by gas chromatography. Hydrogen sulfide was analyzed by three methods:

- Global Geochemistry: Hydrogen sulfide in the sample is precipitated as Ag_2S, and the precipitate weighed to determine H_2S concentration.
- Core Laboratories: Gas chromatography.
- D'Appolonia (in the field): Tutwiler Method.

Isotopes in gases were analyzed by mass spectroscopy after chemical treatment of samples. Commercially available standards, and Global Geochemistry Corporation's own calibrated working standards were used in all analyses.

Other Quality Control measures are documented in D'Appolonia (1982, Appendix B). For example, most analyses by Global Geochemistry were performed in duplicate. Split samples were also sent to various laboratories.

4.2.2 Limitations

Because methods vary among laboratories, split samples were routinely distributed among laboratories to promote obtaining reasonable results. Multiple samples were sent to individual laboratories to increase the reliability of the data, and to provide an internal check on consistency.

4.3 SUMMARY OF RESULTS

4.3.1 General Properties

Gas compositions are summarized in Table C.7 and Table C.8 for ERDA-6 and WIPP-12, respectively. A wide variation exists in the measured gas compositions of samples from both wells, in part because of air contamination of the samples. However, compositional differences exist that probably reflect inherent differences between ERDA-6 and WIPP-12 gases. As shown in Tables C.7 and C.8, carbon dioxide (CO_2) is a major constituent in most ERDA-6 samples. Hydrogen sulfide (H_2S) tends to be higher in ERDA-6 gas (see D'Appolonia, 1982, Tables 6.9-C2 and 12.20-C3, for H_2S determined by the Tutwiler Method); while methane (CH_4) and heavier hydrocarbons comprise a larger proportion of most WIPP-12 gas. Student's "t" and Mann-Whitney tests were used to analyze differences in the means/populations of the hydrogen sulfide, carbon dioxide, and methane data from ERDA-6 and WIPP-12. Significant differences between wells were observed at a greater than 99.8% confidence level for all parameters for both tests. Gas samples from both wells contain appreciable concentrations of nitrogen (N_2). Because no oxygen and argon were observed, this nitrogen cannot be attributed to air contamination.

4.3.2 Proportions and Volume Estimates of Phases

Data discussed in the preceding paragraph were treated thermodynamically in order to estimate phase proportions and compositions of phases present downhole.

Boiling Point Elevation

The boiling point elevation of an ideal, pseudo-binary mixture[1] consisting of a volatile (low boiling point, high vapor pressure) phase and a non-volatile phase can be calculated. For the WIPP-12 gas, the volatile phase consists mainly of methane; however, nitrogen and ethane are considered part of the volatile phase and are treated identically to methane. The "non-volatile" phase is hydrogen sulfide. Figure C-23 shows the critical point elevation curve for the CH_4-H_2S binary mixture (Katz et al., 1959). The boiling point elevation for a mixture of 75 percent methane 25/percent hydrogen sulfide, corresponding to the mean WIPP-12 gas composition for Flow Test 3 as analyzed by Global Geochemistry (D'Appolonia, 1982, Table 12.20-C7), was also calculated and plotted, with details shown on Figure C-24. At points along the curve where ideal gas laws poorly represent gas behavior (i.e., at pressures along the curve above the critical points of the individual gases alone), the curve shape was estimated by smooth-fit techniques using the most ideal (i.e., most volatile) gas as a constraint. At the maximum downhole pressure measured in WIPP-12, 12.7 MPa (about 1840 psia, 125 atm), and the downhole temperature, 26.7°C (80°F), the distribution of phases appears to be approximately 30 percent gas and 70 percent liquid. Consequently, only 30 percent of the moles collected as gas at the surface is expected to exist as gas downhole. After correcting for the effects of downhole pressure on (ideal) gas volume, the estimated in-situ volume of gas will be approximately 7 ml gas/liter of brine. This volume has been considered when estimating the compressibility and volume of fluid in the reservoir (see Part III, Hydrology, Sections 3.3.5 and 3.4.4).

---

(1) The system is pseudo-binary because all volatile components were lumped together and treated along with methane. Similarly, significant nonvolatiles were treated with hydrogen sulfide. The effects of the resulting mixture on inputs to the calculation were computed by weighting the components according to molar proportions.

Composition of Liquid and Gas Phases

A composition-temperature plot was constructed for the binary system methane (CH_4) - hydrogen sulfide (H_2S). Initial calculations were based on Raoult's Law, but did not produce meaningful results at small concentrations of the "non-volatile" phase. For consistency, these portions of Figure C-25 have been derived primarily from the boiling point elevation diagram. As shown in the diagram, under downhole conditions at WIPP-12, and an initial composition of 75 percent methane/25 percent hydrogen sulfide, an approximate liquid composition is 68 percent methane. Similarly, the vapor phase is expected to approach 92 percent methane. This result agrees with an intuitive estimate that the downhole gas will be composed dominantly (if not entirely) of non-condensible gases (i.e., methane and nitrogen). The condensible and soluble gas, hydrogen sulfide, probably does not exist as a gas in significant amounts downhole.

These approximations apply to WIPP-12 only. A similar treatment for ERDA-6 is not necessary because the downhole pressure at ERDA-6 is about 14.2 MPa (2060 psia; 140 atm). At 27°C, and in their observed concentrations, carbon dioxide, methane, hydrogen sulfide, and nitrogen result in a supercritical fluid at all pressures above 9.3 MPa (1350 psia, 92 atm; Katz et al., 1959). This is primarily due to the high proportions of the condensible gases hydrogen sulfide and carbon dioxide. At downhole pressures, individual gas solubilities indicate that the fluid is totally miscible in the brine. The compressibility of the brine, therefore is unchanged, and calculations of reservoir volume are unaffected.

4.3.3 Isotopes

A summary of the isotopic compositions of gases from ERDA-6 and WIPP-12 is shown in Table C.9. A complete data listing is given in D'Appolonia (1982, Tables 6.7-C7, 6.7-C8, and 12.7-C7).

$\delta^{34}S$ in Hydrogen Sulfide

Sulfur isotopes in hydrogen sulfide show depletion in ^{34}S (see Figure C-26). This result suggests isotope fractionation by bacterial sulfate reduction (bacteria will preferentially metabolize ^{32}S versus ^{34}S; Nielsen, 1979). In ERDA-6, the $\delta^{34}S$ values are consistently lower (-20.46 °/oo) than in WIPP-12 (-14.36 °/oo). This difference may be due to less favorable conditions in WIPP-12 for bacterial processes (i.e., more sluggish sulfate reduction). Alternatively, WIPP-12 may have been mixed with an isotopically heavier H_2S, such as that generated by thermogenic processes (see discussion for methane).

Further evidence for a biogenic origin of hydrogen sulfide is found by comparing $\delta^{34}S$ in hydrogen sulfide with that in the sulfate of the brine. $\Delta(SO_4^{2-} - H_2S)$ values in WIPP-12 average +22.57 °/oo and in ERDA-6 are +29.43 °/oo. These delta values are close to the range reported for fractionation due to bacterial reduction of sulfate (+15 °/oo Harrison and Thode, 1958; +25 °/oo to +65 °/oo Nielson, 1979). In contrast, isotopic equilibrium which occurs at elevated temperatures in the absence of bacterial sulfate reduction is:

$$\delta_{SO_4} - \delta_{H_2S} \approx \Delta(SO_4 - H_2S) \approx +80 \text{ °/oo} \quad \text{(Sakai, 1968; Faure, 1977)}$$

Thus, the signature of bacterial action on the isotopic composition in sulfide and sulfate suggests that only limited interaction could be occurring between brine sulfate and hydrogen sulfide in the reservoirs, and that the reservoirs have never been exposed to high temperatures.

δD in Hydrogen Sulfide

Both the ERDA-6 and WIPP-12 gases are strongly fractionated toward depletion in deuterium. Average δD values are -570 °/oo and -544 °/oo for ERDA-6 and WIPP-12, respectively. This strong fractionation probably reflects the partitioning of deuterium between water (becoming heavier) and hydrogen sulfide (becoming lighter) as H_2S gas is evolved during liquid/gas separation. This exchange occurs rapidly (Clayton et al., 1966), and has been utilized as a commercial technique for manufacturing "heavy water."

Given the comparatively large abundance of hydrogen sulfide in the wells, and the strong fractionation observed, there was initially some concern that the brine samples may have been enriched in deuterium during hydrogen sulfide production. Mass balance calculations have shown that this is not the case. The deuterium content of the brine has not been affected significantly by hydrogen sulfide generation.

$\delta^{13}C$ and δD in Methane

Comparison of the $\delta^{13}C$ and δD values of ERDA-6 and WIPP-12 methanes reveals a significant difference between reservoirs. Specifically, ERDA-6 methane has a $\delta^{13}C$ value that is more negative than -60 °/oo. This indicates that ERDA-6 methane was derived almost entirely from biogenic processes (such as bacterial respiration and elimination; Fuex, 1977; Rice and Claypool, 1981). This origin is also supported by the relative absence of heavy or "wet" hydrocarbons (e.g. ethane, propane, and/or butane; see Table C.7b) which would attend thermogenic processes. In contrast, the $\delta^{13}C$ of WIPP-12 methanes are less negative than -50 °/oo. This value for the carbon isotope indicates a probable thermogenic origin (Schoell, 1980). However, some contribution of biogenic methane cannot be ruled out. The interpretation of a dominantly thermogenic origin for WIPP-12 methane is supported by the presence of heavy hydrocarbons (ethane and propane; see Table C.8b). This thermogenic interpretation requires that portions of the gas were derived from a deeper and separate source than the brines. The greater depth of the source is inferred from temperature requirements. The separateness of the source is inferred from several lines of evidence including: 1) the low permeability of the rock; 2) the relatively unaltered chemical condition of the brine; and 3) the lack of physical evidence for deep rock-water interaction. Mechanisms for this gas evolution and collection are discussed in Section 5.1.4.

$\delta^{13}C$ and $\delta^{18}O$ in Carbon Dioxide

The isotopic composition of carbon dioxide in the ERDA-6 gas is shown in Table C.9 and plotted in Figure C-27. As shown in the figure, the $\delta^{18}O$ in the carbon dioxide is not in equilibrium with the atmosphere. This poor agreement indicates that the reservoirs and the surface (or surface-equilibrated waters) are not connected. The $\delta^{18}O$ values for the Castile brine waters consistently plot + 10 °/oo from the atmospheric (ocean equilibrated) reference. This difference coincides exactly with the enrichment of the brines relative to SMOW (see Figure C-19). Therefore, the oxygen in the brines and associated carbon dioxide appear to be in equilibrium.

If one proposed mechanism for explaining some of the $\delta^{18}O$ enrichment in the ERDA-6 brine is correct (i.e., exchange with carbonates), then the enrichment in $\delta^{13}C$ observed in the carbon dioxide is probably due to the leaching of the minerals, and equilibration at 27°C with the dissolved carbonates. The difference between the $\delta^{13}C$ in carbon dioxide and that in dissolved carbonate is about 7 °/oo to 9 °/oo. This difference is in the range for carbonate-CO_2 equilibrium (Faure, 1977).

4.3.4 Statement of Findings

The bulk chemical and isotopic data for the ERDA-6 and WIPP-12 gases have been reviewed and analyzed. The important findings relative to these gases are summarized below:

- The gases obtained from ERDA-6 do not exist as identifiable gases under downhole conditions. Instead, they are fluids which will have compressibilities similar to the brine. Accordingly, ERDA-6 gases do not affect estimates of brine reservoir volumes (see Part III, Hydrology, Sections 3.3.5 and 3.4.3).

- Because gases exsolve as pressure is released during sampling, the volatiles and gas/liquid ratios obtained from WIPP-12 consitute an overestimate of downhole gas. The actual amount of gas downhole is

closer to 30 percent of that obtained at the surface, or about 7 ml gas/liter brine when corrected for temperature and pressure. The downhole gas is nearly pure methane and nitrogen. This information has been included in brine compressibility and reservoir volume calculations (see Part III, Hydrology, Sections 3.3.5 and 3.4.4).

- Methanes from ERDA-6 and WIPP-12 were generated by different processes. ERDA-6 methane has been produced by bacterial processes (i.e., it is primarily biogenic), while WIPP-12 methane has had a much more significant contribution from thermogenic sources (i.e., thermally driven decay of organic material is significant).

- Hydrogen sulfide in both wells has been produced primarily by bacterial reduction of sulfate, although a thermogenic contribution for some of the WIPP-12 hydrogen sulfide is likely.

- Carbon dioxide is in isotopic equilibrium with brine waters, whereas hydrogen sulfide is not in equilibrium with sulfate in brine.

- Brine gases are very reducing in both reservoirs (methane and hydrogen sulfide are present). Evidence of communication with the atmosphere or other more oxidizing sources is not apparent. The chemically distinct nature of the gases implies no communication between the reservoirs.

5.0 DISCUSSION OF THE DATA AS RELATED TO ISSUES

In this section, the chemical data will be discussed in terms of their relevance to identified issues. For ease of presentation, the discussion will start with an explanation for the origin of the brine. This explanation will help to frame subsequent interpretations by placing the discussion of issues in a mechanistic context.

5.1 ORIGIN OF THE BRINE

5.1.1 Introduction

In most cases, the interpretation of complex data will result in more than one credible working model. This is especially true when selected data sets (such

as trace element variation, etc.) are viewed without the perspective of the total chemistry. Fortunately, when the collective data are considered, a "best", or "most likely" (commonly the simplest) explanation for the observed trends often emerges. Such is the case for the origin of the WIPP-12 and ERDA-6 brines.

To help focus this investigation, an informal hierarchy of data has been established. This hierarchy relates loosely to the importance or weight ascribed to the data, and is derived from the observation that major components of systems are often the most reliable indicators of genesis. Greater confidence can be placed in major/minor element trends because their systematics are less likely to be perturbed by materials or processes which occur infrequently. As an illustration, trace element trends may lend themselves to ambiguous interpretations as a result of strong partitioning by accessory (or trace) phases (e.g., compare Green and Ringwood, 1967, with O'Hara, 1971). Accordingly, the major and minor element chemistries of the brines and gases will be used to interpret the basic origin of the brine. Isotope geochemistry will be used to refine the basic model and to increase the level of detail.

5.1.2 Major and Minor Element Chemistry

The composition of the ERDA-6 and WIPP-12 brines could only have been produced by:

- Dissolution of evaporite minerals (e.g., halite, sylvite, etc.) by a non-seawater source.
- Evaporative concentration of seawater.

To investigate these possibilities, the major and minor element chemistries of the brine have been determined.

During these determinations, the bromide concentrations of the brines were routinely measured. Bromide is of special importance because it is used to determine brine origins (Holser, 1966; Valyashko, 1956; Braitsch, 1971;

Carpenter, 1978; Collins, 1975). Because of this importance, bromide concentrations were measured using two analytical techniques (colorimetric and titrimetric analysis). Recommended ASTM procedures for high ionic strength solutions were also employed. Blind standards were analyzed to determine the accuracy of methods. To summarize the analytical results:

- The two techniques produced concentrations which agreed within the range of analytical error.
- Accuracy was greater than ninety percent as determined by comparison of analyses to known standard compositions.
- The concentration of bromide at ERDA-6 is about 880 mg/l and at WIPP-12 it is about 510 mg/l.

All other major and minor element solutes were also measured using standard, approved techniques, and are referenced to bromide concentration in Table C.10. The results were used to determine whether the brines were generated by dissolution of evaporite minerals or by seawater concentration. Analysis of these models is discussed below.

Dissolution Model.

When a fresh-water source dissolves minerals, the total dissolved solids of the solution increases. To determine if the brines were produced by dissolution (i.e., derived from meteoric waters or waters of dehydration), a simple mass balance model was constructed.

The calculation treats two potential ground-water sources completely; rain (or deionized) water, and the Capitan reef ground water (Lambert, 1978). Simultaneously, the model evaluates waters of dehydration of gypsum (taken as equivalent to rain bulk chemistry, but with a different isotopic identity). In the calculation, the original compositions of the fresh waters have been

modified by assuming that dissolution of evaporite minerals takes place[1]. Published concentrations for bromide minerals of the Delaware Basin (Holser, 1966; Adams, 1969) were used to increase the bromide concentration in the water. For both simplicity and conservatism, only the minerals halite, sylvite, carnallite, thenardite, and calcite were used in the calculations. This simplifies the calculation by avoiding uncharacterized incongruent dissolution of minerals. It is conservative because a maximum amount of bromide is introduced into solution by dissolving these phases. The calculation was ended when the major element chemistry of the model brines equalled or approached the chemistry of the Castile brines. Evaluation of the model's results requires consideration of two factors: (1) the relative masses of minerals required to form the brine, and (2) the agreement between calculated and measured solute/bromide ratios.

Figure C-28 summarizes the results of the calculation for several major components. It can be seen that agreement in the solute/bromide ratios is poor. Moreover, the relative proportions of dissolving phases required to transform the ground water or dehydration water sources to Castile brines are believed to be unrealistic.

Dissolution/precipitation paths for ground waters from the Bell Canyon and Salado formations were also calculated using the water quality data presented in Lambert (1978). However, to arrive at compositions similar to ERDA-6 and WIPP-12 brines, chloride phases must be precipitated. When starting with Bell

(1) In some cases, components were subtracted by assuming common reactions such as calcite reacting to form dolomite and removing Mg from solution. Calculations for the Salado and Bell Canyon encountered this problem frequently. In many of these cases an obvious mechanism for depletion was not apparent. Consequently, the Salado and Bell Canyon ground waters could not be treated completely.

Canyon waters, magnesium and calcium phases must also be removed. For Salado waters, potassium and magnesium must be precipitated in addition to chloride. As precipitation of chloride phases also removes bromide, the resultant bromide concentration is always less than the starting concentration. In most instances, the starting concentration of the bromide in the Salado and Bell Canyon ground waters will be less than the concentration in ERDA-6 and WIPP-12; therefore, no credible dissolution/precipitation path can be employed. Furthermore, to arrive at the correct concentrations, sodium phases must be dissolved. However, the only abundant sodium phase is halite. Halite also contains chloride which must be removed. Therefore, no straightforward, simple pathway of dissolution/precipitation can be calculated.

Seawater Evaporation Model.

The solute/bromide plots (used above to evaluate the dissolution model) can also be used to determine if the Castile brines have been derived from seawater.

As shown in Section 3.3.2, the major and minor element compositions of the brines can best (and perhaps only) be explained by concentration of seawater. Figures C-4 through C-14 illustrate this relationship and show a consistent variation of dissolved components relative to both bromide and chloride.

Several deviations from the seawater curves are apparent in the plots and in Table C.10. For example, all of the chloride versus solute graphs plot slightly but consistently higher in chloride than the seawater reference. As discussed below, this implies some dissolution of a chloride phase.

Valyashko (1956) and Braitsch (1971) noted that chloride/bromide ratios in open seawater were approximately 300 (wt/wt) (see Table C.10). At the beginning of NaCl precipitation, the ratio is approximately 70 (wt/wt). The average WIPP-12 chloride/bromide ratio is 360 (wt/wt), which exceeds the seawater ratio. This elevated value suggests some dissolution of halite by

the brine. The ERDA-6 brine, however, has an average chloride/bromide ratio of 207 (wt/wt). This ratio more closely resembles evaporating seawater with only minor (or without) halite dissolution.

Verification of halite dissolution in both wells is obtained by performing mass balance calculations in which sodium and chloride are removed from the brine compositions according to the stoichiometry of halite (i.e., 1 mole Na: 1 mole Cl). The results of these calculations for ERDA-6 show that dissolution of halite alone is responsible for the elevated sodium and chloride concentrations (i.e., excess above concentrated seawater) in those brines. Similar calculations for WIPP-12 show that an additional sodium phase has also been dissolved. Most probably that phase is glauberite, $CaNa_2(SO_4)_2$. Evidence for glauberite dissolution may be found in thermodynamic calculations and in the sulfate/bromide plot (Figure C-6). Specifically, solubility calculations (after Harvie and Weare, 1980) show that the WIPP-12 brine is probably saturated with glauberite (ERDA-6 brine is possibly saturated) (Tables C.3 and C.4). Furthermore, the sulfate/bromide ratio in WIPP-12 brine is slightly above the seawater reference. This implies that sulfate (in addition to sodium) was present in one of the phases that was dissolved by the brine.

Somewhat stronger than the sodium and chloride deviation is the enrichment of the brines in lithium and boron (see Table C.10 and Figure C-14). Such enrichment in connate brines is relatively common (e.g., Collins, 1970, 1976; Vine, 1979). The enrichment, however, is inconsequential to evaluations of site stability. Nevertheless, possible mechanisms for lithium and boron enrichment will be discussed. These discussions are speculative, and the exact origin of the lithium and boron increases is unclear.

One possibility for the enrichment is that addition of lithium and boron attends diagenesis of the brines. Such enrichment has been reported in the pore waters of restricted marine basins (Collins, 1970). Furthermore, alkali enrichment during diagenesis has apparently occurred in the Delaware Basin,

giving rise to the commercial potash deposits that overlie the Castile (Lambert, 1978, and in preparation). A possible mechanism for this alkali enrichment may be the decomposition of organic marine material. Brown algae (e.g., order Fucales) and red algae (e.g., Rhodymenia palmata) are potential sources for potassium and lithium, respectively (Borovik-Romanova, 1969).

Perhaps more likely than diagenetic enrichment is that the elevated lithium and boron concentrations derive from chemical weathering of (or ion exchange with) terrigenous materials. The southwestern United States is well-known for anomalously high lithium contents in igneous rocks and in sediments (Vine, 1975). Furthermore, high lithium and boron concentrations are commonly associated with sedimentary uranium deposits (Vine, 1979). Deposits of this type are common in New Mexico. Consequently, the chemical weathering of igneous and/or sedimentary sources may have enriched the Permian seawater of the Delaware Basin in lithium and boron. Terrigenous clays in the Castile may also have exchanged with brines to enrich the brines in lithium to a minor degree.

Another deviation from the seawater curves may be found in plots of magnesium/bromide (Figure C-9). These plots are perhaps the most significant divergence from the seawater reference, but they are easily explained. The magnesium depletion results primarily from the reaction of calcite to dolomite which commonly attends the diagenesis of carbonate (e.g., Shephard, 1963):

$$CaCO_3 + Mg^{2+} + CO_3^{2-} = CaMg(CO_3)_2$$

calcite + dissolved material = dolomite

Verification that such a reaction took place is confirmed by the presence of dolomite near fractures and contacts (see Part II, Geology, Section 4.1.3). Mass balance calculations indicate that sufficient dolomite is present in fractures to account for the observed magnesium depletion. For example, at ERDA-6, 0.1 percent dolomite in the fractures is required to account for the reduced magnesium content of the brine. This amount agrees well with X-ray and petrographic observations of dolomite abundances.

Summary

The collective major and minor element chemistry implies that ERDA-6 and WIPP-12 brines were both derived from seawater, and that subsequently each had distinct histories. WIPP-12 brine probably originated as seawater concentrated by evaporation. During transport and collection in the fractured host rock (see Part II, Geology, Section 4.3.3), the condensed seawater reacted with calcite in the host rock to form dolomite. Perhaps at the same time, but probably later, the brine dissolved halite and another sodium-bearing phase (probably glauberite). ERDA-6 had a similar history but did not dissolve glauberite and probably dissolved only minor amounts of halite. The higher bromide content of the ERDA-6 brines probably indicates a more extended period of seawater concentration.

5.1.3 Isotopic Geochemistry

While the major and minor elements of the brines clearly indicate a link to ancient seawater, the isotopic data are somewhat ambiguous in their support of any particular model for the origin of the WIPP brines. Consequently, the isotopic data are discussed below in terms of general agreement or disagreement with proposed models of origin. This can be contrasted with the less equivocal approach taken above for major and minor element chemistries.

Dissolution Model - Ground Water

Previous studies have demonstrated (Lambert, 1978, and in preparation) that the isotopic chemistry of Delaware Basin ground waters fractionate as water travels across the basin. This fractionation results in an increase in both δD and $\delta^{18}O$, and has been attributed to exchange with marine clays (Lambert, 1978, and in preparation). The Castile brines are proposed to be part of this continuum, and their isotopic chemistry is also said to be the result of exchange with clays.

While such a process is reasonable for explaining the regional trend, it is less credible for explaining the composition of reservoir brines. Considering the exchange of structural water only, if the montmorillonite-water

fractionation factor (0.938; Savin and Epstein, 1970) is used to model the isotopic change in water, around 50 batch equilibrations are required to transform water from a δD of -20 °/oo (least negative juvenile ground water) to a δD of -1.0 °/oo (brine value). Mass balance calculations based on interlayer (or exchangeable) water exchange indicate that there is probably only enough clay to fractionate less than one percent of the water in the reservoirs. To fractionate the 8.0×10^9 moles of water in the WIPP-12 reservoir (see Part III, Hydrology, Section 3.4.4) would require at least 6.7×10^8 moles of clay along the water's flow path. A conservative estimate of the fracture surface of 2.67×10^9 m^2 can be derived from the fracture spacing and cross-sectional area of the reservoir (see Part III, Hydrology, Section 3.4.4, and assume continuous fractures across the entire area of influence). If the average depth of alteration across the fracture is on the order of 1 mm, then the maximum 0.1 percent clay content of the rock (found at contacts, see Table C.11) is insufficient for producing the isotopic shift from ground water to brine. Given the conservative assumptions employed, fractionation by clay has probably not contributed significantly to the isotopic character of the brine. If the mechanism is operative, then either the brine followed a very complex and tortuous path, or the zone of alteration is much more extensive than that sampled by coring.

The mass balance calculations discussed above indicate that clay is unlikely to alter known Delaware Basin ground waters to the point where they resemble the isotopic chemistries of the Castile brines. This does not, however, rule out the potential for another mechanism having caused such a shift. To assess this potential, the relation between TDS and brine isotopes may be considered.

As discussed earlier, the variation of δD (°/oo) and δO^{18} (°/oo) as a function of TDS can sometimes be used to determine the parent liquid of a given water source. The technique requires construction of a linear regression fit through the data, and extrapolation to infinite dilution (i.e., TDS = 0). These regression lines should pass through points for the source water, as long as the mechanism that fractionates the isotopes remains constant, and the

fractionation occurs while the TDS of the water is being developed (Clayton et al., 1966). As observed from Figure C-29, no local Delaware Basin ground waters are safely within the statistically derived 90 percent confidence area of the source, although ground waters from the Bell Canyon and Salado formations plot on the very edge of that confidence zone. Based on the isotopes alone, these ground waters could conceivably have given rise to the brines; however, they are high-TDS ground waters. Mixing of high-TDS waters with concentrated seawater would probably result in alteration of the solute/bromide ratios (i.e., mixing would add mass to the system but not sufficient bromide). If mixing occurred to the extent where the isotopic fingerprint resembled the ground water rather than the brine, mass balance calculations (viz., Hitchon and Friedman, 1969) indicate a ground water:seawater ratio near 2:1 would be required. Such dilution would perturb the bromide ratios to the point where resemblance to seawater curves would not be possible.

Finally, it is instructive to examine the $\delta^{34}S$ values of the sulfate in brine and in the reservoir rock. The value for the rock (~ 12 °/oo) is well within the range for Permian sulfate minerals of the Delaware Basin (Holser and Kaplan, 1966). The value for the sulfate in brine (~ 9 °/oo) is isotopically lighter than the rock. If the sulfate in brine were generated by dissolving the rock, then the $\delta^{34}S$ value for the brine should be <u>at least</u> equal to that of the rock[(1)]. However, bacterial sulfate reduction has produced H_2S from the brine. This process fractionates light sulfur into the gas and makes the residual brine heavier. Consequently, the combination of anhydrite dissolution, and bacterial sulfate reduction would have produced brines that are heavier than the reservoir rock.

Therefore, the isotopic geochemistries of the Castile brines do not support the contention that dissolution of rock by ground water has produced the reservoir fluids. Furthermore, ground waters have probably not contributed to reservoir formation. The basis for these conclusions includes:

---

(1) In order to be less than the rock, pyrite (or a related phase) would have to be precipitated. No such phases are reported in the Castile.

- Mass balance constraints do not permit fractionation of δD over the range required, using any known mechanism.

- Delaware Basin ground waters that have isotopic compositions within the possible range of source waters are all high TDS waters. Mixing of these waters with brine would perturb the major element chemistry.

- The $\delta^{34}S$ values for sulfate in brine are consistently less than the $\delta^{34}S$ values of the rock, which precludes dissolution.

Waters of Dehydration

As noted earlier (Section 5.1.2), at an extreme, the bulk chemistry of meteoric water and waters of dehydration would be similar (very low TDS); however, their isotopic identities would be distinctly different. The isotopic difference results from the fact that waters of dehydration of gypsum are fractionated at least twice from meteoric water. The first fractionation occurs during the evaporation of seawater (e.g., Sofer and Gat, 1975) which later precipitates gypsum. The second fractionation occurs when gypsum nucleates in the seawater (Sofer, 1978). A third fractionation is probable subsequent to gypsum dehydration to anhydrite (i.e., back reaction of isotopes with anhydrite), but is not kinetically favored, and is unlikely to reach equilibrium (Lloyd, 1968). The net effect of the fractionation mechanisms is dependent upon the conditions prevailing during seawater evaporation (Sofer and Gat, 1975). However, a plausible range, assuming no back reaction with anhydrite, is shown in Figure C-29. This estimate assumes that the Permian ocean which gave rise to the gypsum (i.e., anhydrite) had an isotopic composition identical to the current SMOW reference.

The ERDA-6 and WIPP-12 brine isotopes plot within the range estimated for waters of dehydration of gypsum. Consequently, on the basis of isotopes, an origin of the brines from waters of dehydration is possible. However, at

least two arguments (based on isotopes) may be raised to weaken this interpretation: 1) The Permian ocean may have been isotopically different from the current ocean. Depending on the magnitude of the difference, the WIPP-12 and ERDA-6 data might not coincide with the dehydration field. 2) The $\delta^{13}C$ and $\delta^{18}O$ data from CO_2 indicate that the brine has reacted with carbonate to generate CO_2 (at ERDA-6). This reaction should increase the $\delta^{18}O$ value of the brine. Mass balance calculations indicate that the shift could be in the range of 3 °/oo to 6 °/oo. Such a shift would displace waters of dehydration from the gypsum crystallization field.

While these arguments weaken the hypothesis that the brines originated as waters of dehydration, they do not preclude the possibility. For example, Kharaka et al. (1973) estimate that the Permian ocean was about 5 °/oo depleted in $\delta^{18}O$ relative to SMOW. If this were true, then the isotopic shift in ancient seawater would compensate for the shift induced by carbonate reaction, i.e., the correspondence between the Castile brines and waters of dehydration of gypsum would remain. Analysis of isotopes, therefore, cannot be used unequivocally to support or condemn the hypothesis that the brines originated from waters of dehydration of gypsum.

Seawater Evaporation Model

If the brines were derived from ancient seawater, then the age of the waters is Permian (the same age as the sediments). As discussed above, the present-day seawater reference (SMOW) may be inappropriate for interpreting the consistency of measured brine isotopes with a seawater evaporation model. For example, on the basis of melted polar ice caps in the Permian, Kharaka et al. (1973) calculated a shift in the δD and $\delta^{18}O$ ocean water references (-5 °/oo and -0.5 °/oo, respectively). The details of this calculation are unclear, but the results provide one estimate of how the isotopic composition of the water in the Permian ocean varies from that of SMOW.

Another method for estimating the isotopic composition of the Permian ocean is to utilize the relation between $\delta^{18}O$ in ocean water and $\delta^{18}O$ in ocean water

sulfate (Kaplan, 1982, personal communication). The current ocean water sulfate has a $\delta^{18}O$ value of about 12.5 °/oo (Claypool et al., 1980). This value is approximately the same as the value found from coexisting sulfate mineral precipitates, i.e., essentially no fractionation of oxygen in sulfate attends precipitation. If the relationship between ^{18}O in seawater and ^{18}O in ocean water sulfate has remained constant with time, and if the dissolved sulfate and precipitating sulfate have always equilibrated to the same extent, then isotopic differences in ancient and modern sulfate minerals reflect the differences of ancient and modern oceans. In contrast to modern sulfate minerals, the Permian sulfates of the Delaware Basin have $\delta^{18}O$ values of about 9 °/oo (Claypool et al., 1980). Employing the assumptions outlined in the previous paragraph, the Permian ocean is calculated to be 3.5 °/oo lighter than the modern ocean (9 °/oo -12.5 °/oo = -3.5 °/oo). The reference value for Permian ocean water $\delta^{18}O$ is therefore -3.5 °/oo. A minimum value for coexisting deuterium may be estimated by using the relationship for Raleigh distillation, i.e., unimpeded evaporation:

$$\delta D = 8(\delta^{18}O) + 5 \qquad \text{(Craig, 1961)}$$

For a $\delta^{18}O$ value of -3.5 °/oo, the resulting δD is -23 °/oo. This estimate, together with the one computed by Kharaka et al. (1973), has been used to define a range for the Permian ocean. The range is depicted as a heavy line in Figure C-30. The stippled area shows a field appropriate for evaporation from these sources.

Of significance is that the Castile brines plot above and to the right of both Permian ocean estimates (see Figure C-31). Although evaporation might be invoked to explain the position of the Castile brines in the shaded area, such an explanation is probably valid only for the enrichment of deuterium, and a portion of the $\delta^{18}O$. Additional enrichment in $\delta^{18}O$ probably has resulted from isotopic exchange between the brines and carbonates (subsequent to removal of the brine from its basin). Mass balance estimates indicate that such exchange could account for at least a 1 °/oo increase in $\delta^{18}O$, and perhaps as much as a 5 °/oo increase.

In addition to the brine isotopes, the isotopes of sulfur in sulfate are consistent with the seawater evaporation model. The $\delta^{34}S$ in brine sulfate is measured as around 8 °/oo to 9 °/oo compared to about 11.5 °/oo in the coexisting rock. This relationship is consistent with the 1.65 °/oo fractionation that might be expected when anhydrite precipitated from ancient seawater (Holser and Kaplan, 1966; Claypool et al., 1980). Moreover, both $\delta^{34}S$ values fall in the range for Permian materials.

The discussion above has been premised on an assumed difference between Permian ocean and present-day seawater. This difference cannot be demonstrated conclusively and is a subject of academic debate. Consequently, whether the isotopic character of the Castile brines can be explained using reasonable processes and the current SMOW reference should be determined.

Mechanisms for increasing the brines in ^{18}O relative to SMOW include:

- Evaporation
- Reaction with carbonates
- Reaction with silicates

By analogy to the discussion above, the $\delta^{18}O$ shift can be accounted for by these mechanisms.

Mechanisms for altering the δD of the brines relative to SMOW include:

- Evaporation
- Reaction with marine clays
- Mixing with other waters

Evaporation could produce the δD values observed in the brines, if the brines followed an evaporation path similar to those for bitterns (see Sofer and Gat, 1975). However, given the low magnesium content of the brines, this explanation does not appear credible. Reaction with marine clays probably could not

produce the observed δD values because there does not appear to be a sufficient mass of clay in the formation. As a result, if no isotopic difference existed between Permian and current oceans, then the isotopic character of the brines is best explained by mixing seawater with low TDS waters. These waters must be low TDS to avoid altering the major and minor element relationships discussed earlier.

One potential mixing model might be that fresh water isotopically similar to that found in some regional meteoric waters ($\delta^{18}O$ = -2 °/oo to -7 °/oo, δD = -10 °/oo to -30 °/oo) mixed with concentrated seawater. If mixing occurred in a 1:1 ratio (see Hitchon and Friedman, 1969), then a source near the edge of the 90 percent confidence field of Figure C-29 would result. To generate the observed isotopes in the brines, that source would then have to be fractionated. In this scenario, at least two possibilities exist:

- The mixing occurred either soon after (or during) the last stages of sedimentation. Evaporation through pores or at the surface then concentrated the heavier isotopes into the residual brine.

- Isotopic fractionation occurred after burial of the mixed solution. Fractionation of hydrogen by hydrous phases (e.g., Savin and Epstein, 1970; Lambert, 1978, and in preparation) enriched the residual brine slightly in deuterium. Reaction with other reservoir rocks (anhydrite and dolomite) enriched the brines in ^{18}O (Lloyd, 1968; Clayton et al., 1966).

Alternatively, seawater underwent concentration by evaporation to generate its major and minor element chemistries and precipitated gypsum during the process. As salinity of the basin increased, the gypsum destabilized and dehydrated to form anhydrite (e.g., Posnjak, 1938). Since waters of dehydration are low TDS, the major/minor element proportions of the seawater would be unchanged by mixing of the two waters. The isotopic identity of the residual brine would be changed, however, and depending on its proportions (at least 1:1 mixing is required), it would plot along the regression line somewhere between the center of the 90 percent confidence field and that

measured for the brines (see Figure C-29). Subsequent evaporation would cause isotopic fractionation and major element concentration trends consistent with those observed for the brine.

One strength of this last alternative is that the linear regression line derived from isotope versus TDS plots (Figures C-20 and C-21) converges on the vertex of the waters of crystallization of gypsum field (Figure C-29). Furthermore, anhydrite pseudomorphs after gypsum may be present in cores taken from the reservoir host rock (see Part II, Geology, Section 4.1.3 and Figure C-18).

The major weakness of the model is the lack of extensive physical evidence for gypsum pseudomorphs. At best, the criteria used to identify gypsum pseudomorphs (i.e., relict cleavages and replacement textures) are subjective and inconclusive. Furthermore, the presence of such textures is not pervasive as might be expected if extensive gypsum dehydration has occurred. Finally, some of the anhydrite grains appear to be primary precipitates. It would be unusual for anhydrite and gypsum to coprecipitate.

Therefore, the isotopic data are not inconsistent with an ancient seawater origin for the brine. The bases for this conclusion are:

- Two models have been evaluated; one in which ancient seawater is isotopically identical to SMOW and another in which the ancient ocean differs from SMOW. Both models can be used to arrive at isotopic values observed without being inconsistent with material abundances existing in the basin. Specifically:

  - Mixing of SMOW with ancient meteoric waters or waters of dehydration of gypsum in proportions near 1:1 could produce waters near the "unfractionated" source of the brines. Subsequent reaction with carbonates and clays or evaporation of the mixtures could produce waters with the isotopic composition of the brines.

- Estimates of Permian ocean water fall below and to the left of the Castile brines. Evaporation of such seawater and isotopic exchange with carbonates are therefore viable mechanisms for generating the Castile brine isotopes.

- The measured $\delta^{34}S$ of the sulfate in the rocks and brines are consistent with Permian-aged materials. Differences between the two sulfates can be attributed to fractionation during precipitation.

- The preferred model for brine origin is ancient seawater modified slightly by reaction with basin minerals. This model is preferred because of its simplicity, and because of a lack of evidence for alternative models.

5.1.4 Gas Compositions

The major element chemistry, and the isotopic ratios of the gases obtained from ERDA-6 and WIPP-12 show differences between the two wells. First, the compositions and proportions of the gases, and their amounts relative to brine are different at each well. (See Figure C-26 and Tables C.7 and C.8). These differences may be attributed to:

- Different sources of generation.

- Different downhole conditions affecting the efficiency of rate-dependent processes.

- Different downhole conditions affecting the equilibrium proportions of coexisting volatile components.

The hydrogen sulfide of WIPP-12 exists both as a gas, and as a dissolved (or miscible) liquid. In contrast the hydrogen sulfide at ERDA-6 exists only as a dissolved phase. At both wells, the hydrogen sulfide has been generated dominantly by bacterial sulfate reduction. This process usually requires still-water conditions. Therefore, the hydrogen sulfide generation probably occurred either in-place in the reservoir, or after collection of pore waters, but prior to reservoir formation. Conditions for hydrogen sulfide production may have been more favorable in the ERDA-6 environment. More likely, however,

the WIPP-12 reservoir contains a thermogenic hydrogen sulfide component. Upward-moving thermogenic hydrogen sulfide might have been trapped along with pore water by the rapid sedimentation of anhydrite during the Permian. Alternatively, the thermogenic hydrogen sulfide could have been acquired by WIPP-12 during the deformation that resulted in the reservoir.

Less ambiguous than the hydrogen sulfide is the origin(s) of methane at the two wells. The methane at ERDA-6 is probably all of biogenic origin. In contrast, the methane of WIPP-12 is dominantly thermogenic with perhaps a minor contribution from biogenic sources. Deformation and flow may have liberated thermogenic methane from the fluid inclusions of the underlying halite. Alternatively, deformation may have disrupted grain boundary contacts, allowing thermogenic methane to diffuse from a deeper source. The less equivocal presence of thermogenic methane at WIPP-12, supports the interpretation of thermogenic hydrogen sulfide at that well.

Nitrogen and carbon dioxide are also present at both wells. Nitrogen may have been generated either by air entrapment, by pyrolysis of organics, or most likely by bacterial processes (e.g., Desulfovibrio denitrificans; Kuznetsov et al., 1963). The carbon dioxide is present in greater amounts than can be attributed to air entrapment. Consequently, it is probably a result of biogenic activity and/or carbonate dissolution.

Of some interest are the different proportions of carbon dioxide and methane at the two wells. ERDA-6 is much richer in CO_2, while WIPP-12 is much richer in methane. Both of these gases are carbon bearing and can coexist at equilibrium. The relative proportions may be a function of different carbon to hydrogen ratios (see Gerlach and Nordlie, 1975). Accordingly, the difference between the two wells may be due to the greater carbon:hydrogen (rock:water) ratio at ERDA-6.

5.1.5 Residence Time

Determination of the length of time that the ERDA-6 and WIPP-12 brines have resided in the fractured anhydrite reservoirs was calculated using the uranium-isotope disequilibrium method (Appendix A). This method utilizes deviations in the $^{234}U/^{238}U$ specific activity ratio from unity to estimate the age of confinement of ground water (Kronfeld et al., 1975; Andrews and Kay, 1978; Barr et al., 1979). Determination by this method of the time of entrapment of fluids, however, is not unequivocal for fluids that might have migrated along uncharacterized flowpaths or that could have complex histories. Significant factors contributing to this uncertainty are that a $^{234}U/^{238}U$ specific activity ratio of the water at the time of its isolation must be inferred, and a model of fluid movement, including potential changes in fluid chemistry created by the lithology of the travel path and eventual trap rock, must be considered. These factors are seldom known, but must be inferred from other geological and hydrological information (see, for example, Andrews et al., 1982). Nevertheless, geologically reasonable inferences can be made that allow bounding calculations of residence time.

Residence time of the ERDA-6 and WIPP-12 brines by the uranium-isotope disequilibrium method was calculated according to various models of origin by Lambert and Carter (in press) on samples collected for that purpose and supplied to Sandia National Laboratories. For the reasons discussed above, an absolute time of residence could not be uniquely determined.

Significantly, however, the activity ratios in the brines are not unity (i.e., the uranium isotopes are not in secular equilibrium). Since secular equilibrium between $^{234}U/^{238}U$ will be established in less than two million years, the excess ^{234}U implies brine and rock have interacted within the last 2×10^6 years. Such interaction is likely to occur when fresh rock surfaces are exposed to brine and ^{234}U is preferentially leached. Therefore, if the brines are trapped Permian seawater, then the initiation of brine collection in fractures must have occurred no more than one to two million years ago (the time for achieving secular equilibrium between ^{234}U and ^{238}U is less than two million years). More rigorous residence time calculations are included in

Appendix A. The results of these calculations, however, are entirely dependent upon model assumptions that cannot yet be verified. Moreover, the uncertainty in the exact history of the fluids may obviate attempts at more precise refinements.

5.1.6 Summary of Brine Fluid Origin

The Castile brine reservoirs appear to have formed from ancient seawater, without a noticeable contribution from any other water source. During the Permian, seawater was trapped in a restricted basin and the water was concentrated by evaporation. During formation of the Castile anhydrite, between 75 percent and 90 percent of the original water volume was lost by subaerial evaporation (gypsum/anhydrite to halite saturation). This distillation increased the TDS of the brine, and enriched it in deuterium and ^{18}O. During chemical precipitation of gypsum/anhydrite, some of the basin water was trapped as sediment pore water. The sediment was subsequently compacted, lithified, and tilted (see Part II, Geology, Section 3.4), and these ancient processes mobilized the brine. After release from the pores, the brine traveled along fractures and bedding planes to a point of collection. This transport is of an unspecifiable distance, but was probably relatively short (i.e., it was not basin-wide). During this ancient transport, perhaps initiated by episodes of regional tilting, the brine reacted with calcite to form dolomite. This depleted the brine in magnesium. Isotope exchange between the brine and carbonates also enriched the brine in heavy oxygen. Minor dissolution of halite and precipitation of quartz also occurred during brine transport, and in the case of WIPP-12, glauberite may have been dissolved. This dissolution elevated the sodium and chloride components of the brine.

When the brine came to rest, biogenic activity may have begun. Since the brine was held in an hydraulically tight environment, gases that were produced by bacterial processes were retained. These gases included hydrogen sulfide and methane, and may have included carbon dioxide and nitrogen. The deformation that gave rise to reservoir formation (see Part II, Geology, Section 4.3.1) remobilized the brine. At this time, the brine probably traveled only

a very short distance (meters to tens of meters). During this mobilization, the thermogenic gases were probably acquired by the reservoir. Since reservoir formation, very little or no introduction of fluids into the reservoirs has occurred. As a result, the fluids have reached (or very closely approached) equilibrium with their environment.

From this description of brine origin, several significant observations may be made. The brines observed in the Castile were derived virtually entirely from waters no longer available as sources. Therefore, brine reservoir formation may be considered inactive or dormant. If dormant, then the frequency and size of additional reservoirs are dependent upon the geomechanical history of the specific areas of interest. The volume of water for forming the reservoir is limited by the amount of pore (i.e., fracture filling) water available.

5.2 EXTENT OF CHEMICAL EQUILIBRATION

The brines, and to a large part, the gas chemistries[1], suggest that components of the reservoirs have equilibrated with the host formations. Since dissolution and transport commonly lead to disequilibrium relations, this equilibration can be taken as an indication of a near-stagnant regime.

5.2.1 Gases

The environments of both brine reservoirs are very reducing (i.e., oxygen is absent). The probable control on this condition is hydrogen sulfide. Figure C-32 is an Eh/pH diagram for aqueous sulfate systems computed for the temperature and pressure conditions that exist downhole (see Part III, Hydrology, Sections 3.4.3 and 3.4.4). The measured Eh and pH of the brines appear to be controlled by the reaction:

(1) The exceptions are major isotopes of CH_4 and H_2S. These gases have been influenced by biogenic activity, and the lack of equilibrium between them and the rest of the reservoir reflects the relatively-low temperature.

$$H_2S + 4H_2O \rightarrow SO_4^{2-} + 10H^+ + 8e^- \quad \text{(Garrels and Christ, 1965)}$$

at an H_2S/SO_4^{2-} ratio near 10^3.

This estimate, however, depends on the accuracy of field-measured Eh and pH. Field measurements of Eh are notoriously difficult and often unreliable. Furthermore, the brine pH and Eh were not measured downhole. As a result, the measurements should be validated by examining a different system.

The carbon gases present downhole can be used to estimate the equilibrium of the brine system. Methane and carbon dioxide equilibrium may be used in conjunction with water to define the active oxygen content:

$$CH_4 + 2O_2 \rightarrow CO_2 + 2H_2O$$

The equilibrium oxygen fugacity (active oxygen content) can be calculated from the well-known equilibrium relation:

$$\Delta G = - RT \ln K$$

and from the mass action expression:

$$K = \frac{[\text{products}]}{[\text{reactants}]} = \frac{f(CO_2)f(H_2O)^2}{f(CH_4)f(O_2)^2}$$

Equilibrium oxygen fugacity can be calculated by using tabulations of free energy (Robie et al., 1978) and/or extrapolations of empirical data (Skippen, 1967). For the measured gas compositions, oxygen fugacity is calculated as 10^{-67} atm for ERDA-6, and 10^{-69} atm for WIPP-12. (These low values are thermodynamic potentials, and not necessarily oxygen concentrations.)

Oxygen fugacity may then be used to calculate Eh (oxidation/reduction potential) using the relation:

$$Eh\ (volts) = 1.23 + 4.96 \times 10^{-5}\ (T°K)\ \log fO_2 - 1.984 \times 10^{-4}\ (T°K)\ pH - (T°K-298)9.196 \times 10^{-4}$$ (Smith et al., 1980)

In this way, theoretical equilibrium Ehs for WIPP-12 and ERDA-6 were calculated as -232mV and -171mV, respectively. These values compare to the average measured values of -225mV and -152mV. Thus, the theoretical results are in surprisingly good agreement with the measured results, being within 12.5 percent of the measurements for both wells. Although it was believed originally that kinetic factors might negate the calculations, the agreement implies that the Eh measurements are reliable, and that the gases are in (or are approaching) chemical equilibrium with the environment (i.e., the calculations were made with equilibrium as an assumption. If that assumption were incorrect, any agreement between the theoretical and measured values would be highly fortuitous.). Equilibrium at a reduced (i.e., negative) Eh is a significant finding given the poor reducing capacity of the reservoir rocks. The approach to equilibrium implies that the brines have been isolated and undisturbed for a long period of time.

5.2.2 Brines

Perhaps a more powerful argument for reservoir/host rock equilibrium can be made by comparing the results of equilibrium saturation calculations with observed phases. These calculations were performed using the equilibrium thermodynamic model developed for brines (Harvie and Weare, 1980). The results of the model predict that both wells are saturated (i.e., in equilibrium) with calcite, dolomite, and probably anhydrite. All of these phases are present in the rocks of both reservoirs. More significantly, the model detects a difference between the brines in that the WIPP-12 brine is probably saturated with halite and glauberite while the ERDA-6 brine is not saturated with halite, and may not be saturated with glauberite. Physical and petrographic observations appear to confirm this relationship. Specifically, fractures in the WIPP reservoir contain secondary halite in addition to anhydrite while the ERDA fractures contain anhydrite, but are devoid of halite.

The significance of this equilibrium is that the brines have little or no potential to dissolve the host rock under present conditions.

5.2.3 Isotopes

In addition to the major element chemistry, the isotopic data appear to support the assertion of equilibrium. Least ambiguous are the $\delta^{34}S$ data obtained on the sulfate in the brine. These values (near 9 °/oo) are centrally located in the field for Permian sulfates (Faure, 1977; Nielsen, 1979; Thode et al., 1961). Since the reservoir rocks are known to be Permian (e.g., Adams, 1944), and since no other materials generally produce $\delta^{34}S$ values near 8 °/oo (see Figure C-22), either the brines were derived directly from Permian seas or the waters have equilibrated with Permian sulfate minerals. In either case, the brines are in equilibrium with the host rock.

In addition to the $\delta^{34}S$ isotopes in sulfate, the $\delta^{13}C$ isotopes in CO_2 and in brine carbonate appear to show equilibration. The observed fractionation Δ 7 to 9 °/oo is consistent with the equilibrium range at 25-30°C (Faure, 1977).

Finally, the $\delta^{18}O$ in carbon dioxide appears to be in equilibrium with the oxygen in water. Figure C-27 presents the data from the Castile brines. For reference, the $\delta^{13}C$ and $\delta^{18}O$ values for atmospheric CO_2 are also shown. The $\delta^{18}O$ values of the Castile brine carbon dioxide are 10 °/oo greater than atmosphere. This 10 °/oo increase is precisely the same as observed for the oxygen of the brine water. Accordingly, the brine water and carbon dioxide are in equilibrium.

5.3 EXTENT OF CHEMICAL ISOLATION

As shown in Sections 2.0-4.0 (above), many chemical similarities exist between ERDA-6 and WIPP-12 brines. These similarities may be attributed to the common origin of the brine reservoir waters (See Section 5.1). Distinct differences between the brines are also apparent, and these differences imply a distinct lack of chemical communication between reservoirs. Moreover, the chemical

differences between the brines and known ground-water sources suggest little or no communication between them.

5.3.1 Gases

Perhaps the strongest evidence for isolation may be found in the gases of the brine reservoirs. Thermodynamic evaluation of the volatile mixtures of the brine show that at least for WIPP-12, a substantial gas (as opposed to super-critical fluid) concentration exists. The fact that these gases have remained trapped by the stratigraphy enclosing the brines attests to the closed nature of the reservoirs. Furthermore, the mobility of gases should lead to mixing of the reservoir volatiles, if communication between them exists. The considerable difference in the compositions of gas mixtures at ERDA-6 and WIPP-12 indicate that mixing has not occurred. Furthermore, the methanes associated with each of the reservoirs are of distinct origins (thermogenic versus bacteria-produced). Based on these differences, communication between the reservoirs appears to be nil.

5.3.2 Brines

As well as the gases, the brine chemistries are indicative of isolation. Figures C-4 through C-16 illustrate the character of the brine reservoirs relative both to other Delaware Basin ground waters and to seawater. While the resemblance to seawater is striking, any continuity between brine compositions and ground waters is lacking. For example, introduction of ground waters into seawater-derived brines should increase the mass of major element components relative to bromide. Such is not the case; in fact, where serious departures from the seawater curves are apparent (e.g., magnesium), those departures are in the negative direction. Thus, the major element/bromide ratios, which are sensitive to slight perturbations (see Carpenter, 1978), indicate that no mixing of seawaters and local ground waters has occurred.

In addition to lack of mixing with ground water, the brine chemistries appear to indicate a lack of communication between reservoirs. Most notably, WIPP-12 brine appears to be saturated with halite while ERDA-6 brine is not. This

difference, along with the perceptible differences in both absolute and relative concentrations of dissolved components and gases, support the interpretation that the reservoirs are not chemically connected. Moreover, given the poor reducing capacity of evaporite rocks, any communication between the reservoirs, or between the reservoirs and a ground water source, would be expected to perturb the Eh of the reservoir. Since the reservoirs appear to be in equilibrium with their surroundings, and since they have distinctly different Eh's, each reservoir appears to be a closed system.

Isotopes

Previous examinations of brine isotopes (Lambert, 1978) have noted the seeming continuity from meteoric Delaware Basin ground waters to the brine reservoirs. These examinations have been made in the absence of the complete data. As a result, one credible interpretation of this trend was a continuous fractionation of the hydrogen and oxygen isotopes from meteroic water to the brine. While the mechanism for deuterium enrichment is uncertain (compare Lambert, 1978, and in preparation; with: Savin and Epstein, 1970; O'Neill and Kharaka, 1976; and Kharaka et al., 1973), one might propose that, at the very least, mixing of waters has occurred. However, the isotope ($\delta^{18}O$ and δD) versus salinity (TDS) plots presented earlier (Figures C-20, C-21, and C-29) argue against such a source. Moreover, mass balance constraints and the major and minor element chemistries of the brines appear to refute this hypothesis.

5.4 SUMMARY OF FINDINGS AS RELATED TO ISSUES

In the sections above, the chemical data have been discussed in terms of issues relevant to the suitability of the proposed WIPP site. The major findings are summarized below:

- The brines are probably derived from ancient seawater. In any case, no ground water currently in the basin contributed significantly to formation of the reservoirs. (For a comparison of the different origin hypotheses see Table C.12.)
- The formation of brine reservoirs can be considered an inactive or dormant process. If dormant, the

formation of brine reservoirs is dependent upon the geomechanical environment of the area. Water for forming the reservoirs is limited to water currently contained in the fracture pore space of the Castile Formation.

- The brine reservoirs are stagnant and have reached equilibrium with their surroundings. Flow into or out of the reservoirs approaches zero.

- The brine reservoirs are not in chemical communication with each other or with other known sources of water. Accordingly, the reservoirs can be considered closed or isolated systems.

- Brine from WIPP-12 is saturated with all major phases of the reservoir rock. Brine from ERDA-6 is saturated with all major phases, but is slightly undersaturated with halite. The potential for brines from either reservoir to dissolve overlying rock is negligible.

LIST OF REFERENCES

Adams, J. E., 1944, Upper Permian Ochoa Series of Delaware Basin, West Texas and Southeastern New Mexico: Amer. Assoc. of Pet. Geol. Bull., v. 28, no. 11, pp. 1596-1625.

Adams, S. S., 1969, Bromine in the Salado Formation, Carlsbad Potash District, New Mexico: New Mexico Bureau of Mines and Mineral Resources, Bulletin 93, Socorro, N.M., 122 pp.

American Public Health Association (APHA), 1980, Standard Methods for the Examination of Water, 15th edition: American Public Health Association, Washington, D.C.

Anderson, R. Y., 1982, Upper Castile Brine Aquifer, Northern Delaware Basin, New Mexico.

Anderson, R. Y. and D. W. Kirkland, 1980, Dissolution of Salt Deposits by Brine Density Flow: Geology, v. 8, pp. 66-69.

Andrews, J. N., I. S. Giles, R. L. F. Kay, D. J. Lee, J. K. Osmond, J. B. Cowart, P. Fritz, J. F. Barker, and J. Gale, 1982, Radioelements, Radiogenic Helium and Age Relationships for Ground Waters From the Granites at Stripa, Sweden: Geochim. Cosmochim. Acta, v. 46, pp. 1533-1543.

Andrews, J. N. and R. L. F. Kay, 1978, The Evolution of Enhanced $^{234}U/^{238}U$ Activity Ratios for Dissolved Uranium and Ground Water Dating: Fourth Int. Conf. Geochronology, Cosmochronology and Isotope Geology, Denver, U.S. Geol. Survey Open-File Report 78-701, p. 11.

Barnes, I. and W. Back, 1964, Dolomite Solubility in Ground Water: Article 160, in U.S. Geol. Survey Prof. Paper 475-D, pp. D179-D180.

Barr, G. E., S. J. Lambert, and J. A. Carter, 1979, Uranium Isotope Disequilibrium in Groundwaters of Southeastern New Mexico and Implications Regarding Age-Dating of Waters: in Isotope Hydrology 1978, v. II, International Atomic Energy Agency, pp. 645-660.

Baumann, H., 1971, The Production of Pure and Perturbed Quartz Surfaces and Their Relation Under Various Treatment: Fortschr. Kolloide u. Polymere, v. 55, pp. 37-44.

Borovik-Romanova, T. H., 1969, Biogeochemistry of the Alkali Elements: Geochemistry International, v. 6, pp. 906-912.

LIST OF REFERENCES
(Continued)

Bottinga, Y. and H. Craig, 1969, Oxygen Isotope Fractionation Between CO_2 and Water, and the Isotopic Composition of Marine Atmospheric CO_2: Earth Planet. Sci. Letters, v. 5, pp. 285-295.

Braitsch, O., 1971, Salt Deposits - Their Origin and Composition: Springer-Verlag, New York, 297 pp.

Carpenter, A. B., 1978, Origin and Chemical Evolution of Brines in Sedimentary Basins: Oklahoma Geol. Survey Circular 79, pp. 60-77.

Chen, C. A. and W. L. Marshall, 1982, Amorphous Silica Solubilities IV, Behavior in Pure Water and Aqueous Sodium Chloride, Sodium Sulfate, Magnesium Chloride, and Magnesium Sulfate Solution Up to 350°C: Geochim. Cosmochim. Acta, v. 46, pp. 279-287.

Claypool, G. E., W. T. Holser, I. R. Kaplan, H. Sakai, and I. Zak, 1980, The Age Curves of Sulfur and Oxygen Isotopes in Marine Sulfate and Their Mutual Interpretation: Chem. Geology, v. 28, pp. 199-260.

Clayton, R. N., I. Friedman, D. L. Graf, T. K. Mayeda, W. F. Meents, and N. F. Shimp, 1966, The Origin of Saline Formation Waters, 1. Isotopic compositions: Jour. of Geophys. Res., v. 71, pp. 3869-3882.

Collins, A. G., 1970, Geochemistry of Some Petroleum Associated Waters from Louisiana: U.S. Bureau of Mines Report Investigation 7326, 31 pp.

Collins, A. G., 1975, Geochemistry of Oilfield Waters: Elsevier Scientific Publishing Company, N.Y., 496 pp.

Collins, A. G., 1976, Lithium Abundances in Oilfield Waters: in Lithium Resources and Requirements by the Year 2000, J. D. Vine, ed., U.S. Geol. Survey Prof. Paper 1005, pp. 116-123.

Craig, H., 1961, Standard for Reporting Concentration of Deuterium and Oxygen - 18 in Natural Waters: Science, v. 133, pp. 1833-1834.

D'Appolonia Consulting Engineers, Inc., 1982, Data File Report - ERDA-6 and WIPP-12 Testing: Westinghouse Electric Corporation and U.S. Department of Energy, Albuquerque, N.M.

Faure, G., 1977, Principles of Isotope Geology: John Wiley and Sons, N.Y., 464 pp.

Freeze, R. A. and J. A. Cherry, 1979, Groundwater: Prentice-Hall, Inc., Englewood Cliffs, New Jersey, 604 pp.

Fuex, A. N., 1977, The Use of Stable Carbon Isotopes in Hydrocarbon Exploration: Jour. of Geochem. Exploration, v. 7, pp. 155-188.

LIST OF REFERENCES
(Continued)

Garrels, R. M. and C. L. Christ, 1965, Solutions, Minerals, and Equilibria: Freeman, Cooper and Company, San Francisco, CA., 450 pp.

Gerlach, T. M. and B. E. Nordlie, 1975, The C-O-H-S Gaseous System Part I, Composition Limits and Trends in Basalt Gases: Amer. Jour. of Sci., v. 275, pp. 353-376.

Grabau, A. W., 1920, Geology of the Non-Metallic Mineral Deposits Other Than Silicates; v. 1 Principles of Salt Deposition: McGraw-Hill Book Company, New York, 435 pp.

Green, D. H. and A. E. Ringwood, 1967, The Genesis of Basaltic Magma: Contrib. Min. Petrol., v. 15, pp. 103-190.

Harrison, A. G. and H. G. Thode, 1958, Mechanisms of the Bacterial Reduction of Sulphate from Isotope Fractionation Studies: Trans. of the Faraday Society, v. 54, pp. 84-92.

Harvey, W. W., M. J. Turner, J. Slaughter, and A. C. Makrides, 1976, Study of Silica Scaling from Geothermal Brines: Progress Report for Period March, 1976 - September, 1976: COO-2607-3, EIC Corporation, Newton, Massachusetts.

Harvie, C. E. and J. H. Weare, 1980, The prediction of Mineral Solubilities in Natural Waters: the Na-K-Mg-Ca-Cl-SO_4-H_2O System from Zero to High Concentration at 25°C: Geochim. Cosmochim. Acta, v. 44, pp. 981-997.

Hiss, W. L., 1975, Water Quality Data From Oil and Gas Wells in Part of the Permian Basin, Southeastern New Mexico and Western Texas: U.S. Geol. Survey Open-File Report 75-579.

Hitchon, B. and I. Friedman, 1969, Geochemistry and Origin of Formation Waters in the Western Canada Sedmentary Basin - I. Stable Isotopes of Hydrogen and Oxygen: Geochim. Cosmochim. Acta, v. 33, pp. 1321-1347.

Holser, W. T., 1966, Bromide Geochemistry of Salt Rocks: in Second Symposium on Salt, J.L. Rau, ed., Northern Ohio Geol. Society, Inc., Cleveland, Ohio, pp. 248-275.

Holser, W. T. and I. R. Kaplan, 1966, Isotope Geochemistry of Sedimentary Sulfates: Chem. Geology, v. 1, pp. 93-135.

Holser, W. T., I. R. Kaplan, H. Sakai, and I. Zak, 1979, Isotope Geochemistry of Oxygen in the Sedimentary Sulfate Cycle: Chem. Geology, v. 25, pp. 1-17.

Iler, R. K., 1979, The Chemistry of Silica: Solubility, Polymerization, Colloid and Surface Properties, and Biochemistry: John Wiley and Sons, N.Y.

LIST OF REFERENCES
(Continued)

Jones, C. L., 1973, Salt Deposits of Los Medanos Area, Eddy and Lea Counties, New Mexico: U.S. Geol. Survey Open-File Report 4339-7, 67 pp.

Kaplan, I. R., 1982, personal communication: President, Global Geochemistry Corp., Canoga Park, California.

Katz, D. L., D. Cornell, R. Kobayashi, F. H. Poettman, J. A. Vary, J. R. Elenbaas, and C. F. Weinaug, 1959, Handbook of Natural Gas Engineering: McGraw-Hill Book Company, N.Y.

Kharaka, Y. K., F. A. F. Berry, and I. Friedman, 1973, Isotope Composition of Oil-Field Brines from Kettleman North Dome, California, and Their Geologic Implications: Geochim. Cosmochim. Acta, v. 37, pp. 1899-1908.

Krauskopf, K. B., 1967, Introduction to Geochemistry: McGraw-Hill Book Company, N.Y., 721 pp.

Kronfeld, J., E. Gradsztajn, H. W. Muller, J. Radin, A. Yaniv, and R. Zach, 1975, Excess Uranium-234: An Aging Effect in Confined Waters: Earth Planet. Sci. Letters, v. 27, pp. 342-349.

Kuznetsov, S. I., M. V. Ivanov, and N. N. Lylaikova, 1963, Introduction to Geological Microbiology: translation by P.T. Broneer (1978), McGraw-Hill Book Company, New York, 245 pp.

Lambert, S. J., 1978, Geochemistry of Delaware Basin Ground Waters: New Mexico Bureau of Mines and Mineral Resources, Circular 159, pp. 33-38.

Lambert, S. J., in preparation, Interim Report: Dissolution of Evaporites in and Around the Delaware Basin, Southeastern New Mexico and Western Texas: SAND82-0461, Sandia National Laboratories, Albuquerque, New Mexico.

Lambert, S. J. and J. A. Carter (in press), Uranium-Isotope Disequilibrium in Brine Reservoirs of the Castile Formation, Northern Delaware Basin, Southeastern New Mexico: SAND83-0144, Sandia National Laboratories, Albuquerque, New Mexico.

Lloyd, R. M., 1968, Oxygen Isotope Behavior in the Sulfate-Water System: Jour. of Geophys. Res., v. 73, pp. 6099-6110.

MacKenzie, F. T. and R. Gees, 1971, Quartz: Synthesis at Earth Surface Conditions: Science, v. 173, pp. 533-535.

Martinez, J. D. (principal author), 1979, An Investigation of the Utility of Gulf Coast Salt Domes for the Storage or Disposal of Radioactive Waste: Institute for Environmental Studies, Louisiana State University, Baton Rouge, LA.

LIST OF REFERENCES
(Continued)

Mercer, J. W. and B. R. Orr, 1979, Interim Data Report on the Geohydrology of the Proposed Waste Isolation Pilot Plant Site, Southeast New Mexico: U.S. Geol. Survey Water-Resources Investigations 79-98, 178 pp.

Midkiff, W. S. and H. P. Foyt, 1976, Amorphous Silica Scale in Cooling Waters: LA-UR-75-2313, submitted to Cooling Tower Institute, Annual Meeting, Houston, Texas, January 1976, Los Alamos Scientific Laboratory, Los Alamos, N.M.

Midkiff, W. S. and H. P. Foyt, 1977, Silica Scale Technology and Water Conservation: LA-UR-76-2500, Submitted to Meeting of the National Association of Corrosion Engineers, March, 1977, San Francisco, Los Alamos Scientific Laboratory, Los Alamos, N.M.

Nielsen, H., 1979, Sulfur Isotopes: in Lectures In Isotope Geology, E. Jager and J. C. Hunziker, eds., Springer-Verlag, New York, 329 pp.

O'Hara, M. J., 1971, Garnet-Peridotite Stability and Occurrence in Crust and Mantle: Contrib. Min. Petrol., v. 32, pp. 48-68.

O'Neill, J. R. and Y. K. Kharaka, 1976, Hydrogen and Oxygen Isotope Exchange Reactions Between Clay Minerals and Water: Geochim. Cosmochim. Acta, v. 40, pp. 241-246.

Posnjak, E., 1938, The System, $CaSO_4$-H_2O: Amer. Jour. of Sci., v. 35A, pp. 247-272.

Powers, D. W., S. J. Lambert, S. E. Shaffer, L. R. Hill, and W. D. Weart (editors), 1978, Geological Characterization Report, Waste Isolation Pilot Plant (WIPP) Site, Southeastern, New Mexico: SAND78-1596, Sandia National Laboratories, Albuquerque, New Mexico.

Rice D. D. and G. E. Claypool, 1981, Generation, Accumulation, and Resource Potential of Biogenic Gas: Amer. Assoc. of Pet. Geol. Bull., v. 65, no. 1, pp. 5-25.

Rittenhouse, G., 1967, Bromine in Oil-Field Waters and Its Use in Determining Possibilities of Origin of These Waters: Amer. Assoc. of Pet. Geol. Bull., v. 51, pp. 2430-2440.

Robie, R. A., B. S. Hemingway, and J.R. Fisher, 1978, Thermodynamic Properties of Minerals and Related Substances at 298.15K and 1 bar and at Higher Temperatures: U. S. Geol. Survey Bull. 1452.

Sakai, H., 1968, Isotopic Properties of Sulfur Compounds in Hydrothermal Processes: Geochem. Jour., v. 3, pp. 29-49.

Savin, S. M. and S. Epstein, 1970, The Oxygen and Hydrogen Isotope Geochemistry of Clay Minerals: Geochim. Cosmochim. Acta, v. 34, pp. 25-42.

LIST OF REFERENCES
(Continued)

Schoell, M., 1980, The Hydrogen and Carbon Isotopic Composition of Methane from Natural Gases of Various Origins: Geochim. Cosmochim. Acta, v. 44, pp. 649-661.

Shepherd, F. P., 1963, Submarine Geology: Harper and Rowe, N.Y., 557 pp.

Skippen, G. B., 1967, Experimental Study of the Metamorphism of Silicious Carbonate Rock: Ph.D. Thesis, Johns Hopkins University, Baltimore, Maryland.

Skelland, A. H. P., 1974, Diffusional Mass Transfer: John Wiley and Sons, N.Y., 501 pp.

Smith, M. J. (principal author), 1980, Engineered Barrier Development for a Nuclear Waste Repository in Basalt: An Integration of Current Knowledge: RHO-BWI-ST-7, Rockwell International, Rockwell Hanford Operations, Richland, Washington.

Snyder, R. P., 1982, personal communication-unpublished file: Geologist, U.S. Geological Survey, Denver, Colorado.

Sofer, A., 1978, Isotopic Composition of Hydration Water in Gypsum: Geochim. Cosmochim. Acta, v. 42, pp. 1141-1149.

Sofer, Z. and J. R. Gat, 1975, The Isotope Composition of Evaporating Brines: Effect of the Isotopic Activity Ratio in Saline Solutions: Earth Planet. Sci. Letters, v. 26, pp.179-186.

Thode, H. G., J. Monster, and H. B. Durford, 1961, Sulphur Isotope Geochemistry: Geochim. Cosmochim. Acta, v. 25, pp. 159-174.

U.S. Environmental Protection Agency (U.S. EPA), 1979, Methods for Chemical Analysis of Water and Wastes: EPA-6004-79-020, Office of Research and Development, U.S. Environmental Protection Agency, Cincinnati, Ohio.

Valyashko, M. G., 1956, Geochemistry of Bromine in the Processes of Salt Deposition and the Use of the Bromine Content as a Genetic and Prospecting Criterion: Geochemistry, no. 6, pp. 570-589.

Vine, J. D., 1975, Lithium in Brines, How, Why and Where to Search: Jour. of Res., U.S. Geol. Survey, v. 3, pp. 479-485.

Vine, J. D., 1979, Lithium Investigations in Sedimentary and Volcanic Rocks: U.S. Geol. Survey Prof. Paper 1150, pp. 15-17.

Weast, R. C. (editor), 1971, Handbook of Chemistry and Physics: Chemical Rubber Company, Cleveland, Ohio.

LIST OF REFERENCES
(Continued)

Weres, O., A. Lee, and L. Tsao, 1980, Kinetics of Silica Polymerization: LBL-7033, Earth Sciences Division, Lawrence Berkeley Laboratory, University of California, Berkeley, California, 256 pp.

White, D. E., J. D. Hem, and G. A. Waring, 1963, Chemical Composition of Subsurface Waters: U.S. Geol. Survey Prof. Paper 440-F.

TABLE C.1
TIME AND DISTANCE RELATIONSHIPS FOR A DIFFUSING GAS

Time (years)	Characteristic Distance[a] (km)	Complete Mixing Distance[b] (km)
1,000	0.79	0.10
10,000	2.51 (77,600 yrs)	0.31
100,000	7.94	1.00
1,000,000	25.12	3.16 (4.9 x 10^6 yrs) [c]
10,000,000	79.45	9.99
100,000,000	251.23	31.58

[a] Extent of diffusion calculated from $x = (2Dt)^{1/2}$ where: x = distance
D = diffusion coefficient
t = time

[b] Calculated from $\frac{C_i}{C_o} = 0.90 = \text{erfc}\ [x/2(Dt)^{1/2}]$

where: C_o = initial concentration
C_i = concentration at time = t
(Freeze and Cherry, 1979)

[c] Dashed line shows times appropriate for ERDA-6 and WIPP-12 reservoir separations.

TABLE C.2

CHEMICAL COMPOSITION OF BRINES
SUMMARY OF STATISTICS
ERDA-6, WIPP-12, AND UNION WELLS[1]

SAMPLE TYPE:		FLOW SAMPLE					FLOW SAMPLE					FLOW SAMPLE				
LABORATORY:		D'APPOLONIA					D'APPOLONIA					D'APPOLONIA				
LOCATION:		ERDA-6					WIPP-12					UNION				
FIELD DETERMINATIONS:	UNITS	NO. OF ANALYSES	MINIMUM	MAXIMUM	AVERAGE[2]	CV[3]	NO. OF ANALYSES	MINIMUM	MAXIMUM	AVERAGE[2]	CV[3]	NO. OF ANALYSES	MINIMUM	MAXIMUM	AVERAGE[2]	CV[3]
Temperature	°C	40	21.9[4]	26.7	26.2[5]	0	59	24.2	28.2	26.7	3	--	--	--	--	--
pH	Standard Units	40	6.0	6.3	6.17	0.8	59	6.4	7.20	7.06	2	4	6.95	7.3	7.10	2
Eh	Millivolts	40	-168	-51	-132	8	59	-239	-195	-225	13	4	-259	-184	-233	14
Specific Gravity	--	39	1.214	1.232	1.216	0.2	59	1.210	1.220	1.215	0.2	4	1.210	1.220	1.216	4
Specific Conductance	µmhos/cm @ 25°C	39	351,000	623,000	473,000	5	59	420,000	599,000	566,000	5	4	499,000	542,000	526,000	0.4
Alkalinity[6]	mg/l	20	2245	2950	2600	5	55	2625	3040	2800	3	3	1955	2320	2100	9
Carbonate	mg/l	20	0	0	0	0	55	0	0	0	0	3	0	0	0	0
Hydroxide	mg/l	20	0	0	0	0	55	0	0	0	0	3	0	0	0	0
Chloride	mg/l	20	170,200	210,900	188,800	3	53	171,000	197,800	182,200	4	3	183,200	185,400	183,900	0.7
Sulfate	mg/l	20	15,200	26,400	19,100	9	48	16,200	21,300	18,900	6	3	18,400	20,100	19,300	4
Total Hardness (as $CaCO_3$)	mg/l	25	2235	8730	2660	6	25	5640	6515	6050	4	3	8950	9160	8970	2
Total Iron	mg/l	19	0.03	0.85	0.22	70	12	0.06	0.69	0.27	70	3	0.13	1.5	0.62	120
Hydrogen Sulfide	mg/l	20	172	837	380	30	59	402	1148	990	18	3	544	612	590	6
LABORATORY DETERMINATIONS:																
pH	Standard Units	10	6.29	6.73	6.42	2	13	7.14	7.80	7.49	3	3	7.3	7.34	7.31	0.4
Specific Conductance	µmhos/cm @ 25°C	10	400,000	510,000	490,000	7	13	480,000	810,000	637,000	14	3	500,000	500,000	500,000	0
Total Dissolved Solids	mg/l	10	320,000	340,000	330,000	3	13	310,000	340,000	328,000	2	3	300,000	510,000	390,000	27
Total Suspended Solids	mg/l	10	32	220	87	80	13	8	92	45	65	3	24	96	70	57
Cations																
Barium	mg/l	10	0.10	2.3	0.76	100	13	<0.1	0.90	<0.31	100	3	1.5	2.0	1.7	16
Calcium	mg/l	10	470	520	490	3	13	280	420	350	10	3	330	350	340	3
Cesium	mg/l	5	2.4	2.6	2.5	3	10	1.2	1.9	1.6	14	--	--	--	--	--
Lithium	mg/l	10	210	270	240	8	13	220	330	280	13	3	355	365	360	2
Magnesium	mg/l	10	230	540	450	19	13	1600	1700	1600	3	3	1900	2300	2100	10
Potassium	mg/l	10	2800	4400	3800	12	13	2500	3300	2900	8	3	3500	4600	3900	16
Sodium	mg/l	10	109,000	116,000	112,000	3	13	112,000	180,000	138,000	12	3	109,000	115,000	111,000	3
Strontium	mg/l	10	14	20	18	12	13	10	26	19	23	3	11	12	12	5
Anions:																
Alkalinity[6]	mg/l	10	2600	2700	2600	2	13	2560	2800	2700	3	3	1500	1600	1500	4
Bromide	mg/l	10	750	990	880	9	13	380	600	510	14	3	430	580	480	17
Chloride	mg/l	10	160,000	180,000	170,000	6	13	160,000	220,000	178,000	8	3	160,000	180,000	170,000	6
Fluoride	mg/l	10	1.6	1.9	1.7	6	13	2.9	4.3	3.4	16	3	0.88	1.0	0.92	8
Iodide	mg/l	5	25	32	28	11	5	16	29	24	22	--	--	--	--	--
Sulfate	mg/l	10	14,000	18,000	16,000	7	13	16,000	20,000	18,000	7	3	20,000	24,000	22,000	10
Nutrients:																
Ammonia (as Nitrogen)	mg/l	10	840	920	870	2	13	320	430	370	11	3	300	340	310	7
Nitrate (as Nitrogen)	mg/l	10	570	680	620	15	13	360	1300	550	63	3	370	480	440	14
Phosphate (as Phosphorus)	mg/l	10	0.26	0.49	0.37	19	13	<0.10	0.8	<0.3	100	3	<0.1	<0.1	<0.1	0
Other Elements:																
Aluminum	mg/l	10	0.20	3.9	2.4	53	13	1.4	3.9	2.9	27	3	2.4	3.4	2.9	18
Boron	mg/l	10	570	890	680	15	13	790	1400	990	16	3	1000	1300	1100	16
Copper	mg/l	10	0.19	0.96	0.40	53	13	0.36	0.86	0.62	30	3	<0.1	0.6	0.3	60
Iron	mg/l	10	2.4	6.9	3.6	37	13	1.5	4.5	2.7	26	3	1.2	3.6	2.8	49
Manganese	mg/l	10	5.6	7.8	6.9	11	13	0.16	0.92	0.71	38	3	0.6	1.0	0.8	25
Silica (as SiO_2)	mg/l	5	34	51	45	17	10	61	73	57	23	--	--	--	--	--
Zinc	mg/l	10	0.39	0.64	0.55	20	13	0.27	0.51	0.37	20	3	<0.1	1.4	0.63	130

NOTES:

(1) Analyses performed by D'Appolonia. Samples containing drilling fluid contamination excluded from this table.

(2) Average = Arithmetic Mean.

(3) CV = Coefficient of Variance (%) = $\frac{\text{Standard Deviation}}{\text{Average}} \times 100$.

(4) Downhole temperature averaged 21.9°C during Activity ERDA-6.8 from 10/31/81 to 11/4/81 (measured at 605 feet below the surface).

(5) Downhole temperature averaged 26.7°C during Activity ERDA-6.9 (measured at approximately 2472 feet below the surface).

(6) Values are reported as mg/l HCO_3^-. However, analyses of inorganic carbon average only 340 mg/l HCO_3^- in WIPP-12 and 980 mg/l HCO_3^- in ERDA-6.

"--" = Parameter not analyzed.

TABLE C.3

EVALUATION OF ERDA-6 BRINE FOR MINERAL SATURATION

Phase	Log (Ksp)	Log (IAP) Calculated Activity Product Range Including Error*	Physical Evidence	Evaluation
Anhydrite	-4.39[a]	-4.65 to -4.21	Secondary anhydrite observed	Probably Saturated
Calcite	-8.35[a]	-8.33 to -7.53	Secondary calcite observed, calcite precipitated	Saturated
Dolomite	-17.0[b]	-16.25 to -14.70	Dolomite observed in fractures	Saturated
Glauberite	-5.31[a]	-5.79 to -5.24	None	Possibly Saturated
Halite	1.57[a]	1.28 to 1.42	None	Not Saturated

The samples evaluated were from Flow Tests 2 and 3. The samples from Flow Test 2 were numbers 24, 28, 30, 36, 39, and 48. The samples from Flow Test 3 were numbers 53, 61, 76, and 99. Compositions of the samples are reported in the ERDA-6 and WIPP-12 Data File Report (D'Appolonia, 1982). Mineral activity products were evaluated at near-neutral pH. Generally, the results were not found to be sensitive to pH, and except for the case of dolomite, no determination of saturation/undersaturation was dependent on pH over the range of interest (pH 6.0-7.0). For dolomite the IAP reported is for the average measured pH of ERDA-6 (pH = 6.4). Other phases investigated were antarcticite, arcanite, bischofite, bloedite, carnallite, epsomite, hexahydrite, kainite, kieserite, labile salt, leonhardtite, leonite, mirabilite, pentahydrite, polyhalite, schoenite, sylvite, and thenardite. All of these phases were undersaturated by more than an order of magnitude.

*Includes errors of measurement and one σ errors of calculation.

[a]Harvie and Weare, 1980

[b]Barnes and Back, 1964

TABLE C.4

EVALUATION OF WIPP-12 BRINE FOR MINERAL SATURATION

Phase	Log (Ksp)	Log (IAP) Calculated Activity Product Range Including Error*	Physical Evidence	Evaluation
Anhydrite	-4.39[a]	-4.63 to -4.19	Possible secondary anhydrite observed	Probably Saturated
Calcite	-8.35[a]	-8.48 to -7.66	None	Saturated
Dolomite	-17.0[b]	-15.86 to -14.35	Dolomite observed in fractures	Saturated
Glauberite	-5.31[a]	-5.55 to -5.02	None	Probably Saturated
Halite	1.57[a]	1.41 to 1.59	Salting out	Probably Saturated

The samples evaluated were from Flow Test 1 and Drill Stem Test DST-3020. The samples from Flow Test 1 were numbers 7, 14, DH-1 (D'Appolonia), DH-2 (D'Appolonia), DH-1 (Core Lab.), and DH-2 (Core Lab.). The sample from DST-3020 was number 22. Compositions of the samples are reported in the ERDA-6 and WIPP-12 Data File Report (D'Appolonia, 1982). Mineral activity products were evaluated at near-neutral pH. Generally, the results were not found to be sensitive to pH. No determination of saturation/undersaturation was dependent on pH over the range of calculations. Other phases investigated were antarcticite, arcanite, bischofite, bloedite, carnallite, epsomite, hexahydrite, kainite, kieserite, labile salt, leonhardtite, leonite, mirabilite, pentahydrite, polyhalite, schoenite, sylvite, and thenardite. All of the phases were undersaturated by more than an order of magnitude.

*Includes errors of measurement and one σ errors of calculation.

[a]Harvie and Weare, 1980

[b]Barnes and Back, 1964

TABLE C.5

ISOTOPIC COMPOSITION OF BRINES
SUMMARY OF STATISTICS
ERDA-6 AND WIPP-12[1]

LABORATORY: LOCATION:		GLOBAL GEOCHEMISTRY ERDA-6					GLOBAL GEOCHEMISTRY WIPP-12				
PARAMETER[2]	UNITS	NUMBER OF ANALYSES	MINIMUM	MAXIMUM	AVERAGE[3]	CV[4]	NUMBER OF ANALYSES	MINIMUM	MAXIMUM	AVERAGE[3]	CV[4]
H_2O											
δD	°/oo	19[5]	-8	+1	-5	50	25[7]	-4	+3	-0.8	170
$\delta^{18}O$	°/oo	16[6]	9.02	9.93	9.51	1	23[8]	9.08	11.23	10.45	5
SO_4^{2-}											
$\delta^{34}S$	°/oo	9[9]	8.64	9.79	8.97	5	21[10]	7.43	8.63	8.21	2
CO_3^{2-}											
$\delta^{13}C$	°/oo	10[11]	3.02	5.16	3.96	24	5[12]	-12.35	-3.28	-9.14	38
$\delta^{18}O$	°/oo	--	--	--	--	--	20[13]	10.28	11.09	10.65	2

NOTES:

(1) Analyses performed by Global Geochemistry Corporation, Canoga Park, California. Contaminated samples excluded.

(2) $\delta x = \left[\frac{R_{Sample}}{R_{Standard}} - 1\right] \times 10^3$

$x = D$, $R = D/H$, Standard = SMOW.

$x = {}^{18}O$, $R = {}^{18}O/{}^{16}O$, Standard = SMOW.

$x = {}^{34}S$, $R = {}^{34}S/{}^{32}S$, Standard = Canon Diablo Triolite (CDT).

$x = {}^{13}C$, $R = {}^{13}C/{}^{12}C$, Standard = Belemnite from Peedee Formation in South Carolina (PDB).

(3) Average = Arithmetic Mean.

(4) CV = Coefficient of Variance (%) = $\frac{\text{Standard Deviation}}{\text{Average}} \times 100$.

(5) Analyses of eight split samples and three duplicates of three of the split samples were performed.

(6) Analyses of eight split samples were performed.

(7) Analyses of eleven split samples and three duplicates of three of the split samples were performed.

(8) Analyses of nine split samples, two individual samples, and three duplicates of three of the split samples were performed.

(9) Analyses of one split sample and seven individual samples were performed.

(10) Analyses of ten split samples and one individual sample were performed.

(11) Analyses of one split sample and eight individual samples were performed.

(12) Analyses of five individual samples were performed.

(13) Analyses of ten split samples were performed. Values reflect analytical technique of bubbling through water (that is, values = $\delta^{18}O$ of water).

"-" = Analyses not performed because the results would reflect the analytical technique of bubbling through water (that is, values = $\delta^{18}O$ of water).

TABLE C.6

ISOTOPIC COMPOSITION OF SELECTED MINERALS
SUMMARY OF STATISTICS
ERDA-6 AND WIPP-12[1]

LABORATORY: LOCATION:		GLOBAL GEOCHEMISTRY ERDA-6					GLOBAL GEOCHEMISTRY WIPP-12				
PARAMETER[2]	UNITS	NUMBER OF ANALYSES	MINIMUM	MAXIMUM	AVERAGE[3]	CV[4]	NUMBER OF ANALYSES	MINIMUM	MAXIMUM	AVERAGE[3]	CV[4]
Anhydrite, SO_4^{2-}											
$\delta^{34}S$	°/oo	4[5]	11.38	11.67	11.52	1	12[6]	11.15	12.47	11.63	3
Calcite, CO_3^{2-}											
$\delta^{13}C$	°/oo	5[7]	6.03	6.74	6.41	5	4[8]	6.40	6.87	6.70	3
$\delta^{18}O$	°/oo	5[7]	32.91	34.17	33.76	2	4[8]	31.71	32.99	32.38	3
Dolomite, CO_3^{2-}											
$\delta^{13}C$	°/oo	--	--	--	--	--	2[9]	-2.02	5.36	1.67	310
$\delta^{18}O$	°/oo	--	--	--	--	--	2[9]	36.39	37.36	36.88	2

NOTES:

(1) Analyses performed by Global Geochemistry Corporation, Canoga Park, California.

(2) $\delta x = \left[\frac{R_{Sample}}{R_{Standard}} - 1\right] \times 10^3$.

$x = {}^{18}O$, $R = {}^{18}O/{}^{16}O$, Standard = SMOW.

$x = {}^{34}S$, $R = {}^{34}S/{}^{32}S$, Standard = Canon Diablo Triolite (CDT).

$x = {}^{13}C$, $R = {}^{13}C/{}^{12}C$, Standard = Belemnite From Peedee Formation in South Carolina (PDB).

(3) Average = Arithmetic Mean.

(4) CV = Coefficient of Variance (%) = $\frac{\text{Standard Deviation}}{\text{Average}} \times 100$.

(5) Analyses of four individual samples collected from 2600 to 2612 feet were performed.

(6) Analyses of ten individual samples and 1 split sample were performed. Samples were collected from 2803 to 3904 feet.

(7) Analyses of three individual samples and one split sample were performed. (Samples were same as in Footnote 5.)

(8) Analyses of two split samples collected from 3324 and 3904 feet were analyzed.

(9) Analyses of two individual samples collected from 2945 and 3017 feet were analyzed.

"--" = Parameter not analyzed.

TABLE C.7a
GAS COMPOSITION (MOLE%)
SUMMARY OF STATISTICS
ERDA-6

PARAMETERS / SAMPLE TYPE:	FLOW SAMPLES									
LABORATORY: / LOCATION:	THURMOND/McGLOTHLIN ERDA-6					GLOBAL GEOCHEMISTRY[1] ERDA-6				
	NO. OF ANALYSES	MINIMUM	MAXIMUM	AVERAGE[2]	CV[3]	NO. OF ANALYSES	MINIMUM	MAXIMUM	AVERAGE[2]	CV[3]
FIELD ANALYSES:										
Hydrogen Sulfide	3	21.41	27.86	24.44	13	--	--	--	--	--
Gas/Liquid Ratio (V/V)[4]	3	0.35	0.54	0.44	30	--	--	--	--	--
LABORATORY ANALYSES:										
Gas Components:										
Hydrogen Sulfide	--	--	--	--	--	3	25.9	31.7	28.4	10
Nitrogen	10	2.33	19.28	11.30	48	3	3.6	17.0	12.5	57
Carbon Dioxide	10	19.88	25.18	23.62	6	3	36.9	46.8	41.5	12
Methane	10	10.96	21.54	15.72	22	3	10.3	15.0	12.1	21
Ethane	10	0.25	0.75	0.51	29	2	0.39	0.39	0.39	0
Propane	10	0.06	0.20	0.14	27	2	0.10	0.10	0.10	0
Iso-Butane	10	0.00	0.02	0.01	86	2	0.00	0.005	0.002	140
N-Butane	10	0.00	0.02	0.01	47	2	0.00	0.012	0.006	140
Iso-Pentane	10	0.00	0.02	0.01	140	--	--	--	--	--
N-Pentane	10	0.00	0.11	0.02	160	--	--	--	--	--
Hexanes[5]	10	0.00	4.21	0.63	200	--	--	--	--	--
Oxygen	--	--	--	--	--	--	--	--	--	--
Argon	--	--	--	--	--	--	--	--	--	--
Unknown	10	32.25	58.04	48.05	17	--	--	--	--	--

NOTES:

[1] Minimum and maximum values based on all analyses. However, mean value calculated excluding air contaminated samples.

[2] Average = Arithmetic Mean.

[3] CV = Coefficient of Variance (%) = $\frac{\text{Standard Deviation}}{\text{Average}} \times 100$.

[4] Volume of gas to volume of brine. Gas volume corrected to standard temperature and pressure.

[5] Includes hexane and higher molecular weight hydrocarbons.

"--" = Parameter not analyzed.

TABLE C.7b
GAS COMPOSITION (MOLE%)
SUMMARY OF STATISTICS
ERDA-6[1]

PARAMETERS								
SAMPLE TYPE:	DOWNHOLE SAMPLES							
LABORATORY:	CORE LABORATORY				GLOBAL GEOCHEMISTRY			
LOCATION:	ERDA-6				ERDA-6			
	NO. OF ANALYSES	MINIMUM	MAXIMUM	AVERAGE[2,4]	NO. OF ANALYSES	MINIMUM	MAXIMUM	AVERAGE[3,4]
LABORATORY ANALYSES:								
Gas/Liquid Ratio (V/V)[5]	4	1.92	2.96	1.92	--	--	--	--
Gas Components:								
Hydrogen Sulfide	4	23.06	44.74	44.74	4	0.96	23.7	23.7
Nitrogen	4	0.91	43.52	0.91	4	40.4	68.9	40.4
Carbon Dioxide	4	26.68	46.16	46.16	4	Present	27.1	27.1
Methane	4	7.30	8.34	7.89	4	0.26	6.4	6.4
Ethane	4	0.28	0.34	0.30	4	0.012	0.21	0.21
Propane	4	0.00	0.02	0.00	4	0.003	0.05	0.05
Iso-Butane	4	0.00	0.00	0.00	4	0.00	0.00	0.00
N-Butane	4	0.00	0.00	0.00	4	0.001	0.01	0.01
Iso-Pentane	4	0.00	0.00	0.00	--	--	--	--
N-Pentane	4	0.00	0.00	0.00	--	--	--	--
Hexanes[6]	4	0.00	0.00	0.00	--	--	--	--
Oxygen	--	--	--	--	4	10.9	20.5	10.9
Argon	--	--	--	--	4	Present[7]	Present[7]	Present[7]
Unknown	--	--	--	--	--	--	--	--

NOTES:

[1] Minimum and maximum values based on all analyses. However, mean value calculated excluding air contaminated samples.

[2] Only one sample analysis reported (DH-2). Air contamination suspected in remaining three samples.

[3] All samples show air contamination. Only one sample analysis reported (DH-4). This sample contained the smallest quantity of oxygen and nitrogen.

[4] Average = Arithmetic Mean.

[5] Volume of gas to volume of brine. Gas volume corrected to standard temperature and pressure.

[6] Includes hexane and higher molecular weight hydrocarbons.

[7] Argon peak present, but could not be quantified.

"--" = Parameter not analyzed.

TABLE C.8a
GAS COMPOSITION (MOLE%)
SUMMARY OF STATISTICS
WIPP-12

PARAMETERS																				
SAMPLE TYPE	FLOW SAMPLES																			
LABORATORY	THURMOND/McGLOTHLIN[1]					GLOBAL GEOCHEMISTRY					CORE LABORATORY					MORCO[2]				
LOCATION:	WIPP-12					WIPP-12					WIPP-12					WIPP-12				
ACTIVITY	FLOW TEST 1					FLOW TEST 3					FLOW TEST 3					FLOW TEST 3				
DESCRIPTION:	NO. OF ANALYSES	MINIMUM	MAXIMUM	AVERAGE[3]	CV[4]	NO. OF ANALYSES	MINIMUM	MAXIMUM	AVERAGE[3]	CV[4]	NO. OF ANALYSES	MINIMUM	MAXIMUM	AVERAGE[3]	CV[4]	NO. OF ANALYSES	MINIMUM	MAXIMUM	AVERAGE[3]	CV[4]
FIELD ANALYSES:																				
Hydrogen Sulfide	3	2.78	6.53	4.91	49	--	--	--	--	--	--	--	--	--	--	50	9.88	17.72	13.40	14
Gas/Liquid Ratio (V/V)[5]	14	0.11	0.24	0.15	20	--	--	--	--	--	--	--	--	--	--	8	1.30	3.82	1.84	35
LABORATORY ANALYSES:																				
Gas Components:																				
Hydrogen Sulfide	--	--	--	--		7	24.1	27.5	25.2	5	5	17.91	19.00	18.60	3	--	--	--	--	--
Nitrogen	6	10.01	33.00	14.10	31	7	8.4	8.8	8.6	2	5	9.25	9.87	9.46	3	571	10	15	12	17
Carbon Dioxide	6	0.07	2.98	1.58	86	7	0.00	0.00	0.00	0	5	0.00	0.10	0.06	60	416	0.10	0.28	0.18	31
Methane	6	59.71	78.32	66.69	15	7	59.4	62.6	61.2	2	5	65.82	66.72	66.13	0.6	416	56	60	58	3
Ethane	6	4.43	5.85	5.24	14	7	4.6	5.6	5.0	7	5	4.79	4.93	4.89	1	416	4.7	5.6	5.1	6
Propane	6	0.75	0.98	0.87	12	7	0.00	0.00	0.00	0	5	0.77	0.93	0.87	6	--	--	--	--	--
Iso-Butane	6	0.03	1.09	0.04	16	--	--	--	--	--	5	Trace	Trace	Trace	--	--	--	--	--	--
N-Butane	6	0.00	0.14	0.11	20	--	--	--	--	--	5	Trace	Trace	Trace	--	--	--	--	--	--
Iso-Pentane	6	0.00	0.08	0.04	71	--	--	--	--	--	5	0.00	0.00	0.00	0	--	--	--	--	--
N-Pentane	6	0.00	0.43	0.15	140	--	--	--	--	--	5	0.00	0.00	0.00	0	--	--	--	--	--
Hexanes[6]	6	0.42	2.13	0.82	35	--	--	--	--	--	5	0.00	0.00	0.00	0	--	--	--	--	--
Oxygen	--	--	--	--	--	7	0.00	0.00	0.00	0	0	--	--	--	--	--	--	--	--	--
Argon	--	--	--	--	--	7	0.00	0.00	0.00	0	0	--	--	--	--	--	--	--	--	--
Unknown	6	0.00	12.27	6.04	71	--	--	--	--	--	0	--	--	--	--	--	--	--	--	--

NOTES

[1] Air contamination from separator suspected in some samples analyzed by Thurmond-McGlothlin, Inc. Midland, Texas. Duplicate analyses also perform by Bell Petroleum Laboratories and Core Laboratories (see D'Appolonia, 1982).

[2] The hydrogen sulfide analyses and gas/liquid ratio determinations were performed by D'Appolonia. Nitrogen, carbon dioxide, methane and ethane values were measured in the field by Morco Inc., Carlsbad, New Mexico.

[3] Average = Arithmetic Mean. Samples that have been contaminated by air were not included in the average.

[4] CV = Coefficient of Variance (%) = $\frac{\text{Standard Deviation}}{\text{Average}} \times 100$.

[5] Volume of gas to volume of brine. Gas volume corrected to standard temperature and pressure.

[6] Includes hexane and higher molecular weight hydrocarbons.

"--" = Parameter not analyzed.

TABLE C.8b
GAS COMPOSITION (MOLE%)
SUMMARY OF STATISTICS
WIPP-12[1]

PARAMETERS										
SAMPLE TYPE:	DOWNHOLE SAMPLES									
LABORATORY:	CORE LABORATORY					GLOBAL GEOCHEMISTRY				
LOCATION:	WIPP-12					WIPP-12				
	NO. OF ANALYSES	MINIMUM	MAXIMUM	AVERAGE[2]	CV[3]	NO. OF ANALYSES	MINIMUM	MAXIMUM	AVERAGE[2]	CV[3]
LABORATORY ANALYSES:										
Gas/Liquid Ratio (V/V)[4]	2	0.511	0.559	0.535	6	--	--	--	--	--
Gas Components:										
Hydrogen Sulfide	2	13.61	27.57	20.59	48	2	7.5	28.2	17.9	82
Nitrogen	2	45.97	59.30	57.64	29	2	49.8	54.4	52.1	6
Carbon Dioxide	2	0.20	0.61	0.41	72	2	Trace	0.48	0.24	140
Methane	2	15.49	23.4	19.45	29	2	5.7	6.4	6.1	8
Ethane	2	0.99	1.46	1.23	27	2	0.17	0.60	0.39	79
Propane	2	0.00	0.26	0.13	140	2	0.015	0.06	0.04	85
Iso-Butane	2	0.00	0.00	0.00	0	2	0.00	0.00	0.00	0
N-Butane	2	0.00	0.00	0.00	0	2	0.001	0.015	0.01	120
Iso-Pentane	2	0.00	0.00	0.00	0	2	0.00	0.00	0.00	0
N-Pentane	2	0.00	0.00	0.00	0	2	0.00	0.00	0.00	0
Hexanes[5]	2	0.00	0.00	0.00	0	2	0.00	0.00	0.00	0
Oxygen	--	--	--	--	--	2	13.4	18.1	15.8	21
Argon	--	--	--	--	--	2	Present[6]	Present[6]	Present[6]	--

NOTES:

(1) All samples have reacted with and been contaminated by air to some degree.

(2) Average = Arithmetic Mean.

(3) CV = Coefficient of Variance (%) = $\frac{\text{Standard Deviation}}{\text{Average}} \times 100$.

(4) Volume of gas to volume of brine. Gas volume corrected to standard temperature and pressure.

(5) Includes hexane and higher molecular weight hydrocarbons.

(6) Argon peak present, but could not be quantified.

"--" = Parameter not analyzed.

TABLE C.9

ISOTOPIC COMPOSITION OF GASES
SUMMARY OF STATISTICS
ERDA-6 AND WIPP-12[1]

LABORATORY: LOCATION:		GLOBAL GEOCHEMISTRY ERDA-6					GLOBAL GEOCHEMISTRY WIPP-12				
PARAMETER[2]	UNITS	NUMBER OF ANALYSES	MINIMUM	MAXIMUM	AVERAGE[3]	CV[4]	NUMBER OF ANALYSES	MINIMUM	MAXIMUM	AVERAGE[3]	CV[4]
H_2S											
δD	°/oo	11[5]	-621	-461	-570	9	16[6]	-564	-522	-544	2
$\delta^{34}S$	°/oo	14[7]	-22.12	-19.63	-20.46	3	19[8]	-15.13	-13.94	-14.36	2
CH_4											
δD	°/oo	3[9]	-321	-229	-264	19	16[6]	-228	-217	-223	1
$\delta^{13}C$	°/oo	9[10]	-65.82	-59.88	-61.96	4	16[6]	-48.86	-48.42	-48.65	0.2
CO_2											
$\delta^{13}C$	°/oo	14[11]	-11.61	-3.14	-4.67	41	--	--	--	--	--
$\delta^{18}O$	°/oo	14[11]	49.02	52.93	51.60	2	--	--	--	--	--

NOTES:

[1] Analyses performed by Global Geochemistry Corporation, Canoga Park, California. Values exclude air-contaminated samples.

[2] $\delta x = \left[\frac{R_{Sample}}{R_{Standard}} - 1\right] \times 10^3$.

x = D, R = D/H, Standard = SMOW.

x = ^{18}O, R = $^{18}O/^{16}O$, Standard = SMOW.

x = ^{34}S, R = $^{34}S/^{32}S$, Standard = Canon Diablo Triolite (CDT).

x = ^{13}C, R = $^{13}C/^{12}C$, Standard = Belemnite From Peedee Formation in South Carolina (PDB).

[3] Average = Arithmetic Mean.

[4] CV = Coefficient of Variance (%) = $\frac{\text{Standard Deviation}}{\text{Average}} \times 100$.

[5] Analyses of five split samples and one individual sample were performed.

[6] Analyses of six split samples and four individual samples were performed (flow samples only).

[7] Analyses of seven split samples were performed.

[8] Analyses of six split samples, four individual samples, and three duplicates of one individual and two of the split samples were performed.

[9] Analyses of three individual samples were performed.

[10] Analyses of four split samples and one individual sample were performed.

[11] Analyses of six split samples and two individual samples were performed.

"--" = Parameter not analyzed; no carbon dioxide detected in WIPP-12 gases.

TABLE C.10

IONIC RATIOS IN SEAWATER AND BRINE
(wt/wt Basis)

SEAWATER OR BRINE	RATIO Li/Br	Na/Br	K/Br	Mg/Br	Ca/Br	Cl/Br	TDS/Br
Seawater	0.003	169	5.4	20	6.2	292	494
Seawater at beginning of gypsum/anhydrite precipitation	0.003	163	6.0	22	2.8	297	492
Seawater at beginning of halite precipitation	0.003	35	5.8	19	0.03	69	129
Seawater at beginning of magnesium sulfate precipitation	0.003	16	8.6	19	0.002	64	109
Seawater at beginning of sylvite precipitation	0.003	1.5	3.0	15	0.0	42	63
ERDA-6 (average)	0.28	144	5.1	0.5	0.57	207	375
WIPP-12 (average)	0.55	276	6.0	3.2	0.73	360	744

Reference: Collins, 1975, Table 7. III

TABLE C.11

MINERALOGICAL COMPOSITION OF SELECTED ROCK SAMPLES
FROM ERDA-6 AND WIPP-12[1]

SAMPLE DEPTH (FT.)	WELL	DESCRIPTION OF LOCATION	Bulk[2]							<5 μ [3]			
			Calcite ($CaCO_3$)	Dolomite ($CaMg(CO_3)_2$)	Anhydrite ($CaSO_4$)	Hemihydrate ($CaSO_4 \cdot {}^1/_2H_2O$)	Halite (NaCl)	Quartz (SiO_2)	Total Clay	Illite	Chlorite	Smectite	Non-expandable Mixed-layer
2851.5-2851.75	WIPP-12	Anhydrite III	--	--	99	tr	--	tr	--	--	--	--	--
2943.3-2943.4	WIPP-12	Anhydrite III, some clays	--	--	99	tr	--	--	tr	100	--	--	--
3016.7-3016.9	WIPP-12	Fracture in Anhydrite III containing brine	--	tr	98	tr	--	tr	--	--	--	--	--
3061.4-3061.6	WIPP-12	Contact Anhydrite III/Halite II	tr	tr	66	tr	33	--	--	--	--	--	--
3120.5-3120.7	WIPP-12	Anhydrite stringer in Halite II	tr	--	98	tr	--	--	tr	--	--	--	100
3276.6-3277.0	WIPP-12	Contact Halite II/Anhydrite II	--	tr	78	tr	21	--	--	--	--	--	--
3325.0-3325.2	WIPP-12	Anhydrite II with laminae	3	tr	96	tr	--	--	tr	57	--	--	43
3384.2-3384.8	WIPP-12	Vugs in Anhydrite II near Halite I contact	9	--	90	tr	--	--	--	--	--	--	--
3385.4-3385.8	WIPP-12	Contact Anhydrite II/Halite I	tr	tr	65	tr	34	--	--	--	--	--	--
3385.4-3385.8	WIPP-12	Anhydrite II near Halite I contact	--	tr	99	tr	--	--	--	--	--	--	--
3893.3-3893.5	WIPP-12	Anhydrite I at contact with Halite I	--	--	100	tr	--	--	--	--	--	--	--
3904.7-3904.9	WIPP-12	Point where Anhydrite I becomes bedded	1	--	98	tr	--	--	tr	--	46	--	54
2611.9-2612.0	ERDA-6	Recrystallized core break in Anhydrite II	2	--	97	tr	--	--	tr	34	30	36	--

NOTES:

[1] Analyses performed by Reservoirs, Inc., Denver, Colorado using a Scintag Pad II Automated Diffractometer with 1000 Series Hi-Purity Germanium Low Energy Photon Detector. Bulk samples were analyzed from 2 to 60 degrees two theta at steps of 0.03 degrees counting 0.5 seconds at each step. Clay samples were analyzed from 2 to 27 degrees two theta. For greater resolution selected samples were analyzed at steps of 0.01 degrees counting 6 to 9 seconds each step for a total scan time of 20 hours. Accuracy using this method is estimated at ± 5 percent and precision at ± 3 percent.

[2] Values expressed as weight percent. "tr" = less than 1 percent.

[3] Values expressed as weight percent of material less than 5 microns in size (clay fraction). The total amount of materials clay sized particles is less than one percent.

"--" = Not present.

TABLE C.12

CORRESPONDENCE BETWEEN CHEMICAL DATA AND HYPOTHETICAL ORIGINS FOR BRINE

Origin	Major/Minor Element Chemistry	Water Isotopes	Other Isotopes	Trace Elements Chemistry	Physical Evidence
1. Meteoric Water	No	No	No	No	Yes
2. Waters of Dehydration	No	Maybe	Maybe	No	Maybe
3. Ancient Seawater	Yes	Yes	Yes	Yes	Yes
4. Mixture of Current Meteoric Water and Seawater	No	Maybe	No	Yes	Yes
5. Mixture of Ancient Low-TDS Meteoric Water and Seawater	Yes	Yes	Yes	Yes	Yes
6. Mixtures of Dehydration Waters and Seawater	Yes	Yes	Yes	Yes	Maybe

"No" indicates data do not support hypothesis.
"Yes" indicates data do support hypothesis.
"Maybe" indicates data may or may not support hypothesis.

TME 3153

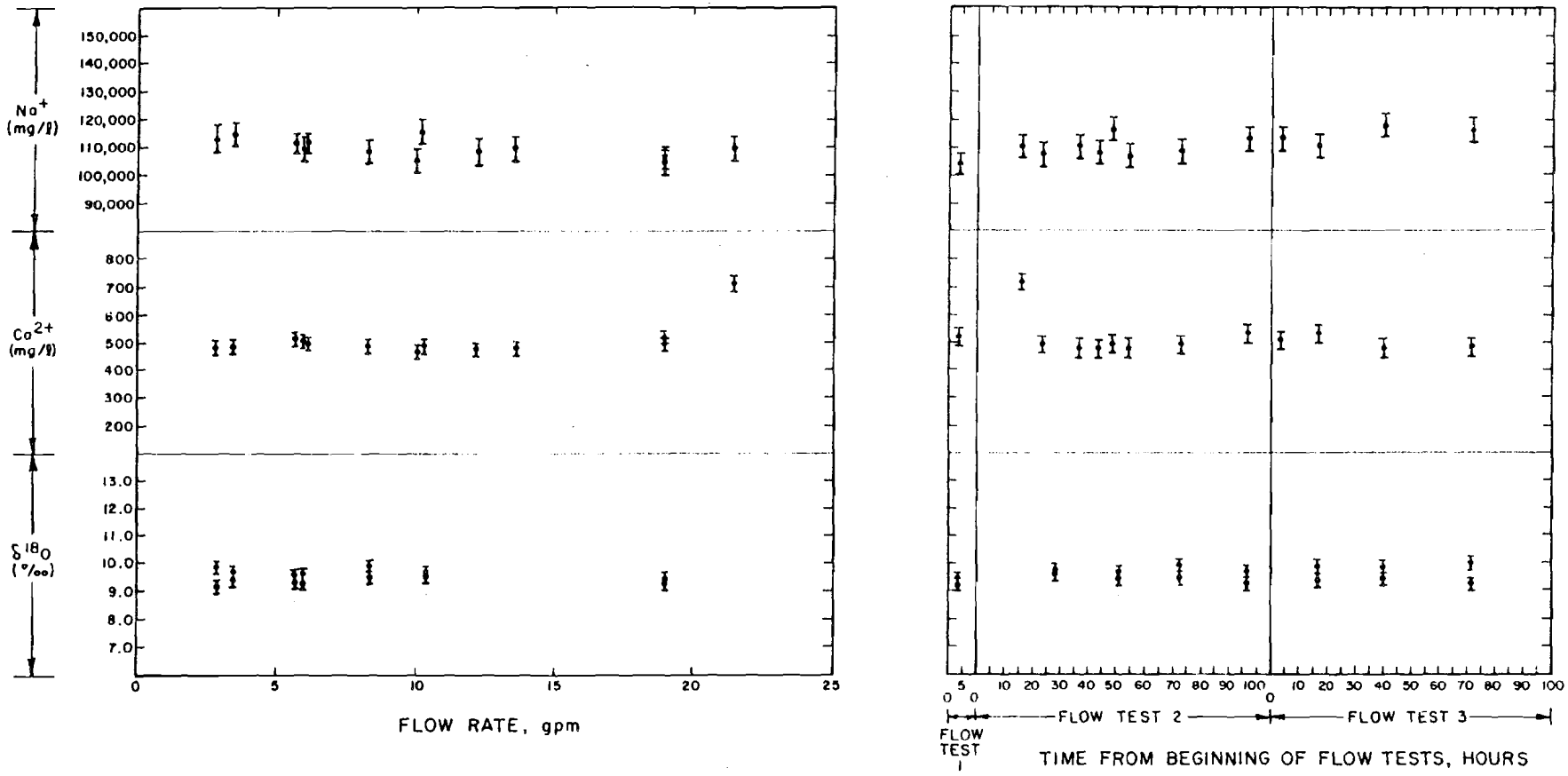

LEGEND:

ERROR BARS[1] —MEASURED VALUE

[1] ERROR BARS REFLECT PERCENT RELATIVE ERROR AS DETERMINED BY D'APPOLONIA'S ANALYSES OF SOLUTIONS WITH KNOWN CONCENTRATIONS.

FIGURE C-1a

CONCENTRATION OF SELECTED PARAMETERS VERSUS FLOW RATE AND FLOW TIME ERDA-6

PREPARED FOR

WESTINGHOUSE ELECTRIC CORPORATION
ALBUQUERQUE, NEW MEXICO

D'APPOLONIA

DRAWN BY BKH 12-8-82
CHECKED BY RLO 12/12/82
APPROVED BY DKS 12/16/82
DRAWING NUMBER NM78-648-832

TME 3153

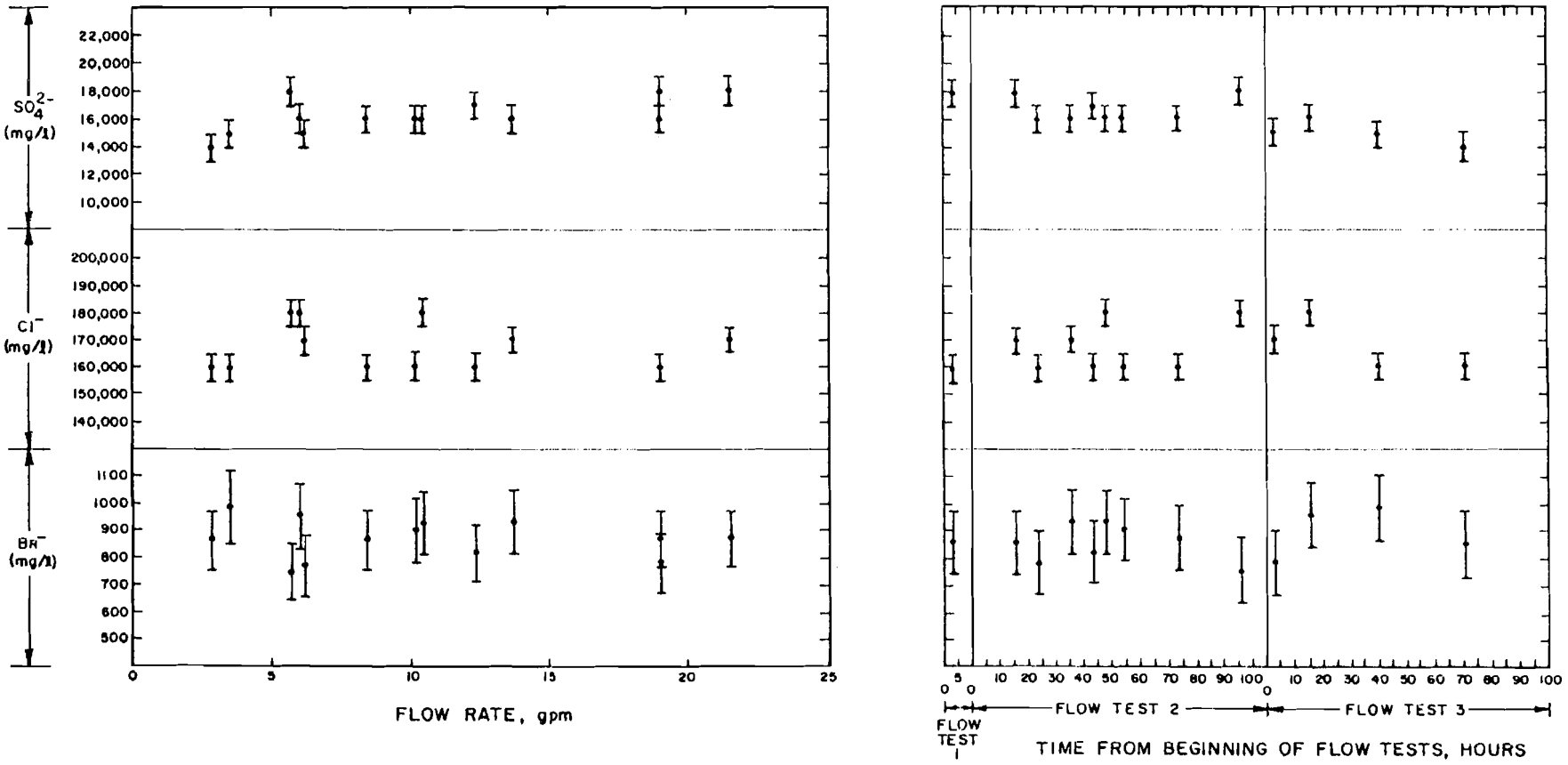

LEGEND:

ERROR BARS[1] {I—MEASURED VALUE

[1] ERROR BARS REFLECT PERCENT RELATIVE ERROR AS DETERMINED BY D'APPOLONIA'S ANALYSES OF SOLUTIONS WITH KNOWN CONCENTRATIONS.

FIGURE C-1b
CONCENTRATION OF SELECTED PARAMETERS VERSUS FLOW RATE AND FLOW TIME
ERDA-6

PREPARED FOR

WESTINGHOUSE ELECTRIC CORPORATION
ALBUQUERQUE, NEW MEXICO

D'APPOLONIA

TME 3153

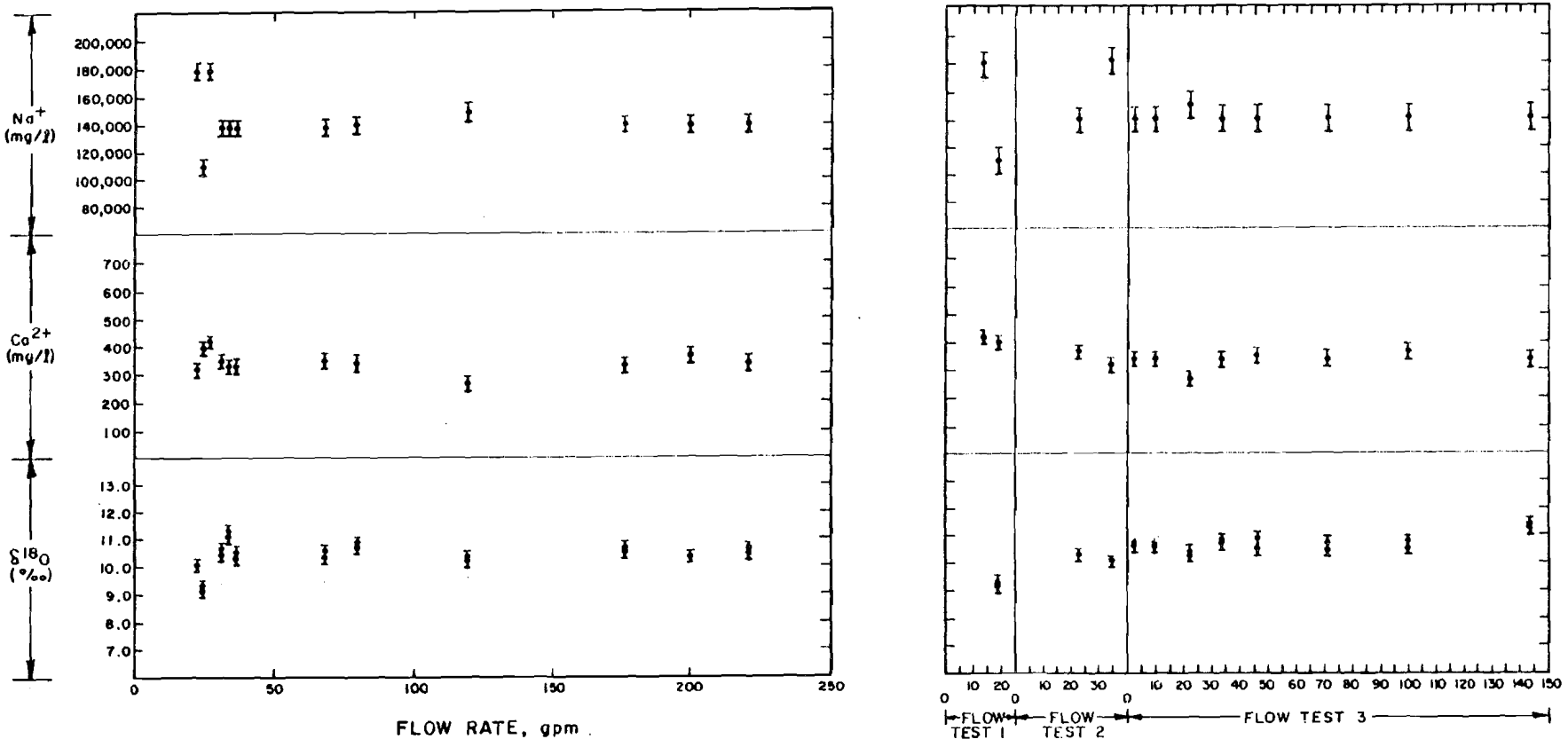

LEGEND:

ERROR BARS[1] {I—MEASURED VALUE

[1] ERROR BARS REFLECT PERCENT RELATIVE ERROR AS DETERMINED BY D'APPOLONIA'S ANALYSES OF SOLUTIONS WITH KNOWN CONCENTRATIONS.

FIGURE C-1c
CONCENTRATION OF SELECTED PARAMETERS VERSUS FLOW RATE AND FLOW TIME
WIPP-12

PREPARED FOR

WESTINGHOUSE ELECTRIC CORPORATION
ALBUQUERQUE, NEW MEXICO

D'APPOLONIA

TNE 3153

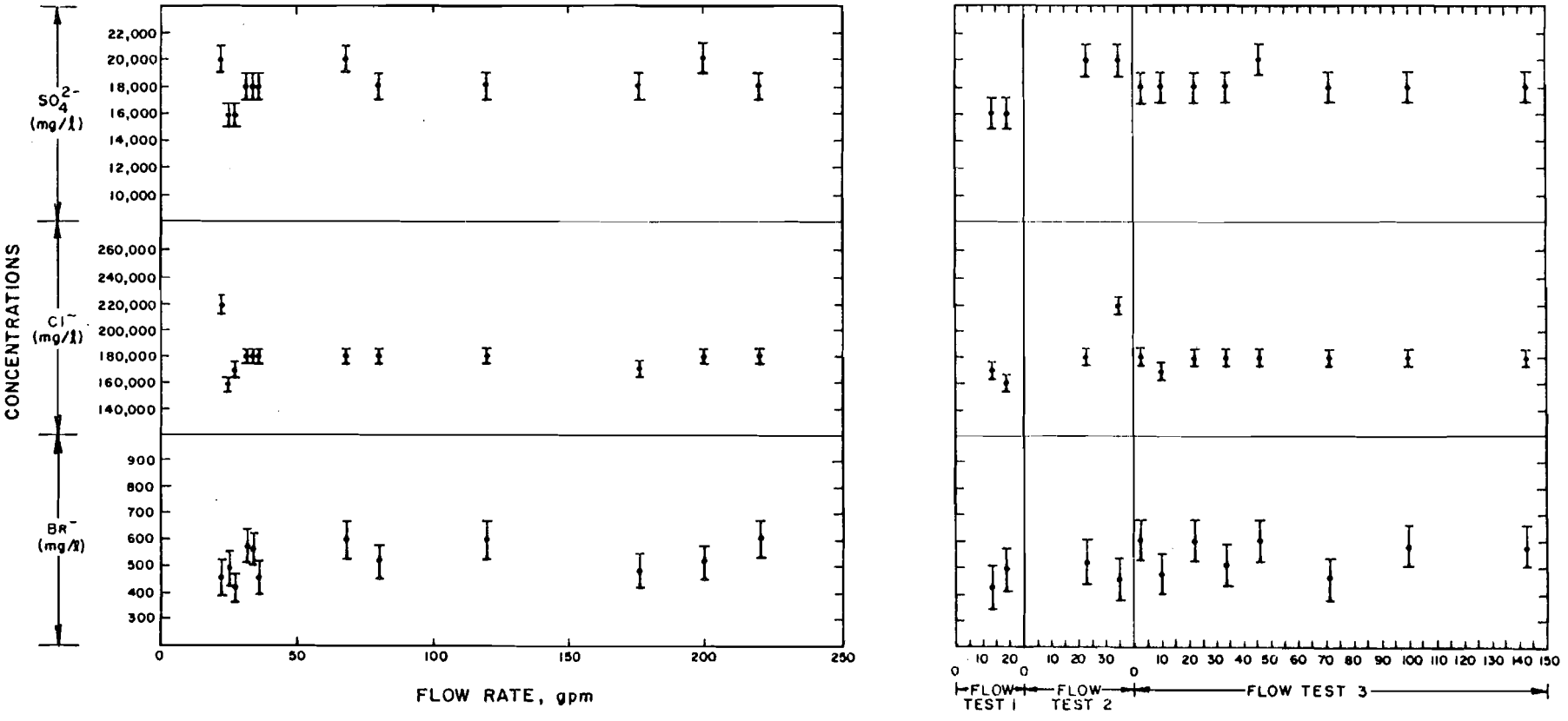

LEGEND:

ERROR BARS[1] —MEASURED VALUE

[1] ERROR BARS REFLECT PERCENT RELATIVE ERROR AS DETERMINED BY D'APPOLONIA'S ANALYSES OF SOLUTIONS WITH KNOWN CONCENTRATIONS.

FIGURE C-1d
CONCENTRATION OF SELECTED PARAMETERS VERSUS FLOW RATE AND FLOW TIME
WIPP-12

PREPARED FOR

WESTINGHOUSE ELECTRIC CORPORATION
ALBUQUERQUE, NEW MEXICO

D'APPOLONIA

TME 3153

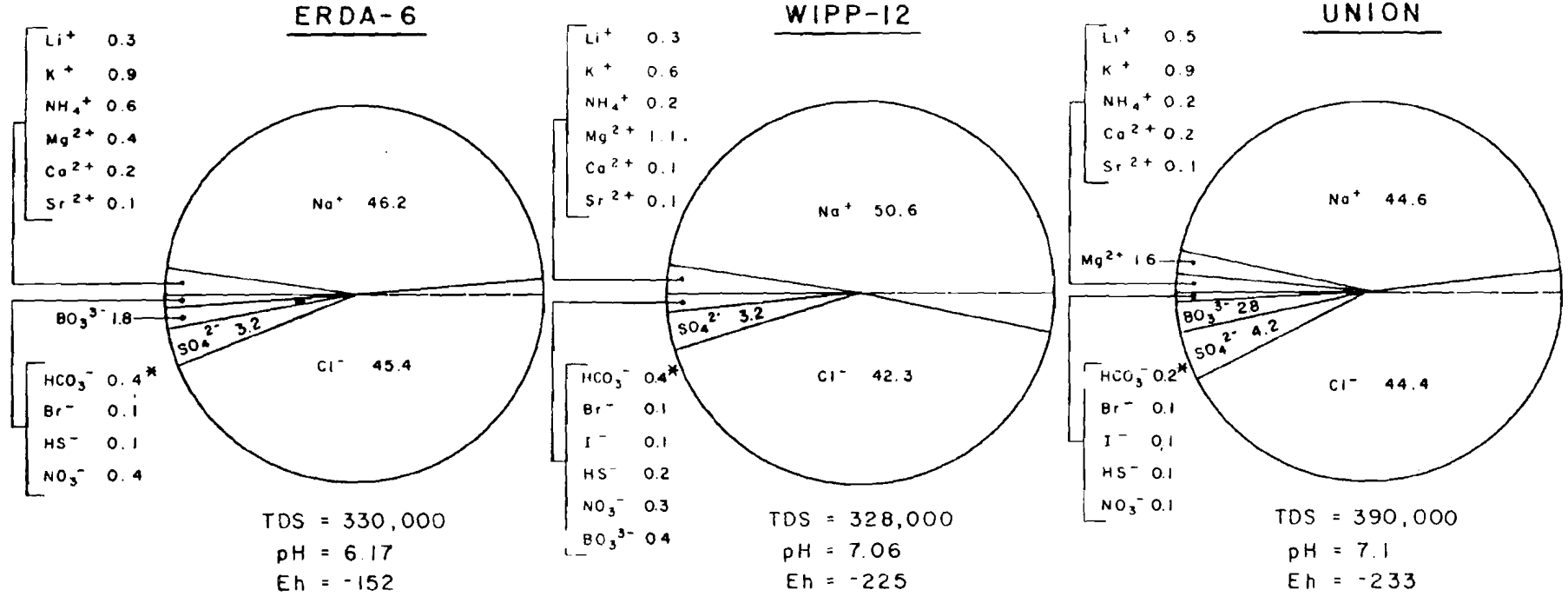

* THESE VALUES ARE EQUAL TO THE ALKALINITY EXPRESSED AS BICARBONATE.

NOTE:
VALUES EXPRESSED IN TERMS OF RELATIVE PERCENT MILLIEQUIVALENTS.

LEGEND

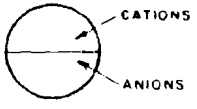

TDS = TOTAL DISSOLVED SOLIDS, MG/L
pH, STANDARD UNITS
Eh, MILLIVOLTS

FIGURE C-2

MEAN COMPOSITION OF BRINES
MAJOR CATIONS AND ANIONS

PREPARED FOR

WESTINGHOUSE ELECTRIC CORPORATION
ALBUQUERQUE, NEW MEXICO

DRAWN BY	EF	CHECKED BY	RLO	DRAWING NUMBER	NM78-648-A109
	9/22/82	APPROVED BY	DKS/OMW		5/10/83

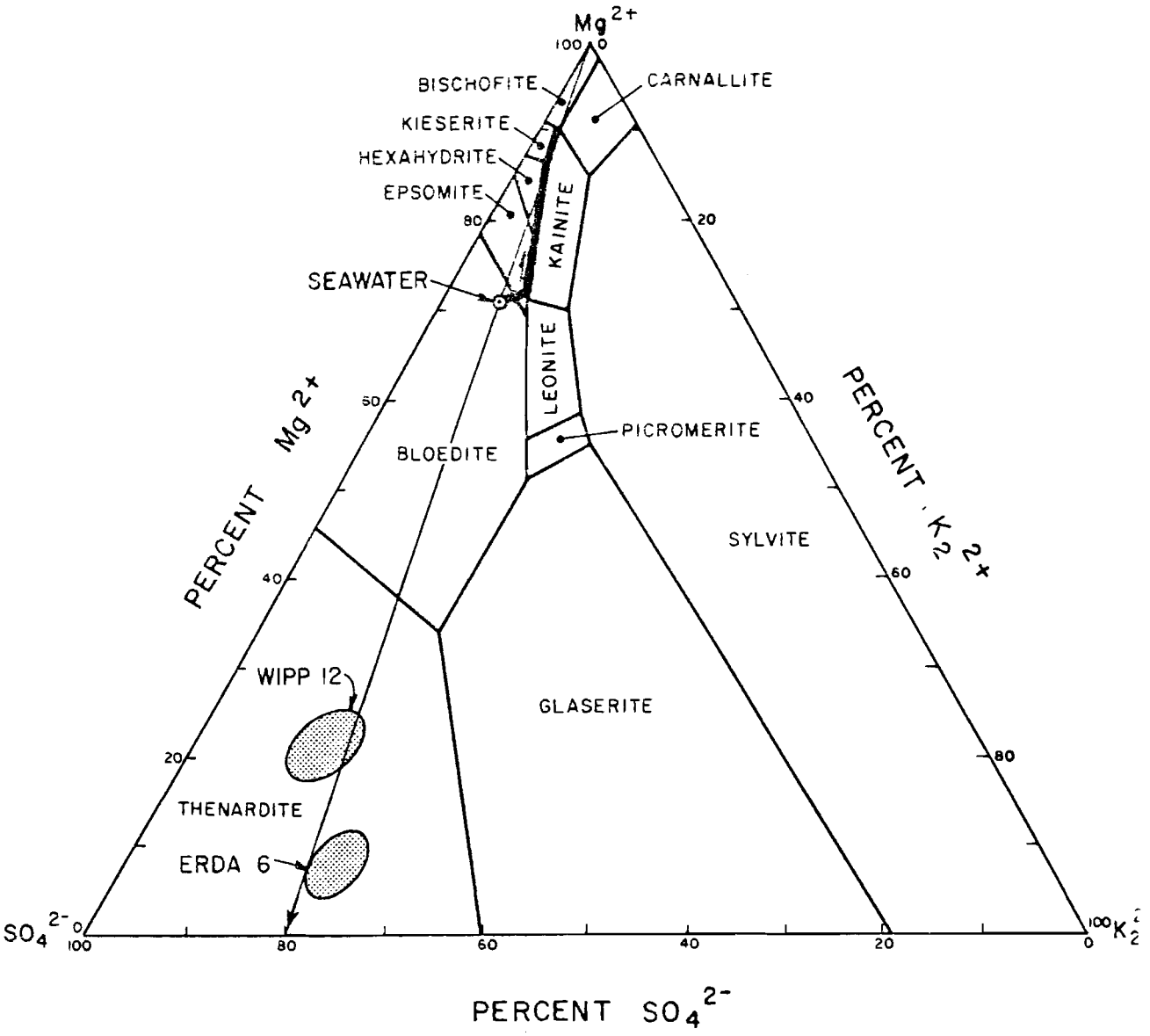

FIGURE C-3

JANECKE DIAGRAM
SHOWING BRINES AND SEAWATER

PREPARED FOR

WESTINGHOUSE ELECTRIC CORPORATIO
ALBUQUERQUE, NEW MEXICO

DRAWN BY	EB 9/10/82	CHECKED BY	RLD 3/11/83	DRAWING NUMBER	NM78-648-A92
		APPROVED BY	DKS/OPW 3/10/83		

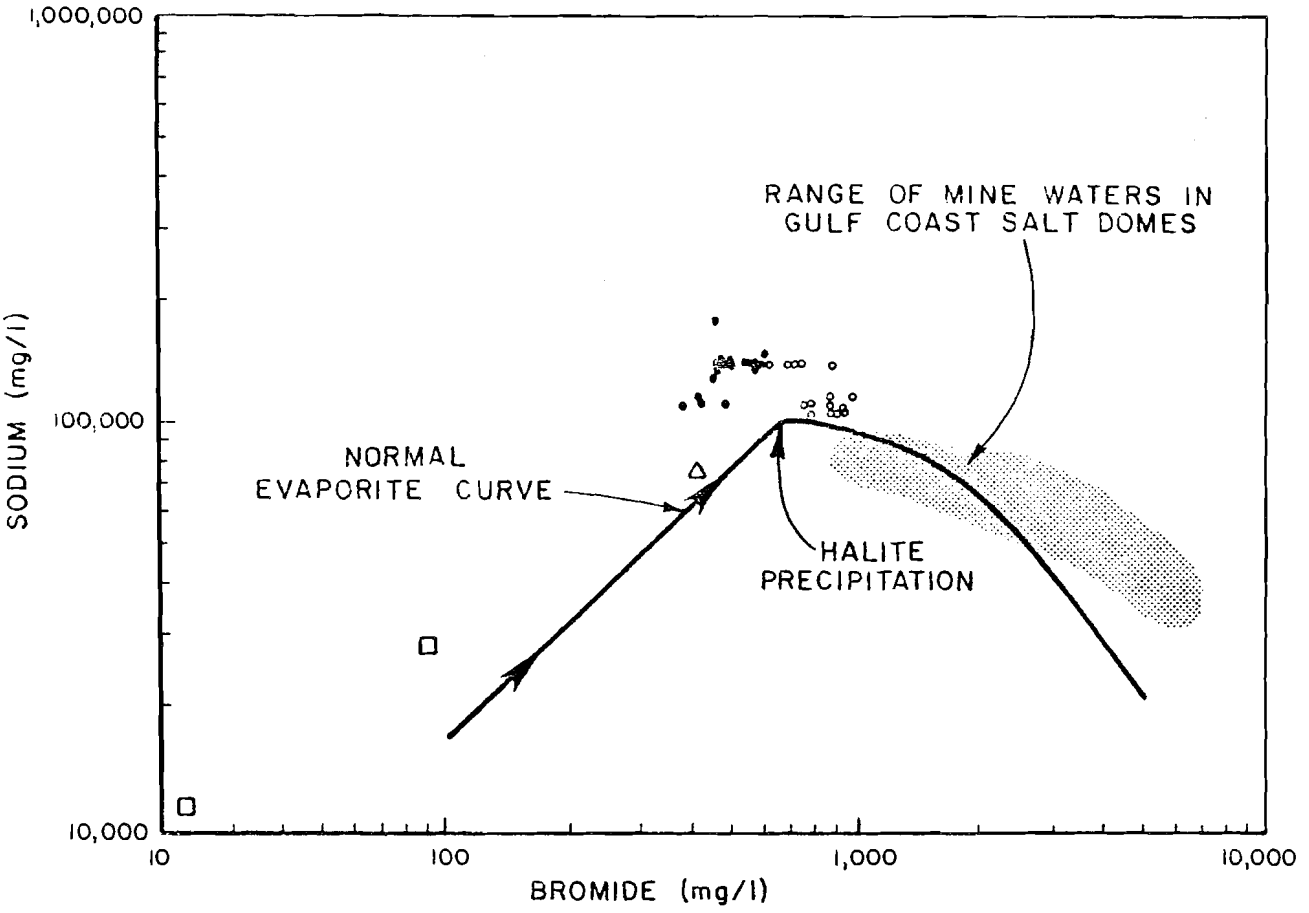

LEGEND

- • WIPP-12 BRINES
- ○ ERDA-6 BRINES
- △ BELL CANYON GROUND WATER
- □ MORROW GROUND WATER

FIGURE C-4

COMPARISON OF CASTILE BRINE SODIUM/BROMIDE RATIOS WITH SEAWATER EVAPORATION TREND

PREPARED FOR

WESTINGHOUSE ELECTRIC CORPORATION
ALBUQUERQUE, NEW MEXICO

D'APPOLONIA

DRAWN BY	EB	CHECKED BY	RLO	3/22/83	DRAWING NUMBER	NM78-648-A93
	9/9/82	APPROVED BY	DKS/JDW	3/18/83		

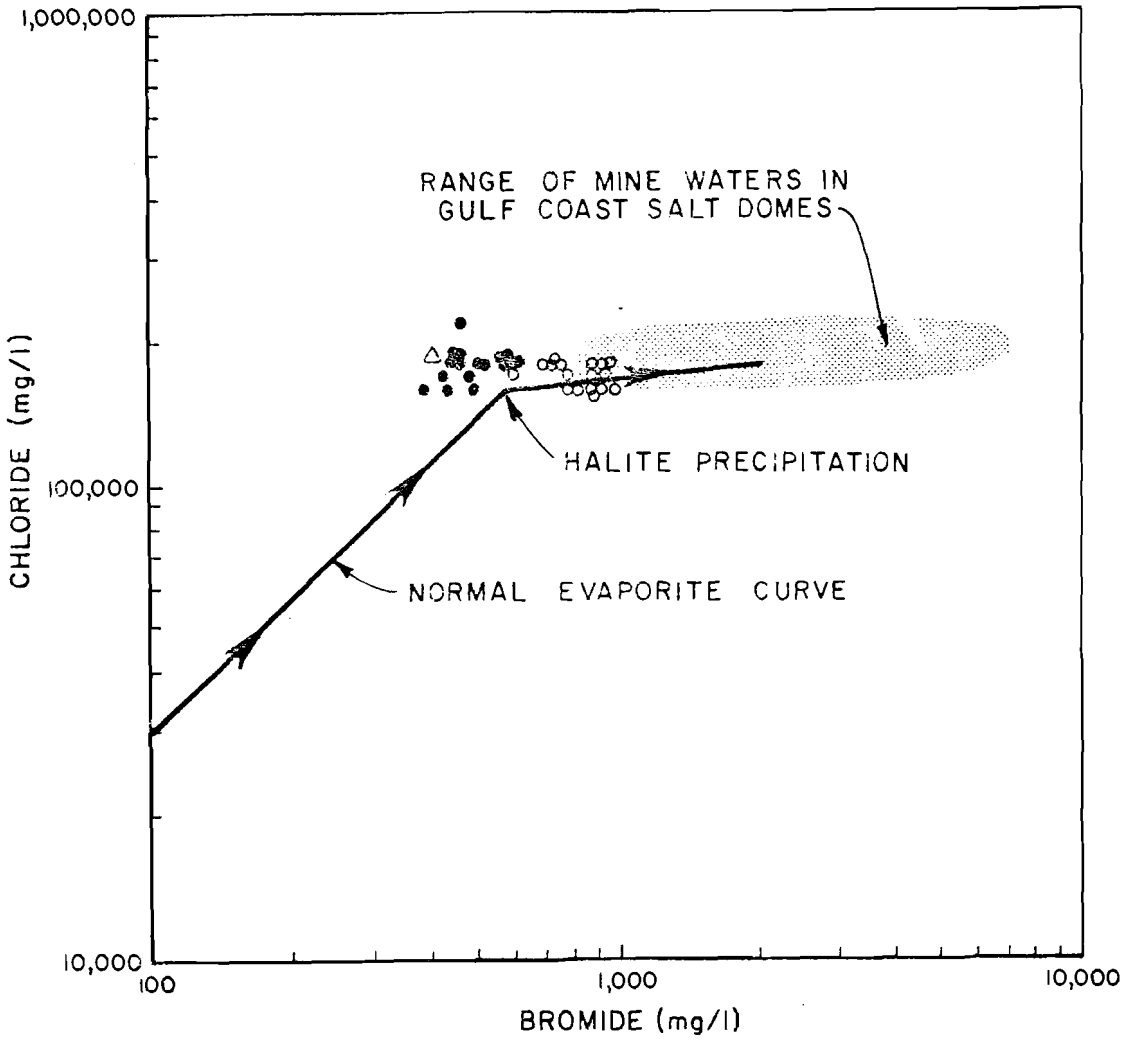

LEGEND

- • WIPP-12 BRINES
- o ERDA-6 BRINES
- Δ BELL CANYON GROUND WATER

FIGURE C-5

COMPARISON OF CASTILE BRINE CHLORIDE/BROMIDE RATIOS WITH SEAWATER EVAPORATION TREND

PREPARED FOR

WESTINGHOUSE ELECTRIC CORPORATION
ALBUQUERQUE, NEW MEXICO

D'APPOLONIA

DRAWN BY	DATE	CHECKED BY	DATE	DRAWING NUMBER
EF	9/17/82	APPROVED BY	3/18/83	NM78-646-A94

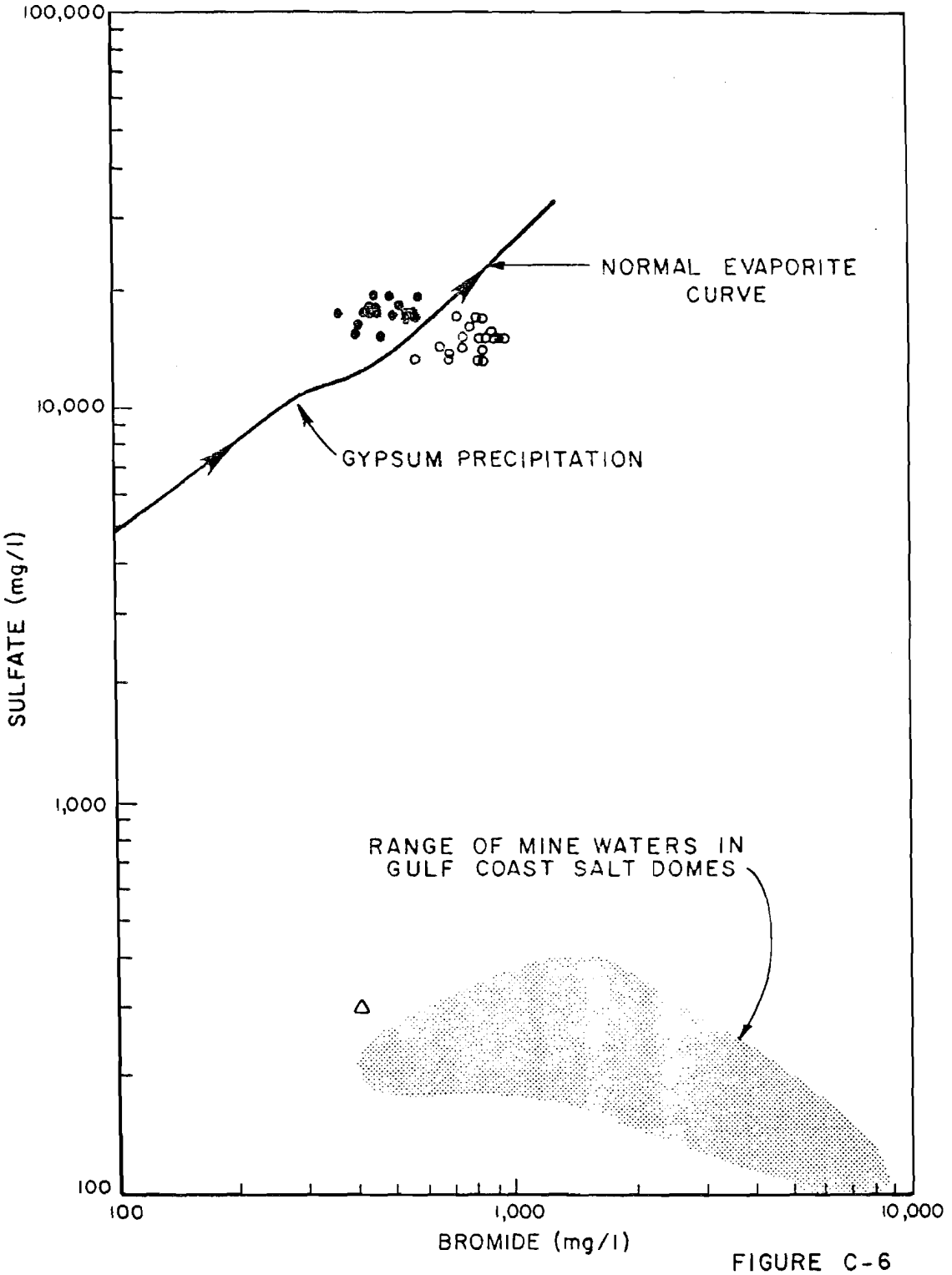

FIGURE C-6

COMPARISON OF CASTILE BRINE SULFATE/BROMIDE RATIOS WITH SEAWATER EVAPORATION TREND

PREPARED FOR

WESTINGHOUSE ELECTRIC CORPORATION
ALBUQUERQUE, NEW MEXICO

LEGEND

- • WIPP-12 BRINES
- ○ ERDA-6 BRINES
- △ BELL CANYON GROUND WATER

D'APPOLONIA

DRAWN BY	CHECKED BY	APPROVED BY	DRAWING NUMBER
EF 9/21/82	ALO DKS/OPW	3/17/83 5/18/83	NM78-648-A96

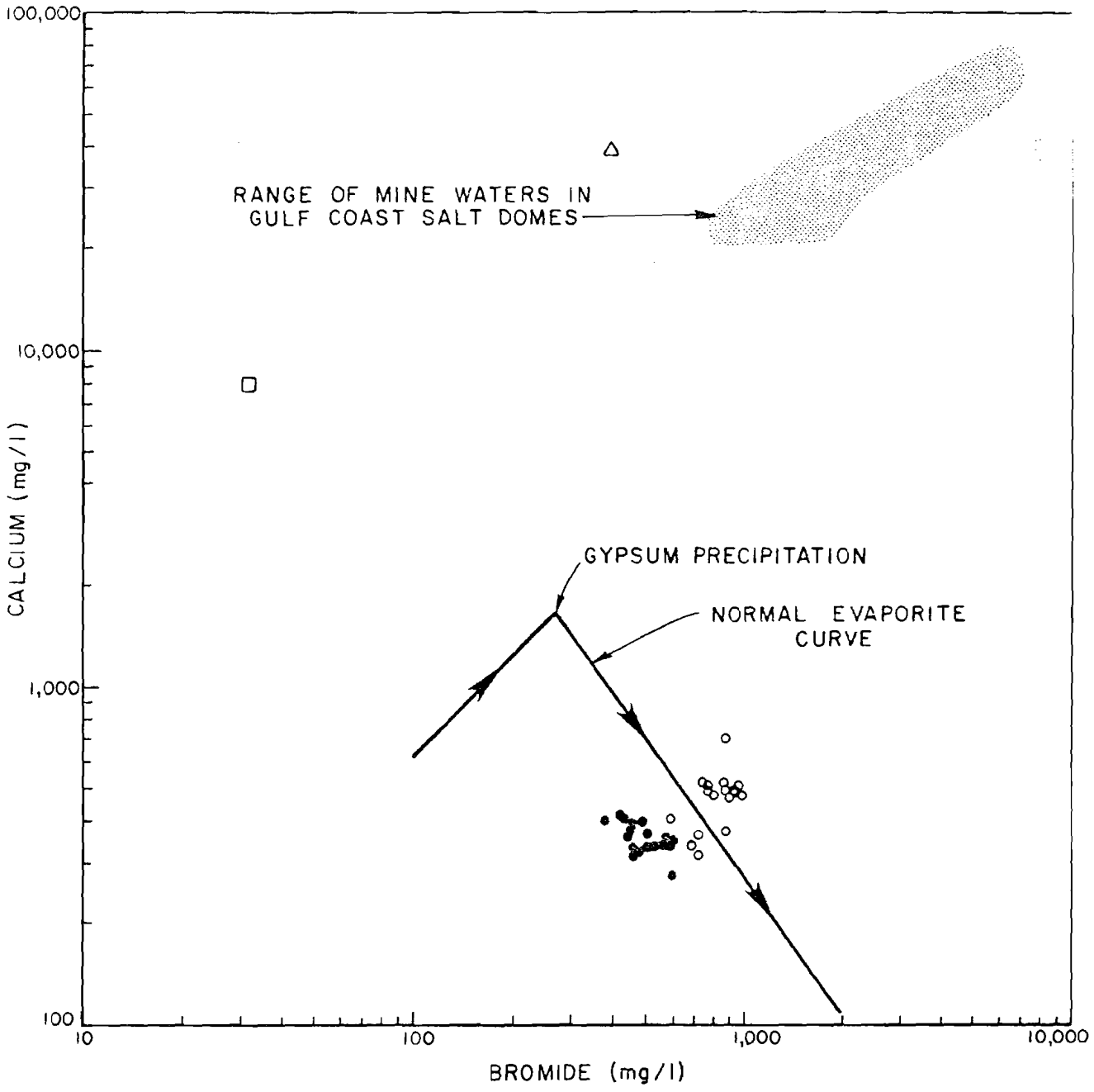

LEGEND

- ● WIPP-12 BRINES
- ○ ERDA-6 BRINES
- △ BELL CANYON GROUND WATER
- □ MORROW GROUND WATER

FIGURE C-7

COMPARISON OF CASTILE BRINE CALCIUM/BROMIDE RATIOS WITH SEAWATER EVAPORATION TREND

PREPARED FOR

WESTINGHOUSE ELECTRIC CORPORATION
ALBUQUERQUE, NEW MEXICO

D'APPOLONIA

DRAWN BY	EB 9/4/82	CHECKED BY	RLO 9/23/82	DRAWING NUMBER NM78-648-A95
		APPROVED BY	DKS/WPW 9/18/82	

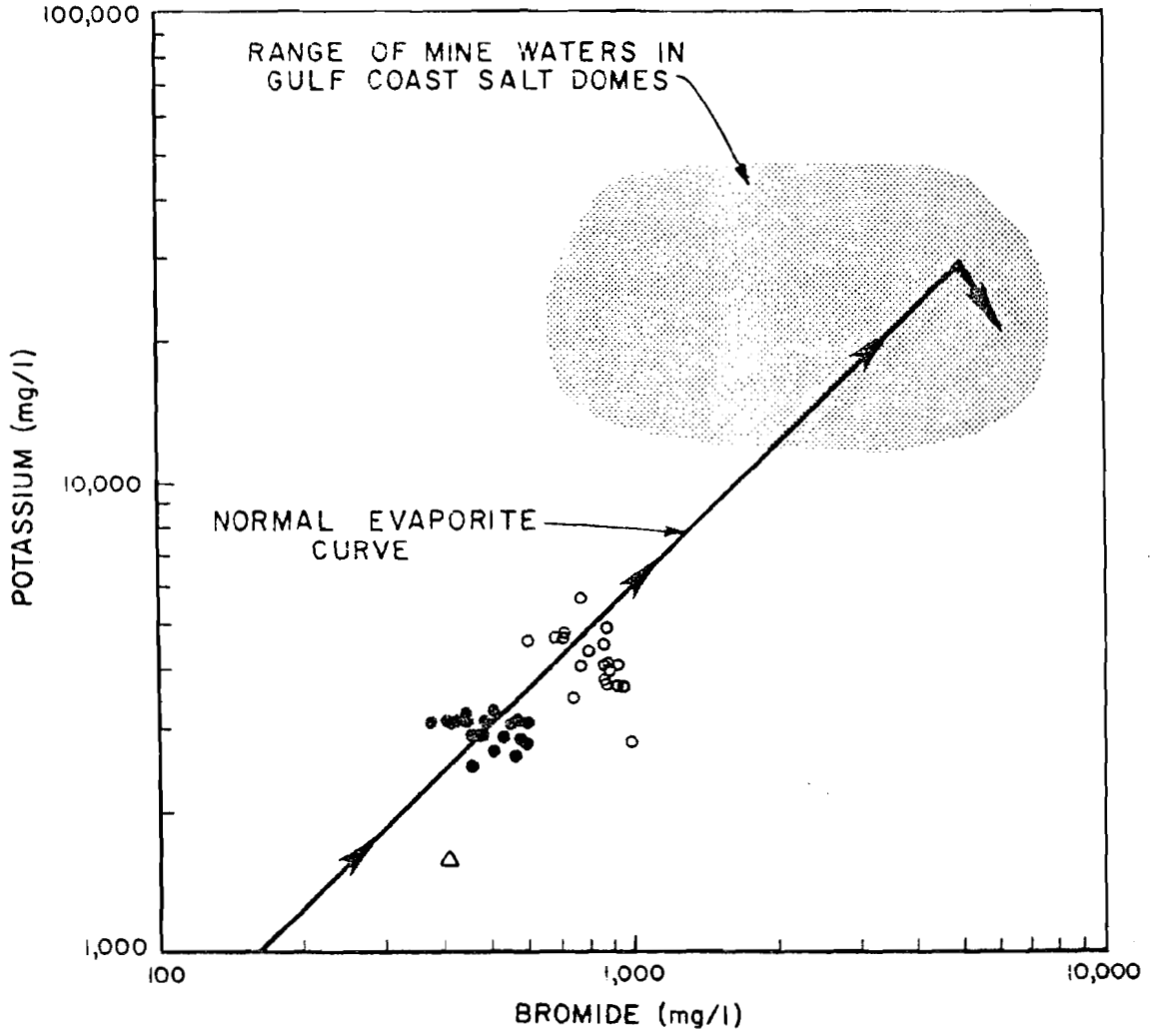

LEGEND

- • WIPP-12 BRINES
- o ERDA-6 BRINES
- Δ BELL CANYON GROUND WATER

FIGURE C-8

COMPARISON OF CASTILE BRINE POTASSIUM/BROMIDE RATIOS WITH SEAWATER EVAPORATION TREND

PREPARED FOR

WESTINGHOUSE ELECTRIC CORPORATION
ALBUQUERQUE, NEW MEXICO

D'APPOLONIA

DRAWN BY	CHECKED BY		DRAWING NUMBER
EB			NM78-648-A97
9/8/82	APPROVED BY		
	DR/oPJ	3/12/83	

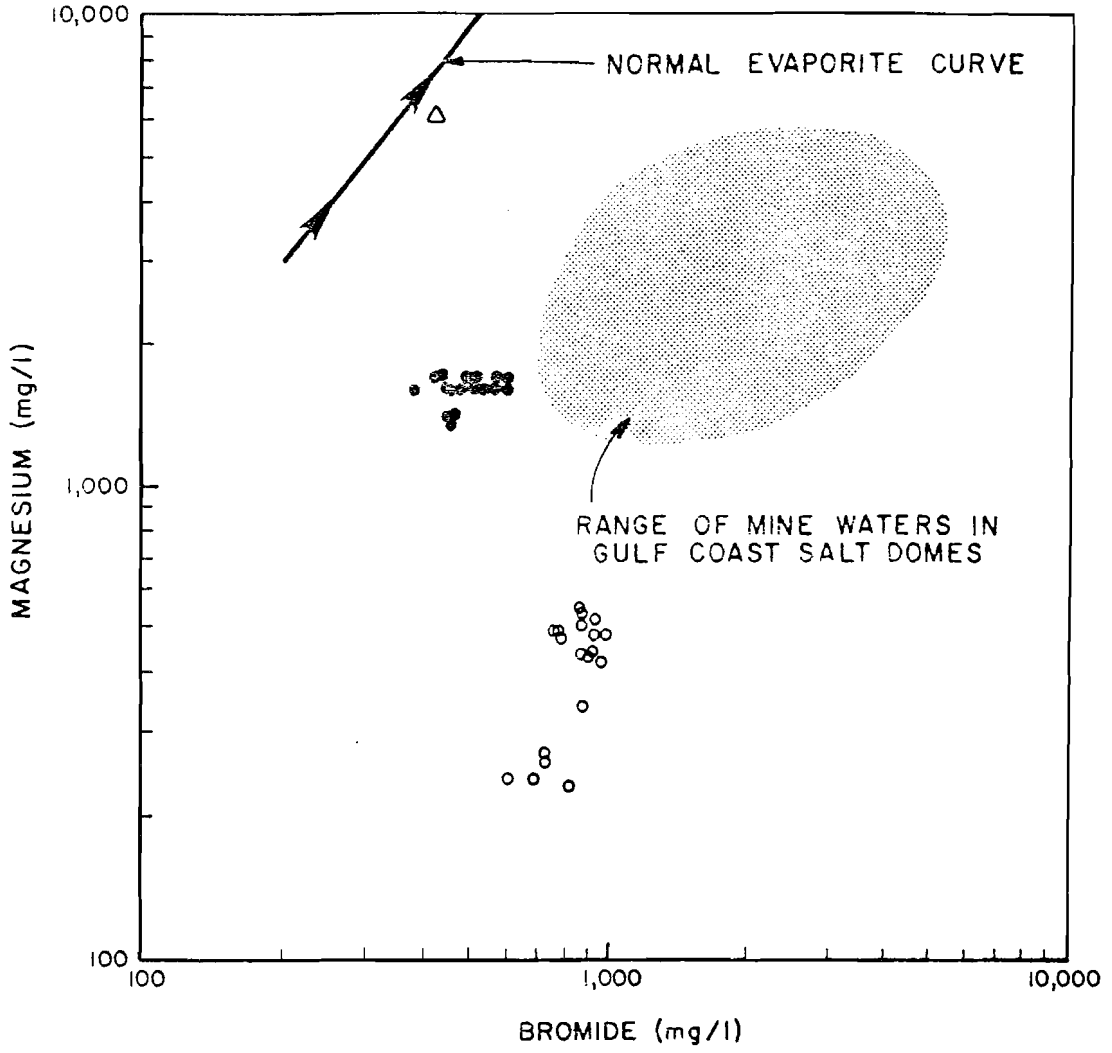

LEGEND

- • WIPP-12 BRINES
- o ERDA-6 BRINES
- △ BELL CANYON GROUND WATER

FIGURE C-9.

COMPARISON OF CASTILE BRINE MAGNESIUM/BROMIDE RATIOS WITH SEAWATER EVAPORATION TREND

PREPARED FOR

WESTINGHOUSE ELECTRIC CORPORATION
ALBUQUERQUE, NEW MEXICO

D'APPOLONIA

DRAWN BY	CHECKED BY	DRAWING NUMBER
EB 9/10/82	APPROVED BY	NM78-648-A98

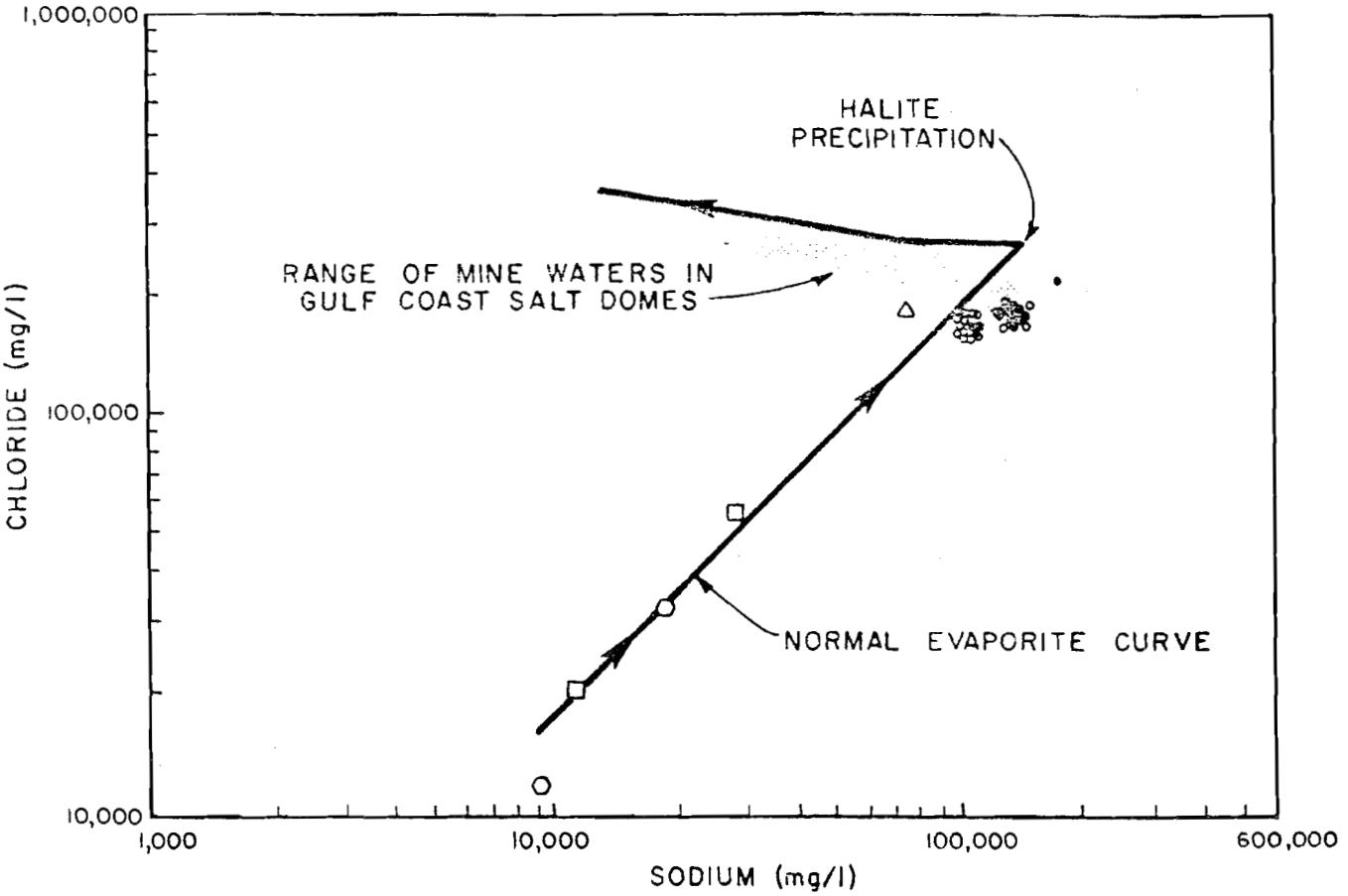

LEGEND

- • WIPP-12 BRINES
- o ERDA-6 BRINES
- △ BELL CANYON GROUND WATER
- □ MORROW GROUND WATER
- ○ RUSTLER GROUND WATER

FIGURE C-10

COMPARISON OF CASTILE BRINE CHLORIDE/SODIUM RATIOS WITH SEAWATER EVAPORATION TREND

PREPARED FOR

WESTINGHOUSE ELECTRIC CORPORATION
ALBUQUERQUE, NEW MEXICO

D'APPOLONIA

DRAWN BY	EF 9/21/82	CHECKED BY	RLC 3/17/83	DRAWING NUMBER NM78-648-A99
		APPROVED BY	DKS/opw 3/13/83	

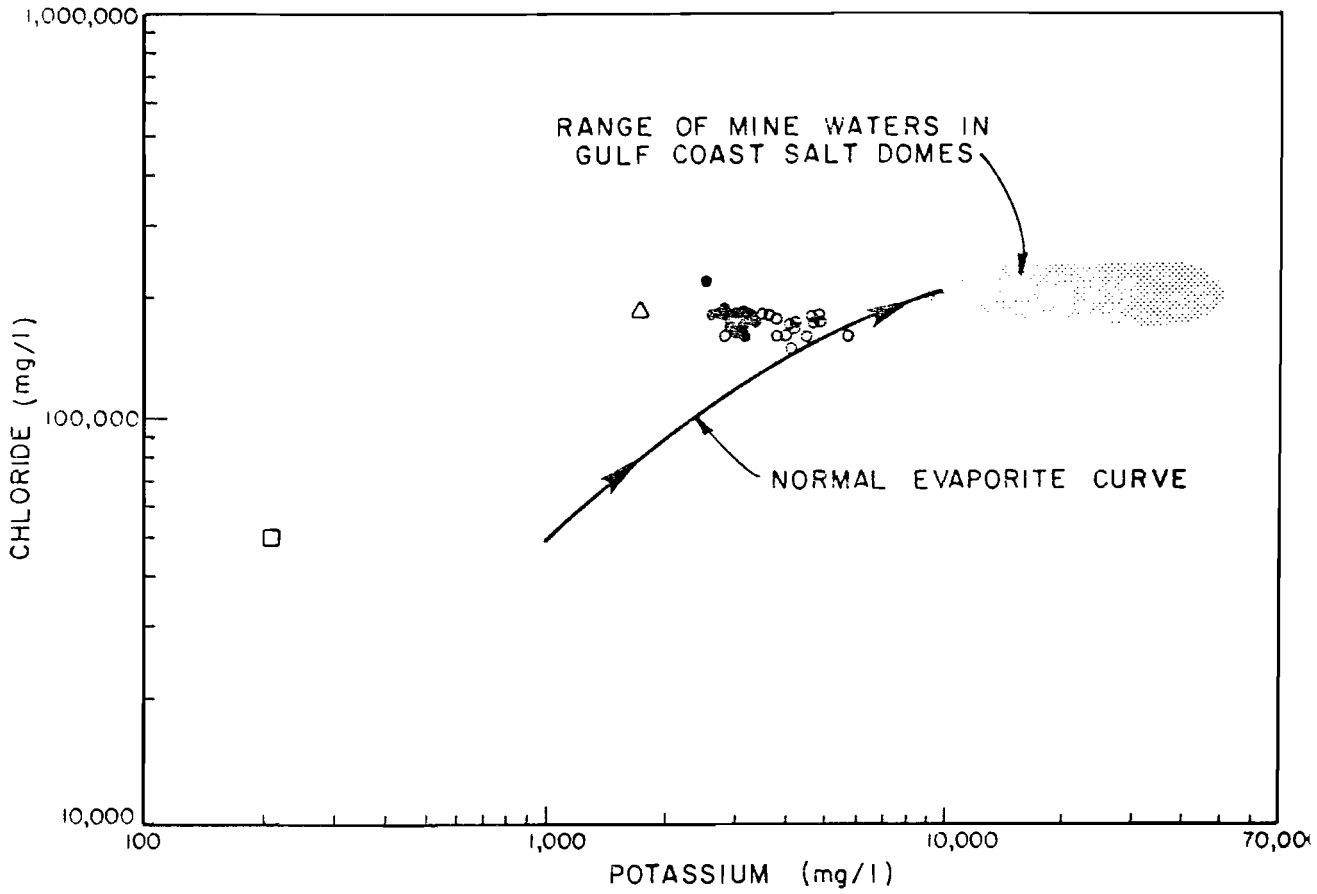

LEGEND

- ● WIPP-12 BRINES
- ○ ERDA-6 BRINES
- △ BELL CANYON GROUND WATER
- □ MORROW GROUND WATER

FIGURE C-11

COMPARISON OF CASTILE BRINE CHLORIDE/POTASSIUM RATIOS WITH SEAWATER EVAPORATION TREND

PREPARED FOR

WESTINGHOUSE ELECTRIC CORPORATION
ALBUQUERQUE, NEW MEXICO

D'APPOLONIA

DRAWN BY	CHECKED BY		DRAWING NUMBER
EB	RLD		NM78-648-A100
9/13/82	APPROVED BY		
	DKS/OPJ	3/18/83	

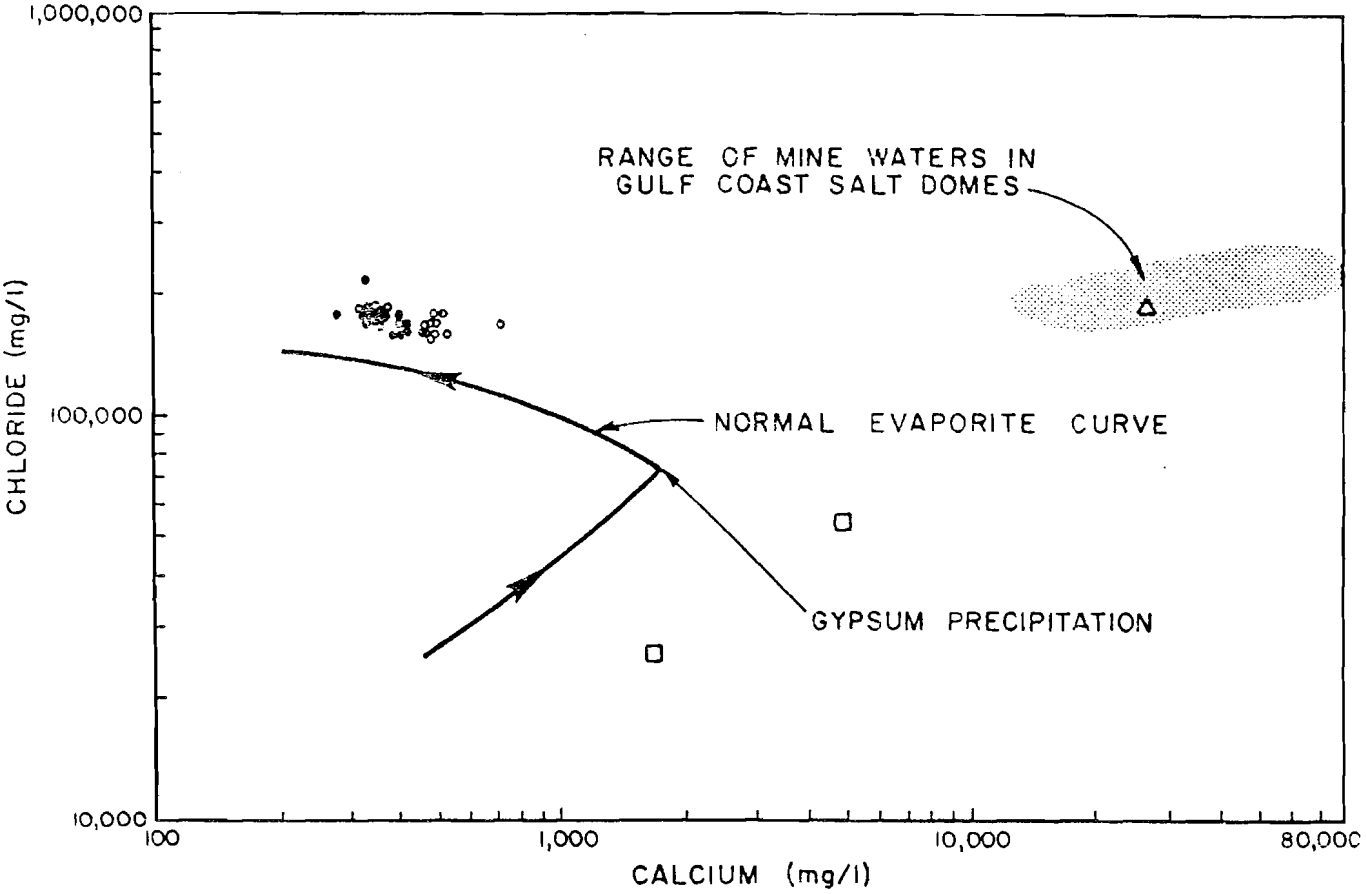

LEGEND

- • WIPP-12 BRINES
- o ERDA-6 BRINES
- △ BELL CANYON GROUND WATER
- □ MORROW GROUND WATER

FIGURE C-12

COMPARISON OF CASTILE BRINE CHLORIDE/CALCIUM RATIOS WITH SEAWATER EVAPORATION TREND

PREPARED FOR

WESTINGHOUSE ELECTRIC CORPORATION
ALBUQUERQUE, NEW MEXICO

D'APPOLONIA

DRAWN BY	CHECKED BY		DRAWING NUMBER
EF		RLD 9/17/82	NM78-648-A101
9/20/82	APPROVED BY	DKS/opm 3/18/83	

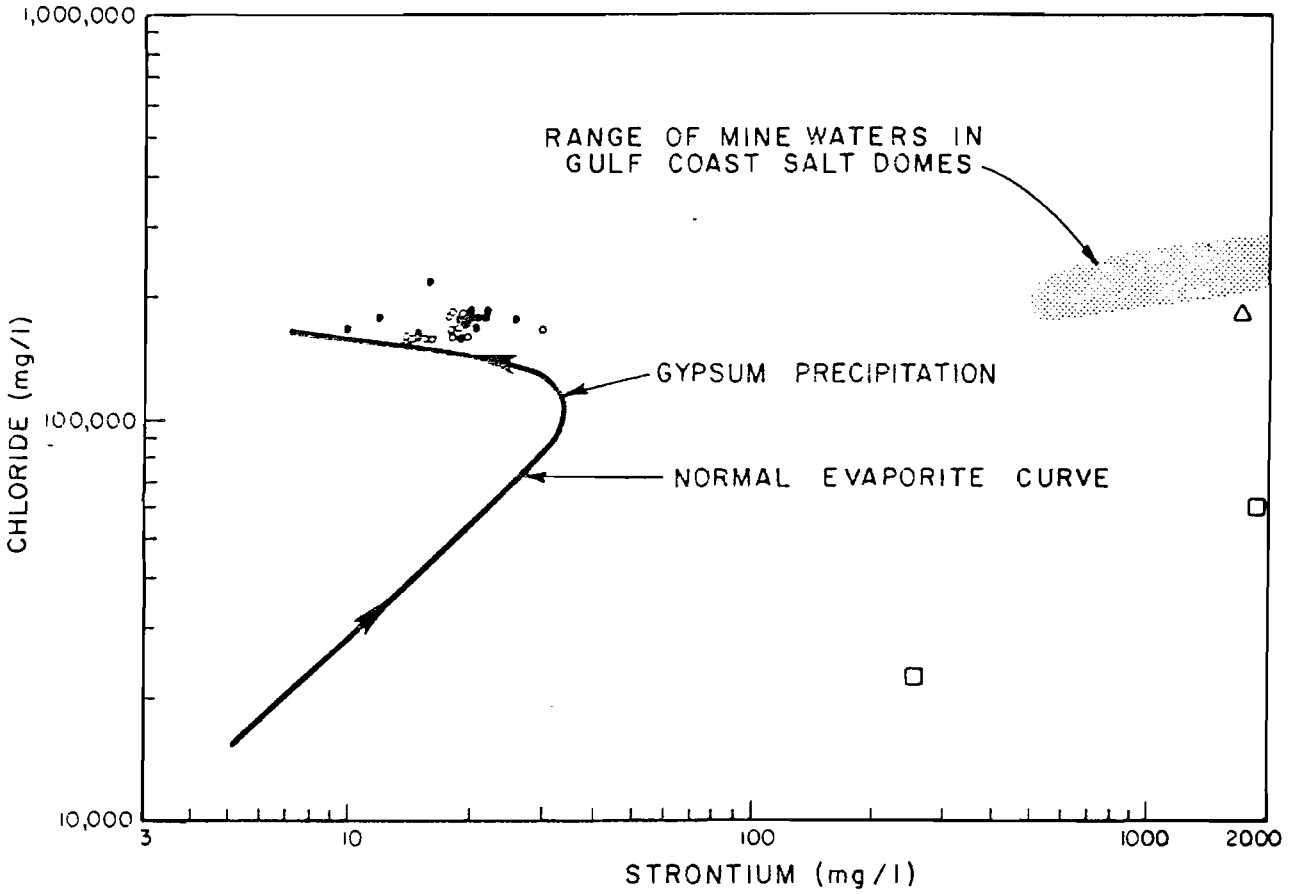

LEGEND

- • WIPP-12 BRINES
- ° ERDA-6 BRINES
- △ BELL CANYON GROUND WATER
- □ MORROW GROUND WATER

FIGURE C-13
COMPARISON OF CASTILE BRINE CHLORIDE/STRONTIUM RATIOS WITH SEAWATER EVAPORATION TREND

PREPARED FOR

WESTINGHOUSE ELECTRIC CORPORATION
ALBUQUERQUE, NEW MEXICO

D'APPOLONIA

DRAWN BY	CHECKED BY	DRAWING NUMBER
EB 9/10/82	APPROVED BY DRS for JPW 3/18/83	NM'78-648-A102

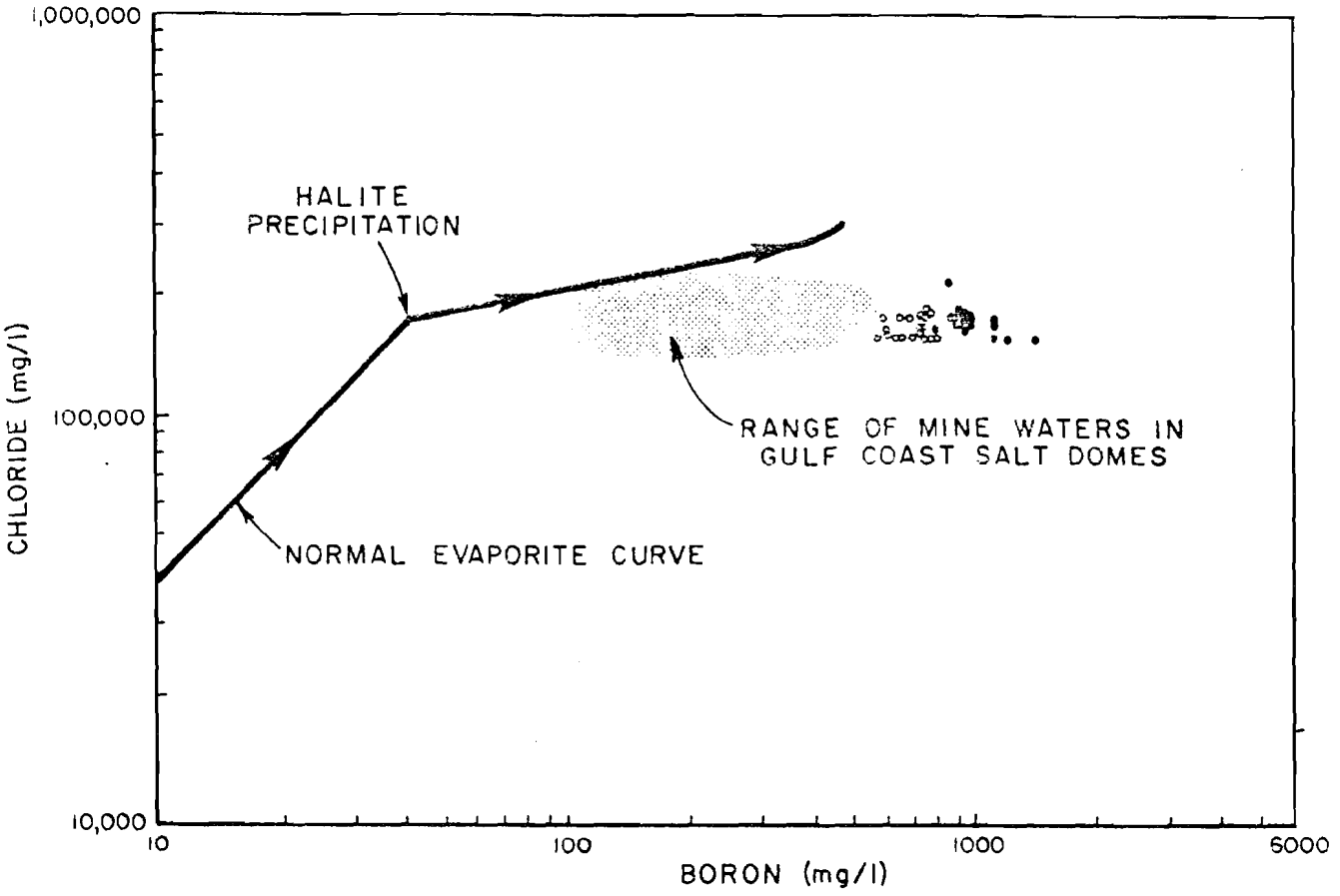

FIGURE C-14

COMPARISON OF CASTILE BRINE CHLORIDE/BORON RATIOS WITH SEAWATER EVAPORATION TREND

PREPARED FOR

WESTINGHOUSE ELECTRIC CORPORATION
ALBUQUERQUE, NEW MEXICO

LEGEND

- • WIPP-12 BRINES
- o ERDA-6 BRINES

D'APPOLONIA

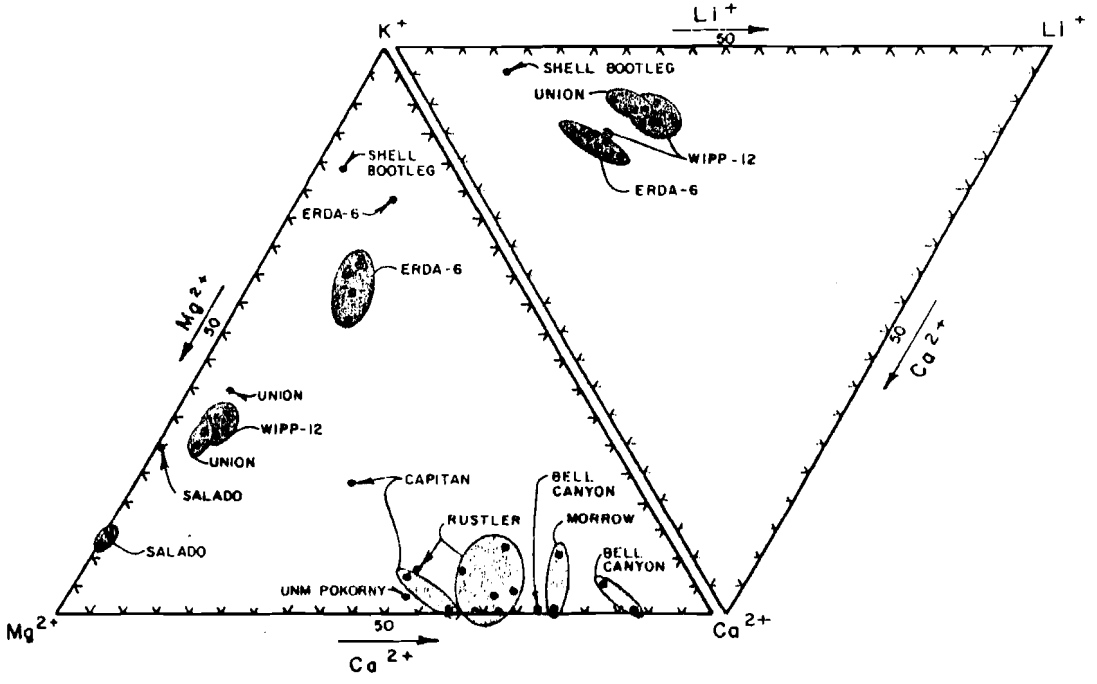

NOTES:

1. CASTILE WELLS = ERDA-6, WIPP-12, UNION, SHELL BOOTLEG AND UNM POKORNY.
2. NUMBERS EXPRESSED IN RELATIVE PERCENT EQUIVALENTS.

FIGURE C-15

COMPARISON OF ERDA-6 AND WIPP-12 BRINES WITH REGIONAL GROUND WATERS

PREPARED FOR

WESTINGHOUSE ELECTRIC CORPORATION
ALBUQUERQUE, NEW MEXICO

REFERENCES:

LAMBERT (1978), HISS (1975), WHITE et al. (1963), SNYDER (1982)

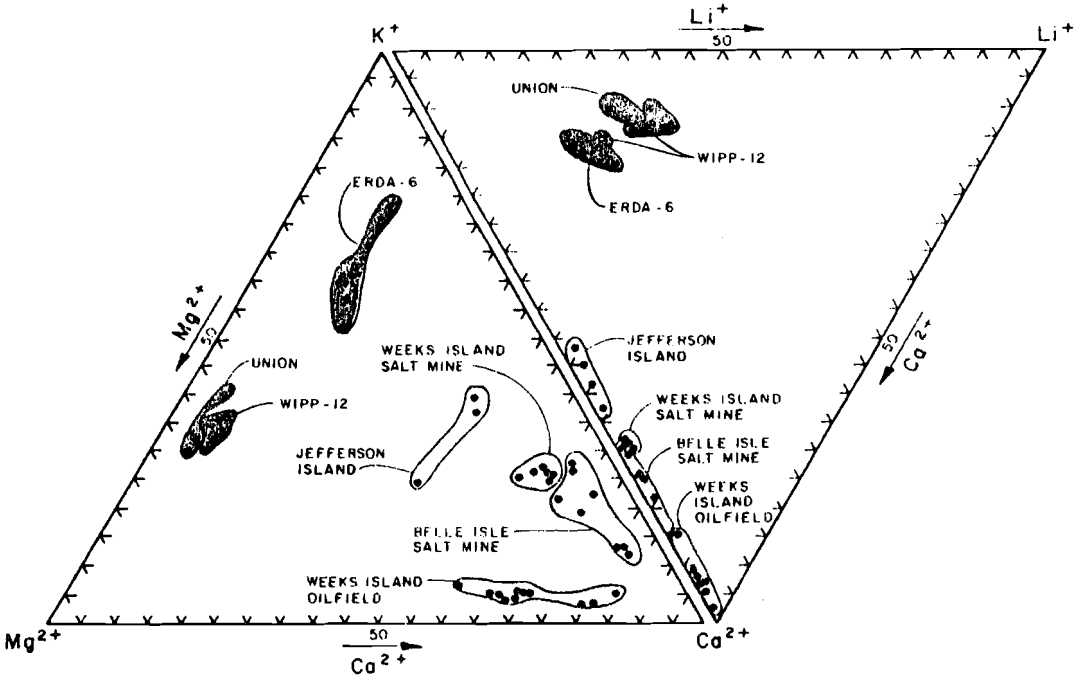

NOTE:

NUMBERS EXPRESSED IN RELATIVE PERCENT EQUIVALENTS.

FIGURE C-16

COMPARISON OF ERDA-6 AND WIPP-12 BRINES WITH METEORIC SEEPS INTO GULF COAST SALT DOMES

PREPARED FOR

WESTINGHOUSE ELECTRIC CORPORATION
ALBUQUERQUE, NEW MEXICO

REFERENCE:

MARTINEZ (1979)

DRAWN BY | BKH | 9-23-82
CHECKED BY | R.L.O. | 3/12/83
APPROVED BY | DRS/DAT | 3/13/83
DRAWING NUMBER NM78-648-844

TME 3153

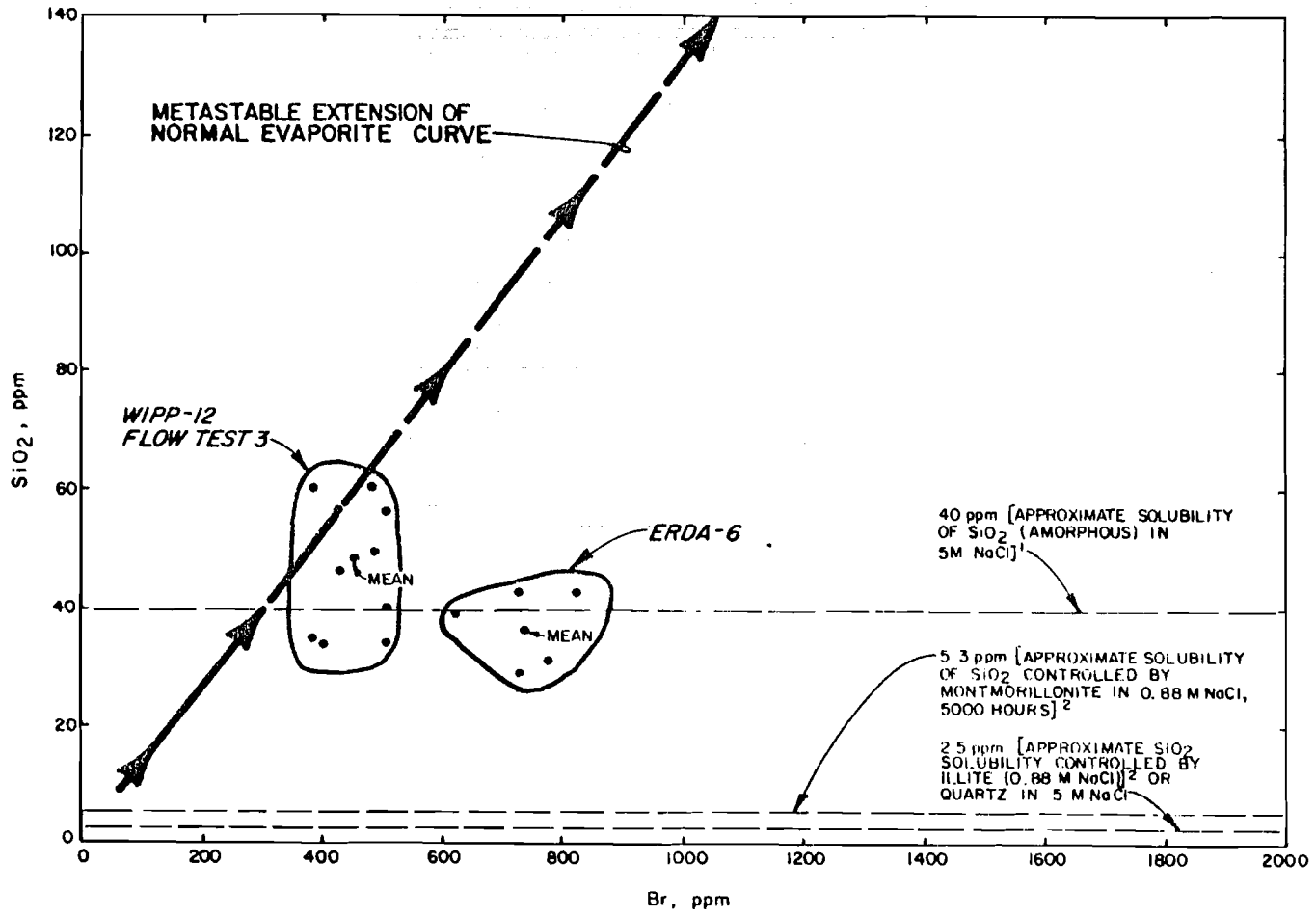

NOTES:
1. CHEN AND MARSHALL (1982).
2. COLLINS (1975).

FIGURE C-17

COMPARISON OF WIPP-12 AND ERDA-6 BRINES' SILICA/BROMIDE RATIOS WITH SEAWATER EVAPORATION AND OTHER CONTROLS ON SILICA

PREPARED FOR

WESTINGHOUSE ELECTRIC CORPORATION
ALBUQUERQUE, NEW MEXICO

IDAHO

DRAWN BY | CHECKED BY | APPROVED BY | DRAWING NUMBER NM79-648-854

TME 3153

DRAWN BY	R. Bricker	CHECKED BY	SRB	12/3/82	DRAWING NUMBER NM78-648-A87
	3 Dec. 82	APPROVED BY	RSP	12-3-82	

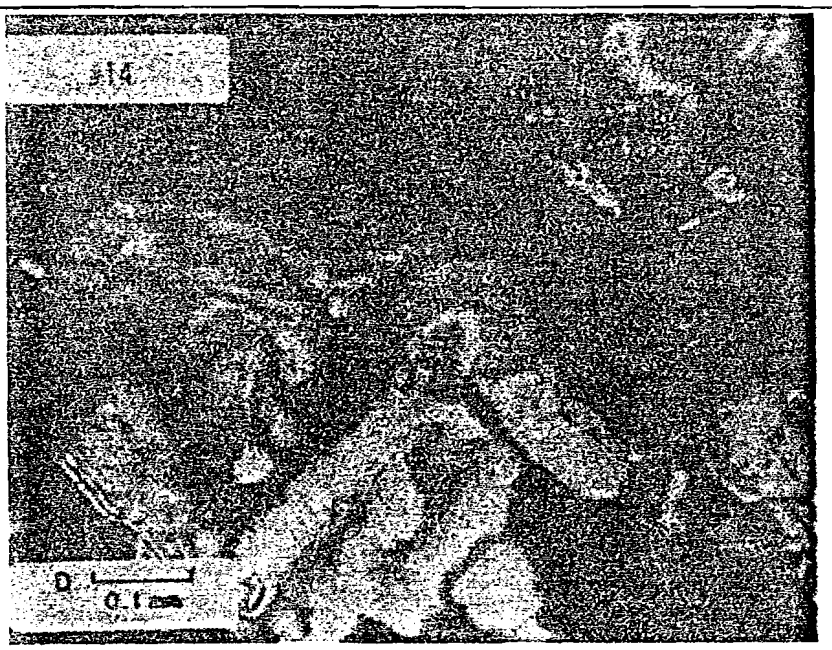

A. PHOTOMICROGRAPH OF WIPP-12 CORE (SAMPLE 14, 3276.6 FT.) SHOWING AUTHIGENIC QUARTZ CRYSTAL IN CENTER OF PHOTO, AT ANHYDRITE II / HALITE II CONTACT

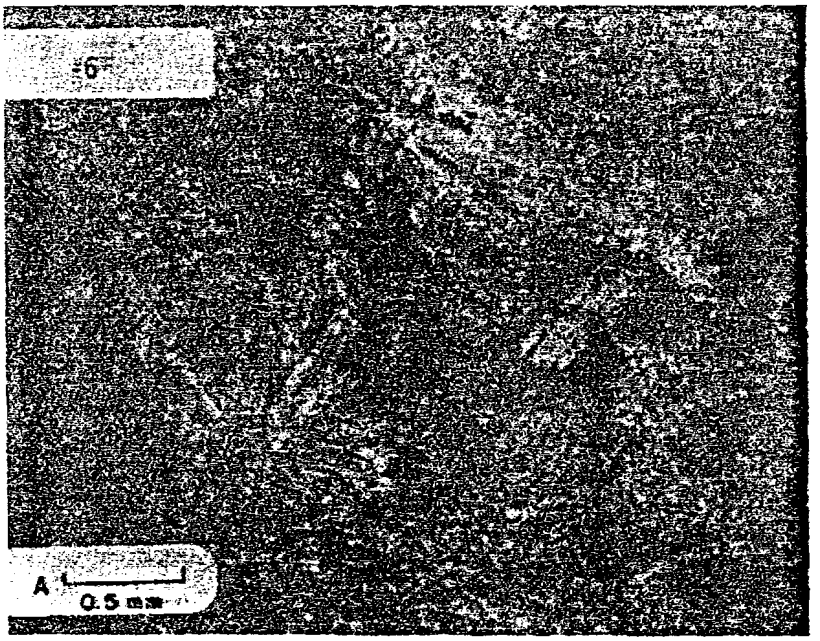

B. PHOTOMICROGRAPH OF WIPP-12 CORE (SAMPLE 6, 2943.3 FT.) SHOWING POSSIBLE PSEUDOMORPHS OF ANHYDRITE AFTER GYPSUM IN ANHYDRITE III. (RADIATING GROUP OF ACICULAR ANHYDRITE CRYSTALS, LEFT OF CENTER)

FIGURE C-18

PHOTOMICROGRAPH OF WIPP-12 CORE

PREPARED FOR

WESTINGHOUSE ELECTRIC CORPORATION
ALBUQUERQUE, NEW MEXICO

NOTE:

PHOTOS TAKEN BY RESERVOIRS, INC., DENVER, CO. DEPTHS ARE FEET BELOW GROUND SURFACE, AS MARKED ON CORE (UNCORRECTED FOR GEOPHYSICS). REFER TO TABLE C-11 FOR MINERALOGIC COMPOSITION.

D'APPOLONIA

08	DRAWN BY	EF 9/20/82	CHECKED BY	RLO 3/17/83	DRAWING NUMBER NM78-648-A105
			APPROVED BY	DKS/CAW 3/18/83	

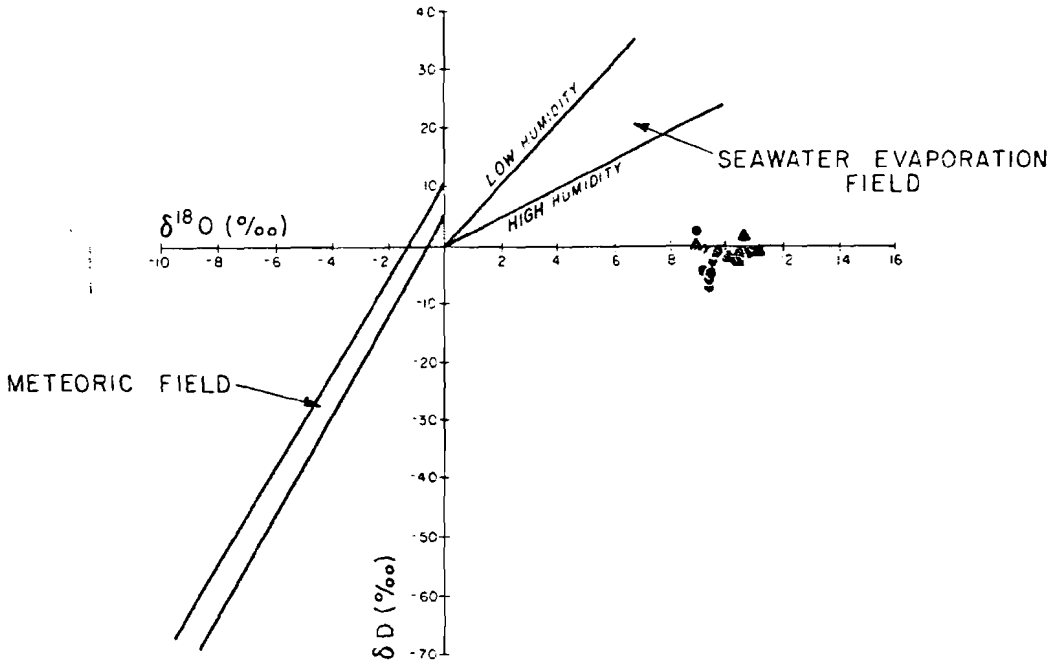

A. RELATION OF $\delta^{18}O$ AND δD OF BRINES TO REFERENCE FIELDS

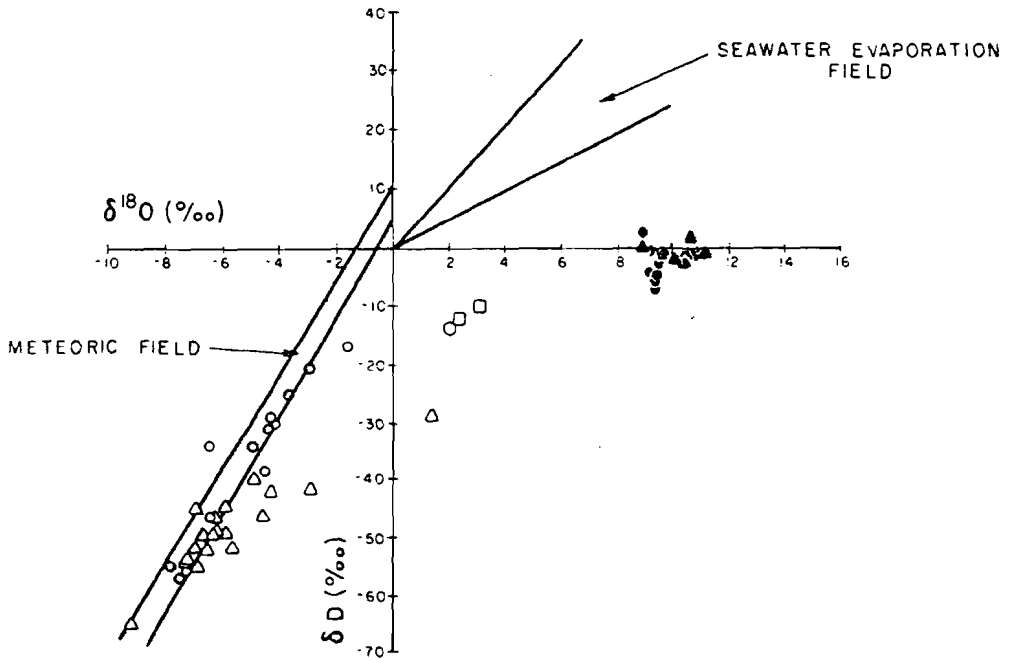

B. RELATION OF $\delta^{18}O$ AND δD OF BRINES TO REGIONAL GROUND WATERS

LEGEND

- ● ERDA-6 BRINES
- ▲ WIPP-12 BRINES
- ○ BELL CANYON GROUND WATER
- ○ CAPITAN GROUND WATER
- □ SALADO GROUND WATER
- △ RUSTLER GROUND WATER

FIGURE C-19

RELATION OF $\delta^{18}O$ AND δD OF BRINES TO REFERENCE FIELDS AND REGIONAL GROUND WATERS

PREPARED FOR

WESTINGHOUSE ELECTRIC CORPORATION
ALBUQUERQUE, NEW MEXICO

D'APPOLONIA

DRAWN BY	MJG	CHECKED BY	RLO	DRAWING NUMBER	NM78-648-A104
	10/18/82	APPROVED BY	DKS/opw		3/18/83

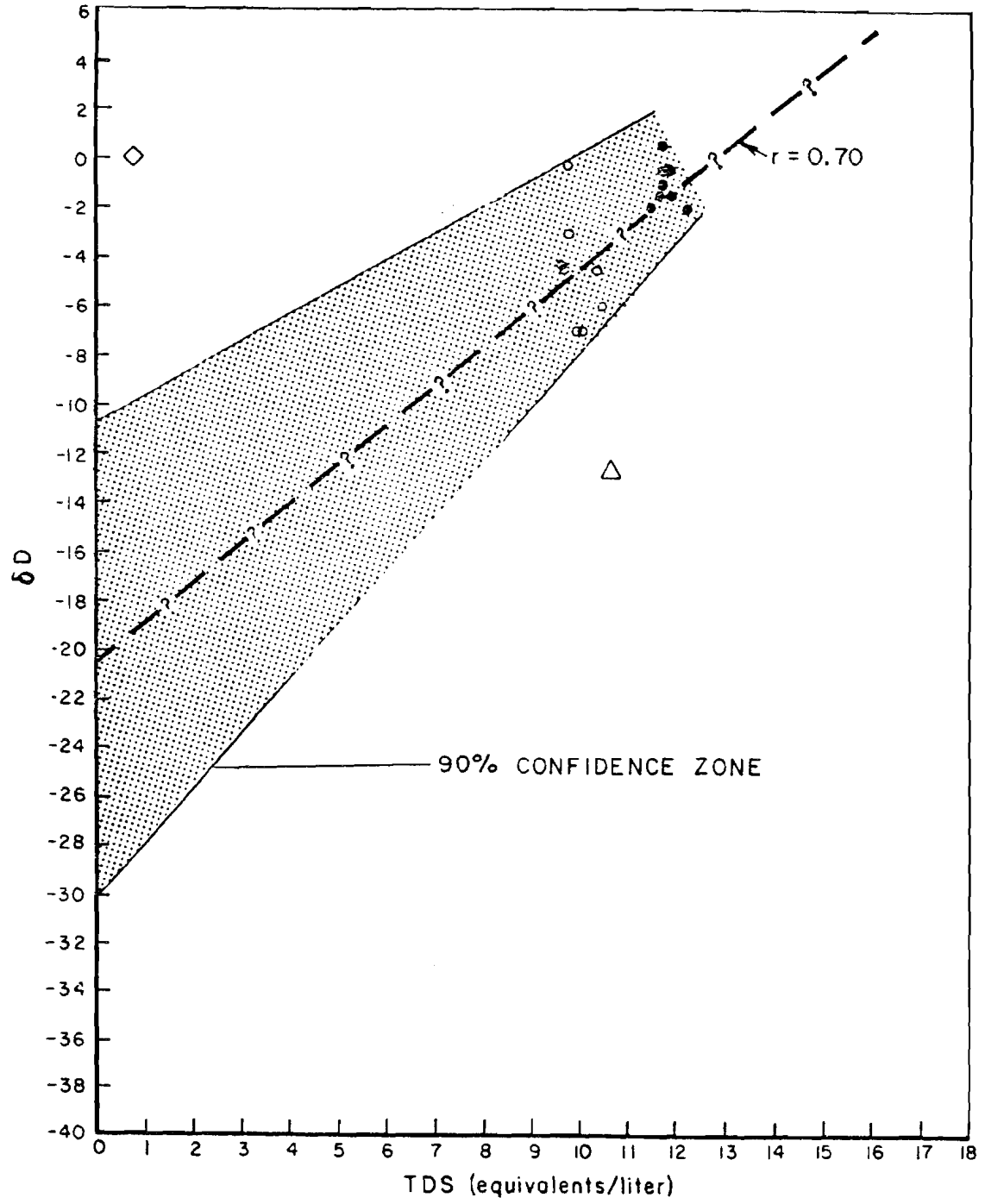

FIGURE C-20

VARIATION OF DEUTERIUM WITH TOTAL DISSOLVED SOLIDS

PREPARED FOR

WESTINGHOUSE ELECTRIC CORPORATION
ALBUQUERQUE, NEW MEXICO

LEGEND:

- ● WIPP-12 BRINE
- ○ ERDA-6 BRINE
- △ BELL CANYON GROUND WATER
- ◇ SMOW

D'APPOLONIA

DRAWN BY	CHECKED BY	DRAWING NUMBER
E.B 9/21/82	APPROVED BY DKS/opw 3/15/83	NM78-648-A103

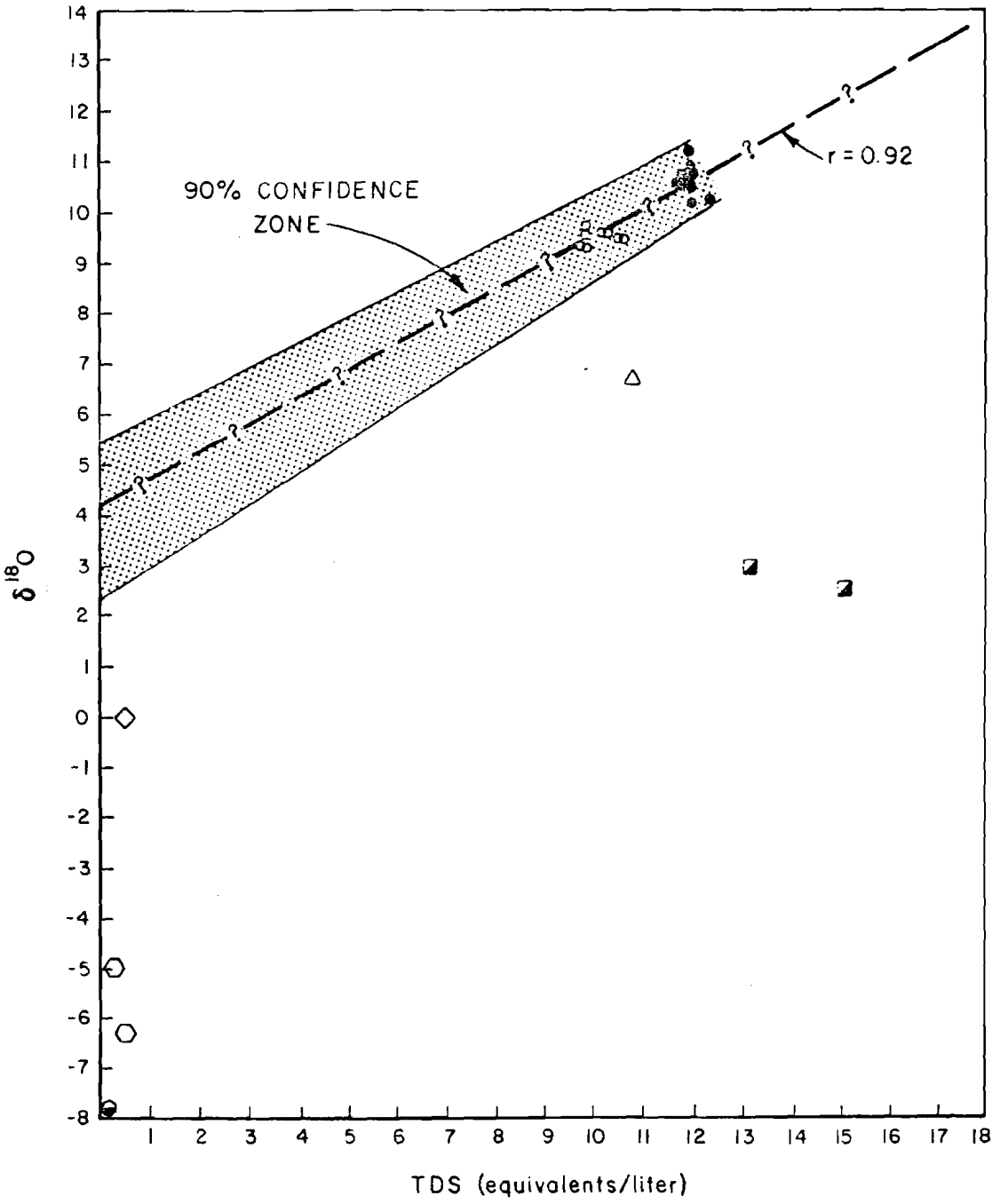

LEGEND:

- ● WIPP-12 BRINE
- ○ ERDA-6 BRINE
- △ BELL CANYON GROUND WATER
- ⬡ RUSTLER GROUND WATER
- ◪ SALADO GROUND WATER
- ◒ CAPITAN GROUND WATER
- ◇ SMOW

FIGURE C-21

VARIATION OF $\delta^{18}O$
WITH TOTAL DISSOLVED SOLIDS

PREPARED FOR

WESTINGHOUSE ELECTRIC CORPORATION
ALBUQUERQUE, NEW MEXICO

02	DRAWN BY	BKH 9-23-82	CHECKED BY		DRAWING NUMBER NM78-648-A116
			APPROVED BY	DKG/OWJ 2/18/83	

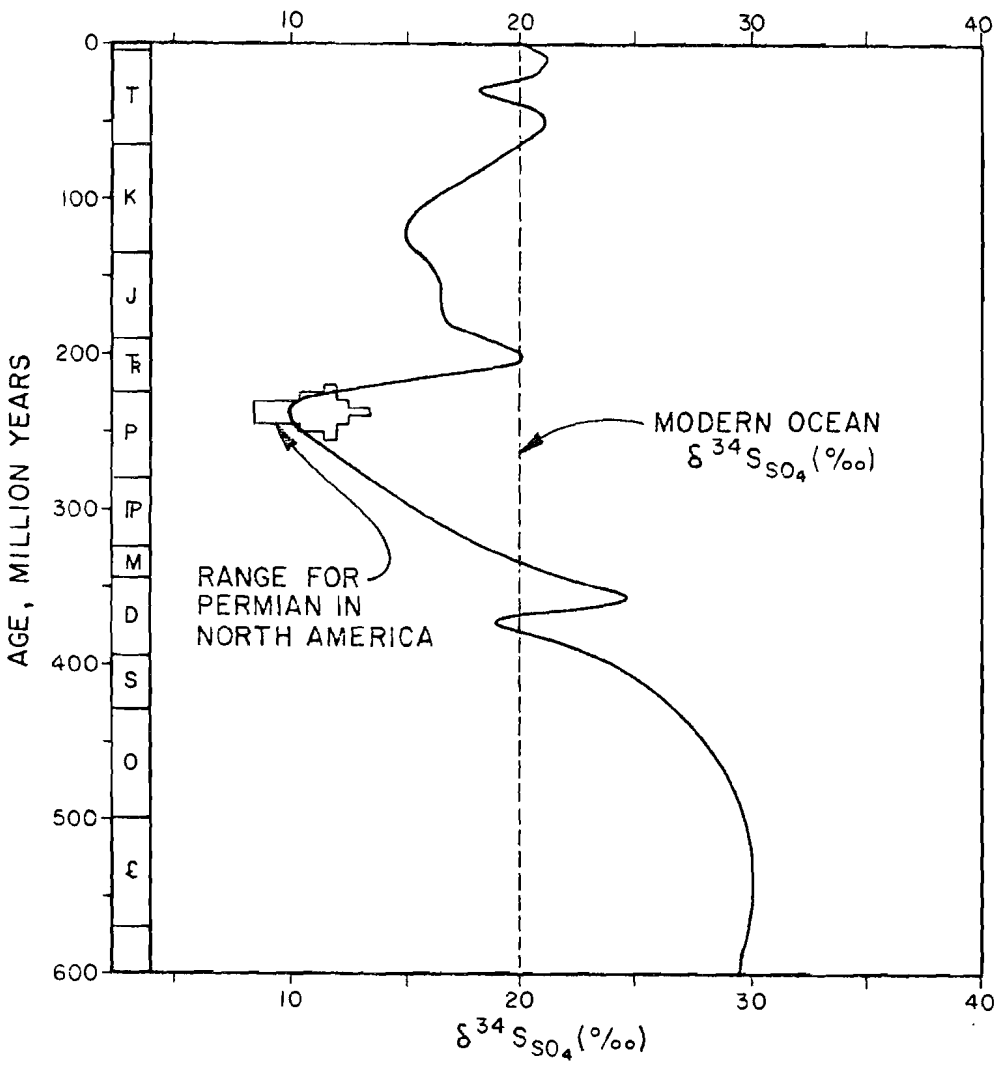

FIGURE C-22

$\delta^{34}S$ VARIATION IN WORLD OCEANS THROUGH TIME

PREPARED FOR

WESTINGHOUSE ELECTRIC CORPORATIO
ALBUQUERQUE, NEW MEXICO

REFERENCE:

DRAWN BY	BKH	CHECKED BY	RLO	3/12/82	DRAWING NUMBER NM78-648-A108
	9-24-82	APPROVED BY	DKS/DAW	3/18/82	

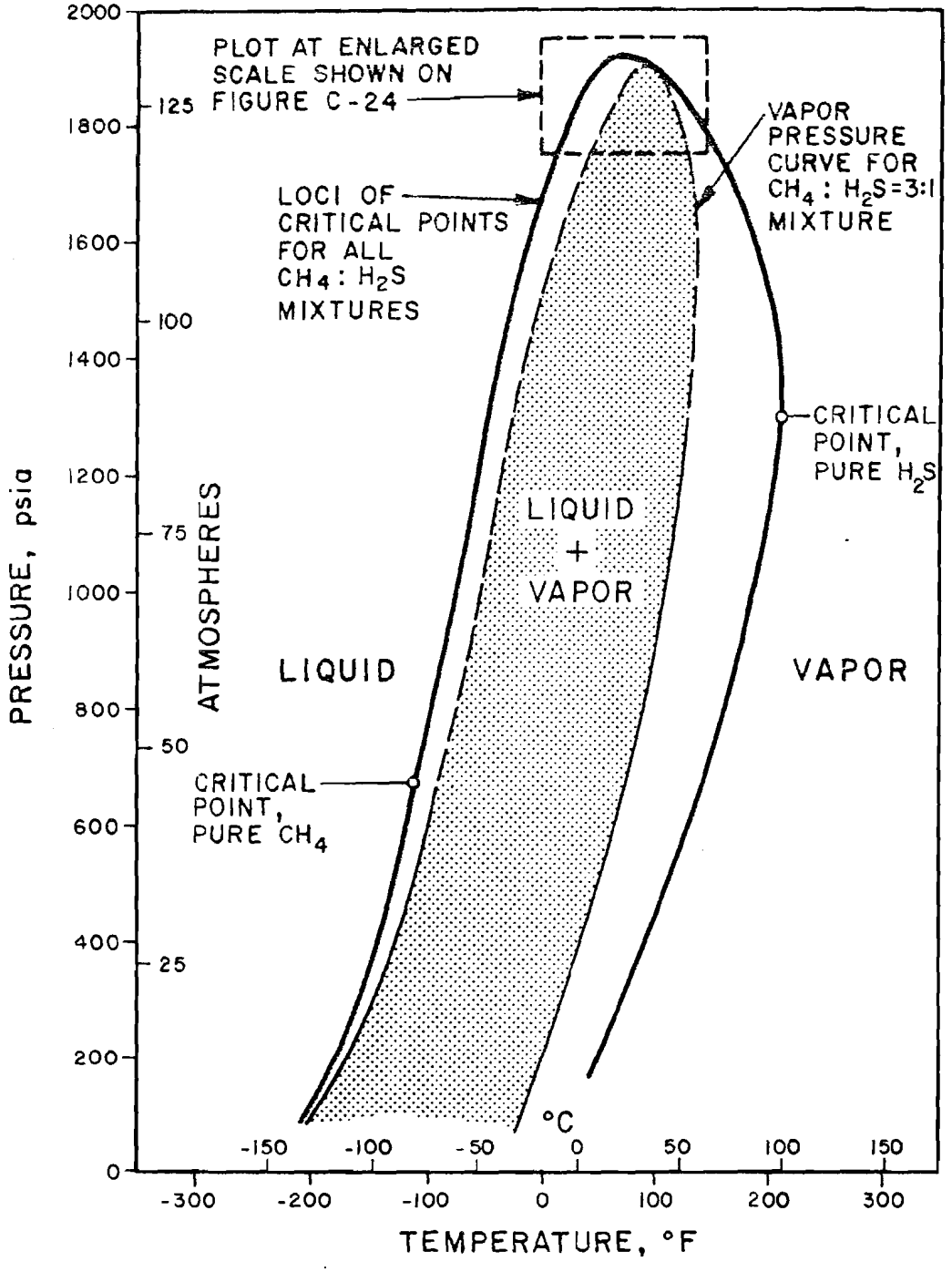

FIGURE C-23

PRESSURE VS. TEMPERATURE
FOR BINARY MIXTURES
CH_4 + H_2S

PREPARED FOR

WESTINGHOUSE ELECTRIC CORPORATION
ALBUQUERQUE, NEW MEXICO

D'APPOLONIA

DRAWN BY	BKH	CHECKED BY	RLO	3/7/83	DRAWING NUMBER NM78-648-A110
	9-24-82	APPROVED BY	DKS/ofw	3/18/83	

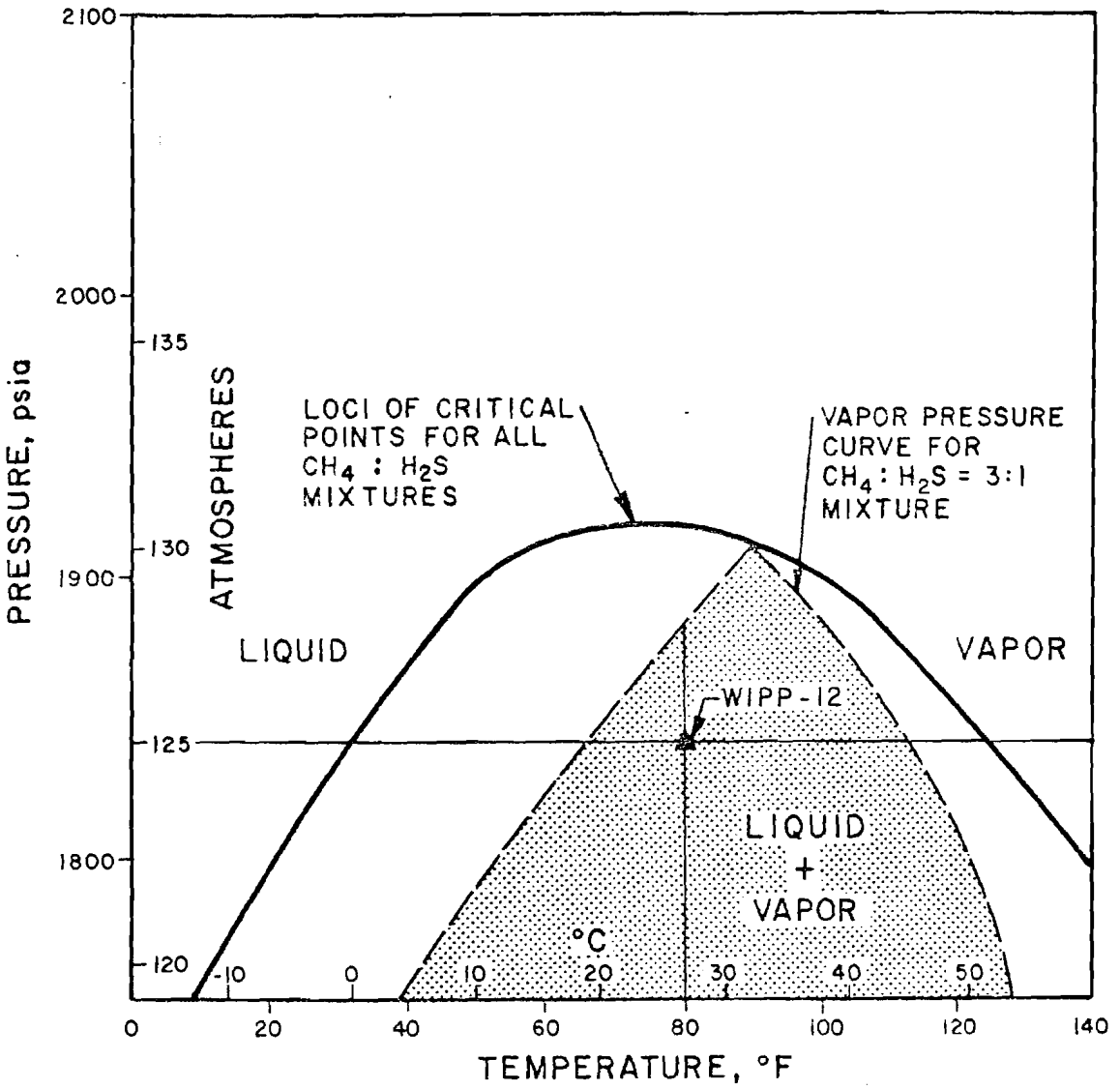

FIGURE C-24

PRESSURE vs TEMPERATURE
FOR BINARY MIXTURES
CH_4 + H_2S
(SCALE ENLARGED)

PREPARED FOR

WESTINGHOUSE ELECTRIC CORPORATION
ALBUQUERQUE, NEW MEXICO

D'APPOLONIA

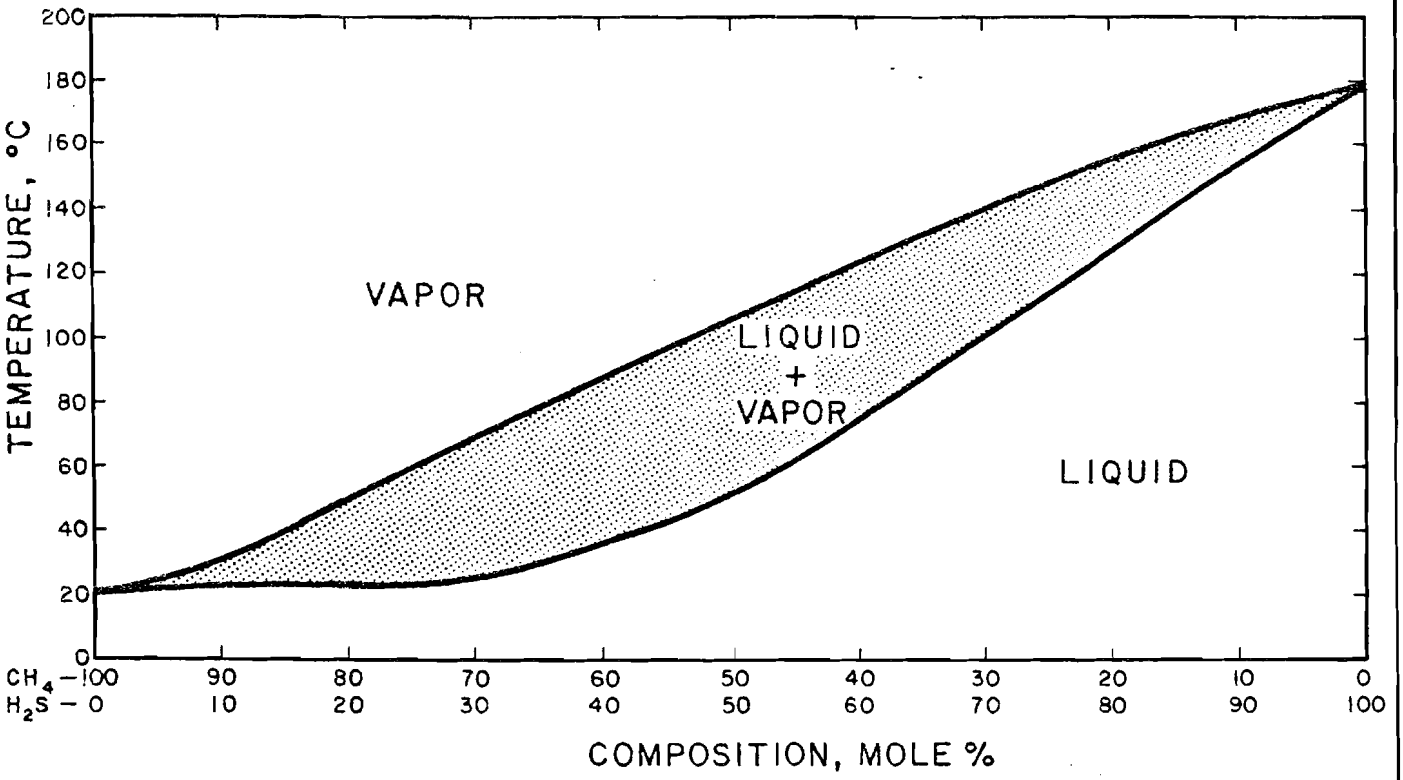

FIGURE C-25

COMPOSITION vs. TEMPERATURE
FOR BINARY MIXTURES
CH_4+ H_2S AT DOWNHOLE PRESSURE

PREPARED FOR

WESTINGHOUSE ELECTRIC CORPORATION
ALBUQUERQUE, NEW MEXICO

D'APPOLONIA

DRAWN BY	EF 9/22/82	CHECKED BY	KEO 3/22/83	DRAWING NUMBER NM78-648-A113
		APPROVED BY	DKS/CAW 3/18/83	

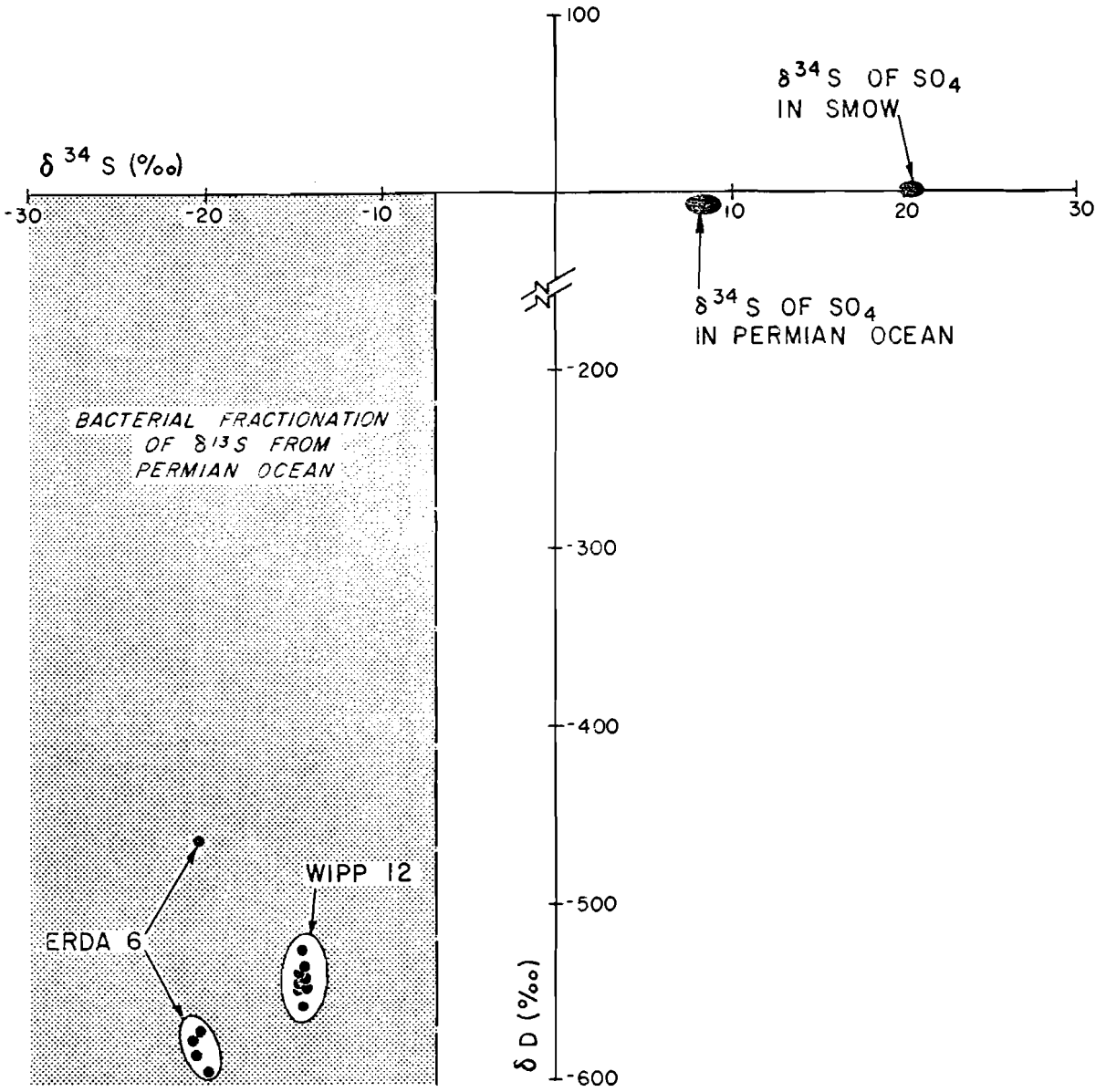

FIGURE C-26

ISOTOPIC COMPOSITION
OF HYDROGEN SULFIDE GAS
FROM ERDA-6 AND WIPP-12

PREPARED FOR

WESTINGHOUSE ELECTRIC CORPORATION
ALBUQUERQUE, NEW MEXICO

REFERENCE

THODE ET AL.(1961)
NIELSEN (1979)
KHARAKA ET AL.(1973)

D'APPOLONIA

DRAWN BY	CHECKED BY	DRAWING NUMBER
EF 9/22/82	APPROVED BY	NM78-648-A114
	RLO 3/17/83	
	DKS/DPJ 3/18/83	

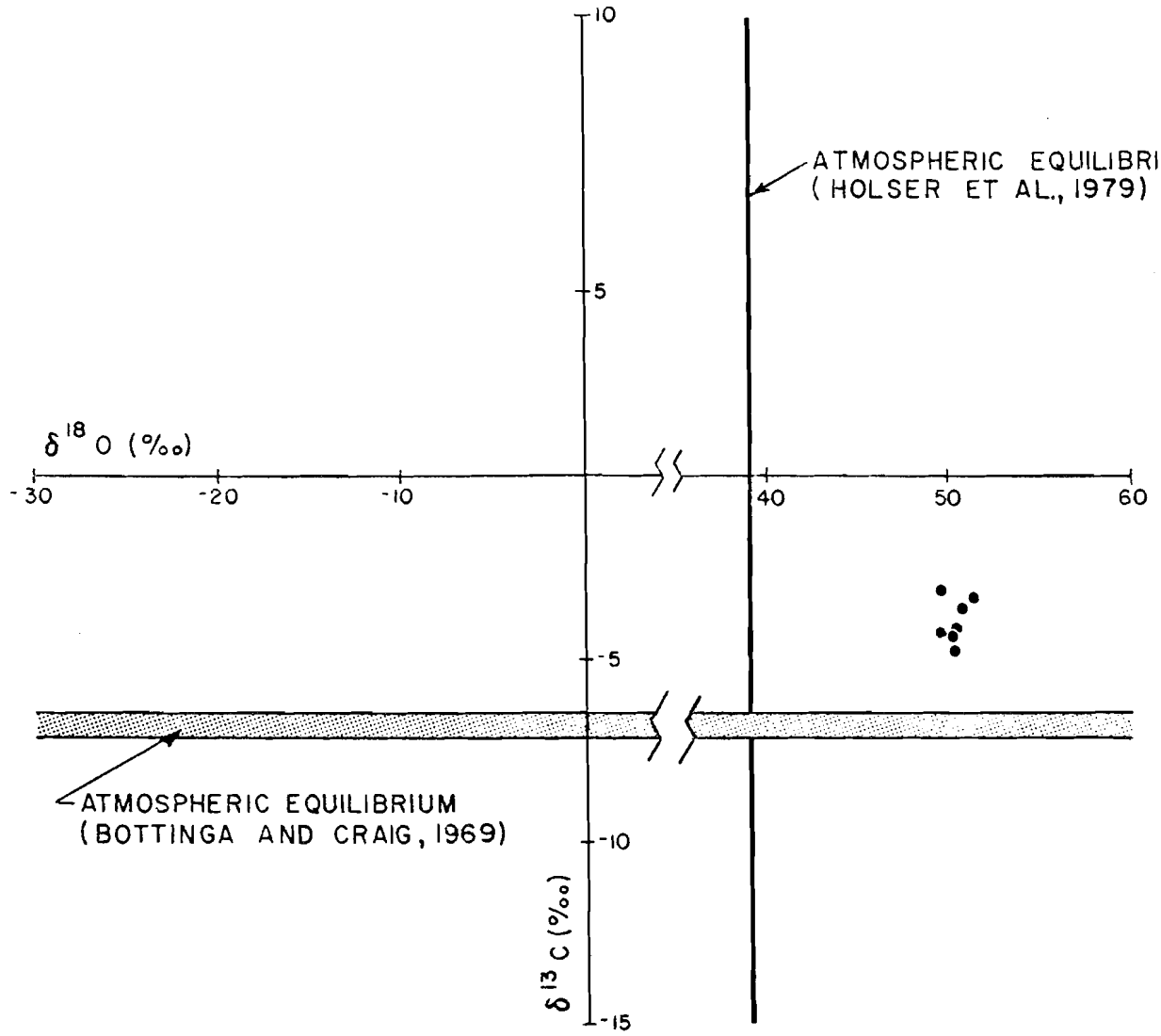

FIGURE C-27

ISOTOPIC COMPOSITION
OF CARBON DIOXIDE GAS
FROM ERDA-6

PREPARED FOR

WESTINGHOUSE ELECTRIC CORPORATION
ALBUQUERQUE, NEW MEXICO

D'APPOLONIA

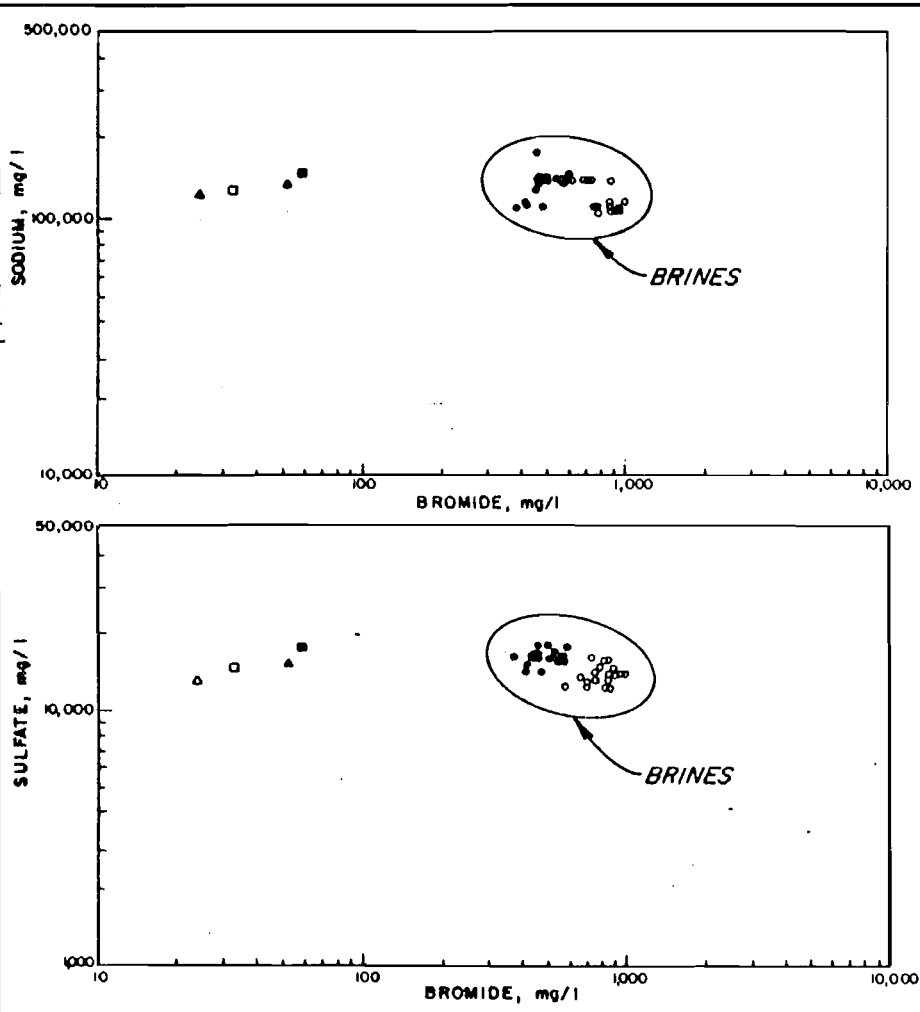

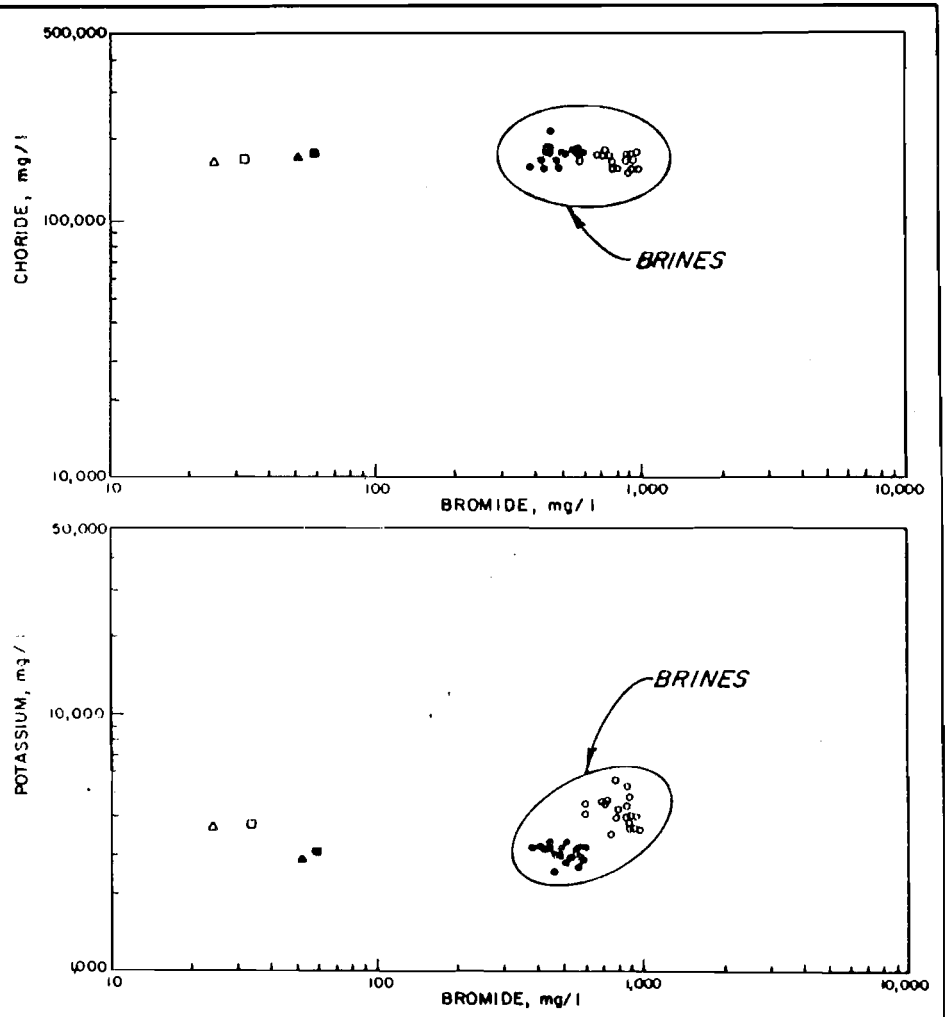

LEGEND:

- WIPP-12 BRINES
- ERDA-6 BRINES

DISSOLUTION PATH:

- DEIONIZED WATER TO ERDA-6
- DEIONIZED WATER TO WIPP-12
- CAPITAN WATER TO ERDA-6
- CAPITAN WATER TO WIPP-12

FIGURE C-28

COMPARISON OF HYPOTHETICAL DISSOLUTION PATHS TO CASTILE BRINES

PREPARED FOR

WESTINGHOUSE ELECTRIC CORPORATION
ALBUQUERQUE, NEW MEXICO

IDAHO

TME 3153

05	DRAWN BY	EF 9/20/82	CHECKED BY	RLO 3/17/83	DRAWING NUMBER	NM78-648-A106
			APPROVED BY	DKS/DMW 3/18/83		

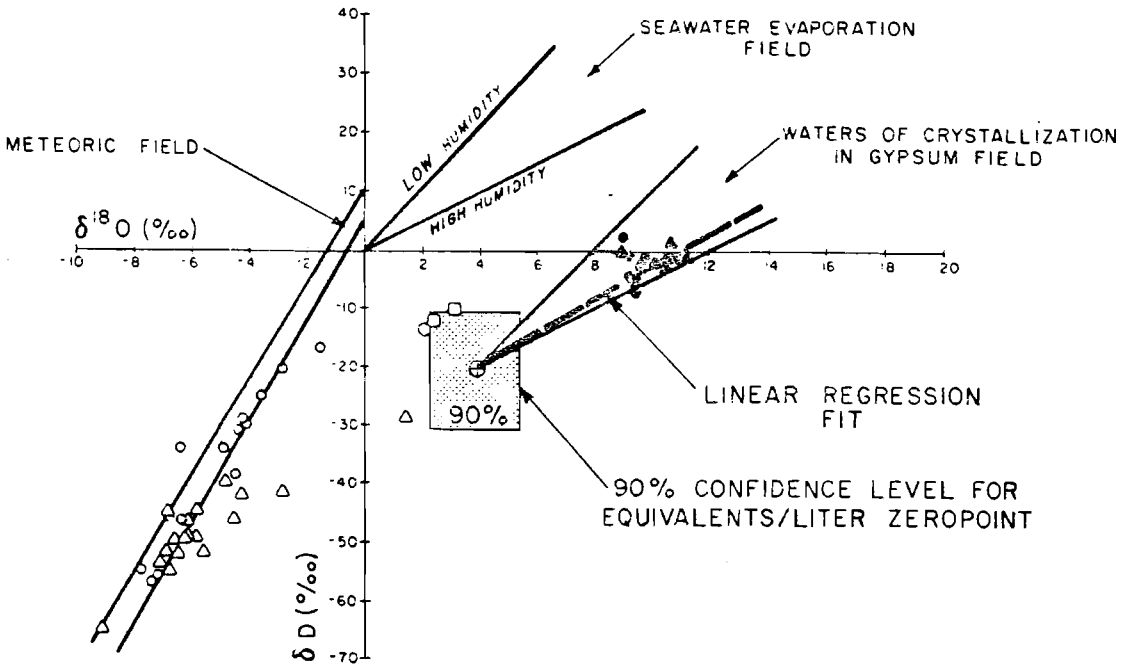

FIGURE C-29

RELATION OF $\delta^{18}O$ AND δD OF BRINES TO POTENTIAL SOURCE WATER

LEGEND

- ● ERDA-6 BRINES
- ▲ WIPP-12 BRINES
- ○ BELL CANYON GROUND WATER
- ○ CAPITAN GROUND WATER
- □ SALADO GROUND WATER
- △ RUSTLER GROUND WATER

PREPARED FOR

WESTINGHOUSE ELECTRIC CORPORATION
ALBUQUERQUE, NEW MEXICO

D'APPOLONIA

06	DRAWN BY	BKH 10-25-82	CHECKED BY	KLC 3/17/83	DRAWING NUMBER	NM78-648-A117
			APPROVED BY	DKS/DAN 3/18/83		

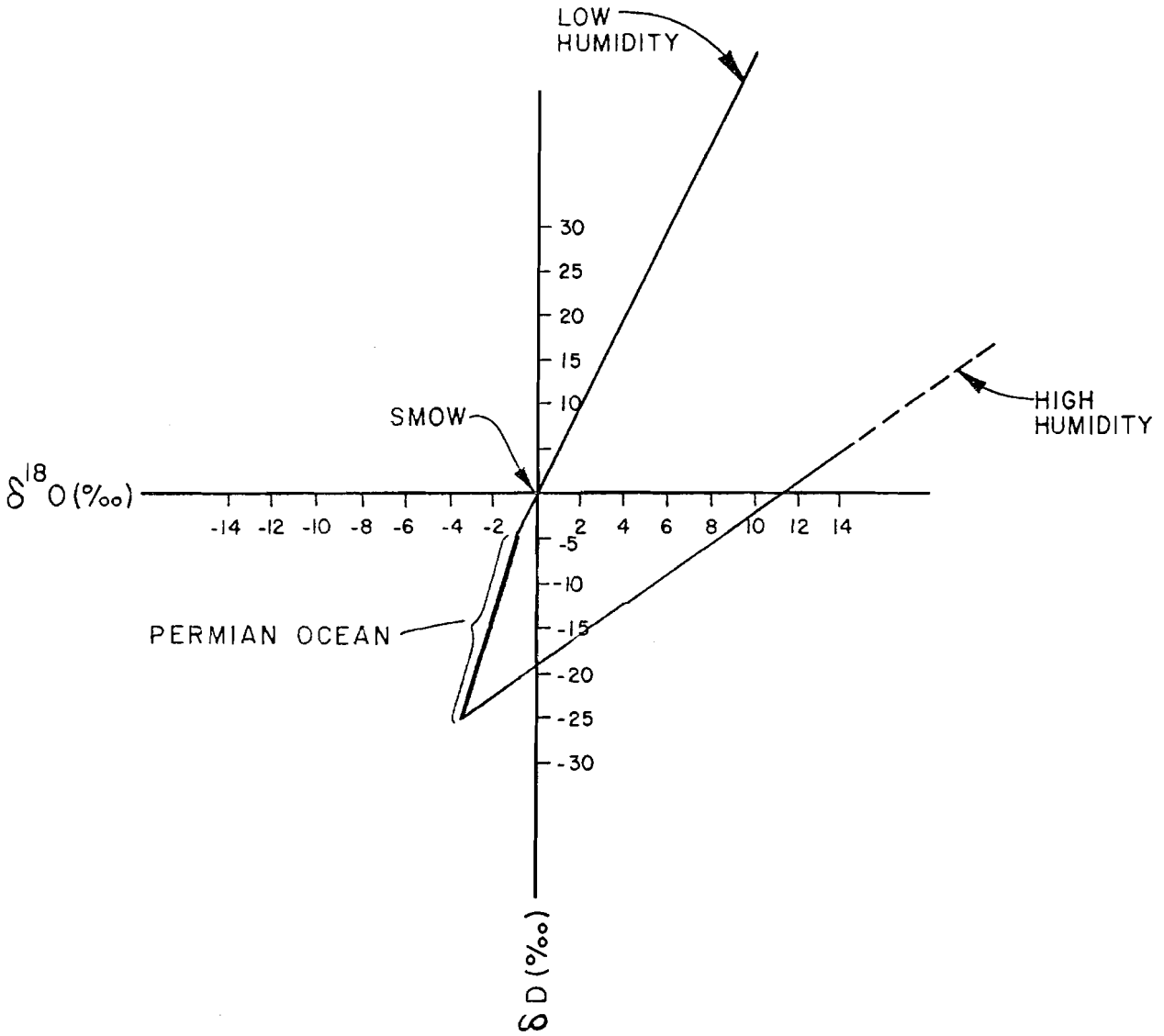

LEGEND:

EVAPORATION FIELD

FIGURE C-30

ESTIMATED PERMIAN OCEAN
REFERENCE FIELDS

PREPARED FOR

WESTINGHOUSE ELECTRIC CORPORATIC
ALBUQUERQUE, NEW MEXICO

D'APPOLONIA

07	DRAWN BY	BKH 10-25-82	CHECKED BY	RZD	3/17/83	DRAWING NUMBER	NM78-648-A118
			APPROVED BY	DKG/DPW	3/18/83		

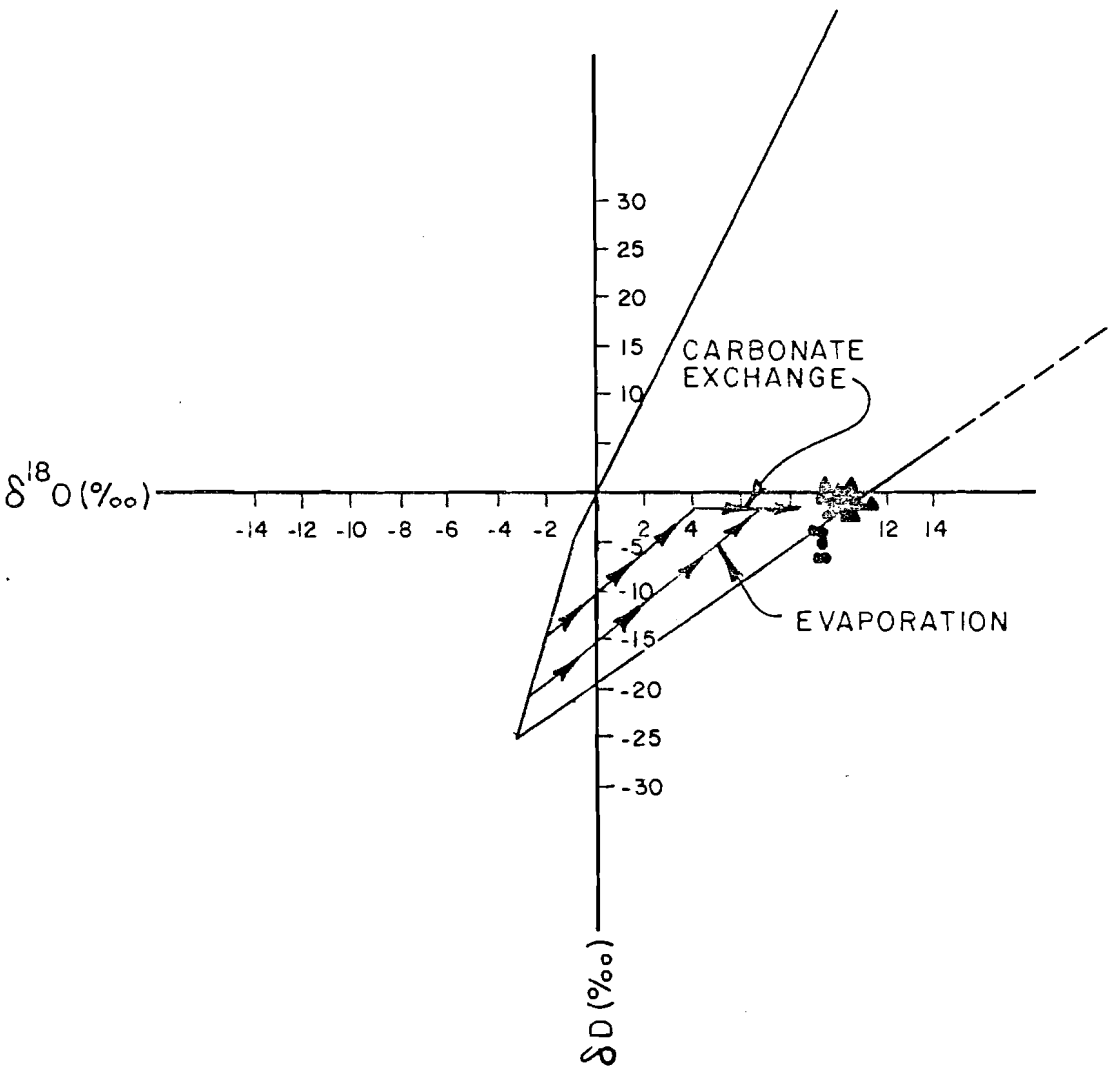

LEGEND:

- • ERDA-6 BRINES
- ▲ WIPP-12 BRINES
- →→→ PROBABLE FRACTIONATION PATH (RANGE)

FIGURE C-31

ISOTOPES OF CASTILE BRINE WATER RELATIVE TO PERMIAN OCEAN

PREPARED FOR

WESTINGHOUSE ELECTRIC CORPORATION
ALBUQUERQUE, NEW MEXICO

D'APPOLONIA

DRAWN BY	EF	CHECKED BY	RLO	3/17/83	DRAWING NUMBER NM78-648-A115
	9/23/82	APPROVED BY	DKS/OPW	3/18/83	

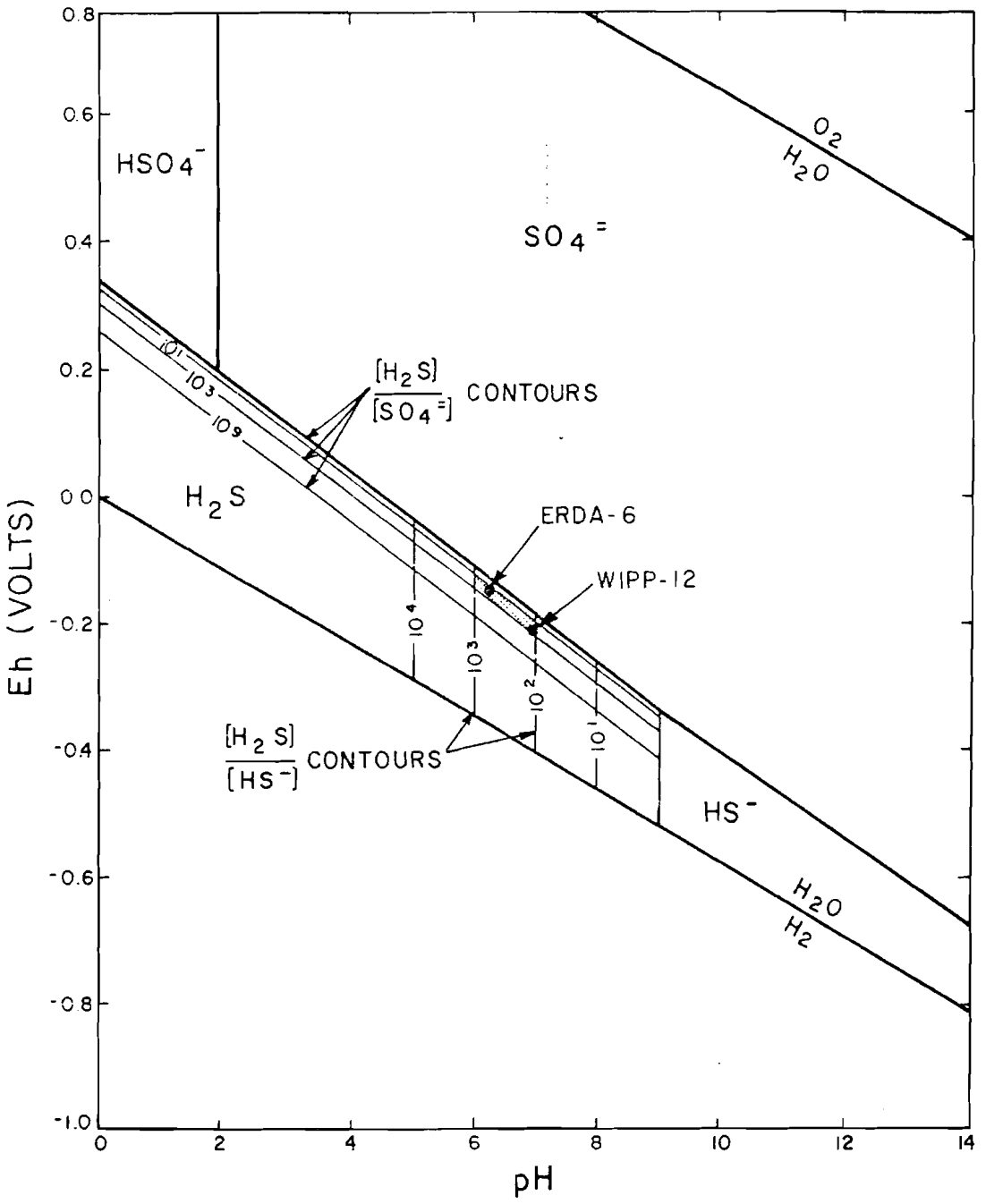

FIGURE C-32

Eh-pH FOR THE SYSTEM S-H_2O
AT DOWNHOLE PRESSURE

PREPARED FOR

WESTINGHOUSE ELECTRIC CORPORATION
ALBUQUERQUE, NEW MEXICO

D'APPOLONIA

PART V - SUMMARY AND CONCLUSIONS

1.0 INTRODUCTION

The analyses and interpretations by three disciplines -- geology, hydrology, and chemistry -- have been integrated to form a model of brine reservoir genesis, and to assess the current and future status of brine reservoirs as they relate to the WIPP site. In particular, the effect of these reservoirs on the potential suitability of the proposed research and development facility for storing transuranic radioactive waste was assessed. The model presented in this summary section represents the hypothesis which encompasses and explains more of the data than any other hypothesis. Alternative hypotheses are presented in the body of the report.

2.0 GENESIS OF PRESSURIZED BRINE RESERVOIRS

The development of the brine reservoirs began in the Permian Period about 235 million years before present. The Castile evaporites, consisting primarily of anhydrite and halite, were deposited at that time (Part II, Section 3.4). During the initial chemical sedimentation (or precipitation) period, the solids were poorly consolidated, and porosity may have been as high as 50 percent (Part II, Section 4.4). Much or all of this pore space was filled with Permian seawater that had been enriched in dissolved solids by evaporation. As a result of that evaporation, some enrichment of deuterium and oxygen-18 in the water also occurred (Part IV, Section 5.1.3).

As sedimentation in the basin continued, the seawater became trapped as an interstitial fluid between individual grains of anhydrite and halite (Part IV, Section 5.1). As compaction increased, grain boundary accretion of halite probably surrounded some of the pore fluids and gave rise to fluid inclusions in halite crystals.

Subsequent to lithification of the sediments, the evaporite sequence was deformed (Part II, Section 4.3). Deformation is represented, in part, by the localized elongate, salt-cored anticlines associated with the Castile brine

reservoirs (Part II, Section 2.3). These features were probably generated by flow of halite in response to differential stress. Mechanisms for salt flow that have been proposed include the following (Part II, Section 4.3.1): (1) halite thickening occurred as a result of gravity foundering (or density contrast between halite and anhydrite) possibly aided by interstitial fluids or small-scale faulting; (2) regional tilting of the basin, which took place in early Tertiary time (about 65 million years ago), Miocene time (between 25 and 12 million years ago), and late Pliocene to Pleistocene time (12 to 1 million years ago) may have caused gravity sliding and thickening of the lower halite against the buttress of the Capitan reef; (3) dehydration of gypsum to form anhydrite with attendant release of water locally reduced the strength of anhydrite and facilitated upward halite movement.

By whatever mechanism, the upward flow of salt deformed the overlying anhydrite and caused it to fracture as a result of extension (Part II, Section 4.3.3). The open fractures acted as unfilled voids to attract the most mobile phases present in the evaporite sequence. Those mobile phases were brine and perhaps some of the associated gases. Flow into the fractures of the anticline released some of the pressure on the brine and resulted in the current reservoir pressure being somewhat less than present lithostatic, but greater than present hydrostatic pressure (Part II, Section 4.3.3). During this local flow of brine, some halite and (in the case of WIPP-12) glauberite were probably dissolved (Part IV, Section 5.1.2)

Most of the brine originated as pore waters associated with the anhydrite. As the magnesium-rich waters migrated toward fractures, they reacted with calcite to yield dolomite (Part IV, Section 5.1.2) This accounts for the presence of dolomite in the anhydrite (Part II, Section 4.1.3). The reaction also greatly enriched the brine in oxygen-18 and depleted it in magnesium (Part IV, Sections 5.1.2 and 5.1.3).

Accompanying brine flow, or somewhat later, methane gas was both generated and trapped in place. In the case of ERDA-6, methane was generated biologically,

whereas in WIPP-12 a portion was produced thermogenically (by the thermal degradation of organic matter) (Part IV, Section 4.3.3). Most of the hydrogen sulfide (liquid) was produced biogenically after the physical processes of reservoir formation were completed. However, a portion of the hydrogen sulfide may have had a thermogenic origin and been trapped similar to the methane (Part IV, Section 4.3.3). At this stage, the evolution of the brine may have been complete. However, minor dissolution of the confining halite beds (top and bottom) may have occurred, resulting in the halite saturation of the WIPP-12 reservoir (Part IV, Section 5.1.3).

3.0 PRESENT STATUS OF PRESSURIZED BRINE RESERVOIRS

The ERDA-6 and WIPP-12 brine reservoirs may be modeled as fractured heterogeneous systems. The volumes of the ERDA-6 and WIPP-12 reservoirs are estimated, within an order of magnitude, to be about 630,000 barrels and about 17,000,000 barrels, respectively. Of these volumes, only three percent or less could be delivered to the surface without pumping if a man-made connection were provided. The vast majority of brine is stored in low-permeability microfractures. About five percent of the overall brine volume in each reservoir is stored in large, open fractures (Part III, Sections 3.4.3 and 3.4.4). The large fractures form an infiltration gallery or extended well, providing a collection mechanism and high-permeability conduit for brine flow. The large fractures provide an initially vigorous flow or pressure-buildup response (Part III, Sections 3.4.3 and 3.4.4). The microfractures provide a slow, sustained response. Given sufficient time, flow from the microfractures can largely replenish any depletion which has occurred in the large fractures.

The Delaware Basin has been tectonically stable for at least the last million years. At present, the Castile brine reservoirs appear to be isolated. There is no evidence to suggest hydraulic or chemical connection between reservoirs, or between reservoirs and other ground-water systems, either at the present or in the past (Part III, Section 3.4.1; Part IV, Section 5.3). Prior to testing, the hydraulic head in WIPP-12 was 4680 ft MSL (for pure water) while

in ERDA-6 it was 5551 ft MSL. If good hydraulic communication between the two wells existed, these hydraulic heads would be nearly equal. Furthermore, the hydraulic heads in both the ERDA-6 and WIPP-12 reservoirs exceed those of local ground waters, including the highest ground-water recharge zones of the basin. Thus, ground water cannot be recharging the brine reservoirs. The maintenance of these elevated hydraulic heads for at least a million years with no recharge potential attests to the lack of flow from the reservoirs to the local ground waters. With flow occuring neither to nor from the reservoirs, hydraulic isolation is maintained. Finally, the gas and brine chemistries of the two reservoirs are distinctly different from each other and from local ground waters. For example, large differences in the gas compositions exist between WIPP-12 and ERDA-6 (Part IV, Section 5.1.4). The gas in WIPP-12 is composed mostly of methane and has little or no carbon dioxide. ERDA-6 contains substantial quantities of carbon dioxide, and more hydrogen sulfide than WIPP-12. Differences observed in the brine composition include boron, bromide, magnesium, potassium, and lithium concentrations (Part IV, Section 3.3.2). Connection between reservoirs would eliminate these differences, especially with respect to the highly mobile gases. Accordingly, if connected in the past, the current brine (and associated gas) compositions of the two reservoirs would be equivalent or more closely related.

In addition to being isolated, the brines appear to be in chemical equilibrium with their surroundings, and they are stagnant (Part IV, Section 5.2). Specifically, the Eh's measured for each well are consistent with theoretical equilibrium calculations for Eh using thermodynamic data for coexisting gas pairs (methane-carbon dioxide) and for dissolved sulfide species (hydrogen sulfide-sulfate). This agreement indicates bulk system equilibrium among solid, liquid, and gas phases. Moreover, the brines are chemically saturated with the primary phases of the reservoir host rock (anhydrite and calcite). WIPP-12 also appears to be saturated with halite, the principal phase of the confining strata. These data further support the contention of equilibrium (Part IV, Section 5.2).

The origin of water in Castile brine reservoirs preferred in previous work (Lambert, 1978; Barr et al, 1979; Lambert, 1983; Lambert and Carter, 1983) is old meteoric groundwater, acquiring its present solutes and D/H and $^{18}O/^{16}O$ ratios during extensive interaction with minerals associated with the evaporite sequence. If this groundwater is inferred to have originated in the nearest highly productive groundwater reservoir, the Capitan Limestone, its probable α_o is 5.14 for the actively recharged region near Carlsbad (Carlsbad Well No. 7).

Hiss (1975) showed that other nearby portions of the Capitan hydrological system (near the postulated groundwater divide) are probably not actively moving. The waters from the Middleton and Hackberry wells, on either side of the divide apparently formed by the Laguna Submarine Canyon system, have α-values of 1.81 and 1.22, respectively (Barr et al, 1979). These wells are inferred to have no direct interconnection with each other, because of their distinct α-values. Further, as discussed by Barr et al (1979), these waters have been isolated from their inferred source of recharge (α_o = 5.14) for 500,000 to 1,100,000 years; the Middleton and Hackberry wells are developed in relatively stagnant portions of the Capitan. Thus, it is not geologically reasonable to use their α values for calculating ages of isolation for the brine reservoirs, since their observed α values

(a) do not represent α values of actively recharged groundwater,
(b) have themselves decreased by radioactive decay since the formation of the brine reservoirs, and
(c) were probably significantly different from their modern (observed) values at the time the brine reservoirs formed.

Given a reasonably fast transit time for water in the "active" portions of the Capitan (Hiss, 1975), and inferring that, for a period of time, the fractured Castile anhydrite was at one time hydrologically connected to the Capitan, this model allows calculations of the age of the end of the hydraulic connection, i.e., entrapment of the fluids within Castile anhydrites. For WIPP 12, the resultant age range is 360,000 to 610,000 years, and for ERDA 6 700,000 to 880,000 years. The latter age is in close agreement with the work of Barr et al (1979).

- Migration of brine made possible by hydraulic and/or chemical disequilibrium and dissolution of halite (Part IV, Section 3.3.5).

Neither of the above mechanisms are feasible in the study area. The proposed horizon for the WIPP facility is separated from the brine-bearing anhydrite horizon by approximately six hundred vertical feet of halite with minor clay interbeddings. The extremely low permeability of halite, combined with the absence of fractures, and the fact that the brines are saturated or nearly saturated with halite, removes from further concern the potential for vertical brine migration.

At present, the brine reservoirs are stable. Moreover, brine reservoirs appear to have been stagnant for at least a million years, as evidenced by permanent hydraulic disequilibrium and distinctly different chemical characteristics. No feasible course of events can be anticipated which could cause the Castile brine reservoirs to have a significant adverse effect on the suitability of the WIPP site for the disposal of TRU waste.

References

Andrews, John N.; and Kay, R. Linden F., 1982, $^{234}U/^{238}U$ activity ratios of dissolved uranium in groundwaters from a Jurassic Limestone aquifer in England: Earth and Planetary Science Letters, v.57, p.139-151.

Barr, G.E.; Lambert, S.J.: and Carter, J.A., 1979, Uranium isotope disequilibrium in groundwaters of southeastern New Mexico and implications regarding age-dating of waters, in Proceedings of the international symposium on isotope hydrology, 1978, v.2: International Atomic Energy Agency, STI/PUB/493, p.645-660.

Fleischer, Robert L., 1982, Alpha-recoil damage and solution effects in minerals: uranium isotopic disequilibrium and radon release: Geochimica et Cosmochimica Acta: v.46, p.2191-2202.

Hiss, W.L., 1975, Stratigraphy and groundwater hydrology of the Capitan aquifer, southeastern New Mexico and western Texas: Unpublished Ph.D. thesis, University of Colorado, Boulder, 501 p.

Kigoshi, Kunihiko, 1971, Alpha-recoil thorium - 234: dissolution into water and the uranium-234/uranium-238 disequilibrium in nature: Science, v.173, p.47-48.

Konfeld, J.; Gradsztajn, E.; and Yaniv, A., 1979: A flow pattern deduced from uranium disequilibrium studies for the Cenomanian carbonate aquifer of the Beersheva Region, Israel: Journal of Hydrology, v.44, p.305-310.

Lambert, Steven J., 1978, Geochemistry of Delaware Basin groundwaters, in Geology and mineral deposits of Ochoan rocks in Delaware Basin and adjacent areas: New Mexico Bureau of Mines and Mineral Resources, Circular 159, p.33-38.

_____: 1983, Dissolution of evaporites in and around the Delaware Basin, southeastern New Mexico and west Texas: Sandia National Laboratories Report SAND82-0461, ?p.

_____; and Carter, J.A., 1983, Uranium-isotope disequilibrium in brine reservoirs of the Castile Formation, northern Delaware Basin, southeastern New Mexico: Sandia National Laboratories Report SAND83-0144.

Osmond, J.K.; and Cowart, J.B., 1976, The theory and uses of natural uranium isotopic variations in hydrology: Atomic Energy Review, v.14, p.621-679.

Urey, H.C., 1947, The thermodynamic properties of isotopic substances: Journal of the Chemical Society, p.562-581.

APPENDIX A

GROUNDWATER RESIDENCE TIME

S. J. Lambert
Sandia National Laboratories

Appendix A

Groundwater Residence Time

Introduction

The uranium-isotope disequilibrium method (the U method) of determining the age of entrapment of groundwaters is dependent on the systematic preferential buildup of ^{234}U with respect to ^{238}U in one part of the groundwater system, and the radioactive decay of ^{234}U (faster than that of ^{238}U) in another part of the system. Deviations of the $^{234}U/^{238}U$ specific activity ratio (α) from unity provide the basis for tracing groundwater flow paths (Kronfeld et al, 1979) and estimating limits to the age of confinement of the water (Barr et al, 1979). Note specifically that the age given is that of entrapment of the water, not necessarily that of initial origin, and that entrapment is defined as the process by which the groundwater ceases to be exposed to new surfaces of fresh, unaltered rock. It must be kept in mind that fresh rock surfaces can be exposed to fluid contact by continuous processes, such as minor fracturing, as well as by more discrete or singular events. Like the well-known carbon-14 method, the U method does not yield an absolute age from a single data point; rather age is some function of the inferred initial and measured final states of the system. Unlike the chlorine-36 and carbon-14 methods, the U method does not depend on a component of groundwater that is purely atmospheric in origin.

The U method allows calculations of residence times to a maximum of approximately 2,000,000 years, well beyond the limit of C-14 (35,000 to 45,000 years). The maximum measurable age is set by analytical limits resulting from the relatively rapid decay of ^{234}U. Even for groundwaters of very high α, say 15, the calculated activity ratio decreases to a value analytically indistinguishable from that at secular equilibrium (1.0) well within 2,000,000 years. The initial conditions inferred in the U method need not be atmospheric. Instead, transit times can be calculated based on the inference that two bodies of groundwater with different α's are now connected or have been connected in the past. The "age" calculated from the U method, based on decrease in α from an inferred initial value at the time of entrapment, is thus entirely dependent on the inferred model of origin and emplacement of the groundwater.

The assumptions fundamental to the U method involve the processes governing the changes in ^{234}U concentration in solution. First, it must be assumed that only radioactive decay diminishes the ^{234}U activity relative to that of ^{238}U. This appears valid, since, in the age range of the U method, it can be assumed that virtually no ^{238}U decays. Second, it is assumed that only preferential leaching of ^{234}U relative to ^{238}U results in α buildup, as discussed by Kigoshi (1971), Andrews and Kay (1982), and Fleischer (1982). Both of these assumptions are reasonable, since a mass difference of 4 out of 238 is insufficient to give rise to appreciable physicochemical isotopic fractionation in exchange, dissolution, or precipitation reactions (Urey, 1947). Thus, the preferential leaching of ^{234}U (daughter of ^{234}Th, itself a daughter product of ^{238}U), a result of damage to the surrounding crystal lattice upon recoil during alpha-decay of ^{238}U, is not reversible.

The work of Barr et al (1979) resulted in the development of two geochronological models, one involving no additional uptake of U from rock along the flow path between inferred source and present occurrence, the other taking into account continuous leaching of additional U from the rock. The no-leaching model:

$$t = \frac{\ell n \left(\frac{\alpha_b - 1}{\alpha_o - 1} \right)}{-\lambda_2}$$

depends only on the $^{234}U/^{238}U$ activity ratio in the groundwater of interest (α_b), its geologically inferred original α (α_o), and λ_2, the radioactive decay constant for ^{234}U ($2.806 \times 10^{-6} a^{-1}$). The leaching model:

$$t = \frac{\ell n \left(\frac{\alpha_b - 1 - fr}{\alpha_o - 1 - fr} \right)}{-\lambda_2}$$

in addition depends on r (the equilibrium ratio of specific activity in rock to that in coexisting water) and f (the composite fractions of ^{234}Th procursor, ^{234}U, and ^{238}U leaching from rock).

The latter equation is equivalent to that developed by Andrews and Kay (1982) for the increase of α in solution as a function of time:

$$\alpha = \frac{^{234}A + {}^{234}\lambda_{Th}\left(\frac{0.235\ {}^{238}\lambda_U}{{}^{234}\lambda_{Th}\ {}^{238}U_s}\right)\left[1-\exp(-{}^{234}\lambda_U t)\right]}{^{238}A}$$

where $^{234}A = {}^{238}A =$ activities of ^{234}U and ^{238}U dissolved from rock by chemical etch processes (no recoil-facilitated preferential leaching)

$^{234}\lambda_{Th} =$ decay constant of ^{234}Th ($10.5\ yr^{-1}$)

$^{238}\lambda_U =$ decay constant pf ^{238}U ($1.537 \times 10^{-10} yr^{-1}$)

$^{234}\lambda_U =$ decay constant of ^{234}U ($2.806 \times 10^{-6} yr^{-1}$)

$^{238}U_s =$ number of ^{238}U atoms within the ^{234}Th recoil range of the continuously leached rock surface.

Discussion

Lambert and Carter (1983) applied both the "leaching" and the "no-leaching" models of Barr et al (1979) to the ERDA 6 and WIPP 12 brine reservoirs in calculating residence times of the respective waters in their anhydrite host rocks. In the "no-leaching" model, it is assumed that trapped fluids do not equilibrate with the rock mass in which they are found, either during flow to the present location or after entrapment. In the "leaching" model, it is assumed that in-place equilibrium is approached. The α for ERDA 6 is between 1.34 and 1.58 at the 95 percent confidence level, (3 replicates), and for WIPP 12 is between 1.74 and 2.54 (8 replicates).

One proposed model for the origin of the Castile brine reservoirs is the migration of primary intergranular pore water (Permian seawater) into the fractures. If this model is correct, and Permian seawater is assumed to have the same composition as present seawater, the initial $^{234}U/^{238}U$ activity ratio (α_o) is constrained to be 1.15 (Osmond and Cowart, 1976).

The brines in the fractured reservoir rock of ERDA 6 and WIPP 12 presently have α-values in the range 1.3 to 2.6. An apparent negative age results from use of the no-leaching model (Barr et al, 1979), since only the inferred α_o and

the observed α are taken to represent the initial and final states of the system in this model. The apparent negative age arises because the α_o is less than the observed α. Since negative ages are of course not real, this implies the α_o selected is wrong (wrong origin) or the no-leaching model does not apply, or both.

An age or residence time can be calculated based on α buildup in a closed, stagnant system of groundwater in contact with host rock; this is the "leaching" model. This is done here using the method of Andrews and Kay (1983) and the values for U content for rock in the ERDA 6 reservoir, 2 parts in 10^6 by wt (Barr et al, 1979) and 0.22×10^{-6} g/kg for the water.

Additional specific assumptions made are that:

a) The brine reached secular equilibrium ($\alpha = 1.0$) at its former location.
b) The brine was emplaced at its present location "instantaneously," i.e., rapidly enough so that no leaching took place along the path of injection.

By this method and under these assumptions, the closed-system "leaching" calculation predicts that the α value of the water should have risen from $\alpha_o = 1.0$ to 1.3 in only 25,000 years and to 1.58 in 50,000 years. Thus, residence times in ERDA 6 and WIPP 12 under these assumptions do not exceed 50,000 years.

If, on the other hand, it is assumed that brine emplacement has been a result of ongoing structural deformation, and that brine continuously equilibrated with the surrounding rock mass until entrapment, the initial α value is indeterminate. The maximum measurable residence time, as described above, becomes no more than 2,000,000 years. In fact, for the specific rock systems of interest here, the maximum measurable age appears to be approximately 800,000 years.

The fact that measured α's in ERDA 6 and WIPP 12 are distinctly greater than 1.0 thus strongly indicates that local residence times for these brines are less than 800,000 to 2,000,000 years, regardless of assumptions about original brine origin and mode or rate of brine emplacement.